



UNIVERSITY OF
LIVERPOOL

Old and New Targets in Antimalarial Drug Discovery

Thesis submitted in accordance with the requirements of the
University of Liverpool for the degree of Doctor of
Philosophy by

Natalie Roberts

September 2016

Declaration

This thesis is the result of my own work. The material contained in this thesis has not been presented, nor is currently being presented, either wholly or in part for any other degree or other qualification.

Natalie Roberts

Department of Chemistry, University of Liverpool

Acknowledgements

I would like to express my sincere gratitude to Professor Paul O'Neill for providing me with the opportunity to undertake this research and ensuring that the past four years have been both challenging and engaging.

Dr Neil Berry, I would like to thank you for being a constant source of advice, encouragement and support. Your guidance and patience have undoubtedly made this process significantly more manageable.

Huge thanks must also go to members of the 4th floor lab, both past and present. The copious amounts of tea and cake have certainly helped to get me through each day and you have all made my time in the lab very enjoyable.

Additionally, I would like to thank the Analytical Services Team for all of their help throughout my time in the department.

My biggest thanks must go to my family. Without all of your endless love and support, none of this would have been possible. I love you all very much.

Mum and Dad, the space here is too short to describe how truly grateful I am for everything you have done for me. You have supported me unconditionally, helped me through the difficult times and always believed in me. Thank you for always being there.

Sam, I am the proudest big sister. You have worked so hard to achieve your dream and I truly admire your strength and determination. Sophie, I am so happy to have you in the family. Thank you both for all the cups of tea, chats and words of encouragement.

Michael, I couldn't have done this without you. You have been an amazing support throughout this process and never lost faith in me. You are always there to listen and never fail to put a smile on my face. I am very excited for what our future holds.

Isabella, words cannot describe how much you mean to me and how much joy and laughter you have brought into my life in such a short space of time. Thank you for giving me the biggest smiles and best cuddles.

Abstract

The increasing emergence of resistance to commonly used therapies has placed a huge strain on the prevention and control of malaria; therefore, there is an urgent need to develop novel antimalarial agents. The aim of this research was to design and synthesise a library of potent antimalarial compounds, with desirable pharmacokinetic profiles, in order to identify a drug candidate suitable for pre-clinical development. This research was divided into two main sections:

- The synthesis of compounds designed to inhibit IspD, a novel target in antimalarial drug discovery
- The late stage development of a series of endoperoxide-based antimalarials, which are derived from the structure of artemisinin

A library of benzisothiazolinone compounds was generated to target the IspD enzyme. Many of these compounds displayed low micromolar inhibitory activity against both enzymatic and phenotypic assays *in vitro* and an investigation into structure-activity relationships around the core of these benzisothiazolinones was also conducted. The most potent compound to emerge, a CH₂ linked benzisoselenazolone, had an IC₅₀ of 0.17 μM against *Pf*IspD and 5.54 μM against *Pf*3D7. These compounds represent a novel class of IspD inhibitor, which have the potential for further development as antimalarial agents.

A number of 1,2,4,5-tetraoxane analogues were also prepared in order to develop an antimalarial agent suitable for a single-dose cure. The most potent analogue, N205, had an IC₅₀ of 1.3 nM and an average mouse survival of 26.3 days (66% cure rate) following a single dose. A less than optimal stability profile for N205 led to the further development of another potent tetraoxane analogue, E209. Optimisation of the synthetic pathway led to the generation of E209 in a series of five high-yielding steps that are suitable for large-scale production. E209 represents the first 1,2,4,5-tetraoxane that is comparable, in terms of both efficacy and PK/PD profiles, to OZ439, and is a candidate for pre-clinical development.

Contributions

IspD

Initial chemoinformatic studies were conducted by Dr Neil Berry at the Department of Chemistry, University of Liverpool. These were used to facilitate the selection of compounds to be screened for activity against the IspD enzyme. High throughput *in vitro* screening was then carried out by BioFocus. Molecular modelling studies used to identify the CH₂ linked series of benzisothiazolinones were conducted by Adam Byrne at the Department of Chemistry, University of Liverpool. *In vitro* biological testing was carried out by the Odom John group at Washington University School of Medicine on St. Louis.

Tetraoxanes

The development and synthesis of RKA182 was carried out by Richard Amewu. The original synthesis of E209 was conducted by Emma Shore. The *in vitro* studies were conducted at the Liverpool School of Tropical Medicine and *in vivo* efficacy studies in mice were conducted at the Swiss Tropical and Public Health Institute (Basel). Solubility, plasma protein binding, rat and mouse pharmacokinetics, and metabolic stability studies were carried out at Monash University. Humanised mouse pharmacokinetic studies were conducted at GSK.

Abbreviations

ACTs	Artemisinin-based combination therapies
ADP	Adenosine diphosphate
ATP	Adenosine triphosphate
BA	Bioavailability
BOC	<i>tert</i> -Butyloxycarbonate
CDP-ME2P	4-Diphosphocytidyl-2 <i>C</i> -methyl-D-erythritol 2-phosphate
CDPME	4-Diphosphocytidyl-2 <i>C</i> -methyl-D-erythritol
CI	Chemical ionisation
CL	Clearance
cMEPP	2 <i>C</i> -Methyl-D-erythritol-2,4-cyclodiphosphate
CMP	Cytidine monophosphate
CoA	Coenzyme A
CTP	Cytidine triphosphate
d	Doublet
DCE	1,2-Dichloroethene
DCM	Dichloromethane
dd	Doublet of doublets
ddd	Doublet of doublet of doublets
DHA	Dihydroartemisinin
DHFR	Dihydrofolate reductase
DHPS	Dihydropteroate synthase
DIPEA	N,N-Diisopropylethylamine
DMAPP	Dimethylallyl pyrophosphate
DMF	Dimethylformamide
DMPK	Drug metabolism and pharmacokinetics
DMSO	Dimethyl sulfoxide
DNA	Deoxyribonucleic acid
DOXP	1-deoxy- <i>D</i> -xylulose-5-phosphate
DPPA	Diphenylphosphoryl azide
dt	Doublet of triplets
DXS	1-Deoxy- <i>D</i> -xylulose-5-phosphate synthase

EDAC	1-Ethyl-3-(3-dimethylaminopropyl)carbodiimide
eq	Equivalents
ES	Electrospray
FPIX	Ferriprotoporphyrin IX
GAP	Glyceraldehyde 3-phosphate
GHMP	Galacto-homoserine-mevalonate-phosphomevalonate
HATU	1-[Bis(dimethylamino)methylene]-1H-1,2,3-triazolo[4,5-b]pyridinium 3-oxide hexafluorophosphate
HIV	Human immune deficiency virus
HMBPP	4-Hydroxy-3-methyl-2-(E)-butenyl-4-diphosphate
HMG-CoA	3-Hydroxy-3-methylglutaryl-CoA
HOBt	Hydroxybenzotriazole
HRMS	High-resolution mass spectrometry
HTS	High throughput screen
IPP	Isopentenyl pyrophosphate
IR	Infrared
IspC	1-Deoxy-D-xylulose-5-phosphate reductoisomerase
IspD	4-Diphosphocytidyl-2C-methyl-D-erythritol cytidyltransferase
IspE	4-Diphosphocytidyl-2C-methyl-D-erythritol kinase
IspF	2C-Methyl-D-erythritol-2,4-cyclodiphosphate synthase
IspG	4-Hydroxy-3-methyl-2-(E)-butenyl-4-diphosphate synthase
IspH	4-Hydroxy-3-methyl-2-(E)-butenyl-4-diphosphate reductase
IV	Intravenous
LAH	Lithium aluminium hydride
LDL	Low-density lipoprotein
LRMS	Low-resolution mass spectrometry
m	multiplet
mCPBA	<i>meta</i> -Chloroperoxybenzoic acid
MEP	2C-methyl-D-erythritol-4-phosphate
MMV	Medicines for Malaria Venture
mp	Melting point
MS	Mass spectrometry
MTO	Methyltrioxorhenium

MVA	Mevalonate
NADP	Nicotinamide adenine dinucleotide phosphate
NMR	Nuclear magnetic resonance
o/n	Overnight
PD	Pharmacodynamics
<i>Pf</i> CRT	<i>Plasmodium falciparum</i> chloroquine resistance transporter
PIFA	[Bis(trifluoroacetoxy)iodo]benzene
PK	Pharmacokinetics
ppm	Parts per million
q	Quartet
rt	Room temperature
s	Singlet
SAR	Structure-activity relationship
SCID	Severe combined immunodeficiency
SERCA	Sarco/endoplasmic reticulum Ca ²⁺ -ATPase
t	Triplet
T _{1/2}	Half-life
td	Triplet of doublets
TEMPO	(2,2,6,6-Tetramethylpiperidin-1-yl)oxyl
TFA	Trifluoroacetic acid
THF	Tetrahydrofuran
TLC	Thin layer chromatography
TPP	Thiamine pyrophosphate
V _d	Volume of distribution
WHO	World Health Organisation

Contents

Title Page	i
Declaration	ii
Acknowledgements	iii
Abstract	iv
Contributions	v
Abbreviations	vi
Chapter I – General Introduction to Malaria	1
Chapter II – Introduction to IspD	37
Chapter III – IspD Inhibitors	78
Chapter IV – A Review of Endoperoxide Antimalarials	211
Chapter V – Novel Tetraoxane Antimalarials	243
Chapter VI - Conclusions	319

Chapter I

General Introduction to Malaria

Table of Contents

1.1 Introduction	3
1.1 The symptoms of malaria	4
1.2 The Parasite	6
1.2.1 Parasite life cycle	7
1.2.2 Haemoglobin degradation	9
1.3 The Mosquito Vector	11
1.3.1 Vector control	11
1.4 Past and Present Drug Therapies	12
1.4.1 Quinoline antimalarials	13
1.4.2 Antifolate compounds	17
1.4.2.1 DHPS inhibitors	17
1.4.2.2 DHFR inhibitors	18
1.4.3 Atovaquone	20
1.4.4 Artemisinin and semi-synthetic derivatives	21
1.4.5 Artemisinin-based combination therapies	24
1.5 Resistance	26
1.6 Research Aims	27
1.6 References	28

1.1 Introduction

Malaria is a potentially life-threatening infectious disease that is transmitted through the bite of an infected female *Anopheles* mosquito.¹ The World Malaria Report 2015 revealed over 214 million cases of malaria in 95 countries, resulting in an estimated 438,000 deaths.² Despite efforts to eliminate malaria, a disease that is preventable and treatable, it remains the world's most significant parasitic disease.^{3,4} The map shown below (Figure 1.1) highlights the prevalence of the disease in the developing countries of sub-Saharan Africa, South America and Southeast Asia.

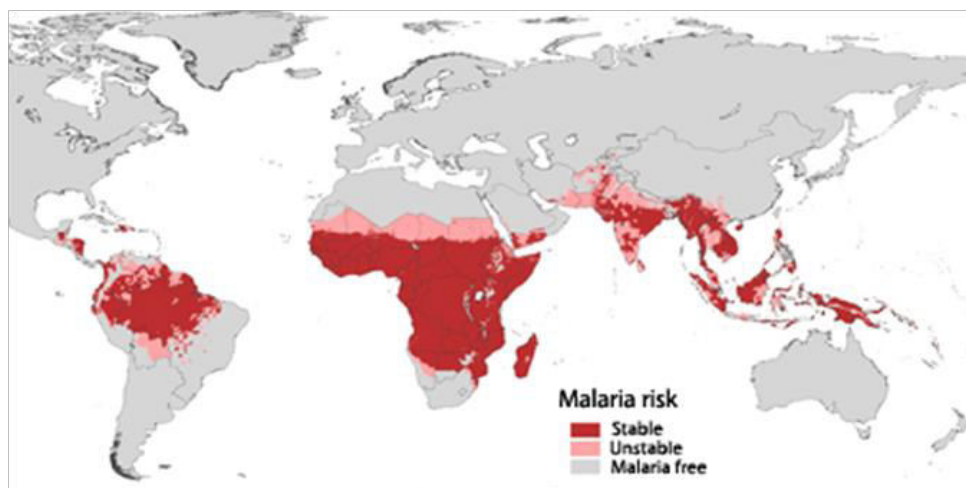


Figure 1.1. Worldwide distribution of *Plasmodium falciparum* malaria categorised by areas of stable transmission (red), unstable transmission (pink) and malaria free (grey)

Reproduced from: The Limits and Intensity of *Plasmodium falciparum* Transmission: Implications for Malaria Control and Elimination Worldwide, R. Snow *et al.*⁵

Sub-Saharan Africa carries the highest burden, with 90% of all malaria deaths occurring in these financially vulnerable countries.⁶ The issue is further complicated by cases of HIV and incidences of war and famine.⁷ Despite malaria being entirely preventable and curable, it remains one of the leading causes of death in children aged under-5 in Africa.⁸

In many areas of sub-Saharan Africa the levels of malaria are stable; transmission occurs throughout the year and there is little variation from one year to the next. As a result, most people will have been exposed to the disease many times since birth, and this instils a degree of immunity in the adult population towards the most severe outcomes of malaria.⁹ However, the risk of serious clinical manifestations in children and pregnant women is high. The lack of naturally acquired immunity in children leads to severe and often life-threatening infections; in fact one in five childhood deaths in sub-Saharan Africa are caused by malaria.¹⁰ Pregnancy leads to a lowering of the immune system and, as a result, pregnant women are four times more likely to contract the disease and suffer from twice as many fatalities in comparison to the general adult population. Contracting the disease whilst pregnant can also lead to premature delivery and low-birth-weight babies.^{11,12}

In areas of unstable malaria transmission such as Southeast Asia and South America, the occurrence of infection is more sporadic and transmission varies throughout the year. There is no opportunity for protective immunity to develop, and therefore the whole population is equally vulnerable.¹³

Malaria imposes significant costs on both individuals and governments. The disease has a huge financial impact on developing countries and, as a result, significantly hinders economic growth; it is therefore both a cause and consequence of poverty.¹⁴ The correlation between malaria and poverty is compelling and the gap in prosperity between countries with and without malaria continues to grow.¹⁵

1.1 The symptoms of malaria

The symptoms of malaria usually present themselves around 10-15 days after being bitten and can become life threatening if left untreated. The disease can be characterised as either uncomplicated or severe, depending on the nature and severity of the symptoms.¹⁶

Typical symptoms of uncomplicated malaria include a fever, chills, nausea, vomiting, diarrhoea, headaches, and general malaise.¹⁷ In fact, the symptoms of this disease are often mistaken for flu, which can lead to a delay in diagnosis and increase the risk of severe complications.¹⁸

Manifestations of severe malaria include seizures, neurological problems, severe anaemia, pulmonary oedema, haemoglobinuria, cardiovascular collapse, and shock.¹⁹ Early detection and prompt treatment are therefore crucial in curing this deadly disease and preventing long-term effects.^{20,21}

One of the biggest issues facing both the treatment and eradication of malaria is the increasing emergence of resistance to the most commonly used front-line drug therapies. Therefore there is an urgent need for the development of novel drug compounds targeting malaria.^{22,23}

1.2 The Parasite

Malaria is caused by protozoan parasites of the genus *Plasmodium*. Over 200 species of this parasite have been identified and there are 4 distinct species that are known to infect humans: *Plasmodium falciparum*, *Plasmodium ovale*, *Plasmodium malariae* and *Plasmodium vivax*.

P. falciparum is responsible for the most severe strain of malaria and has the highest complication and mortality rates of all four species.²⁴ It is estimated that *P. falciparum* is not only responsible for 50% of all malaria infections worldwide but for 75% of infections and 90% of the deaths that occur in sub-Saharan Africa.²⁵ *P. falciparum* malaria can develop within eight days of being bitten and can rapidly become more severe with complications such as dehydration, shock, respiratory problems, and liver and/or kidney failure. Anaemia is also common as the parasite feeds off host haemoglobin and leaves the host weak and drowsy.²⁶ In particularly severe cases, cerebral malaria may develop as a result of erythrocytes containing the mature forms of the parasite adhering to the vascular endothelium.²⁷ This leads to sequestration and obstruction of small vessels and can result in a reduced blood flow to the brain. A reduced blood, and therefore oxygen, flow can cause the brain to swell leading to seizures, comas and even brain damage.²⁸

P. vivax is found in more temperate regions and is responsible for the majority of malaria cases outside of Africa, as the parasite can survive at lower temperatures than *P. falciparum*.²⁹ Although it is rarely fatal the symptoms of *vivax* malaria can be very debilitating and relapses are common as the hypnozoite stage of the parasite can remain dormant within the liver for anywhere between several months and four years after contracting the disease.³⁰ This allows the parasite to hide and wait for the optimal transmission time. Tropical strains of *P. vivax* are associated with multiple relapses with short time intervals between; however, much longer time intervals are observed between relapses in temperate regions.³¹ Repeated attacks throughout childhood and adult life can be severely

detrimental to the well-being, development and economic performance of an individual.³²

P. ovale was discovered and named by J. W. W. Stephens in 1922 and was characterised by a tertian fever and the oval shape of infected erythrocytes in patients.³³ This species is found in sub-Saharan Africa and islands in the western Pacific.³⁴ Symptoms appear around 12 to 20 days post-exposure and include bouts of fever, chills, nausea, diarrhoea, and oedema. Relapse is common after treatment and can occur up to four years after initial infection as a result of hypnozoites that remain dormant in the liver.³⁵

P. malariae is wide-spread throughout sub-Saharan Africa, southeast Asia, Indonesia, and on many of the islands of the western Pacific.³⁶ This species is the least prevalent of the four and the clinical manifestations are much milder. Although the symptoms of this strain are not as severe as *P. falciparum* and *P. vivax*, it can remain active in the host for extended periods of time, leading to chronic infection. The parasite load in the blood of infected patients is lower than that of the other malaria species due to its longer developmental life cycle in the host. This allows for the host to develop immunity at an earlier stage and reduces the severity of symptoms.³⁷ The symptoms include a fever, which appears at characteristic three-day intervals, and general flu-like symptoms. Although the morbidity rate is low for this particular species, it can still contribute to deaths through incidences of anaemia and reduced resistance to other infections.

In recent years, cases due to a fifth species have been recorded in humans - *P. knowlesi*; a species that infects long-tailed and pig-tailed macaques in Southeast Asia. However, the method of transmission is thought to be zoonotic rather than from person to person (via a mosquito vector) and incidences of infection have been low and sporadic.³⁸

1.2.1 Parasite life cycle

The parasite life cycle involves two stages: the sexual stage, which takes part inside a mosquito vector, and the asexual stage, which takes part inside a human host (see Figure 1.2). When an infected mosquito takes a blood meal from a host it injects a small amount of saliva that contains immature forms of the parasite known as sporozoites.³⁹ At the same time, a secretion containing an anti-coagulant and local anaesthetic are administered in order to prevent the host from realising they have been bitten.⁴⁰ The immature sporozoites enter the bloodstream and travel to the liver where they enter the host's hepatocytes. These sporozoites remain in the liver for up to one week, where they begin multiplying asexually to form thousands of merozoites. Some sporozoites may develop into hypnozoites (*P. vivax* and *P. ovale*), which can remain dormant for extended periods of time before being activated.⁴¹ The merozoites formed are expelled from the liver and go on to invade circulating erythrocytes. Whilst inside the red blood cell the parasite will break down host haemoglobin in order to obtain amino acids required for development and to provide the extra space required for growth.⁴² At the same time the parasite enters the schizont stage by rapidly replicating its DNA.⁴³ Mature merozoites can rupture erythrocytes in order to be released back into the bloodstream so that they may go on to infect more cells. Antigens and toxic metabolites are released from infected erythrocytes upon rupturing, and this causes the high temperature associated with a malarial infection.⁴⁴ Although most merozoites will continue the replicative cycle, some will differentiate into gametocytes. These gametocytes will circulate for up to 7 days, ready to be taken up by a female mosquito. The change in environment from a warm-blooded host to the gut of a mosquito vector stimulates the development of gametocytes into gametes.⁴⁵ Fertilisation between male and female gametes forms diploid zygotes, which will undergo the processes of meiosis and differentiation to form motile ookinetes. Ookinetes escape the gut and further differentiate into oocysts, which divide many times to produce large numbers of sporozoites. These sporozoites migrate to the salivary gland of the mosquito, ready to be injected next time a blood meal is taken, thus completing the life cycle.^{46,47,48}

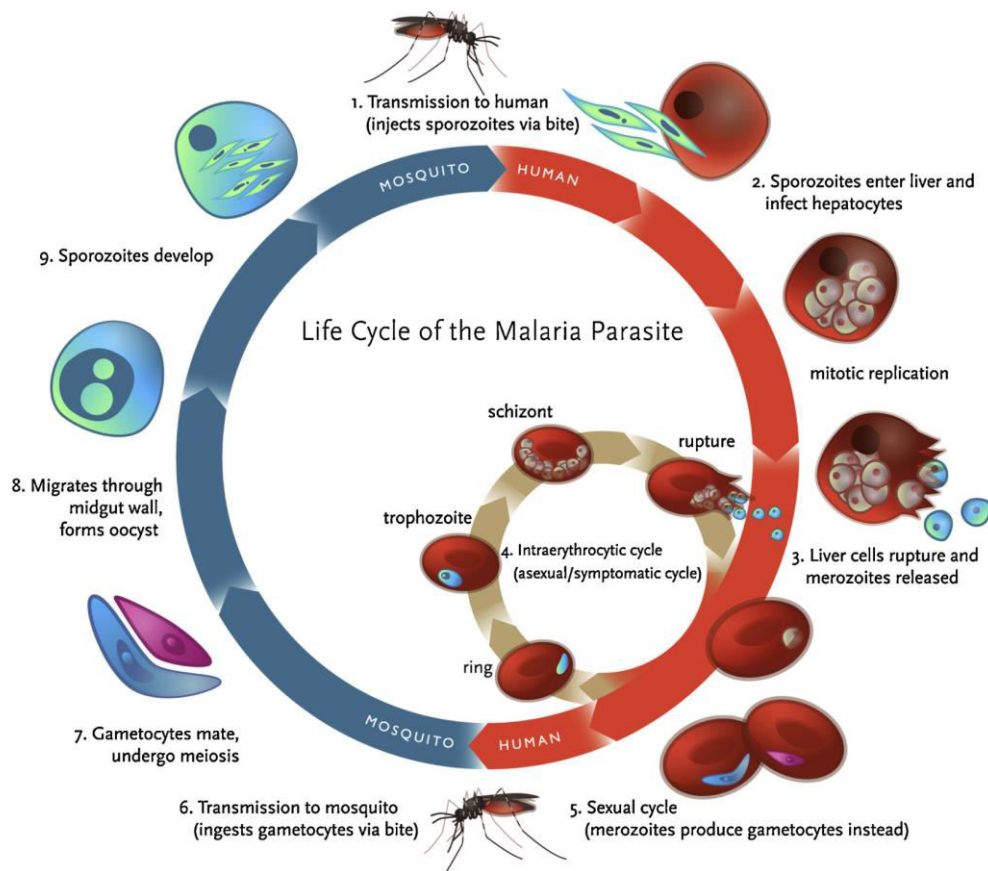


Figure 1.2. Life cycle of the malaria parasite
 Figure reproduced from: Antimalarial drug resistance: a review of the biology and strategies to delay emergence and spread, E.Y. Klein ⁴⁹

1.2.2 Haemoglobin degradation

Haemoglobin is an important nutrient source for the intraerythrocytic stages of the parasite life cycle and its catabolism takes place within an acidic digestive vacuole.⁵⁰ Due to the parasite's limited capability for de-novo synthesis of amino acids, the host's haemoglobin is used as the source for those it requires for growth and development.⁵¹

As the parasite develops within an erythrocyte, the host cell's cytoplasm is taken-up through the endolysosomal system; the cytoplasm is ingested by the cytosome and packaged into double-membrane vesicles, which translocate to the

digestive vacuole.⁵² The contents of the vesicle are released into the digestive vacuole and haemoglobin degradation is initiated by aspartic haemoglobinase I (see Figure 1.3).⁵³ A second enzyme, plasmepsin II, cleaves the resulting acid denatured product resulting in the formation of ferriprotoporphyrin IX (FPIX), or free heme, and globin.⁵⁴ Cysteine protease enzymes cleave globin into smaller peptides that are exported back out into the cytoplasm where they are hydrolysed into amino acids used for parasite growth. However, FPIX is toxic to the parasite and it can cause lethal disruptions to membranes and proteins. It is therefore sequestered into a non-toxic, crystalline substance known as hemazoin.⁵⁵

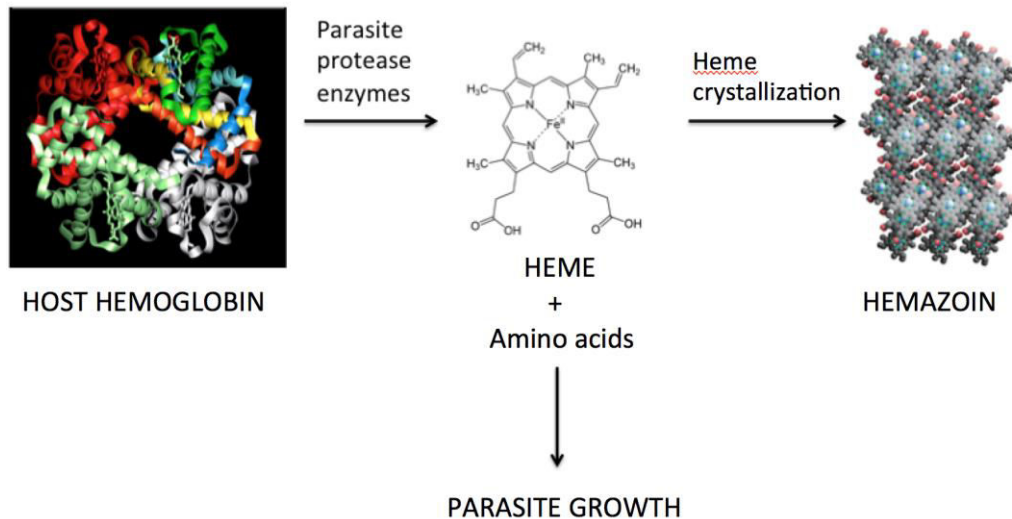


Figure 1.3. Haemoglobin degradation and heme crystallization pathway: Host haemoglobin is broken down to amino acids for parasite growth and resulting free heme is converted to non-toxic, crystalline hemazoin

Figure adapted from: Malaria: Drugs, Disease and Post-genomic Biology ⁵⁴

1.3 The Mosquito Vector

Of around 430 species of *Anopheles* mosquitoes, approximately 30 are of importance as vectors of the malaria parasite. The first three stages of the development of anophelines are aquatic and last 5-14 days depending on the climate. Eggs are laid directly on water and larvae hatch within a few days; the larvae then feed on algae, bacteria and other microorganisms before metamorphosing into pupae.⁵⁶ Once the adult mosquito emerges it will mate within a few days and can live for up to one month. Females feed on nectar and other sources of sugar like males, but pregnant females also require a blood meal for the development of their eggs. Once a blood meal has been taken, the female will rest for a few days before laying her eggs and continuing the cycle.⁵⁷

1.3.1 Vector control

A number of strategies can be implemented for vector control and these have been developed as a result of the biology and behavior of the *Anopheles* mosquito. Long lasting insecticidal nets and indoor residual spraying have proven to be the two most important and effective methods of vector control in endemic areas.⁵⁸ The use of insecticidal nets has reduced the mortality rate by an estimated 55% in children under the age of five in sub-Saharan Africa, not only through a reduction in malaria deaths but also through the reduction of deaths from other causes that can be exacerbated by malaria.⁵⁹ Indoor residual spraying involves spraying the indoor walls and ceilings of homes and is effective if implemented with high-level coverage. Both of these methods are successful in controlling species with a preference to feed and/or rest indoors.⁶⁰

For those that feed and/or rest outside, source management is the best control method. This involves targeting the larval stages of the mosquito and can be instigated either through the destruction of breeding sites or the application of insecticides to larval habitats.⁶¹ The main issue with larval source management is that their habitats may be small, widely dispersed and transient. Therefore

source management is a useful tool for supplementing other methods, but alone can be ineffective.⁶²

1.4 Past and Present Drug Therapies

Although there are a number of preventative steps that can be taken in order to decrease the risk of contracting malaria, such as mosquito repellents and insecticide-treated mosquito nets, the burden of prevention and control of the disease still lies heavily on the drug treatments available.⁶³

Each parasite species presents its own unique challenges for treatment and eradication. In order for treatments to be effective, a prompt and precise diagnosis is necessary. *P. falciparum* for example must be diagnosed quickly and differentiated from other strains in order to minimize serious complications.⁶⁴ Traditional diagnostic techniques involve analysis of a blood smear, usually stained with Giemsa, under a microscope. However, microscopy methods can be unreliable and inconsistent and rely heavily on the quality of reagents, of the microscope and the experience of the technician. Diagnostic tools are constantly improving and methods such as Polymerase Chain Reaction are able to accurately differentiate between all four species and detect parasites down to very low levels.⁶⁵

There are three key aspects to consider from both a treatment and eradication perspective. The first is the liver stage of the parasite's life cycle. Both *P. vivax* and *P. ovale* form hypnozoites whilst inside hepatocytes. These inactive forms can lay dormant for long periods of time and relapses of infection will occur unless they are completely eradicated.⁴¹ The second factor to consider is the time it takes for gametocytes to appear in the blood stream. For *P. vivax* it is soon after infection, whereas it may be several days after the initial fever occurs for *P. falciparum*.⁶⁶ An effective treatment against *P. vivax* therefore must not only prevent the development of the parasite in the intraerythrocytic stages of development, but also kill existing gametocytes in circulation. Finally the

replication time in the host varies between species: *P. falciparum*, *P. vivax* and *P. ovale* all cause tertian fevers due to lysis of red blood cells after each replication cycle, which takes roughly 48 hours.⁶⁷ The symptoms of *P. malariae* are much milder as a result of slower replication. *P. knowlesi* however replicates much more rapidly and it is therefore of the utmost importance to treat this strain at the onset of symptoms.⁶⁸

1.4.1 Quinoline antimalarials

One of the first widely used antimalarials was quinine (Figure 1.4), a natural product extracted from the bark of the *Cinchona calisaya* tree.⁶⁹ The structure of this compound was elucidated in 1908 and it was predicted that the quinoline core was key to the antimalarial activity of this compound.⁷⁰

Modifications of the quinoline core led to the discovery of chloroquine (see Figure 1.4), which proved to be one of the most important antimalarial drugs of the 20th century.⁷¹ Chloroquine proved to be highly effective and well tolerated, and quickly established itself as the drug of choice for the treatment of uncomplicated malaria and chemoprophylaxis. This 4-aminoquinoline compound was found to be a potent blood schizonticide, which was effective against the intraerythrocytic stages of all parasite strains. Due to its weakly basic nature, chloroquine rapidly accumulates within the acidic food vacuole of the parasite and is thought to exert its mechanism of action through inhibition of heme polymerisation.⁷² This allows for levels of free heme to accumulate, which is a toxic and reactive metabolite, and inhibition of the crucial detoxification process proves lethal to the parasite.⁷³

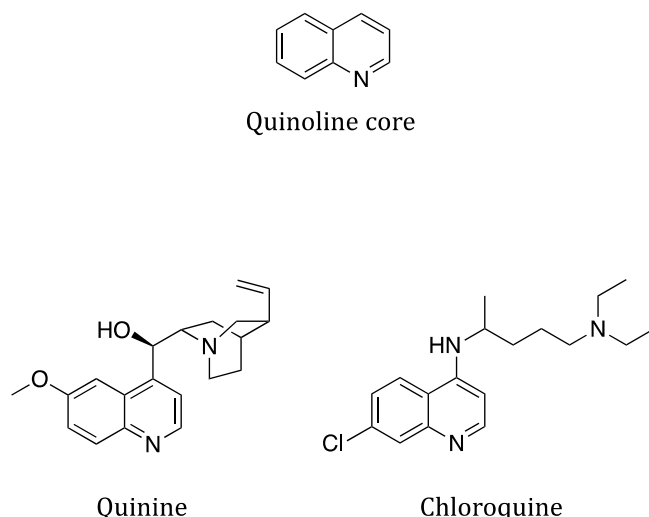


Figure 1.4. The structures of two key antimalarials derived from a quinoline core:
Quinine and chloroquine

Chloroquine resistance has developed as a result of mutations to the chloroquine resistance transporter (*PfCRT*), an integral membrane protein located on the membrane of the food vacuole.⁷⁴ Mutations in this transporter result in an increased ability for chloroquine to escape from the food vacuole, preventing levels from accumulating high enough to inhibit heme polymerisation. In fact, chloroquine efflux is found to be 40 to 50 times faster in resistant strains compared to sensitive strains.⁷⁵ This mechanism of resistance has been validated through the use of drugs that inhibit chloroquine efflux; when used in combination with such compounds the effects of chloroquine resistance are reversed. One such compound is the antibiotic azithromycin (Figure 1.5), a slow acting macrolide that targets the 70S ribosomal subunit of the apical complex.⁷⁶ Azithromycin has insufficient efficacy to be used as a single agent, however when used in a combination therapy with chloroquine a synergistic effect is observed, even against chloroquine resistant strains of *P. falciparum*.⁷⁷ This highlights the potential of such combinations to be developed as prophylactic agents. The development of resistance to chloroquine had a huge impact on world health and therefore placed an urgent need on the discovery of novel antimalarials to replace it.⁷⁸

with neuropsychiatric reactions and links to depression and other mental health problems.⁸⁴

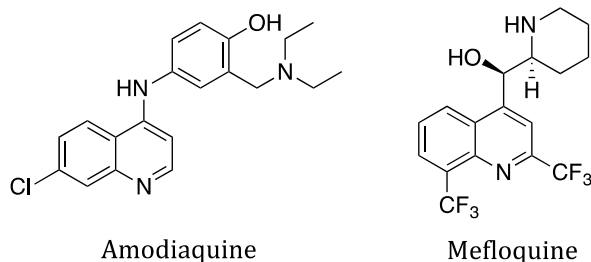


Figure 1.6. The 4-aminoquinoline, amodiaquine, and the quinoline methanol, mefloquine, developed to target chloroquine resistant strains of *P. falciparum*

Primaquine (Figure 1.7) is an 8-aminoquinoline and the only drug approved to eliminate hypnozoites in the treatment of *P. vivax* and *P. ovale* malaria.⁸⁵ It is also the only compound known to be active against mature gametocytes of *P. falciparum*. Battles in the Pacific during World War II resulted in an urgent need for a drug that could prevent the relapse of malaria.⁸⁶ Studies focused on 8-aminoquinolines as another known compound in this class, pamaquine, proved highly effective at eliminating hypnozoites but was too toxic for use. Thousands of compounds were screened for their activity and primaquine came top; however, its mechanism of action is poorly understood. This drug could generate reactive oxygen species or potentially interfere with the electron transport chain in the parasite. This compound should be avoided in patients with a glucose-6-phosphate dehydrogenase deficiency, as potentially life-threatening hemolysis can occur; therefore, screening should be carried out before administering primaquine.⁸⁷ Primaquine is currently administered in combination with a blood schizonticide to effectively eliminate all stages of the parasite.⁸⁸

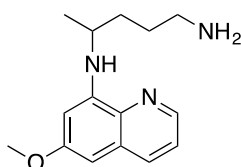


Figure 1.7. The structure of primaquine; the only drug approved to eliminate the hypnozoite stages of *P. vivax* and *P. ovale* infection

1.4.2 Antifolate compounds

Antifolate agents used to treat malaria can be subdivided into two different classes: inhibitors of dihydropteroate synthase (DHPS), class I inhibitors, and inhibitors of dihydrofolate reductase (DHFR), class II inhibitors.

DHPS is found exclusively in the parasite and is responsible for the *de novo* synthesis of essential folate co-enzymes. As humans do not synthesise folate *de novo*, DHPS provides a selective target for antimalarial drug development.⁸⁹ DHFR is found in both the parasite and humans. This enzyme helps to maintain a constant supply of reduced folate, which is essential for a whole host of one-carbon transfer reactions, including the synthesis of nucleotides required for DNA synthesis.⁹⁰ Selectivity for parasite DHFR is therefore essential in order to prevent the occurrence of adverse side effects.⁹¹

1.4.2.1 DHPS inhibitors

A number of sulfonamide and sulfone containing compounds, including sulfadoxine and dapson (Figure 1.8), were found to inhibit DHPS in malaria parasites by competing with the natural substrate, *p*-aminobenzoic acid.⁹²

Dapsone is the most potent inhibitor of DHPS to date and was synthesised in 1908 in the search for molecules to produce azodyes. It wasn't until many years later that its antimalarial properties were discovered. This compound is also active against mycobacteria and has been used in the treatment of leprosy.⁹³

Dapsone was used in combination with chlorproguanil (sold commercially as Lapdap™) to treat uncomplicated malaria; however, it was withdrawn in 2008 due to toxicity issues observed in Phase III trials.⁹⁴

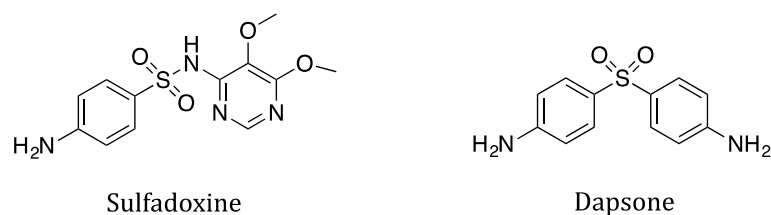


Figure 1.8. DHPS inhibitors: Sulfadoxine and dapsone

DHPS inhibitors interrupt the *de novo* synthesis of folate but the parasite is able to overcome the effects of this by obtaining the folate it needs from exogenous sources in the host. As a result, many of the compounds developed to inhibit this enzyme, including sulfadoxine, have insufficient potency when used as single agents.⁹⁵ However, it was found that these inhibitors have a more potent and synergistic effect when used in combination with DHFR inhibitors.⁹⁶

1.4.2.2 DHFR inhibitors

Proguanil (Figure 1.9) was the first reported antifolate antimalarial and was developed by Imperial Chemical Industries during World War II. It is a pro-drug and is metabolised within the body to the active agent, cycloguanil.⁹⁷ Proguanil is used as a prophylactic agent in the prevention of malaria in combination with atovaquone (see 1.4.3). This combination, known as Malarone®, is the only other therapy, aside from primaquine, that is approved and effective in clearing parasites from the liver. Chlorproguanil (Figure 1.9) is the chlorinated analogue of proguanil, which was used in the combination therapy, Lapdap™. Chlorproguanil is also a pro-drug and undergoes metabolism *in vivo* to produce the active metabolite, chlorcycloguanil.⁹⁸

The most widely used antimalarial of this class is pyrimethamine (Figure 1.9), which is a derivative of 2,4-diaminopyrimidine. It has been used in numerous combination therapies with DHPS inhibitors, including sulfadoxine, which have potent activity against *P. falciparum*.⁹⁹

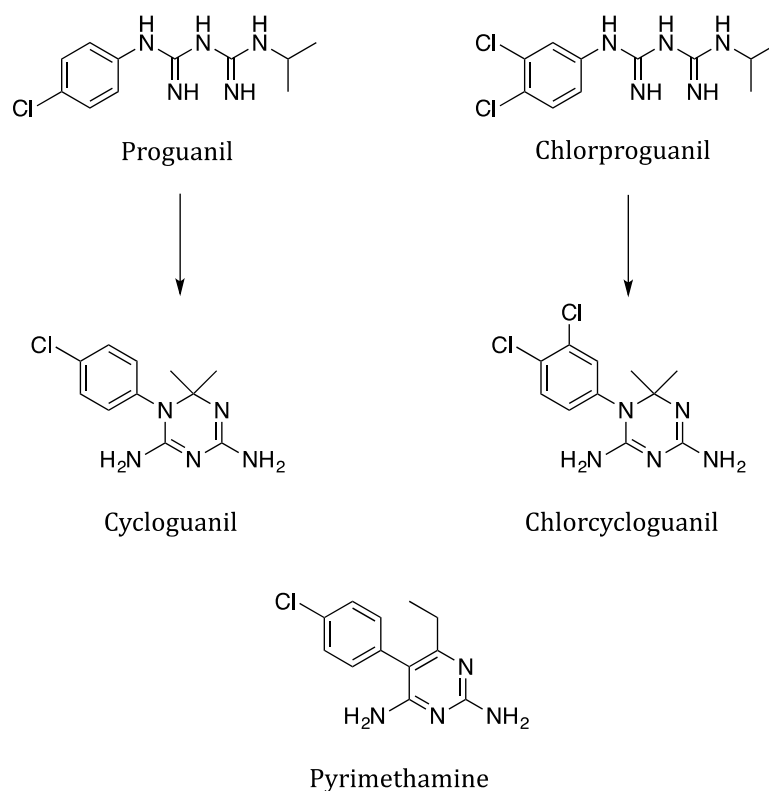


Figure 1.9. Structures of key DHFR inhibitors

These compounds are an important class of antimalarial agents, as they are capable of arresting DNA replication in the parasite; however, resistance is now widespread due to mutations readily occurring in the DHFR enzyme.^{100,91} DHFR inhibitors prevent tetrahydrofolate synthesis by competing for the active site of the enzyme with the natural substrate dihydrofolate. Many of the compounds developed to inhibit DHFR bind rigidly within the active site, and lack the torsional freedom and flexibility observed with dihydrofolate binding. Single point mutations within the active site can therefore have a big impact on drug accommodation without affecting the binding of the natural substrate.^{101,102}

One of the most common mutations known to cause resistance to pyrimethamine is S108N. The NH₂ moiety of asparagine 108 interferes with the chlorine atom of pyrimethamine, resulting in the drug being displaced from the active site. The same effect is also observed for cycloguanil and chlorproguanil.¹⁰³

Future inhibitors of DHFR could therefore be designed with greater flexibility, as seen in the natural substrate. Therefore, single-point mutations developed to

disrupt inhibitor binding may also disrupt dihydrofolate binding significantly enough to be detrimental to parasite survival.^{104,105}

1.4.3 Atovaquone

Atovaquone (Figure 1.10) is an orally bioavailable, metabolically stable hydroxynaphthoquinone that is derived from lapachol, a natural product isolated from the bark of the *Handroanthus impetiginosus* tree.¹⁰⁶ This compound exhibits its antimalarial action through irreversibly binding to the mitochondrial cytochrome *bc₁* complex and inhibiting the natural substrate, ubiquinone. Blocking the electron transport chain ultimately inhibits *de novo* pyrimidine synthesis, leading to parasite death.^{107,108}

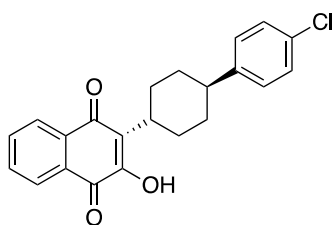


Figure 1.10. Structure of atovaquone

Resistance to atovaquone develops rapidly when used alone, due to single point mutations occurring in the cytochrome *b* gene. A single mutation in the active site, Y268S, causes resistance by reducing hydrophobic interactions between atovaquone and cytochrome *bc₁*.¹⁰⁹ The important contact between histidine 181 of the iron-sulfur protein chain and the hydroxyl group of atovaquone is also lost as a result of the Y268S mutation.¹¹⁰ Atovaquone is therefore forced to bind at an alternative binding site, away from the substrate binding pocket, leading to significantly reduced efficacy.¹¹¹

However, when atovaquone is combined with a second drug, resistance develops much more slowly. In fact the combination of atovaquone with proguanil (Malarone™) is the current therapy of choice for antimalarial prophylaxis for travellers.¹¹²

1.4.4 Artemisinin and semi-synthetic derivatives

In 2015, the Nobel Prize in Physiology or Medicine was divided, one half jointly to William C. Campbell and Satoshi Ōmura "for their discoveries concerning a novel therapy against infections caused by roundworm parasites" and the other half to Youyou Tu "for her discoveries concerning a novel therapy against Malaria".¹¹³ Youyou Tu was part of a secret drug discovery programme during the Vietnam War known as "Project 523", which was tasked with finding an alternative therapy to treat malaria due to the increasing emergence of chloroquine resistance in soldiers along the Ho Chi Minh trail. Tu and her team screened thousands of traditional Chinese remedies and discovered that sweet wormwood, which had been used for centuries to treat febrile illnesses, had promising antimalarial properties. A lengthy extraction process led to the isolation of artemisinin (Figure 1.11), the active component of the herb.¹¹⁴

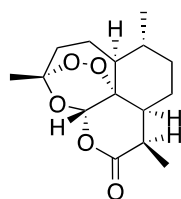


Figure 1.11. The chemical structure of artemisinin, the active antimalarial component of sweet wormwood or *Artemisia annua*

Artemisinin proved 100% effective when tested against parasitemia in both *P. berghei*-infected mice and *P. cynomolgi*-infected monkeys. During this time of the Cultural Revolution in China there were no facilities for conducting trials of new drugs, therefore Tu and her team acted as the first group of volunteers to be administered with the drug, in order to determine whether artemisinin could be used safely in humans.¹¹⁵

Fast-forward to today, and we now know artemisinin to be a powerful, well-tolerated antimalarial agent, which is effective against the most severe, and chloroquine resistant, strains of malaria. This sesquiterpene lactone contains a 1,2,4-trioxane moiety, and this feature is the basis for its unique mechanism of

action.¹¹⁶ Despite displaying very rapid parasite clearance times and fast fever resolution, its therapeutic value is greatly limited by its poor solubility in both oil and water. This results in poor and erratic absorption upon oral administration, and usually translates to poor bioavailability.¹¹⁷ The drug also undergoes extensive first pass metabolism, producing inactive metabolites such as deoxyartemisinin and dihydroxydeoxyartemisinin. As Figure 1.12 shows, both metabolites have lost the 1,2,4-trioxane moiety, which is the key for the antimalarial activity of artemisinin. These factors therefore triggered a search for a series of semi-synthetic analogues with improved pharmacological profiles.¹¹⁸

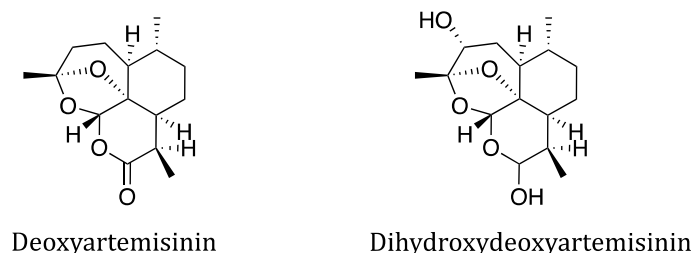
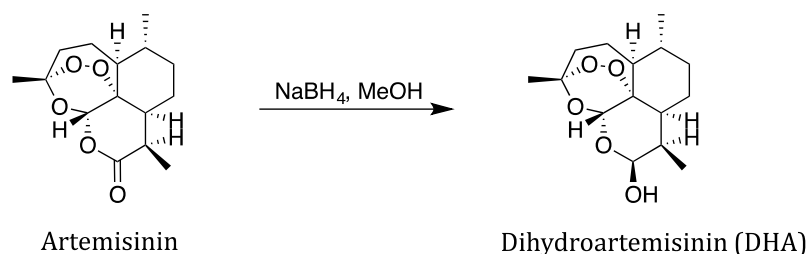


Figure 1.12. Structures of the inactive metabolites of artemisinin

The most easily accessible moiety of artemisinin is the lactone group; therefore this was the main focus for the first generation of semi-synthetic derivatives. Reduction of the lactone to a lactol, using sodium borohydride produces dihydroartemisinin (DHA – Scheme 1.1). These conditions are unusually mild, as lactone reductions usually require harsher reducing agents such as lithium aluminium hydride. The peroxy group survives sodium borohydride reduction however the use of stronger agents leads to degradation of the trioxane.¹¹⁹

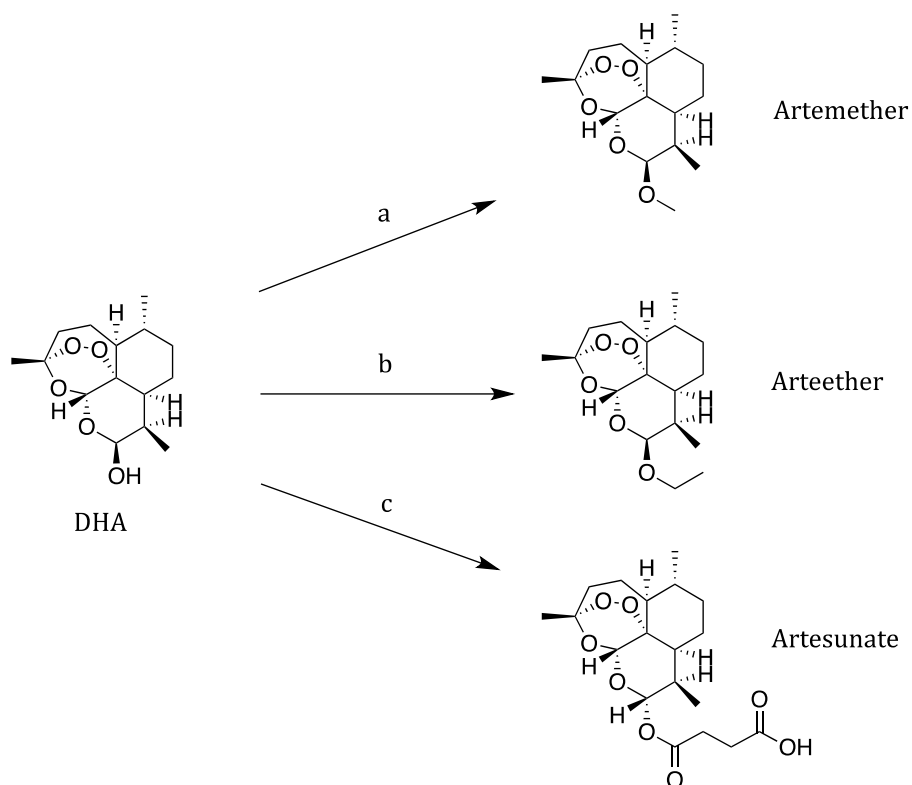


Scheme 1.1. The conversion of artemisinin to dihydroartemisinin

DHA proved to be a more potent blood schizonticide but a loss of stability was observed *in vivo*; therefore, the hydroxyl group was used as a handle for the introduction of a number of different groups to improve both stability and solubility.¹²⁰

Artemether and arteether are both produced from DHA as shown in Scheme 1.2.¹²¹ The advantage of these compounds is their improved solubility in oil, allowing for formulation and administration as an intramuscular injection. *In vivo* these compounds undergo rapid metabolism to the more potent DHA. However, for cases of severe and complicated malaria, a more rapid systemic availability is required that intramuscular preparations cannot meet. As a result, a water-soluble drug for intravenous injection was sought after. This led to the development of artesunate, the succinate ester of DHA, formed by esterification of DHA using succinic anhydride (Scheme 1.2).¹²² Artesunate has improved solubility and pharmacokinetic profiles compared to the ether analogues and can be formulated in a number of ways; including tablets for oral administration or as the sodium salt for IV administration.¹²³

Both artmetheter and artesunate are now commonly used in artemisinin-based combination therapies.¹²⁴



Scheme 1.2. Synthesis of semi-synthetic artemisinin analogues from dihydroartemisinin **a**) i) trimethyl orthoformate (5 eq), methanol, rt, 15 mins ii) acetyl chloride, 10-15°C, 3 hrs.¹²⁵ **b**) BF₃.Et₂O, benzene/ethanol (3:1), reflux, 1 hr.¹²¹ **c**) succinic anhydride, triethylamine, THF, rt, 1 hr.¹²⁶

Artemisinin based compounds have a distinct pharmacodynamic advantage over other antimalarial drugs as they accelerate parasite clearance by eliminating the young, ring-stage parasites, which circulate in the bloodstream.¹²⁷ This prevents further maturation and sequestration of these parasites, leading to the rapid therapeutic response observed and the high success rates in treatment of severe malaria.¹²⁸

1.4.5 Artemisinin-based combination therapies

Despite the semi-synthetic analogues of artemisinin having potent activities and improved pharmacological profiles, parasite recrudescence following artemisinin-based monotherapies is high. This could be a consequence of the short half-lives of these compounds, or a result of the parasite entering a period of dormancy to

protect itself in the presence of the drug, before recovering at a later date to resume growth.¹²⁹

As a result, artemisinin-based combination therapies (ACTs) are now recommended for the treatment of uncomplicated *P. falciparum* infection. These therapies combine artemisinin-based compounds with another drug that has a longer duration of action and an alternative mechanism of action. This creates a highly efficient, fast acting antimalarial agent with a reduced likelihood of resistance developing.¹³⁰

If two drugs are administered in combination, simultaneous mutations in two genes are required to encode resistance, providing both drugs elicit different mechanisms of action. Therefore the chance of being spontaneously resistant to both drugs is extremely low compared to one drug used in monotherapy. Combination therapies therefore not only increase efficacy but also delay the input of mutations encoding for resistance.^{131,132}

Artemether/lumefantrine (Coartem) was the first fixed-dose ACT recommended by WHO for the treatment of uncomplicated *P. falciparum* infection in sub-Saharan Africa and it has also proved effective against multi drug resistant strains of *P. falciparum* in Southeast Asia.¹³³ ACTs are crucial for curtailing the spread of resistance; therefore they must be both affordable and accessible to everyone.

1.5 Resistance

The development of resistance to the most commonly used drug therapies against malaria can have a devastating impact on efforts to control and eradicate the disease.¹³⁴ The development of chloroquine resistance had a huge impact on public health and the increasing emergence of resistance to artemisinin-based compounds could prove catastrophic if full-blown resistance were to appear in Africa.¹³⁵ There is an ever-urgent need for the development of new drug compounds but how can resistance be controlled and why does it occur in the first place?

There are a number of reasons why resistance can, and has occurred, to many commonly used antimalarial drugs. These include:

- Unregulated and poorly administered drug use
- Vector and parasite biology
- Substandard or counterfeit forms of a drug
- Use of antimalarial monotherapies
- Pharmacokinetics
- Poor patient compliance

Antimalarial drug use cannot be strictly regulated in all countries, and individuals in some countries will even self-administer as a result of being exposed to the virus many times. Without proper screening it is difficult to choose the correct treatment and many countries have limited access to these services. The availability of sub-standard and counterfeit drugs is also high in developing nations and their low prices make them attractive options for people suffering with financial problems.¹³⁶ Drug pharmacokinetics can also result in the emergence of resistance; a long half-life for example can lead to sub therapeutic drug concentrations, which can select for drug tolerant parasites.^{137,138}

Patient compliance can be enhanced by convenient dosing regimens, for example with extended release formulations and sometimes it may also be possible to re-

introduce a drug to an area when resistance towards it has waned. The development of resistance comes at a fitness cost to the parasite and it is therefore detrimental to keep this mutation once the drug is withdrawn from use.¹¹²

The best way in which to contain and curtail the spread of resistance is to adhere strictly to treatment guidelines; however, this is very difficult in areas of high migration across borders and in areas of political and social unrest, where access to medical care may be disrupted.¹³⁹ Governments of endemic countries also need to take targeted regulatory measures to remove artemisinin-based monotherapies along with antimalarials that do not meet international quality standards.

Resistance is less common in artemisinin-based compounds and ACTs are, for now, the best therapies to help delay the emergence of resistance; however, there is an ever urgent need for the development of novel antimalarial drug compounds.¹³²

1.6 Research Aims

The primary aim of this research was to design and synthesise a library of novel antimalarials, with the ultimate goal of identifying a compound suitable for preclinical development. The first part of this thesis will discuss the synthesis of a series of substituted benzisothiazolinone compounds, which were designed to inhibit a new target in antimalarial drug discovery: IspD. The second section will then provide an overview of the optimisation of a group of tetraoxane antimalarials. These are a class of endoperoxide compounds developed from artemisinin, which is one of the most important antimalarial agents to be discovered.

1.6 References

- 1 WHO | Malaria Factsheet,
<http://www.who.int/mediacentre/factsheets/fs094/en/>, (accessed December 2016).
- 2 World Malaria Report 2015,
<http://www.who.int/malaria/publications/world-malaria-report-2015/report/en/>, (accessed December 2016).
- 3 WHO | Water-related Diseases,
http://www.who.int/water_sanitation_health/diseases-risks/diseases/malaria/en/, (accessed December 2016).
- 4 J. M. Crutcher and S. L. Hoffman, in *Medical Microbiology*, ed. S. Baron, University of Texas Medical Branch, Galveston (TX), 4th edn, 1996, ch. 83.
- 5 C. A. Guerra, P. W. Gikandi, A. J. Tatem, A. M. Noor, D. L. Smith, S. I. Hay and R. W. Snow, *PLoS Med.*, 2008, **5**, e38.
- 6 WHO | Fact Sheet: World Malaria Report 2015,
<http://www.who.int/malaria/media/world-malaria-report-2015/en/>, (accessed December 2016)
- 7 J. Sachs and P. Malaney, *Nature*, 2002, **415**, 680–685.
- 8 WHO | Children: reducing mortality,
<http://www.who.int/mediacentre/factsheets/fs178/en/>, (accessed December 2016).
- 9 M. Sylvie, C. Pierre and M. Jean, *Biodiversity of Malaria in the World*, John Libbey Eurotext, 2008.
- 10 K. Artavanis-Tsakonas, J. E. Tongren and E. M. Riley, *Clin. Exp. Immunol.*, 2003, **133**, 145–152.
- 11 L. J. Bruce-Chwatt, *Br. Med. J. (Clin. Res. Ed.)*, 1983, **286**, 1457–1458.
- 12 H. L. Guyatt and R. W. Snow, *Clin. Microbiol. Rev.*, 2004, **17**, 760–769.
- 13 M. Martchera and O. Prosper, *Dynamic Models of Infectious Diseases: Volume 1: Vector-Borne Diseases*, ed. V. S. H. Rao and R. Durvasula, Springer-Verlag, New York, 1st edn, 2013, ch. 2, p. 7.
- 14 WHO, http://www.who.int/malaria/publications/atoz/brochure_rbm.pdf,

- (accessed December 2016).
- 15 CDC - Malaria Worldwide - Impact of Malaria,
https://www.cdc.gov/malaria/malaria_worldwide/impact.html, (accessed December 2016).
 - 16 A. Bartoloni and L. Zammarchi, *Mediterr. J. Hematol. Infect. Dis.*, 2012, **4**,
DOI: 10.4084/MJHID.2012.026
 - 17 NHS - Malaria - Symptoms,
<http://www.nhs.uk/Conditions/Malaria/Pages/Symptoms.aspx>,
(accessed December 2016).
 - 18 M. P. Grobusch and P. G. Kremsner, *Curr. Top. Microbiol. Immunol.*, 2005,
295, 83–104.
 - 19 S. Sarkar, K. Saha and C. S. Das, *Lung India*, 2010, **27**, 154–157.
 - 20 G. Pasvol, *Br. Med. Bull.*, 2005, **75**, 29–47.
 - 21 A. Trampuz, M. Jereb, I. Muzlovic and R. M. Prabhu, *Crit. Care*, 2003, **7**, 315–
323.
 - 22 S. Crunkhorn, *Nat. Rev. Drug Discov.*, 2016, **15**, 232–233.
 - 23 F. W. Muregi, H. N. Wamakima and F. T. Kimani, *Curr. Pharm. Des.*, 2012,
18, 3505–3521.
 - 24 WHO | International travel and health - Malaria,
<http://www.who.int/ith/diseases/malaria/en/>, (accessed December
2016).
 - 25 R. W. Snow and J. A. Omumbo, in *Disease and Mortality in Sub-Saharan
Africa*, ed. D.T. Jamison, R. G. Feacham, M. W. Makgoba, E. R. Bos, F. K.
Baingana, K. J. Hoffman and K. O. Rogo, The International Bank for
Reconstruction and Development/ The World Bank, Washington (DC), 2nd
edition, 2006, ch. 14..
 - 26 K. Haldar and N. Mohandas, *Hematology Am. Soc. Hematol. Educ. Program*,
2009, 87–93.
 - 27 G. van der Wal, W. I. M. Verhagen and A. S. M. Dofferhoff, *Neth. J. Med.*,
2005, **63**, 180–183.
 - 28 A. M. Dondorp, E. Pongponratn and N. J. White, *Acta Trop.*, 2004, **89**, 309–
317.
 - 29 E. Petersen, C. Severini and S. Picot, *Travel Med. Infect. Dis.*, 2013, **11**, 51–

- 59.
- 30 M. Imwong, G. Snounou, S. Pukrittayakamee, N. Tanomsing, J. R. Kim, A. Nandy, J.P. Guthmann, F. Nosten, J. Carlton, S. Looareesuwan, S. Nair, D. Sudimack, N. P. J. Day, T. J. C. Anderson and N. J. White, *J. Infect. Dis.*, 2007, **195**, 927–33.
- 31 N. J. White, *Malar. J.*, 2011, **10**, 297.
- 32 K. Mendis, B. J. Sina, P. Marchesini and R. Carter, *Am. J. Trop. Med. Hyg.*, 2001, **64**, 97–106.
- 33 W. E. Collins and G. M. Jeffery, *Clin. Microbiol. Rev.*, 2005, **18**, 570–581.
- 34 F. B. K. Faye, L. Konaté, C. Rogier and J.F. Trape, *Trans. R. Soc. Trop. Med. Hyg.*, 1998, **92**, 522–525.
- 35 CDC - Treatment of Malaria: Guidelines for Clinicians, https://www.cdc.gov/malaria/diagnosis_treatment/clinicians2.html, (accessed December 2016).
- 36 W. E. Collins and G. M. Jeffery, *Clin. Microbiol. Rev.*, 2007, **20**, 579–592.
- 37 M. C. Bruce, A. Macheso, M. R. Galinski and J. W. Barnwell, *Parasitology*, 2007, **134**, 637–650.
- 38 N. J. White, *Clin. Infect. Dis.*, 2008, **46**, 172–173.
- 39 A.-K. Mueller, F. Kohlhepp, C. Hammerschmidt and K. Michel, *Int. J. Parasitol.*, 2010, **40**, 1229–1235.
- 40 E. Calvo, D. M. Mizurini, A. Sá-Nunes, J. M. C. Ribeiro, J. F. Andersen, B. J. Mans, R. Q. Monteiro, M. Kotsyfakis and I. M. B. Francischetti, *J. Biol. Chem.*, 2011, **286**, 27998–28010.
- 41 L. Hulden and L. Hulden, *Malar. J.*, 2011, **10**, 1–6.
- 42 D. E. Goldberg, A. F. Slater, A. Cerami and G. B. Henderson, *Proc. Natl. Acad. Sci. U. S. A.*, 1990, **87**, 2931–2935.
- 43 N. Gerald, B. Mahajan and S. Kumar, *Eukaryot. Cell*, 2011, **10**, 474–482.
- 44 Q. Chen, M. Schlichtherle and M. Wahlgren, *Clin. Microbiol. Rev.*, 2000, **13**, 439–450.
- 45 T. J. Templeton, D. B. Keister, O. Muratova, J. L. Procter and D. C. Kaslow, *J. Exp. Med.*, 1998, **187**, 1599–1609.
- 46 V. Soulard, H. Bosson-Vanga, A. Lorthiois, C. Roucher, J.-F. Franetich, G. Zanghi, M. Bordessoulles, M. Tefit, M. Thellier, S. Morosan, G. Le Naour, F.

- Capron, H. Suemizu, G. Snounou, A. Moreno-Sabater and D. Mazier, *Nat. Commun.*, 2015, **6**, 7690.
- 47 T. Bousema, L. Okell, I. Felger and C. Drakeley, *Nat. Rev. Microbiol.*, 2014, **12**, 833–840.
- 48 G. A. Josling and M. Llinás, *Nat. Rev. Microbiol.*, 2015, **13**, 573–587.
- 49 E. Y. Klein, *Int. J. Antimicrob. Agents*, 2013, **41**, 311–317.
- 50 N. Klonis, O. Tan, K. Jackson, D. Goldberg, M. Klemba and L. Tilley, *Biochem. J.*, 2007, **407**, 343–354.
- 51 M. L. Ginger, *Philos. Trans. R. Soc. B Biol. Sci.*, 2006, **361**, 101–118.
- 52 S. Tomavo, C. Slomianny, M. Meissner and V. B. Carruthers, *PLoS Pathog.*, 2013, **9**, 1-8.
- 53 D. E. Goldberg, A. F. Slater, A. Cerami and G. B. Henderson, *Proc. Natl. Acad. Sci. U. S. A.*, 1990, **87**, 2931–2935.
- 54 D. E Goldberg, in *Malaria: Drugs, Disease and Post-genomic Biology*, ed. D. Sullivan and S. Krishna, Springer Science & Business Media, Berlin, 2006, vol. 1, ch. 8, pp. 275–291.
- 55 S. E. Francis, I. Y. Gluzman, A. Oksman, A. Knickerbocker, R. Mueller, M. L. Bryant, D. R. Sherman, D. G. Russell and D. E. Goldberg, *EMBO J.*, 1994, **13**, 306–317.
- 56 S. Jain, V. Rana, A. Tridibes, S. Sunil and R. K. Bhatnagar, *Parasit. Vectors*, 2015, **8**, 1–20.
- 57 CDC – Anopheles Mosquitoes, <https://www.cdc.gov/malaria/about/biology/mosquitoes/>, (accessed December 2016).
- 58 WHO - Vector control and insecticide resistance, http://www.who.int/malaria/areas/vector_control/insecticide_resistance/en/, (accessed December 2016).
- 59 WHO - Core vector control methods, http://www.who.int/malaria/areas/vector_control/core_methods/en/, (accessed December 2016).
- 60 AIRS, Indoor Residual Spraying, <http://www.africaairs.net/about/indoor-residual-spraying/>, (accessed December 2016).
- 61 WHO - Larval source management: a supplementary malaria vector

- control measure,
http://apps.who.int/iris/bitstream/10665/85379/1/9789241505604_eng.pdf?ua=1, (accessed December 2016).
- 62 CDC - Larval Control and Other Vector Control Interventions,
https://www.cdc.gov/malaria/malaria_worldwide/reduction/vector_control.html, (accessed December 2016).
- 63 M. W. Roederer, H. McLeod and J. J. Juliano, *Bull. World Health Organ.*, 2011, **89**, 838–845.
- 64 N. Tangpukdee, C. Duangdee, P. Wilairatana and S. Krudsood, *Korean J. Parasitol.*, 2009, **47**, 93–102.
- 65 S. P. Johnston, N. J. Pieniazek, M. V. Xayavong, S. B. Slemenda, P. P. Wilkins and A. J. da Silva, *J. Clin. Microbiol.*, 2006, **44**, 1087–1089.
- 66 A. F. Vallejo, J. García, A. B. Amado-Garavito, M. Arévalo-Herrera and S. Herrera, *Malar. J.*, 2016, **15**, 1–9.
- 67 D. Rifkind and G. Freeman, *The Nobel Prize Winning Discoveries in Infectious Diseases*, Elsevier Science, Amsterdam, 2005.
- 68 J. N. Burrows and R.E. Sinden, in *Neglected Diseases and Drug Discovery*, ed. M. J. Palmer and T. N. C. Wells, Royal Society of Chemistry, Cambridge, 1st edn, 2011, ch. 5, pp. 112-133.
- 69 J. Achan, A. O. Talisuna, A. Erhart, A. Yeka, J. K. Tibenderana, F. N. Baliraine, P. J. Rosenthal and U. D'Alessandro, *Malar. J.*, 2011, **10**, 1–12.
- 70 P. M. O'Neill, P. G. Bray, S. R. Hawley, S. A. Ward and B. K. Park, *Pharmacol. Ther.*, 1998, **77**, 29–58.
- 71 WHO - Essential Medicines List,
<http://www.who.int/medicines/publications/essentialmedicines/en/>, (accessed December 2016).
- 72 A. F. Slater, *Pharmacol. Ther.*, 1993, **57**, 203–35.
- 73 S. Q. Toh, A. Glanfield, G. N. Gobert and M. K. Jones, *Parasit. Vectors*, 2010, DOI: 10.1186/1756-3305-3-108.
- 74 D. J. Krogstad, I. Y. Gluzman, D. E. Kyle, A. M. Oduola, S. K. Martin, W. K. Milhous and P. H. Schlesinger, *Science*, 1987, **238**, 1283–1285.
- 75 R. E. Martin and K. Kirk, *Mol. Biol. Evol.*, 2004, **21**, 1938–1949.
- 76 R. M. Chico, R. Pittrof, B. Greenwood and D. Chandramohan, *Malar. J.*, 2008,

DOI:10.1186/1475-2875-7-255.

- 77 C. Ohrt, G. D. Willingmyre, P. Lee, C. Knirsch and W. Milhous, *Antimicrob. Agents Chemother.*, 2002, **46**, 2518–2524.
- 78 T. E. Wellems and C. V Plowe, *J. Infect. Dis.*, 2001, **184**, 770–776.
- 79 S. M. Attia, *Oxid. Med. Cell. Longev.*, 2010, **3**, 238–253.
- 80 T. Johansson, U. Jurva, G. Grönberg, L. Weidolf and C. Masimirembwa, *Drug Metab. Dispos.*, 2009, **37**, 571–579.
- 81 K. H. Rieckmann, G. M. Trenholme, R. L. Williams, P. E. Carson, H. Frischer and R. E. Desjardins, *Bull. World Health Organ.*, 1974, **51**, 375–377.
- 82 A. Dassonville-Klimpt, A. Jonet, M. Pillon, C. Mullie and P. Sonnet, in *Science against Microbial Pathogens: Communicating Current Research and Technological Advances*, Formatex Research Center, Badajoz, 2011, vol. 1, ch. 3, pp. 23-35.
- 83 M. Foley and L. Tilley, *Int. J. Parasitol.*, 1997, **27**, 231–240.
- 84 R. L. Nevin, P. P. Pietrusiak and J. B. Caci, *Malar. J.*, 2008, **7**, 1–5.
- 85 D. Fernando, C. Rodrigo and S. Rajapakse, *Malar. J.*, 2011, **10**, 1–12.
- 86 J. K. Baird and S. L. Hoffman, *Clin. Infect. Dis.*, 2004, **39**, 1336–1345.
- 87 WHO - Safety of 8-aminoquinoline antimalarial medicines,
<http://www.who.int/malaria/publications/atoz/9789241506977/en/>,
(accessed December 2016).
- 88 M. A. Biamonte, J. Wanner and K. G. Le Roch, *Bioorg. Med. Chem. Lett.*, 2013, **23**, 2829–2843.
- 89 A. Nzila, S. A. Ward, K. Marsh, P. F. G. Sims and J. E. Hyde, *Trends Parasitol.*, 2005, **21**, 334–339.
- 90 B. S. Askari and M. Krajinovic, *Curr. Genomics*, 2010, **11**, 578–83.
- 91 Y. Yuthavong, *Microbes Infect.*, 2002, **4**, 175–182.
- 92 A. Nzila, *Drug Discov. Today*, 2006, **11**, 939–944.
- 93 G. Kannan, J. Vasantha, N. V. Rani, P. Thennarasu, K. Kousalya, P. Anuradha and C. U. Reddy, *Indian J. Pharm. Sci.*, 2009, **71**, 456–460.
- 94 D. J. Jollow, T. P. Bradshaw and D. C. McMillan, *Drug Metab. Rev.*, 1995, **27**, 107–124.
- 95 P. Schlagenhauf-Lawlor and Maia Funk-Baumann, *PDQ Travelers' Malaria*, PMPH-USA, Shelton, 2007.

- 96 Y. Zhang and S. R. Meshnick, *Antimicrob. Agents Chemother.*, 1991, **35**, 267–271.
- 97 A. Nzila, in *Treatment and Prevention of Malaria: Antimalarial Drug Chemistry, Action and Use*, ed. H. M. Staines and S. Krishna, Springer, Basel, 1st edn, 2012, ch. 6, pp. 113–125.
- 98 D. Greenwood, in *Antimicrobial Chemotherapy*, ed. D. Greenwood, Oxford University Press, Oxford, 5th edn, 2007, ch. 5, pp. 77–91
- 99 A. Nzila, *J. Antimicrob. Chemother.*, 2006, **57**, 1043–54.
- 100 M. L. Gatton, L. B. Martin and Q. Cheng, *Antimicrob. Agents Chemother.*, 2004, **48**, 2116–23.
- 101 Q. J. Baca, D. M. Coen, D. E. Golan, in *Principles of Pharmacology: The Pathophysiologic Basis of Drug Therapy*, ed. A. H. Tashjian and E. J. Armstrong, Lippincott Williams & Wilkins, Philadelphia, 2011, ch. 32, 563–580.
- 102 Y. Yuthavong, J. Yuvaniyama, P. Chitnumsub, J. Vanichtanankul, S. Chusacultanachai, B. Tarnchompoo, T. Vilaivan and S. Kamchonwongpaisan, *Parasitology*, 2005, **130**, 249–259.
- 103 A. Sardarian, K. T. Douglas, M. Read, P. F. Sims, J. E. Hyde, P. Chitnumsub, R. Sirawaraporn and W. Sirawaraporn, *Org. Biomol. Chem.*, 2003, **1**, 960–964.
- 104 A. Gregson and C. V. Plowe, *Pharmacol. Rev.*, 2005, **57**, 117–145.
- 105 B. Tarnchompoo, C. Sirichaiwat, W. Phupong, C. Intaraudom, W. Sirawaraporn, S. Kamchonwongpaisan, J. Vanichtanankul, Y. Thebtaranonth and Y. Yuthavong, *J. Med. Chem.*, 2002, **45**, 1244–1252.
- 106 L. R. Cruz, T. Spangenberg, M. V. G. Lacerda and T. N. C. Wells, *Malar. J.*, 2013, **12**, 1–12.
- 107 E. S. Kaneshiro, D. Sul and B. Hazra, *Antimicrob. Agents Chemother.*, 2000, **44**, 14–8.
- 108 T. Rodrigues, F. Lopes and R. Moreira, *Curr. Med. Chem.*, 2010, **17**, 929–956.
- 109 B. A. Akhoun, K. P. Singh, M. Varshney, S. K. Gupta, Y. Shukla and S. K. Gupta, *PLoS One*, 2014, **9**, DOI: 10.1371/journal.pone.0110041.
- 110 S. B. Christensen and I. C. Bygbjerg, in *Bioactive Compounds from Natural Sources, Second Edition: Natural Products as Lead Compounds in Drug*

- Discovery*, ed. C. Tringali, CRC Press, Boca Raton, 2nd edn, 2011, ch. 15, pp. 525–560.
- 111 M. Korsinczky, N. Chen, B. Kotecka, A. Saul, K. Rieckmann and Q. Cheng, *Antimicrob. Agents Chemother.*, 2000, **44**, 2100–2108.
- 112 J. M. Peters, N. Chen, M. Gatton, M. Korsinczky, E. V. Fowler, S. Manzetti, A. Saul and Q. Cheng, *Antimicrob. Agents Chemother.*, 2002, **46**, 2435–2441.
- 113 E. Callaway and D. Cyranoski, *Nature*, 2015, **526**, 174–175.
- 114 Y. Tu, *Nat. Med.*, 2011, **17**, 1217–1220.
- 115 U. S. Neill, *J. Clin. Invest.*, 2011, **121**, 3768–3773.
- 116 L. Cui and X. Su, *Expert Rev. Anti. Infect. Ther.*, 2009, **7**, 999–1013.
- 117 J. D. Steyn, L. Wiesner, L. H. du Plessis, A. F. Grobler, P. J. Smith, W.C. Chan, R. K. Haynes and A. F. Kotzé, *Int. J. Pharm.*, 2011, **414**, 260–266.
- 118 T. Gordi, D. X. Huong, T. N. Hai, N. T. Nieu and M. Ashton, *Antimicrob. Agents Chemother.*, 2002, **46**, 1026–1031.
- 119 G. A. Balint, *Pharmacol. Ther.*, 2001, **90**, 261–265.
- 120 S. Parapini, P. Olliaro, V. Navaratnam, D. Taramelli and N. Basilico, *Antimicrob. Agents Chemother.*, 2015, **59**, 4046–4052.
- 121 A. Brossi, B. Venugopalan, L. Dominguez Gerpe, H. J. C. Yeh, J. L. Flippen-Anderson, P. Buchs, X. D. Luo, W. Milhous and W. Peters, *J. Med. Chem.*, 1988, **31**, 645–650.
- 122 M. Degani, S. Narkhede, Y. Pedgaonkar, S. Chavan, M. K. Sharma, WO pat., 2008087667 A1, 2008.
- 123 Q. Li and P. Weina, *Pharmaceuticals*, 2010, **3**, 2322–2332.
- 124 T. K. Mutabingwa, *Acta Trop.*, 2005, **95**, 305–315.
- 125 C. P. Bapat, S. J. Dheer and S. K. Dhamale, WO Pat., 2009109989, 2009.
- 126 R. S. Bhakuni, A. P. Kahol, T. Singh and S.P.S. Khanuja, WO Pat., 2004050661, 2004.
- 127 F. Terkuile, N. J. White, P. Holloway, G. Pasvol and S. Krishna, *Exp. Parasitol.*, 1993, **76**, 85–95.
- 128 R. Udomsangpetch, B. Pipitaporn, S. Krishna, B. Angus, S. Pukrittayakamee, I. Bates, Y. Suputtamongkol, D. E. Kyle and N. J. White, *J. Infect. Dis.*, 1996, **173**, 691–698.
- 129 A. Codd, F. Teuscher, D. E. Kyle, Q. Cheng and M. L. Gatton, *Malar. J.*, 2011,

- 10**, 56.
- 130 WHO | Q&A on artemisinin resistance,
http://who.int/malaria/media/artemisinin_resistance_qa/en/, (accessed December 2016).
- 131 J. Woodcock, J. P. Griffin and R. E. Behrman, *N. Engl. J. Med.*, 2011, **364**, 985–987.
- 132 I. Hastings, *Trends Parasitol.*, 2011, **27**, 67–72.
- 133 C. Weiyuan, *Bull. World Health Organ.*, 2009, **87**, 743–744.
- 134 H. C. Slater, J. T. Griffin, A. C. Ghani and L. C. Okell, *Malar. J.*, 2016, **15**, 1–11.
- 135 J. F. Trape, *Am. J. Trop. Med. Hyg.*, **64**, 12–17.
- 136 K. Karunamoorthi, *Malar. J.*, 2014, **13**, 1–13.
- 137 I. Petersen, R. Eastman and M. Lanzer, *FEBS Lett.*, 2011, **585**, 1551–1562.
- 138 I. M. Hastings, W. M. Watkins and N. J. White, *Philos. Trans. R. Soc. Lond. B. Biol. Sci.*, 2002, **357**, 505–519.
- 139 M. Helble, *Bull. World Health Organ.*, 2011, **89**, 68–72.

Chapter II

Introduction to IspD

Table of Contents

2.1 Introduction	39
2.1.1 Isoprenoids	39
2.1.2 The mevalonate pathway	43
2.1.3 The MEP pathway	47
1-Deoxy- <i>D</i> -xylulose-5-phosphate synthase (DXS)	48
1-Deoxy- <i>D</i> -xylulose-5-phosphate reductoisomerase (IspC)	49
4-Diphosphocytidyl-2 <i>C</i> -methyl- <i>D</i> -erythritol cytidyltransferase (IspD)	51
4-Diphosphocytidyl-2 <i>C</i> -methyl- <i>D</i> -erythritol kinase (IspE)	53
2 <i>C</i> -Methyl- <i>D</i> -erythritol-2,4-cyclodiphosphate synthase (IspF)	53
4-Hydroxy-3-methyl-2-(<i>E</i>)-butenyl-4-diphosphate synthase (IspG)	54
4-Hydroxy-3-methyl-2-(<i>E</i>)-butenyl-4-diphosphate reductase (IspH)	55
2.1.4 Why target the MEP pathway?	56
2.1.5 Inhibitors of the MEP pathway	57
2.2 Why Target IspD?	64
2.3 Aim	64
2.4 Lead Template Identification	65
2.5 Proposed Mechanism of Action	67
2.6 Structure-Activity Relationship Exploration	69
2.7 References	71

2.1 Introduction

2.1.1 Isoprenoids

The isoprenoid family consists of over 35,000 members, which include biologically important compounds such as sterols, terpenes and ubiquinone.¹ Sterols are a subgroup of steroids that contain a hydroxyl moiety in the 3-position of the A-ring. One of the best-known sterols, cholesterol, is shown below in Figure 2.1.² This group of compounds play integral roles in cell membrane structure and act as precursors to fat soluble vitamins and steroid hormones.^{3, 4} Terpenes are aromatic hydrocarbons that are produced by a large variety of plants and some insects.⁵ They are important biosynthetic building blocks and readily undergo chemical modification, including rearrangements of the carbon skeleton and oxidations, forming compounds such as terpenoids.⁶ Terpenes are major components of resin and are the primary constituents of essential oils.⁷ A well-known example of this diverse class of compounds is artemisinin, and the structure of this sesquiterpene lactone is also shown below in Figure 2.1.⁸ Ubiquinone (Figure 2.1) is present in the mitochondria of most eukaryotes.⁹ This lipid soluble molecule is an important component of the electron transport chain and participates in aerobic cellular respiration, producing ATP.¹⁰

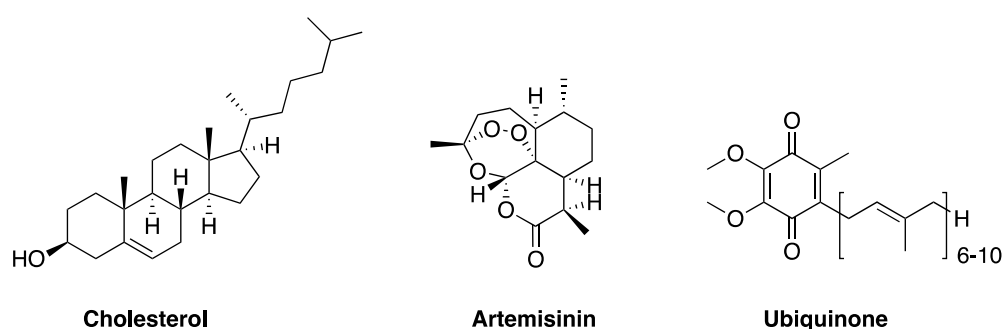


Figure 2.1. The structures of cholesterol, artemisinin and ubiquinone, which are all members of the isoprenoid family

A number of rearrangements, oxidations, repetitions, and cyclisations of a branched isoprene unit are responsible for providing this vast array of molecules. Isopentenyl pyrophosphate (IPP) and dimethylallyl pyrophosphate (DMAPP) (Figure 2.2) are the universal building blocks for this large and diverse group of natural products.^{11,12}

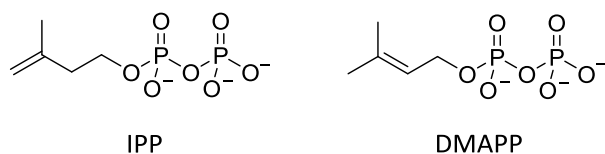


Figure 2.2: The structures of isopentenyl pyrophosphate (IPP) and dimethylallyl phosphate (DMAPP)

Mammals, archaea and fungi synthesise IPP and DMAPP exclusively through a coenzyme A (CoA)-dependant pathway, known as the mevalonate pathway (MVA).¹³ This pathway uses a series of seven enzymes to synthesise the important isoprenoid precursors via a key intermediate, mevalonate (Figure 2.3). As the MVA pathway leads to the production of cholesterol, it has been studied extensively, and is an important drug target for the prevention and treatment of cardiovascular disease.¹⁴

Previously it was thought that this biosynthetic pathway was the only route to IPP and DMAPP; however, in recent years it has been discovered that plant chloroplasts, algae, apicomplexa and eubacteria use an alternative method known as the 1-deoxy-*d*-xylulose 5-phosphate (DOXP) or 2*C*-methylerythritol 4-phosphate (MEP) pathway (Figure 2.3).^{15, 16}

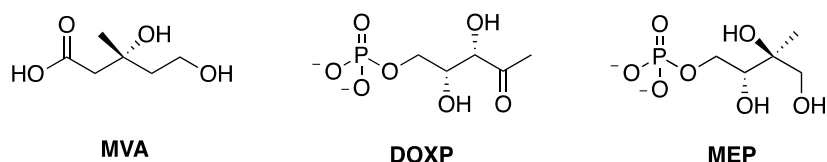


Figure 2.3. The structures of mevalonate (MVA), 1-deoxy-*d*-xylulose 5-phosphate (DOXP) and 2*C*-methylerythritol 4-phosphate (MEP)

Higher plants are known to utilise both biosynthetic pathways for isoprenoid production. In cytoplasmic components of plant cells, the mevalonate pathway is responsible for the synthesis of isoprenoids, and in plastid components, the non-mevalonate pathway produces a large number of other isoprenoids.^{16,17}

Apicomplexa are a large phylum of parasitic protists, which include malaria parasites, and can be distinguished by an apical complex structure along with an additional plastid organelle, known as the apicoplast.¹⁸ The apicoplast is of similar origin to plant chloroplasts but it is non photosynthetic in nature. Apicomplexa do not contain the necessary machinery of the MVA pathway, therefore isoprenoid biosynthesis takes place exclusively via the MEP pathway within the apicoplast.¹⁹

Isoprenoid biosynthesis is essential for cell survival and these molecules are involved in a number of vital cellular functions, including membrane structure, electron transport and cell signalling.²⁰ Ubiquinone (Figure 2.1) for example, is found in the hydrophobic region of the inner mitochondrial membrane and is known to act as a mobile electron carrier in the production of ATP by oxidative phosphorylation.^{21,22} Dolichol (Figure 2.4), which is located on the membrane of the endoplasmic reticulum, is responsible for the formation of a precursor oligosaccharide for *N*-linked glycosylation; an essential process required for both the structure and function of proteins.²³ Menaquinones (Figure 2.4) form a family of vitamin K₂ homologues (varying isoprenoid chain lengths) that are required for a wide variety of functions, including coagulation and bone mineralisation.²⁴

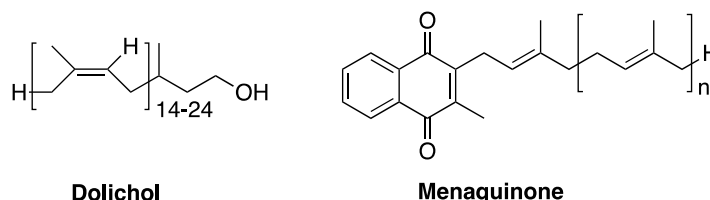


Figure 2.4. The general structures of dolichol and menaquinones

Definitive reasons for the malaria parasite's requirement for isoprenoids remain unclear, and this is further complicated as a number of the parasite's essential

developmental pathways rely heavily on scavenging from the host's red blood cells. For example, the parasite has limited capability for *de novo* synthesis of cholesterol and will instead salvage this essential molecule from host erythrocytic membranes. Furthermore, ATP production is a result of glycolysis rather than mitochondrial respiration.²⁵ However, an active mitochondrial electron transport chain is essential for the regeneration of ubiquinone, which in turn acts as an electron acceptor for dihydroorotate dehydrogenase; an essential enzyme for pyrimidine biosynthesis.²⁶ The parasite is also known to express protein prenyltransferases that are responsible for the post translational modification of proteins through the attachment of isoprenyl groups to cysteine residues. This is important for both protein-protein and protein-membrane interactions.²⁷ Finally, several carotenoids (including β -carotene, see Figure 2.5) have been identified in cultured *P. falciparum*, and inhibition of their biosynthesis leads to an increased sensitivity of the parasite to high environmental oxygen concentrations; suggesting that these tetraterpene pigments may function as important antioxidants.²⁸ Despite a lack of understanding of isoprenoid biology in *P. falciparum*, it is clear that they are vital for a diverse range of cellular processes and are essential to parasite growth and development.

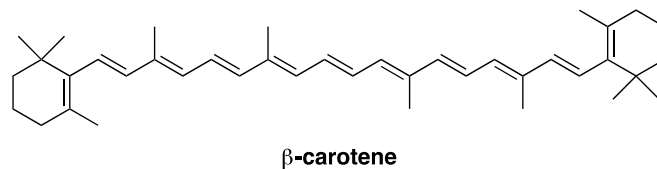
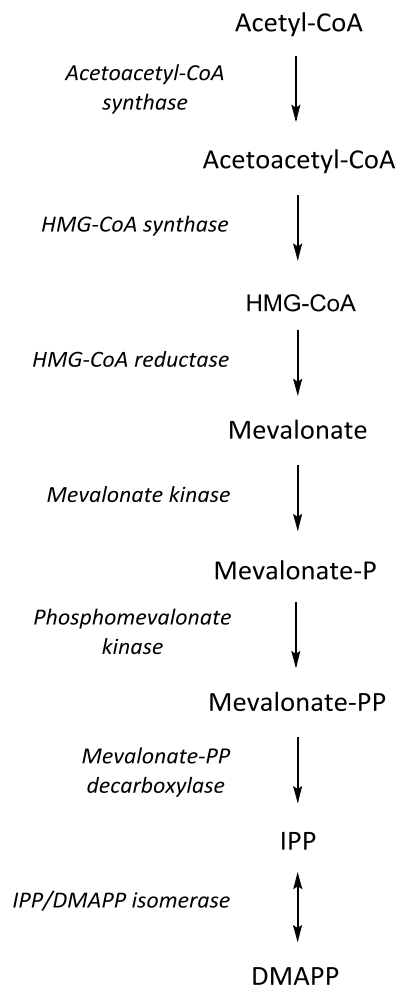


Figure 2.5. The structure of β -carotene, a carotenoid found in the intraerythrocytic stages of *P. falciparum*²⁸

2.1.2 The mevalonate pathway

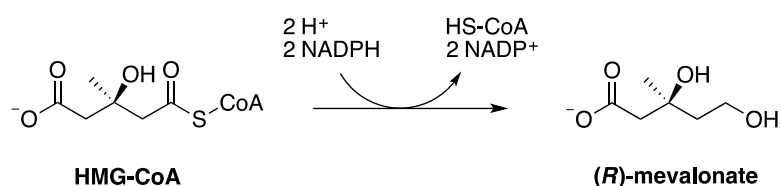
The mevalonate pathway was discovered in yeasts and animals in the 1950s. This synthetic route uses 2 molecules of acetyl-CoA to produce the isoprenoid precursors, IPP and DMAPP, in a series of 7 catalytic steps.

The upper part of the MVA pathway is universal across eukaryotes, archaea and eubacteria, and leads to the production of a mevalonate intermediate in 3 steps. However the lower MVA pathway differs from eukaryotes to archaea. Scheme 2.1 outlines the synthesis of IPP and DMAPP from acetyl-CoA in eukaryotes.



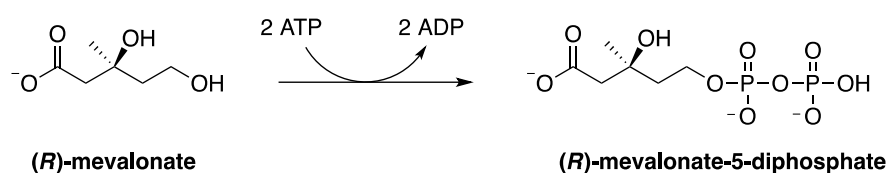
Scheme 2.1. Representation of the mevalonate pathway for isoprenoid biosynthesis in eukaryotes

HMG-CoA reductase is the catalyst for this rate-limiting step in isoprenoid biosynthesis and has therefore become the focus of drug therapies aimed at reducing levels of low-density lipoprotein (LDL) cholesterol in plasma circulation; a major risk factor in coronary heart disease.³² Statins are a class of drug designed to competitively inhibit HMG-CoA reductase, thereby reducing cholesterol synthesis in the liver, and are used widely for the treatment of high blood pressure and cardiovascular disease.³³



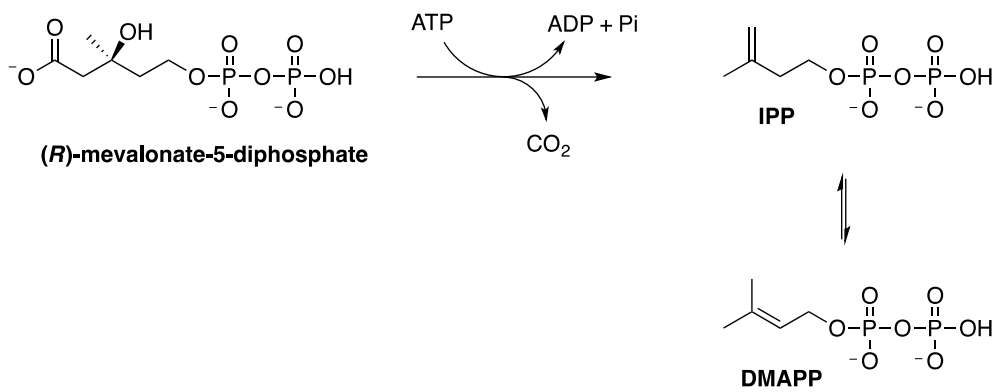
Scheme 2.4. The formation of (*R*)-mevalonate from HMG-CoA, catalysed by HMG-CoA reductase

The next two steps involve phosphorylation of (*R*)-mevalonate to (*R*)-mevalonate-5-diphosphate sequentially by two kinase enzymes: mevalonate kinase and phosphomevalonate kinase (Scheme 2.5). ATP acts as the high-energy phosphate-donating molecule in both transformations.



Scheme 2.5. The formation of (*R*)-mevalonate-5-diphosphate from (*R*)-mevalonate

The final step in the pathway sees the decarboxylation of (*R*)-mevalonate-5-diphosphate to produce IPP. The enzyme responsible for this conversion is mevalonate diphosphate decarboxylase, which recognises and binds both (*R*)-mevalonate-5-diphosphate and ATP. An initial phosphorylation occurs to produce a reactive intermediate, which undergoes sequential dephosphorylation and decarboxylation. The products of this transformation are IPP, CO₂, inorganic phosphate and ADP (Scheme 2.6).³⁴ Some of the IPP produced is converted to DMAPP by an isomerase enzyme, thus completing the synthesis of these crucial isoprenoid building blocks.



Scheme 2.6. The transformation of (*R*)-mevalonate-5-diphosphate into IPP and DMAPP

2.1.3 The MEP pathway

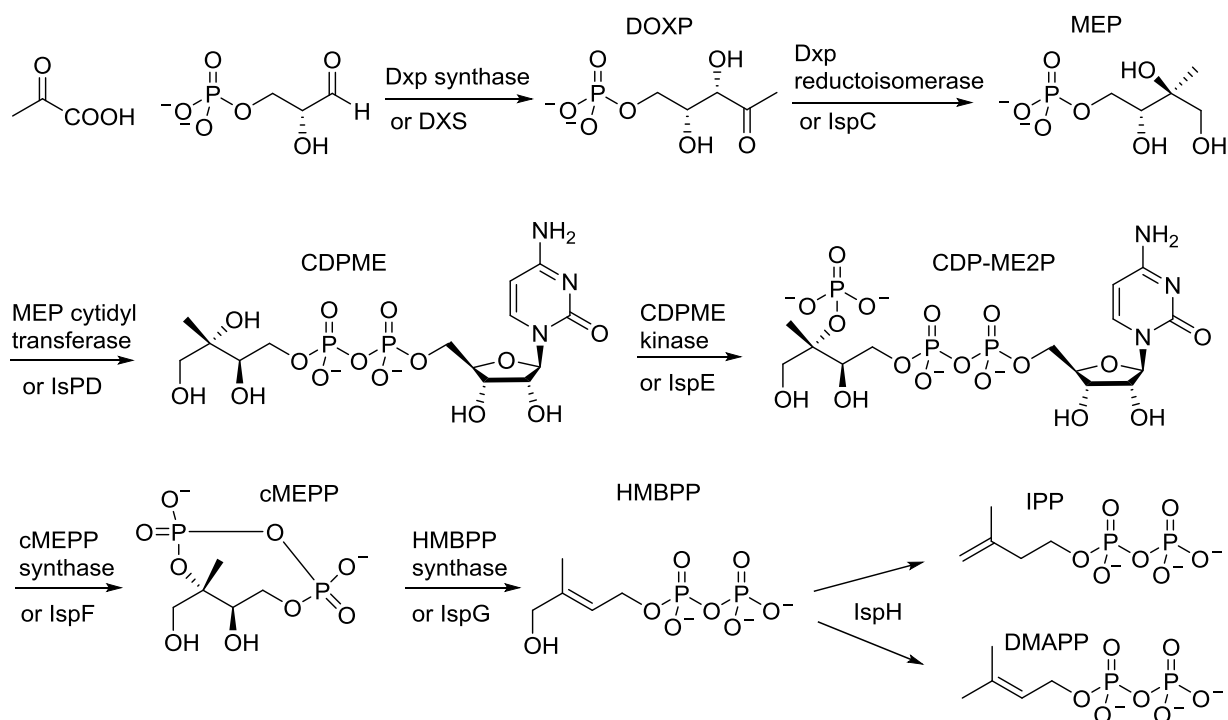
The first indications that the mevalonate pathway might not be the sole route to isoprenoid biosynthesis came in 1966, when Goodwin and co-workers discovered that isotopically labelled mevalonic acid was heavily incorporated into sterols and beta-amyrin in higher plants, whereas there was very little to no incorporation into carotene and phytol (from chlorophyll).³⁵

Further evidence for an alternate pathway emerged in 1977 when Bach and Lichtenthaler investigated the effects of mevinolin on plant growth. Mevinolin is a potent HMG-CoA reductase inhibitor, which strongly inhibited sterol biosynthesis, as was expected. However, it exhibited no effect on the accumulation of other isoprenoids such as mitochondrial ubiquinone, plastid prenylquinones, chlorophylls and carotenoids.³⁶

Work by Kreuz and Kleinig in the 1980s led to the discovery that neither spinach or daffodil chloroplasts use mevalonate, phosphomevalonate or diphosphomevalonate for the synthesis of IPP, yet IPP was still incorporated into plastid polyprenoids in large quantities. The enzymes of the mevalonate pathway couldn't be isolated from these plant chloroplasts either. An alternate pathway was not ruled out at this stage but a number of other possible explanations were postulated to explain these anomalies.³⁷

It wasn't until research into the biosynthesis of bacterial hopanoids (which have structural and functional similarities to sterols), by Rohmer *et al* in the 1990s, led to the discovery of a second and alternate pathway to isoprenoid biosynthesis: the MEP pathway. Isotopic labelling studies not only helped to identify this mevalonate independent route but also determined that glyceraldehyde 3-phosphate and pyruvate were the first precursors of IPP.¹⁶

Since this discovery there has been much research into the elucidation of the enzymes, substrates and reaction mechanisms of this pathway. The MEP pathway is now thought to be catalysed over a series of eight steps, by nine enzymes in total; seven of which have been structurally characterised (Scheme 2.7).

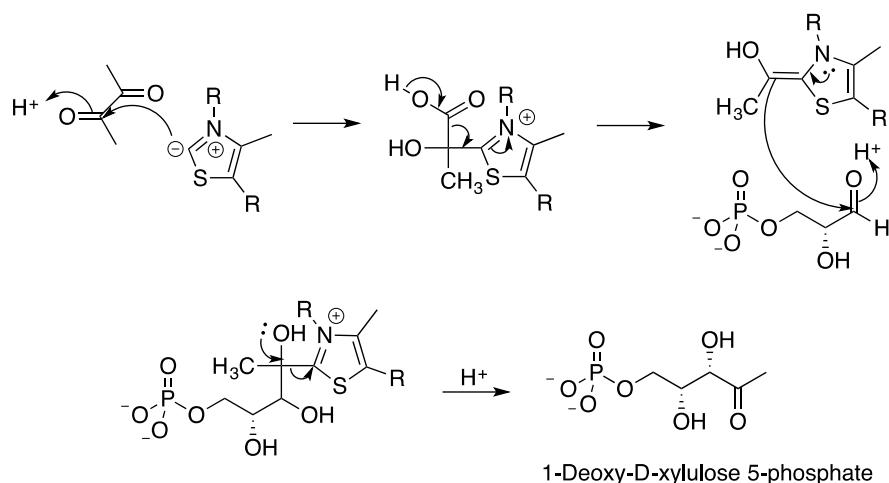


Scheme 2.7. Isoprenoid biosynthesis via the MEP pathway

1-Deoxy-*D*-xylulose-5-phosphate synthase (DXS)

DXS is the enzyme that catalyses the first, and rate limiting, step of the MEP pathway. The pathway begins with a condensation reaction between pyruvate and glyceraldehyde 3-phosphate (GAP) to produce a molecule of 1-deoxy-*D*-xylulose-5-phosphate (DOXP), using the cofactor thiamine pyrophosphate (TPP). The product, DOXP, is also used for the biosynthesis of thiamine (Vitamin B₁) and pyridoxol (Vitamin B₆) as well as isoprenoid formation.³⁸

The proposed mechanism for this step is shown in Scheme 2.8. Deprotonation of the C2 position on the thiazolium ring of TPP generates a reactive ylide species. The C2 carbon then attacks pyruvate in a nucleophilic addition reaction. Decarboxylation generates an active pyruvate intermediate, which can isomerise between the enamine and α -carbanion forms. Activated pyruvate then attacks the aldehyde of GAP and a subsequent rearrangement yields DOXP, with regeneration of the active ylide.^{39, 40}



Scheme 2.8. Proposed mechanism for the synthesis of 1-deoxy-*D*-xylulose-5-phosphate (DOXP) from pyruvate and glyceraldehyde 3-phosphate

1-Deoxy-*D*-xylulose-5-phosphate reductoisomerase (IspC)

IspC catalyses the first committed step in the MEP pathway which involves an intramolecular isomerisation and concomitant reduction of DOXP to generate 2*C*-methyl-*D*-erythritol-4-phosphate (MEP). This enzyme has been studied in great detail and has been key to the elucidation of this pathway since it was discovered to be the molecular target for the antimicrobial agent fosmidomycin.^{41, 42}

There are over 30 published crystal structures for this enzyme. The majority are for *E. coli* and *M. tuberculosis*; however, 3 exist for *P. falciparum*. IspC is known to exist as a homodimer, with each monomer made up of 3 different domains:

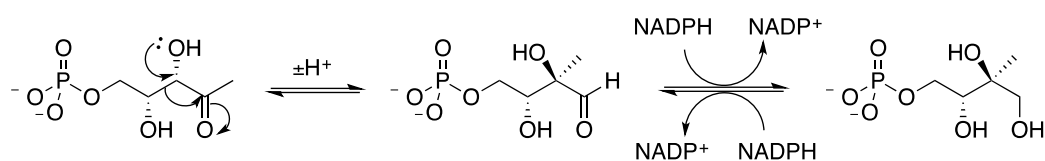
- An N-terminal domain that binds the cofactor NADPH
- A central connective domain that contains active site residues, with positively charged, lipophilic and metal binding regions
- A C-terminal helical domain that has structural functions

The first step of the transformation generates a branched aldehyde derivative known as 2*C*-methyl-*D*-erythrose-4-phosphate which is subsequently reduced to MEP in an NADPH dependant step that sees transfer of a hydride from the cofactor to the aldehyde

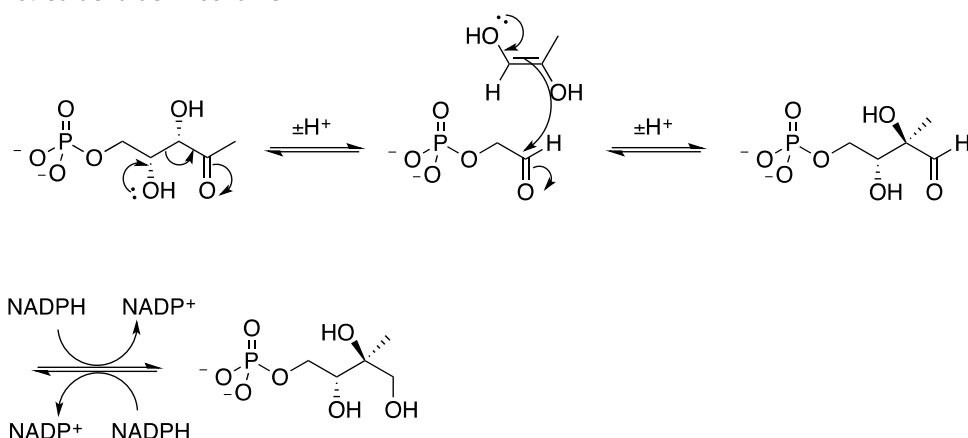
intermediate. The mechanism is believed to be ordered sequentially, with the co-factor binding first, before a divalent cation (Mg^{2+} , Mn^{2+} or Co^{2+}) polarises and orientates both the substrate and reaction intermediate.⁴³

Formation of the aldehyde intermediate has been shown to proceed by cleavage of the bond between C3 and C4 of DOXP and the formation of a new bond between C1 and C3. Both a sigmatropic rearrangement and a retro-aldol/aldol mechanism have been proposed for this step and they are shown in Scheme 2.9. A hydride/methyl shift mechanism has been ruled out as it is not consistent with labelling studies.⁴⁴ There is no definitive evidence for either mechanism but a sigmatropic rearrangement could potentially be favoured due to the stringent fragment containment required for a retro-aldol type mechanism.⁴⁵

Sigmatropic Rearrangement



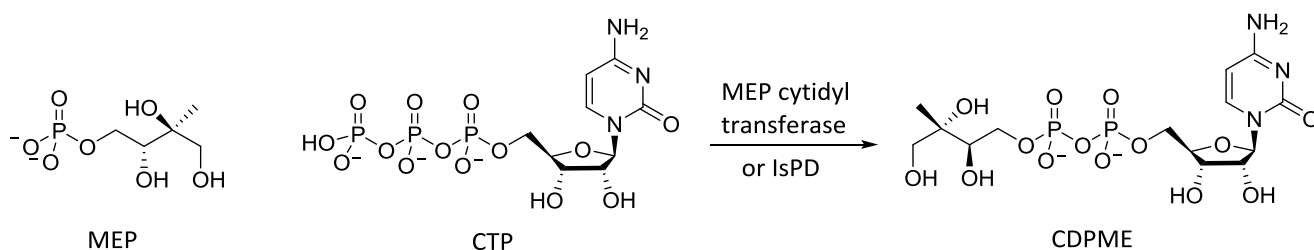
Retroaldol/aldol mechanism



Scheme 2.9. Two proposed mechanisms for the conversion of 1-deoxy-*D*-xylulose-5-phosphate (DOXP) to 2C-methyl-*D*-erythritol-4-phosphate (MEP)

4-Diphosphocytidyl-2C-methyl-D-erythritol cytidyltransferase (IspD)

IspD catalyses the third step in the MEP pathway, which is a coupling reaction between MEP and cytidine triphosphate (CTP) that produces 4-diphosphocytidyl-2C-methyl-D-erythritol (CDPME) with release of pyrophosphate (Scheme 2.10). IspD is part of a family of nucleotidyltransferases that specifically transfer phosphorus containing nucleotide groups.

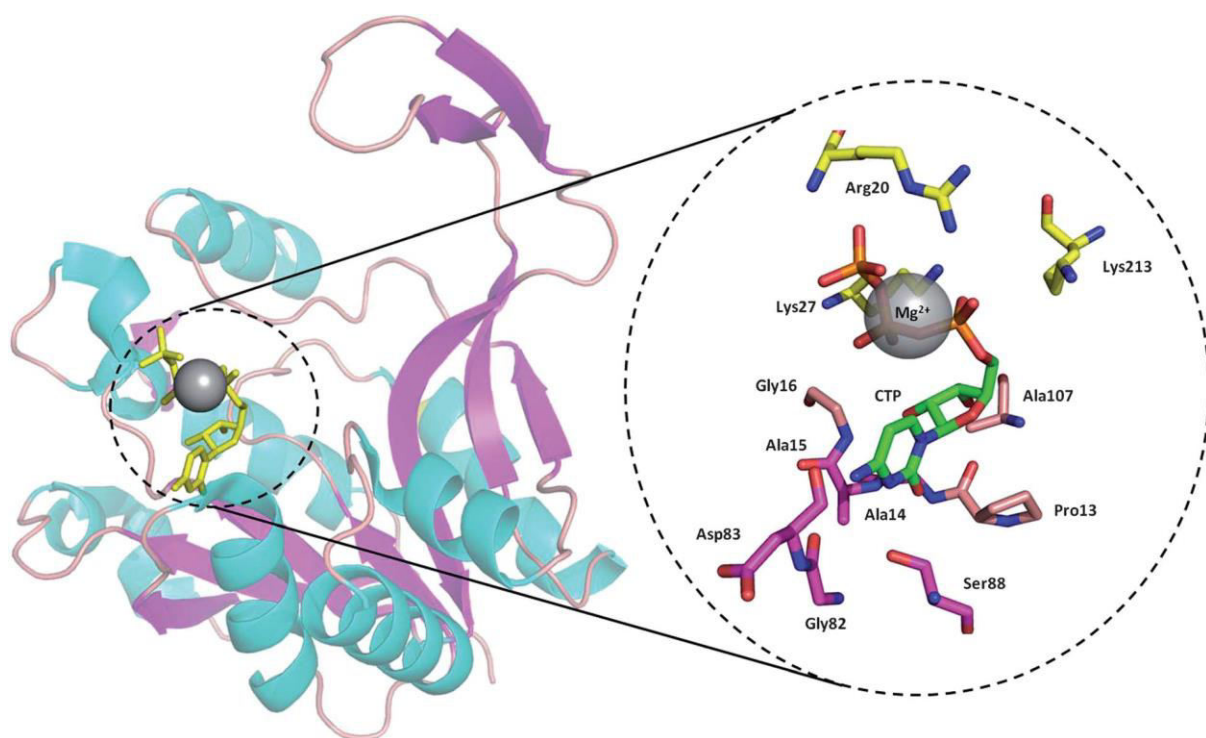


Scheme 2.10. Coupling reaction between 2C-methyl-D-erythritol-4-phosphate (MEP) and cytidine triphosphate (CTP) to produce 4-diphosphocytidyl-2C-methyl-D-erythritol (CDPME), catalysed by 4-diphosphocytidyl-2C-methyl-D-erythritol cytidyltransferase (IspD)

More than a dozen X-ray crystal structures have been published for IspD and show the enzyme to be a C2 symmetric homodimer. Each subunit has a single α/β domain which is constructed around a twisted β sheet. An extended β -arm from each monomer associates to form a dimer interface (Figure 2.6). The interlocking arms form part of the binding site and are responsible for cytidyltransferase activity. Mg^{2+} has been postulated to be necessary for the enzyme's catalytic activity, as it coordinates to the α -, β - and γ -phosphate oxygens of CTP and the α -phosphate oxygen of CDPME, which assists in neutralizing the developing negative charge as the reaction proceeds. The active site is selective for the cytidine base through a number of hydrogen bonding interactions and steric constrictions within the binding pocket, which prevents larger purine bases from coordinating. Along with a magnesium ion, a basic active site also helps to bind the phosphate groups of the substrates, and both lysine and arginine (Lys27 and Arg20 in *E. Coli*, Figure 2.6) help to stabilise the highly negative pentavalent transition state that is proposed to be formed during the coupling reaction.^{38, 46}

Like IspC, an ordered, sequential mechanism takes place where Mg^{2+} coordinates first followed by CTP to form an ion pair, and then MEP. Two mechanisms are possible for nucleotidyltransferases and these involve either a dissociative or associative route. A dissociative mechanism would involve the formation of a highly reactive metaphosphate intermediate on CTP through loss of pyrophosphate, which could be trapped by the 4-phosphate of MEP. An associative mechanism would proceed by nucleophilic attack on the α -phosphate of CTP by the 4-phosphate of MEP, leading to a highly charged transition state and subsequent loss of pyrophosphate.⁴⁷

A small number of inhibitors of IspD have been identified and will be discussed later (Section 2.1.5). The highly polar nature of the active site has presented a significant challenge in the search for effective inhibitors of this enzyme.



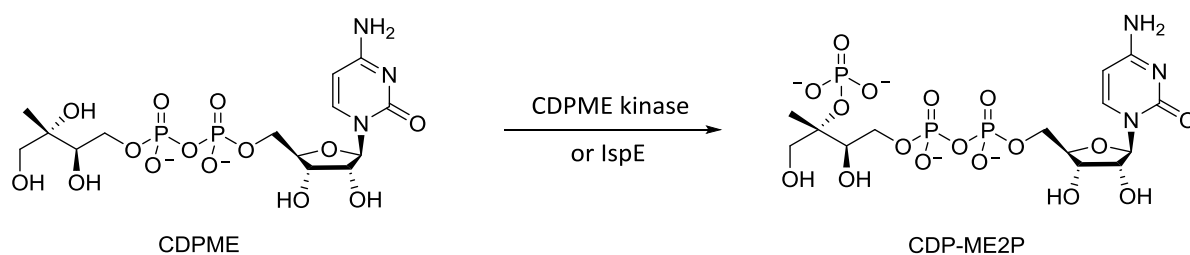
“Tertiary structure of the IspD monomer with CTP-bound from E. coli (PDB code: 1152), with a close-up image of the CTP binding site. α -helices and β -sheets are shown in cyan and purple cartoon format in the overall structure. In the close-up image, cytosine binding residues are shown in purple stick representation, ribose binding residues in tan stick representation, and phosphate binding residues in yellow stick representation. Mg^{2+} is shown as a gray sphere. CTP is coloured by element, with carbon in green.”³⁸

Figure 2.6. The tertiary structure of an IspD monomer

Figure reproduced from: The MEP pathway and the development of inhibitors as potential anti-infective agents, 2012, Hale *et al.*³⁸

4-Diphosphocytidyl-2*C*-methyl-*D*-erythritol kinase (IspE)

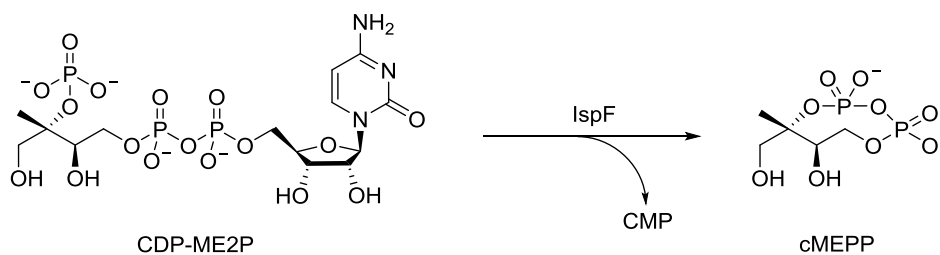
IspE is the fourth enzyme in this pathway and is a member of the galacto-homoserine-mevalonate-phosphomevalonate (GHMP) kinase superfamily. In this step, the hydroxyl group in the 2-position of CDPME is phosphorylated in an ATP dependant reaction, to give 4-diphosphocytidyl-2*C*-methyl-*D*-erythritol 2-phosphate as the product (CDP-ME2P) (Scheme 2.11).⁴⁸



Scheme 2.11. The phosphorylation of 4-diphosphocytidyl-2*C*-methyl-*D*-erythritol (CDPME) to form 4-diphosphocytidyl-2*C*-methyl-*D*-erythritol 2-phosphate (CDP-ME2P) catalysed by IspE

2*C*-Methyl-*D*-erythritol-2,4-cyclodiphosphate synthase (IspF)

IspF catalyses the transformation of CDP-ME2P to produce 2*C*-methyl-*D*-erythritol-2,4-cyclodiphosphate (cMEPP) with the release a molecule of cytidine monophosphate (CMP) (Scheme 2.12). A divalent cation is required for this reaction to take place; however, there is no dependence on any other cofactor. IspF genes are tightly linked to IspD on the *E. coli* chromosome and some eubacteria even contain bi-functional proteins that have an *N*-terminal IspD domain and a *C*-terminal IspF domain, therefore providing further evidence for the involvement of this enzyme in the MEP pathway.⁴⁹



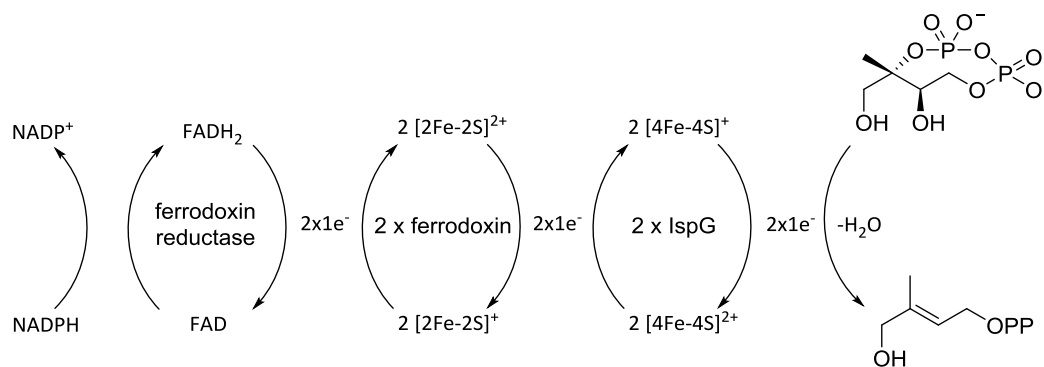
Scheme 2.12. The transformation of 4-diphosphocytidyl-2*C*-methyl-*D*-erythritol 2-phosphate (CDP-ME2P) to 2*C*-methyl-*D*-erythritol-2,4-cyclodiphosphate (cMEPP), catalysed by IspF

The proposed mechanism involves an intramolecular cyclisation, where the terminal phosphate of CDP-ME2P attacks the β -phosphate, generating a pentacoordinate transition state that is stabilised by a divalent cations. The pentacoordinate intermediate then collapses to produce cMEPP and CMP.^{15, 38}

4-Hydroxy-3-methyl-2-(*E*)-butenyl-4-diphosphate synthase (IspG)

IspG is the sixth enzyme in the pathway and it catalyses a complex elimination/reduction reaction that converts cMEPP to 4-hydroxy-3-methyl-2-(*E*)-butenyl-4-diphosphate (HMBPP). IspG is an iron-sulfur protein that utilises a [4Fe-4S] cluster to carry out a double 1 e⁻ transfer, with the assistance of flavodoxin/flavodoxin reductase and NADP/NADPH.⁵⁰

Elucidation of the structure and mechanism of this enzyme have been hampered due to the sensitivity of the iron-sulfur cluster to oxygen. The proposed reaction mechanism (Scheme 2.13) shows a complex system of successive redox reactions, which generates a free radical intermediate of the substrate. Elimination of water leads to the generation of HMBPP; however, the exact sequence of electron transfer and bond-breaking steps is however still in dispute.⁵¹



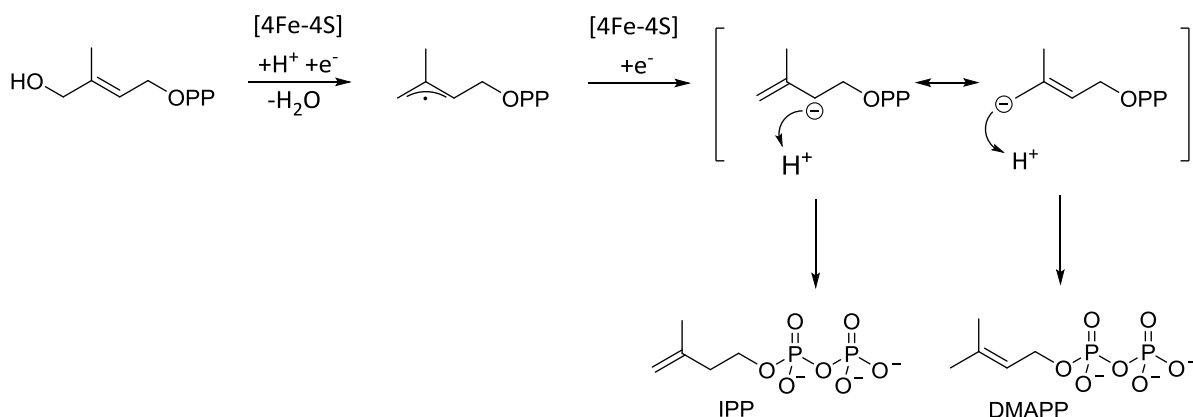
Scheme 2.13. Hypothetical biogenetic scheme for IspG activity⁵⁰

4-Hydroxy-3-methyl-2-(*E*)-butenyl-4-diphosphate reductase (IspH)

IspH is the final enzyme of the MEP pathway and catalyses the production of IPP and DMAPP from HMBPP. This iron-sulfur protein is responsible for the branching of the carbon backbone, which provides diversity in the downstream isoprenoid products. Under kinetic control, IPP and DMAPP are synthesised in a 6:1 ratio. The reaction can be brought to thermodynamic equilibrium by IPP isomerases. IspH has no inherent isomerase activity, therefore the formation of the two isomers relies solely on the final protonation step of the reaction pathway.⁵²

The production of IPP and DMAPP from HMBPP requires a two e^- transfer, like IspG, and also utilises flavodoxin and flavodoxin reductase as an electron transponder. Similarly, structure and mechanistic elucidation have proven difficult due to the sensitivity of the iron-sulfur cluster.

Stereochemical studies and the use of substrate analogues have led to the development of a hypothetical reaction mechanism (Scheme 2.14). The first step involves formation of a carbanion from the hydroxyl group at C1 of HMBPP and the apical iron ion of the redox cluster. Transfer of a proton to the oxygen atom at C1 and of one electron to the alkene moiety results in the cleavage of the carbon-oxygen bond at C1. This produces an allyl radical, which can be stabilised by interactions with the iron-sulfur cluster. Transfer of a second electron from an external source results in the formation of an allyl anion. In the final irreversible step, transfer of a proton can occur to either C1, which produces DMAPP, or C2, which results in IPP production.⁵³



Scheme 2.14. Proposed reaction mechanism of IspH catalysis

With structural information now available for all enzymes of the MEP pathway, there is huge potential for the development of inhibitors as novel anti-infectives.⁵⁴

2.1.4 Why target the MEP pathway?

Scientific investigation into the genes and proteins of the MEP pathway has progressed rapidly, and an in depth understanding of each step has provided a great opportunity for research directed at drug development.⁵⁴ This pathway has been genetically validated as essential in a vast array of organisms, and therefore presents an attractive target for the development of antimicrobial therapies. A number of serious diseases such as malaria, tuberculosis and sexually transmitted infections could be targeted through this pathway, and of particular importance to this project is the presence of MEP enzymes in all intraerythrocytic stages of *P. falciparum*, presenting an opportunity for the development of therapeutics against this most serious strain of malaria.^{55, 56}

As isoprenoids are derived from an alternate pathway in mammals, the MEP pathway provides a target that should have a favourable therapeutic index; an aspect that is highly valued in drug development.⁵⁷

The enzymes of the MEP pathway are also good targets for the development of novel herbicides, due to their presence in the plastid compartment of plants.⁵⁸ Furthermore, plants provide a very good test-system for novel antimicrobial agents targeting the MEP

pathway due to their ease of handling.⁵⁹ Finally, the enzymes of the MEP pathway could be exploited for designed biosynthesis of natural products. As plant tissue extractions typically yield low isoprenoid concentrations, alternative methods to produce high-value terpenoid compounds, such as the antimalarial drug artemisinin or the anticancer drug taxol, could prove highly lucrative.⁶⁰

2.1.5 Inhibitors of the MEP pathway

Inhibitors of DXS

A number of inhibitors have been reported for the first enzyme in this pathway that exhibit structures quite different from the natural substrates. Ketoclofazone (**1**) is a breakdown product of the soil applied herbicide clomazone, and has demonstrated antibacterial activity against *Haemophilus influenzae*, a pathogenic bacterium. However, the parent compound, clomazone, is not an inhibitor of DXS. The inhibitory activity of ketoclofazone can be suppressed through the addition of DOXP, the natural product of this enzyme, thus confirming DXS as the target of this compound.⁶¹

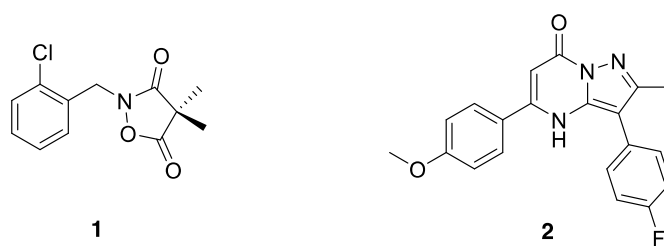


Figure 2.7. The structures of DXS inhibitors ketoclofazone (**1**) and 2-methyl-3-(4-fluorophenyl)-5-(4-methoxyphenyl)-4*H*-pyrazolo[1,5-*a*]pyrimidin-7-one (**2**)

Ketoclofazone has also been shown to lower chlorophyll and carotenoid levels in barley leaves, and also exhibits an IC_{50} of 0.1 mM against *Chlamydomonas*, a genus of green algae.⁶² The exact binding site of ketoclofazone is yet to be identified; however, it is known to coordinate to an inhibitor-binding site away from the active site where the natural substrates pyruvate and GAP bind. As this compound was originally designed as

an herbicidal agent, derivitisation could provide a number of analogues with more potent antibacterial activity.

2-Methyl-3-(4-fluorophenyl)-5-(4-methoxyphenyl)-4*H*-pyrazolo[1,5-*a*]pyrimidin-7-one (**2**) was developed as a result of a target-based approach to identify inhibitors of DXS in *M. tuberculosis* by Kozikowski et al.⁶³ This structure activity relationship study of a small, focused library of compounds, resulted in the discovery of this DXS inhibitor that has an IC₅₀ of 10.6 μM against *M. tuberculosis*.⁶³

Inhibitors of IspC

The in depth knowledge and understanding of the structure and function of IspC is, in part, due to the discovery that fosmidomycin (**3**) is a potent antimalarial compound.

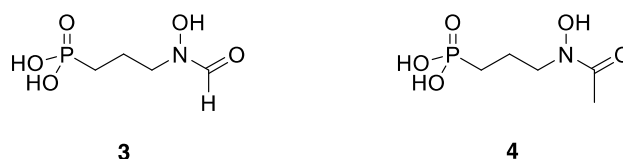


Figure 2.8. The structures of IspC inhibitors fosmidomycin (**3**) and FR-900098 (**4**)

Fosmidomycin and its *N*-acetyl analogue, FR-900098 (**4**), were discovered in 1980 by Fujisawa Pharmaceutical Company Ltd whilst they were investigating phosphonic acid antibiotics for the treatment of urinary tract infections. These novel compounds were very well tolerated and showed huge promise as safe and effective antibacterial agents (fosmidomycin MIC₅₀ = 32 μg/mL vs. carbapenem-resistant *K. pneumoniae*). High rates of recrudescence and poor half-lives (fosmidomycin half-life = 1.14h following IV administration) hindered the progression of these drug therapies.^{64, 65} It wasn't until many years later that fosmidomycin was discovered to be an inhibitor of isoprenoid biosynthesis, and more specifically an inhibitor of the IspC enzyme.⁶⁶

In 1999, Beck *et al.* reported that both fosmidomycin and FR-900098 showed inhibition of *P. falciparum* in submicromolar concentrations. Part of their research also tested these compounds against 3 different drug resistant strains of *P. falciparum* that showed

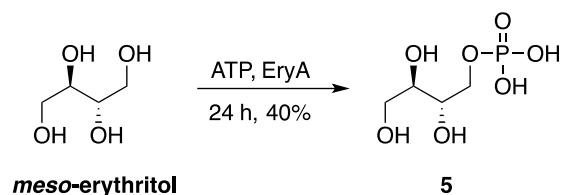
varying levels of sensitivity to chloroquine and pyrimethane. Both compounds showed efficient inhibition of all 3 strains, highlighting the potential of these agents to target multidrug resistant parasites. The group then treated mice infected with *P. vinkei* and found that these drug compounds were not only well tolerated but also very efficient at eliminating parasites, even at low concentrations. Recrudescence was observed after a 4-day dosing regimen but treatment over the course of eight days saw the mice fully cured.^{66, 67}

Studies of fosmidomycin administered in combination with clindamycin showed a therapy that was well tolerated and provided rapid clearance of *P. falciparum* in African children, with the combination being superior to either drug used on its own. However, clinical trials data showed poor efficacy of this combination in children under the age of three. Subsequent trials have replaced clindamycin with piperaquine.^{68, 69}

The hydroxamic acid moiety of fosmidomycin (which is known to be a metal chelator) is postulated to coordinate to the metal cation in the active site of the enzyme. This interaction could hold the inhibitor in place, whilst the phosphonate group binds to the phosphate-recognising pocket. A number of analogues have since been developed, including compounds that replace the phosphonate with phosphate, constrain the propyl chain and even alkylate the hydroxamic acid group; however, none of these analogues have matched the low nanomolar activity of fosmidomycin against both *P. falciparum* and *E. coli*.⁷⁰

Inhibitors of IspD

There are fewer inhibitors known for IspD than the first two enzymes in the pathway. In 2003, Cane and co-workers demonstrated the weak inhibitory activity of *L*-erythritol-4-phosphate (**5**, IC₅₀ = 1.36 mM). Using an erythritol kinase inhibitor extracted from *Brucella abortus*, the group were able to synthesise the desmethyl analogue of the natural substrate for IspD (Scheme 2.15).⁷¹



Scheme 2.15. Synthesis of *L*-erythritol-4-phosphate (**5**) from *meso*-erythritol catalysed by EryA (extracted from *Brucella abortus*)

More recently, a series of novel herbicidal agents targeting IspD have been developed. This group of azolopyrimidines were identified from a high-throughput screen of 100,000 compounds and tested for the inhibition of IspD in *Arabidopsis thaliana*.

The most active compound, 6-benzyl-5-chloro-[1,2,4]triazolo[1,5-*a*]pyrimidin-7-ol (**6**) has an IC_{50} of 140 nM against the plant. Of particular interest is the binding site of these azolopyrimidine inhibitors. Rather than binding in the active site of the enzyme, they instead bind to an allosteric pocket that is in close proximity, which causes a reduction in the size of the active site.⁷²

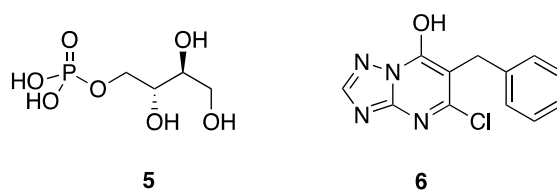


Figure 2.9. The structures of IspD inhibitors *L*-erythritol-4-phosphate (**5**) and 6-benzyl-5-chloro-[1,2,4]triazolo[1,5-*a*]pyrimidin-7-ol (**6**)

Despite some promising data from the azolopyrimidines, there is still huge scope for the design and synthesis of novel inhibitors of IspD, particularly those targeting malaria parasites.

Inhibitors of IspE

Diederich *et al.* reported the first series of water-soluble, cytosine-based inhibitors of IspE, which were originally designed to target IspD. The most potent inhibitor of this series (**7**) had an IC_{50} value of 1.67 mM against *E. coli* IspE. Furthermore, co-

crystallisation studies of the most potent inhibitor complexed with *Aquifex aeolicus* IspE, revealed that this compound binds almost solely through the nucleobase moiety in the CDPME binding pocket and avoids the polar side pocket.⁷³

The group extended this research further to improve potency and water solubility. A structure-activity relationship study conducted with a different set of compounds identified the most potent inhibitor to be compound **8**, which has an IC₅₀ value of 6 μM against *E. coli* IspD, highlighting the improved activity of these 2nd generation inhibitors.⁷⁴

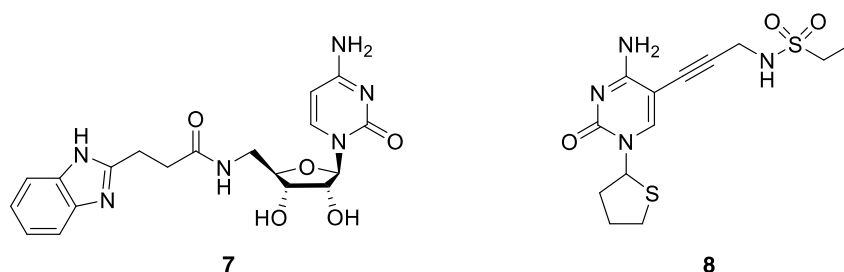


Figure 2.10. The first (**7**) and second (**8**) generation analogues designed to inhibit IspE

Inhibitors of IspF

Diederich *et al.* reported the first inhibitors designed to target IspF, in 2005. A series of fluorescent analogues of cytidine were designed as a result of molecular modelling studies, with the most potent analogue, **9**, exhibiting a weak IC₅₀ value of 3 mM against *E. coli* IspF. Fluorescent labelling also gave an important insight into the binding site for this first generation of inhibitors and allowed for the development of a second generation of inhibitors based on a cytosine core.⁷⁵

A number of cytosine derivatives were then synthesised, which displayed much improved activity profiles against the enzyme. This includes compound **10**, which had low millimolar activity against the enzyme. Despite the cytosine portion being present in the native substrate, the side chain of these cytosine analogues is very different from the highly charged polar side chain of both CDP-ME2P and the first generation fluorescent inhibitors. This suggests that the important binding interaction for these

compounds is with the cytidine binding pocket, and not with the phosphate binding site.⁷⁶

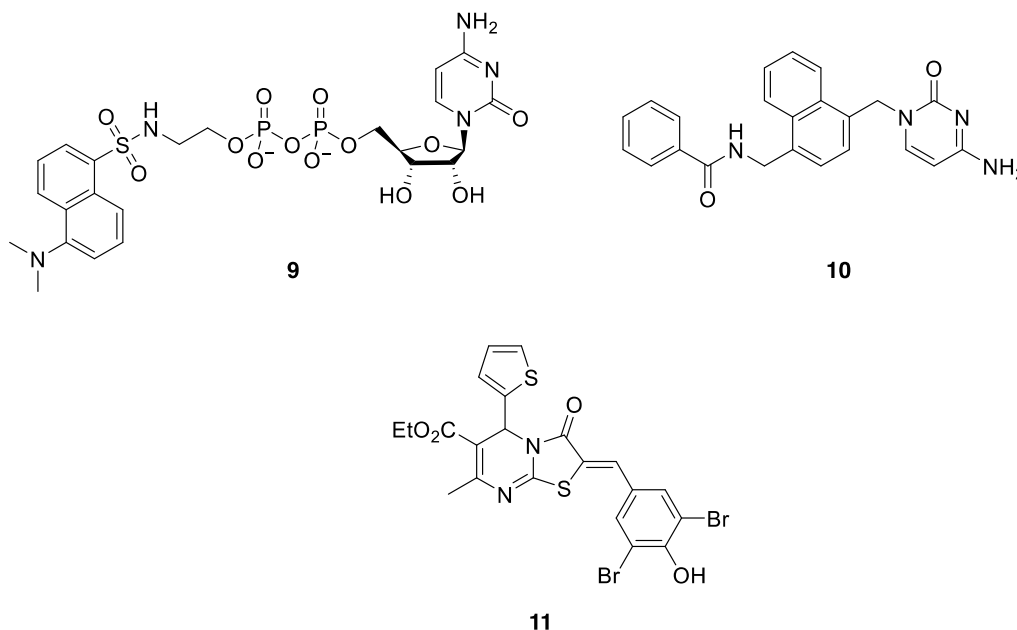


Figure 2.11. The first (**9**), second (**10**) and third (**11**) generation analogues designed to inhibit IspF

As a result of this research, a screening campaign of a large library of compounds aided in the identification of a thiazolopyrimidine derivative (**11**), which displayed single digit micromolar activity against both *P. falciparum* and *M. tuberculosis*. At each stage of this research, the drug compounds developed improved in efficacy as a result of a more in depth understanding of the enzyme's structure, highlighting just how useful X-ray crystallisation studies can be in supporting drug design.⁷⁷

Inhibitors of IspG and IspH

There are fewer known inhibitors of the last two enzymes in the pathway, possibly due to the structure and function of these iron-sulfur proteins only recently being established, and with many questions regarding their mechanism of action still unanswered.

There is little literature precedence for inhibitors of IspG; however, Oldfield *et al.* recently published their results from spectroscopic investigations on the mechanism of action of IspG. As part of this study they identified an alkyne compound, propargyl diphosphate (**12**), as being a good inhibitor (750 nM) of IspG, potentially through the formation of a metallacycle with the iron-sulfur cluster.⁷⁸

Oldfield *et al.* also applied these spectroscopic techniques to IspH, and identified the mechanism of action of a group of pyridine inhibitors of IspH. The most potent of these compounds (**13**) had an IC₅₀ value of 9.1 μM against *A. aeolicus* and was found to exert its inhibitory effect by directly binding to the unique fourth iron ion in the [4Fe-4S] cluster, via a Lewis acid/base mechanism. These results suggest that the development of compounds containing strong Lewis bases e.g. imidazole analogues, could result in a more potent inhibitory effect.⁷⁹

The group also discovered that alkyne diphosphates not only inhibit IspG but IspH as well, and published their findings on the first group of potent inhibitors of IspH. The most active compound (**14**) had an IC₅₀ value of 0.45 μM vs. the enzyme, and again was thought to exert its mechanism of action through the formation of a metallacycle with iron-sulfur redox centre. This data suggests that metallacycles could act as reactive intermediates in both IspG and IspH catalysis, and the compounds developed could potentially inhibit other iron-sulfur proteins.⁸⁰

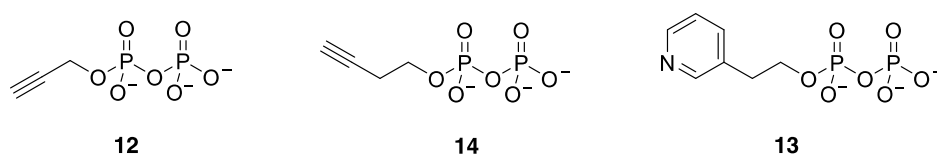


Figure 2.12. Inhibitors designed to target IspG and IspH

2.2 Why Target IspD?

IspD is an essential enzyme for isoprenoid biosynthesis in the *Plasmodium* parasite and is absent from mammalian cells; therefore, targeting this enzyme would impart selective toxicity to the parasite with fewer potential side effects for the host.^{81, 82} The enzyme has recently been genetically validated as a target for novel antimalarial compounds targeting *P. falciparum*, as the pathway is present in all intraerythrocytic stages of the parasite.⁸³ Further verification arises from the potent antimalarial activity of fosmidomycin, which targets another enzyme in the pathway, IspC.⁸⁴

There are fewer known inhibitors of IspD than some other steps in the pathway, thus providing huge scope for the development of novel molecules to inhibit this important biosynthetic step.³⁸ Furthermore, many of the inhibitors already designed to target this pathway are very polar and charged molecules with weak inhibitory activities. The design of a novel series of more potent inhibitors with drug-like properties would be advantageous.⁸⁵ Finally, the emergence of resistance to currently used therapies has created an urgent need for novel antimalarials, therefore this enzyme provides a promising target for the development of commercially viable therapies against the world's most significant parasite.⁸⁶

2.3 Aim

The aim of this project was to identify a new lead-template and explore structure-activity relationships (SAR) around this template by production of a library of novel compounds targeting the IspD enzyme. These inhibitors will be tested *in vitro* for their activity against both the *P. falciparum* IspD enzyme and whole cell 3D7, a chloroquine sensitive but sulfadoxine resistant strain of *P. falciparum*.

2.4 Lead Template Identification

In order to identify a lead template for this SAR study a high throughput screen (HTS), aided by chemoinformatics, was carried out. A computational chemistry approach was used to facilitate the selection of compounds to be screened for activity against the enzyme. The aim was to identify a subset of 5,000 compounds to be screened via HTS from a combined BioFocus library of roughly 500,000 compounds. This library was queried for compounds that fell into a number of different categories:

- Compounds with structural similarities to the natural substrates of IspD
- Compounds with structural similarities to the natural substrates of IspC
- Compounds with structural similarities to known IspD inhibitors $\leq 1 \mu\text{M}$
- Compounds with structural similarities to known IspC inhibitors $\leq 1 \mu\text{M}$
- Compounds containing metal chelating moieties
- Compounds containing bioisosteres of diphosphate

The rationale behind searching for compounds with structural similarities to the natural substrates for, and known inhibitors of, IspD is that structurally similar compounds are more likely to exhibit similar properties.⁸⁷ IspC was also included in this search as fosmidomycin, which is a substrate-like IspC inhibitor, has some activity against IspD.⁸⁸ Furthermore, spill over activity against a second enzyme could help to delay the development of resistance.⁸⁹ Metal chelators were also included in the search due to the presence of a divalent cation, believed to be Mg^{2+} , in the active site that helps to bind and orientate the natural substrates as well as assisting in neutralising the large amount of negative charge generated in the reaction.⁹⁰ Finally, compounds containing bioisosteres of diphosphate would be desirable as they could potentially mimic the chemical nature of MEP and/or CTP, whilst instilling a more drug-like nature to the compound.

The compounds were ranked for similarity using the Tanimoto co-efficient, which is a metric used for comparing the similarity and diversity of sample sets, where 1 is identical and lower values indicate increasing dissimilarity.⁹¹ For this set of compounds a threshold of >0.7 was applied. This resulted in the initial 500,000 structures being filtered to a combined subset of 23,000.

The molecules from the combined subset were then computationally docked into structures of both IspC and IspD and ranked according to their GOLDScore, which is a predictor of binding affinity.⁹² Finally, this combined subset was filtered for calculated solubility and compounds possessing a calculated logS (mol/L) > -3.5 were selected.

A total of 4,750 compounds fulfilled the above criteria, and a further 250 compounds with Tanimoto values between 0.2 and 0.4 were added in order to maximise diversity.⁹³ A *P. falciparum* IspD assay developed by our collaborators in Washington University was then transferred to BioFocus and the 5,000 selected compounds were screened and serialized into 5-point dose-response curves.

Following a filter for compound purity, a total of 54 compounds were identified that had a purity of greater than 70% and an IC₅₀ value of less than 20 μM against the enzyme. 10 potential chemotypes were identified and the most potent inhibitor (**15**), featuring a benzisothiazolinone core, had an IC₅₀ value of 480 nM.

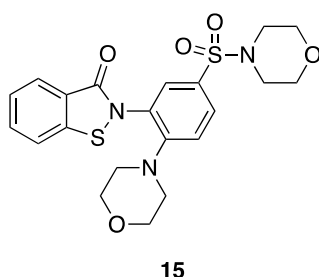
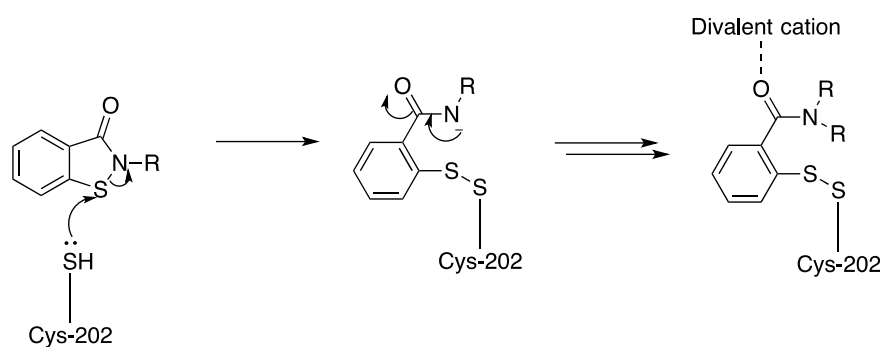


Figure 2.13. Structure of the most potent compound (**15**) identified from the HTS (480 nM)

A benzisothiazolinone core not only featured in the most potent molecule but also in many of the top 54 compounds identified from the HTS, highlighting the potential for the development of a SAR study. Furthermore, there was no previous literature precedence for the use of these compounds against enzymes of the MEP pathway. Therefore a benzisothiazolinone core formed the basis of the lead template for this project.

2.5 Proposed Mechanism of Action

Although a number of IspD crystal structures have been solved for *M. tuberculosis* and various strains of *E. coli*, a crystal structure for *PflspD* has yet to be determined.³⁸ Therefore, an IspD homology model was developed from *E. coli* IspD.⁹⁴ Molecular docking showed that IspD inhibitors bind within the CTP-binding pocket of the enzyme, which places the S-N bond at the core of the benzisothiazolinone close to a cysteine residue (Cys-202). It was therefore proposed that the thiol group of this active site cysteine could interact with the sulfur atom of the benzisothiazolinone core, forming a covalent disulfide adduct (Scheme 2.16).



Scheme 2.16. Proposed mechanism of covalent inhibition between benzisothiazolinone and a key cysteine residue in the active site

The negative charge that is generated during the benzisothiazolinone ring opening could be neutralised through interaction with a magnesium cation that has been proposed to be present in the IspD active site (Figure 2.15).⁹⁵ This covalent interaction would block the natural substrate from binding and result in inhibition of this crucial step in the MEP pathway.

Evidence to support this theory comes from the significant decrease in activity that is observed when a mutation of Cys-202 to Ala-202 is introduced. This decrease in activity could be a consequence of the loss of covalent adducts, or an altered fit of the inhibitor within the CTP-binding pocket.

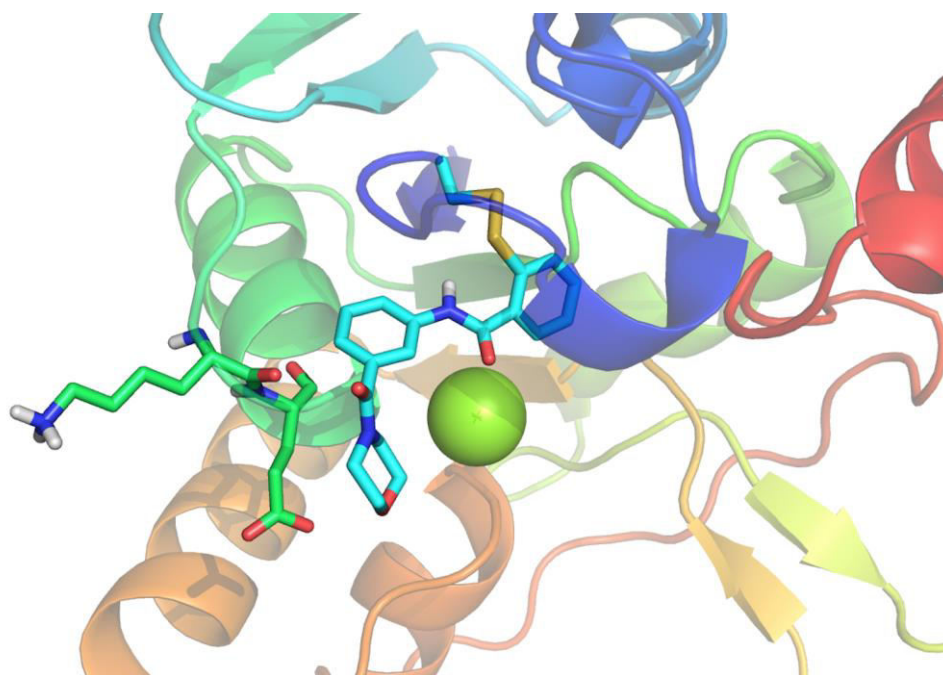


Figure 2.15. Illustration of IspD homology model with benzisothiazolinone **1** (see Chapter 3) docked into the active site. Protein is represented as coloured cartoon; ligand shown as stick structure: C-light blue, N-dark blue, O-red, H- grey; Mg²⁺ depicted as green sphere. Disulfide adduct is depicted in yellow and the resulting negative charge on oxygen is neutralised through interaction with Mg²⁺. Image created using PyMOL Molecular Graphics System, Version 1.5.0.4

Covalent inhibition can further be confirmed if the apparent potency of the inhibitor increases over time, which is a direct result of an increasing number of irreversible interactions with the enzyme. This effect was indeed observed between benzisothiazolinone compounds and the *Pf*IspD homology model, whereas no significant change was observed between benzisothiazolinone compounds and the mutant IspD-C202A model (manuscript in preparation).

The proposed mechanism of action of these benzisothiazolinone compounds is covalent inhibition through the formation of a disulfide adduct with a key cysteine residue in the CTP binding pocket of IspD.

2.6 Structure-Activity Relationship Exploration

6 key modifications to the benzisothiazolinone core were proposed as part of this SAR exploration (Figure 2.14):

- Incorporation of a substituted mono-aryl moiety – to help identify the optimal side chain
- Modification of the A-ring – to probe the sterics and electronics around this portion of the molecule
- Incorporation of a pyridyl moiety into the A-ring – to increase the solubility of these compounds, increase the number of interactions within the active site through hydrogen bonding, enhance the reactivity of the S-N bond and provide a site for metal coordination.
- Incorporation of a pyridyl moiety into the B-ring – for the same reasons as above and to also observe the difference in activity by changing the position of the pyridyl moiety.
- Incorporation of a CH₂ linker – to allow for greater flexibility and rotation around this portion of the molecule.
- Replacement of the S-N bond with Se-N – organoseleniums are utilised in a number of drug compounds and the lower bond dissociation energy for Se-N compared to S-N could enhance biological activity.⁹⁶

The results of biological testing data would then allow for the effect of each modification on IspD inhibition to be compared.

The results of this SAR exploration are discussed in detail in Chapter III.

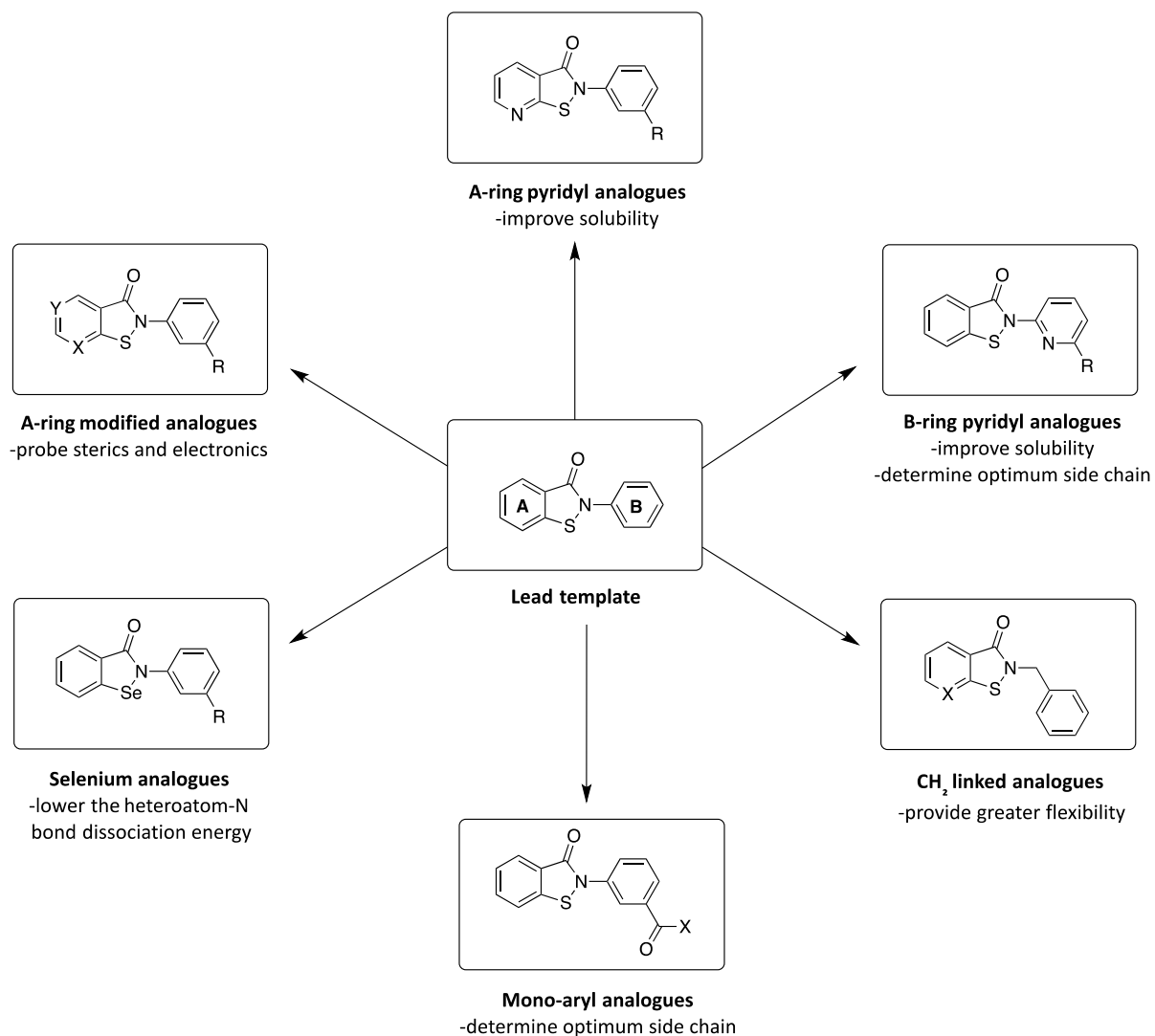


Figure 2.14. Overview of the SAR exploration around the lead template

2.7 References

1. H. K. Lichtenthaler, in *The Chemistry and Biology of Volatiles*, ed. A. Herrmann, Wiley, Hoboken, 1st edn, 2011, ch. 2, pp. 11-48.
2. E. Fahy, S. Subramaniam, H. A. Brown, C. K. Glass, A. H. Merrill, R. C. Murphy, C. R. H. Raetz, D. W. Russell, Y. Seyama, W. Shaw, T. Shimizu, F. Spener, G. van Meer, M. S. VanNieuwenhze, S. H. White, J. L. Witztum and E. A. Dennis, *J. Lipid Res.*, 2005, **46**, 839-862.
3. P. Goluszko and B. Nowicki, *Infect. Immun.*, 2005, **73**, 7791-7796.
4. J.A. Svoboda, in *Biochemistry and Function of Sterols*, ed. E. J. Parish and W. D. Nes, Taylor & Francis, Boca Raton, 1st edn, 1997, ch. 3, pp. 55-64.
5. F. Gleason, in *Plant Biochemistry*, Cram101, USA, 1st edn, 2016, ch. 7, 184-197 .
6. N. Theis and M. Lerda, *Int. J. Plant Sci.*, 2003, **164**, S93-S102.
7. S. Kaur, R. Dayal, V. K. Varshney and J. P. Bartley, *Planta Med.*, 2001, **67**, 883-886.
8. D. L. Klayman, *Science*, 1985, **228**, 1049.
9. P. Cardol, *Biochim. Biophys. Acta*, 2011, **1807**, 1390-1397.
10. T. Gabaldón, D. Rainey and M. A. Huynen, *J. Mol. Biol.*, 2005, **348**, 857-870.
11. J. Gershenzon and N. Dudareva, *Nat. Chem. Biol.*, 2007, **3**, 408-414.
12. B. Zhang, K. M. Watts, D. Hodge, L. M. Kemp, D. A. Hunstad, L. M. Hicks and A. R. Odom, *Biochemistry*, 2011, **50**, 3570-3577.
13. E. D. Beytia and J. W. Porter, *Annu. Rev. Biochem.*, 1976, **45**, 113-142.
14. C. Stancu and A. Sima, *J. Cell Mol. Med.*, 2001, **5**, 378-387.
15. W. N. Hunter, *J. Biol. Chem.*, 2007, **282**, 21573-21577.
16. M. Rohmer, *Nat. Prod. Rep.*, 1999, **16**, 565-574.
17. V. S. Dubey, R. Bhalla and R. Luthra, *J. Biosci.*, 2003, **28**, 637-646.
18. E. Maréchal and M.-F. Cesbron-Delauw, *Trends Plant Sci.*, 2001, **6**, 200-205.
19. L. Imlay and A. R. Odom, *Curr. Clin. Microbiol. Rep.*, 2014, **1**, 37-50.
20. S. Heuston, M. Begley, C. G. M. Gahan and C. Hill, *Microbiology*, 2012, **158**, 1389-1401.
21. G. Lenaz and M. L. Genova, *Biochim. Biophys. Acta*, 2009, **1787**, 563-573.
22. B. Søballe and R. K. Poole, *Microbiology*, 1999, **145**, 1817-1830.
23. A. Helenius and M. Aebi, *Science*, 2001, **291**, 2364-2369.

24. J. W. J. Beulens, S. L. Booth, E. G. H. M. van den Heuvel, E. Stoecklin, A. Baka and C. Vermeer, *Br. J. Nut.*, 2013, **110**, 1357-1368.
25. A. R. Odom, *PLoS Pathog*, 2011, **7**, 10.1371/journal.ppat.1002323.
26. H. J. Painter, J. M. Morrissey, M. W. Mather and A. B. Vaidya, *Nature*, 2007, **446**, 88-91.
27. W. A. Maltese, *Fed. Am. Soc. Ex. Biol.*, 1990, **4**, 3319-3328.
28. R. Tonhosolo, F. L. D'Alexandri, V. V. de Rosso, M. L. Gazarini, M. Y. Matsumura, V. J. Peres, E. F. Merino, J. M. Carlton, G. Wunderlich, A. Z. Mercadante, E. A. Kimura and A. M. Katzin, *J. Biol. Chem.*, 2009, **284**, 9974-9985.
29. D. A. Bochar, J. Freisen, C. V. Stauffacher and V. W. Rodwell, in *Comprehensive Natural Products Chemistry*, eds. K. Nakanishi and O. Meth-Cohn, Pergamon, Oxford, 1999, pp. 15-44.
30. H. Rudney and J. J. Ferguson, *J. Biol. Chem.*, 1959, **234**, 1076-1080.
31. H. M. Miziorko and M. D. Lane, *J. Biol. Chem.*, 1977, **252**, 1414-1420.
32. E. S. Istvan and J. Deisenhofer, *Science*, 2001, **292**, 1160-1164.
33. A. Endo, *J. Lipid Res.*, 1992, **33**, 1569-1582.
34. S. Dhe-Paganon, J. Magrath and R. H. Abeles, *Biochemistry*, 1994, **33**, 13355-13362.
35. K. Treharne, E. Mercer and T. Goodwin, *Biochem. J.*, 1966, **99**, 239-245.
36. T. J. Bach and H. K. Lichtenthaler, *Z. Naturforsch.*, 1982, **37**, 46-50.
37. K. Kreuz and H. Kleinig, *Planta*, 1981, **153**, 578-281.
38. I. Hale, P. M. O'Neill, N. G. Berry, A. Odom and R. Sharma, *MedChemComm*, 2012, **3**, 418-433.
39. S. Handa, *FEBS Open Bio*, 2013, **3**, 124-129.
40. M. Rohmer, M. Seemann, S. Horbach, S. Bringer-Meyer and H. Sahm, *J. Am. Chem. Soc.*, 1996, **118**, 2564-2566.
41. H. Jomaa, J. Wiesner, S. Sanderbrand, B. Altincicek, C. Weidemeyer, M. Hintz, I. Turbachova, M. Eberl, J. Zeidler and H. K. Lichtenthaler, *Science*, 1999, **285**, 1573-1576.
42. S. Steinbacher, J. Kaiser, W. Eisenreich, R. Huber, A. Bacher and F. Rohdich, *J. Biol. Chem.*, 2003, **278**, 18401-18407.
43. P. J. Proteau, *Bioorg. Chem.*, 2004, **32**, 483-493.

44. D. Arigoni, S. Sagner, C. Latzel, W. Eisenreich, A. Bacher and M. H. Zenk, *Proc. Natl. Acad. Sci.*, 1997, **94**, 10600-10605.
45. T. Grawert, M. Groll, F. Rohdich, A. Bacher and W. Eisenreich, *Cell. Mol. Life Sci.*, 2011, **68**, 3797-3814.
46. S. B. Richard, A. M. Lillo, C. N. Tetzlaff, M. E. Bowman, J. P. Noel and D. E. Cane, *Biochemistry*, 2004, **43**, 12189-12197.
47. S. B. Richard, M. E. Bowman, W. Kwiatkowski, I. Kang, C. Chow, A. M. Lillo, D. E. Cane and J. P. Noel, *Nat. Struct. Mol. Biol.*, 2001, **8**, 641-648.
48. H. Lüttgen, F. Rohdich, S. Herz, J. Wungsintaweekul, S. Hecht, C. A. Schuhr, M. Fellermeier, S. Sagner, M. H. Zenk, A. Bacher and W. Eisenreich, *Proc. Natl. Acad. Sci.*, 2000, **97**, 1062-1067.
49. S. Herz, J. Wungsintaweekul, C. A. Schuhr, S. Hecht, H. Lüttgen, S. Sagner, M. Fellermeier, W. Eisenreich, M. H. Zenk, A. Bacher and F. Rohdich, *Proc. Natl. Acad. Sci.*, 2000, **97**, 2486-2490.
50. M. Seemann, B. Tse Sum Bui, M. Wolff, M. Miginiac-Maslow and M. Rohmer, *FEBS Lett.*, 2006, **580**, 1547-1552.
51. M. Seemann, B. Tse Sum Bui, M. Wolff, D. Tritsch, N. Campos, A. Boronat, A. Marquet and M. Rohmer, *Angew. Chem. Int. Ed.*, 2002, **41**, 4337-4339.
52. F. Rohdich, S. Hecht, K. Gärtner, P. Adam, C. Krieger, S. Amslinger, D. Arigoni, A. Bacher and W. Eisenreich, *Proc. Natl. Acad. Sci.*, 2002, **99**, 1158-1163.
53. T. Gräwert, I. Span, A. Bacher and M. Groll, *Angew. Chem. Int. Ed.*, 2010, **49**, 8802-8809.
54. T. Masini, B. S. Kroezen and A. K. H. Hirsch, *Drug Discov. Today*, 2013, **18**, 1256-1262.
55. M. B. Cassera, F. C. Gozzo, F. L. D'Alexandri, E. F. Merino, H. A. del Portillo, V. J. Peres, I. C. Almeida, M. N. Eberlin, G. Wunderlich, J. Wiesner, H. Jomaa, E. A. Kimura and A. M. Katzin, *J. Biol. Chem.*, 2004, **279**, 51749-51759.
56. A. R. Odom and W. C. Van Voorhis, *Mol. Biochem. Parasitol.*, 2010, **170**, 108-111.
57. D. J. Huggins, W. Sherman and B. Tidor, *J. Med. Chem.*, 2012, **55**, 1424-1444.
58. M. Rodriguez-Concepcion, *Curr. Pharm. Des.*, 2004, **10**, 2391-2400.
59. K. Lichtenthaler Hartmut, J. Zeidler, J. Schwender and C. Müller, *Z. Naturforsch.*, 2000, **55**, 305-313.

60. V. J. J. Martin, D. J. Pitera, S. T. Withers, J. D. Newman and J. D. Keasling, *Nat. Biotech.*, 2003, **21**, 796-802.
61. Y. Matsue, H. Mizuno, T. Tomita, T. Asami, M. Nishiyama and T. Kuzuyama, *J. Antibiot.*, 2010, **63**, 583-588.
62. J. Zeidler, J. Schwender, C. Mueller and H. K. Lichtenthaler, *Biochem. Soc. Trans.*, 2000, **28**, 796-798.
63. J. Mao, H. Eoh, R. He, Y. Wang, B. Wan, S. G. Franzblau, D. C. Crick and A. P. Kozikowski, *Bioorg. Med. Chem. Lett.*, 2008, **18**, 5320-5323.
64. E. Iguchi, M. Okuhara, M. Kohsaka, H. Aoki and H. Imanaka, *J. Antibiot.*, 1980, **33**, 19-23.
65. T. Murakawa, H. Sakamoto, S. Fukada, T. Konishi and M. Nishida, *Antimicrob. Agents Chemother.*, 1982, **21**, 224-230.
66. B. Lell, R. Ruangweerayut, J. Wiesner, M. A. Missinou, A. Schindler, T. Baranek, M. Hintz, D. Hutchinson, H. Jomaa and P. G. Kremsner, *Antimicrob. Agents Chemother.*, 2003, **47**, 735-738.
67. H. Jomaa, J. Wiesner, S. Sanderbrand, B. Altincicek, C. Weidemeyer, M. Hintz, I. Türbachova, M. Eberl, J. Zeidler, H. K. Lichtenthaler, D. Soldati and E. Beck, *Science*, 1999, **285**, 1573-1576.
68. S. Borrmann, A. A. Adegnika, P.-B. Matsiegui, S. Issifou, A. Schindler, D. P. Mawili-Mboumba, T. Baranek, J. Wiesner, H. Jomaa and P. G. Kremsner, *J. Infect. Dis.*, 2004, **189**, 901-908.
69. M. Lanaspá, C. Moraleda, S. Machevo, R. González, B. Serrano, E. Macete, P. Cisteró, A. Mayor, D. Hutchinson, P. G. Kremsner, P. Alonso, C. Menéndez and Q. Bassat, *Antimicrob. Agents Chemother.*, 2012, **56**, 2923-2928.
70. L. Kuntz, D. Tritsch, C. Grosdemange-Billiard, A. Hemmerlin, A. Willem, T. J. BACH and M. Rohmer, *Biochem. J.*, 2005, **386**, 127-135.
71. A. M. Lillo, C. N. Tetzlaff, F. J. Sangari and D. E. Cane, *Bioorg. Med. Chem. Lett.*, 2003, **13**, 737-739.
72. M. C. Witschel, H. W. Höffken, M. Seet, L. Parra, T. Mietzner, F. Thater, R. Niggeweg, F. Röhl, B. Illarionov, F. Rohdich, J. Kaiser, M. Fischer, A. Bacher and F. Diederich, *Angew. Chem. Int. Ed.*, 2011, **50**, 7931-7935.

73. C. M. Crane, A. K. H. Hirsch, M. S. Alpey, T. Sgraja, S. Lauw, V. Illarionova, F. Rohdich, W. Eisenreich, W. N. Hunter, A. Bacher and F. Diederich, *ChemMedChem*, 2008, **3**, 91-101.
74. A. K. H. Hirsch, M. S. Alpey, S. Lauw, M. Seet, L. Barandun, W. Eisenreich, F. Rohdich, W. N. Hunter, A. Bacher and F. Diederich, *Org. Biomol. Chem.*, 2008, **6**, 2719-2730.
75. C. M. Crane, J. Kaiser, N. L. Ramsden, S. Lauw, F. Rohdich, W. Eisenreich, W. N. Hunter, A. Bacher and F. Diederich, *Angew. Chem. Int. Ed.*, 2006, **45**, 1069-1074.
76. C. Baumgartner, C. Eberle, F. Diederich, S. Lauw, F. Rohdich, W. Eisenreich and A. Bacher, *Helv. Chim. Acta*, 2007, **90**, 1043-1068.
77. J. G. Geist, S. Lauw, V. Illarionova, B. Illarionov, M. Fischer, T. Gräwert, F. Rohdich, W. Eisenreich, J. Kaiser, M. Groll, C. Scheurer, S. Wittlin, J. L. Alonso-Gómez, W. B. Schweizer, A. Bacher and F. Diederich, *ChemMedChem*, 2010, **5**, 1092-1101.
78. W. Wang, J. Li, K. Wang, C. Huang, Y. Zhang and E. Oldfield, *Proc. Natl. Acad. Sci.*, 2010, **107**, 11189-11193.
79. W. Wang, J. Li, K. Wang, T. I. Smirnova and E. Oldfield, *J. Am. Chem. Soc.*, 2011, **133**, 6525-6528.
80. K. Wang, W. Wang, J.-H. No, Y. Zhang, Y. Zhang and E. Oldfield, *J. Am. Chem. Soc.*, 2010, **132**, 6719-6727.
81. W. Wu, Z. Herrera, D. Ebert, K. Baska, S. H. Cho, J. L. DeRisi and E. Yeh, *Antimicrob. Agents Chemother.*, 2015, **59**, 356-364.
82. S. D. Fontaine, B. Spangler, J. Gut, E. M. W. Lauterwasser, P. J. Rosenthal and A. R. Renslo, *ChemMedChem*, 2015, **10**, 47-51.
83. L. S. Imlay, C. M. Armstrong, M. C. Masters, T. Li, K. E. Price, R. L. Edwards, K. M. Mann, L. X. Li, C. L. Stallings, N. G. Berry, P. M. O'Neill and A. R. Odom, *ACS Infect. Dis.*, 2015, **1**, 157-167.
84. R. K. Dhiman, M. L. Schaeffer, A. M. Bailey, C. A. Testa, H. Scherman and D. C. Crick, *J. Bacteriol.*, 2005, **187**, 8395-8402.
85. L. Di and E. H. Kerns, in *Drug-Like Properties: Concepts, Structure Design and Methods from ADME to Toxicity Optimization*, Elsevier Science, Amsterdam, 2nd edn, 2015, ch. 2, pp. 5-13.
86. K. T. Andrews, G. Fisher and T. S. Skinner-Adams, *Int. J. Parasitol. Drugs Drug Resist.*, 2014, **4**, 95-111.

87. A. A. Alex and R. I. Storer, in *Metabolism, Pharmacokinetics, and Toxicity of Functional Groups: Impact of the Building Blocks of Medicinal Chemistry in ADMET*, ed. D. A. Smith, Royal Society of Chemistry, Cambridge, 1st edn, 2010, ch. 1, pp. 1-61.
88. F. S. Buckner, N. C. Waters and V. M. Avery, *Int. J. Parasitol. Drugs Drug Resist.*, 2012, **2**, 230-235.
89. K. R. Sakharkar, M. K. Sakharkar and R. Chandra, in *Post-Genomic Approaches in Drug and Vaccine Development*, 1st edn, River Publishers, San Francisco, 2015, vol. 5, ch. 1, 1-22.
90. J. Anastassopoulou and T. Theophanides, in *Bioinorganic Chemistry: An Inorganic Perspective of Life*, ed. D. P. Kessissoglou, 1st edn, Springer Netherlands, Dordrecht, ch. 17, pp. 209-218.
91. D. Bajusz, A. Rácz and K. Héberger, *J. Cheminform.*, 2015, **7**, 1-13.
92. CCDC: Support and Resources, <https://www.ccdc.cam.ac.uk/support-and-resources/support/case/?caseid=5d1a2fc0-c93a-49c3-a8e2-f95c472dcff0>, (accessed December 2016).
93. V. J. Gillet, in *Molecular Diversity in Drug Design*, ed. P. M. Dean and R. A. Lewis, Springer, New York, 1999, ch.2, pp. 43-66.
94. L. A. Kelley and M. J. E. Sternberg, *Nat. Protoc.*, 2009, **4**, 363-371.
95. N. H. William, *Curr. Top. Med. Chem.*, 2011, **11**, 2048-2059.
96. S. W. May, *Expert Opin. Investig. Drugs*, 1999, **8**, 1017-1030.

Chapter III

IspD Inhibitors

Table of Contents

3.1 Introduction	81
3.2 Mono-aryl Analogues	82
3.2.1 Rationale	82
3.2.2 Synthesis	83
3.2.3 Results	94
3.2.4 Conclusion	95
3.3 A-ring Modification	96
3.3.1 Rationale	96
3.3.2 Synthesis	97
3.3.2.1 2-Phenylbenzo[<i>d</i>]isothiazol-3(2 <i>H</i>)-one	97
3.3.2.2 2-Phenylisothiazolo[5,4- <i>b</i>]pyridin-3(2 <i>H</i>)-one	99
3.3.2.3 5-Chloro-2-phenylbenzo[<i>d</i>]isothiazol-3(2 <i>H</i>)-one	101
3.3.2.4 5-Methoxy-2-phenylbenzo[<i>d</i>]isothiazol-3(2 <i>H</i>)-one	103
3.3.2.5 7-Methoxy-2-phenylbenzo[<i>d</i>]isothiazol-3(2 <i>H</i>)-one	105
3.3.2.6 7-Nitro-2-phenylbenzo[<i>d</i>]isothiazol-3(2 <i>H</i>)-one	106
3.3.3 Results	108
3.3.4 Conclusion	110
3.4 A-ring Pyridyls	111
3.4.1 Rationale	111
3.4.2 Synthesis	112
3.4.3 Results	116
3.4.4 Conclusion	117
3.5 B-ring Pyridyls	118
3.5.1 Rationale	118
3.5.2 Synthesis	118
3.5.2.1 Amine solubilising groups	120
3.5.2.2 Amide solubilising side chains	121
3.5.3 Results	123
3.5.4 Conclusion	125

3.6 CH₂ Linked Compounds	125
3.6.1 Rationale	125
3.6.2 Benzisothiazolinone CH ₂ linked analogues	126
3.6.2.1 Synthesis	126
3.6.2.2 Results	128
3.6.3 Pyridoisothiazolone CH ₂ linked analogues	129
3.6.3.1 Synthesis	129
3.6.3.2 Results	134
3.6.4 5-OMe CH ₂ linked analogues	136
3.6.4.1 Synthesis	136
3.6.4.2 Results	137
3.6.5 Conclusion	138
3.7 Selenium analogues	139
3.7.1 Rationale	139
3.7.2 Synthesis	140
3.7.3 Results	143
3.7.4 Conclusion	146
3.8 Summary	147
3.9 Experimental	150
3.9.1 General procedures	151
3.9.2 Experimental for compounds 1-75	155
3.9 References	203

3.1 Introduction

This chapter will discuss the rationale behind the development of each series in this structure-activity relationship study, which is highlighted below in Figure 3.1. The synthetic routes to each analogue will be reviewed in detail and the resulting *in vitro* and *in vivo* testing data will be analysed and compared across each series.

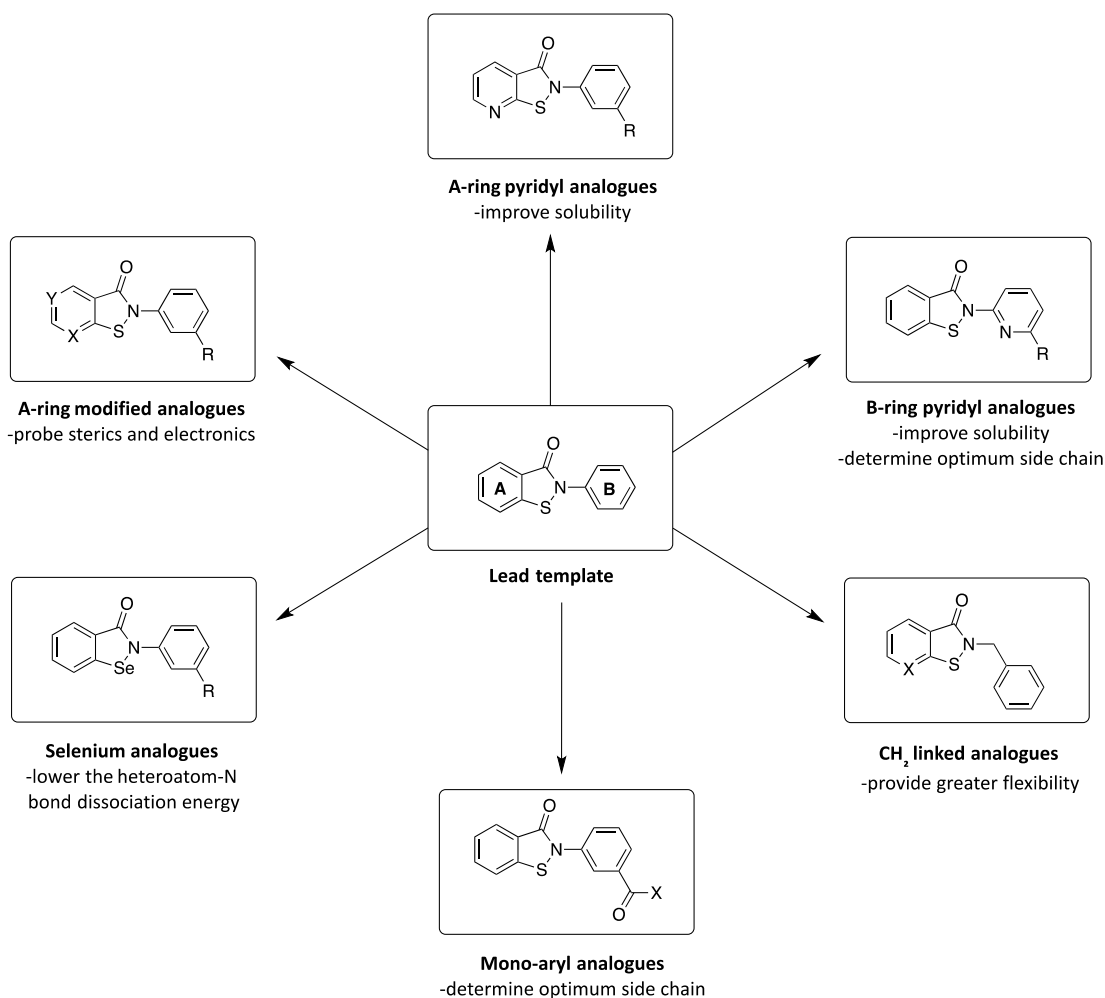


Figure 3.1. Overview of the SAR exploration around the lead template

3.2 Mono-aryl Analogues

3.2.1 Rationale

This small series of mono-aryl compounds (Figure 3.2) was initially designed in order to help identify the optimum side chain for the benzisothiazolinone core. The effects of bi-aryl, CH₂ linked and pyridyl-substituted side chains will be discussed later in this chapter.

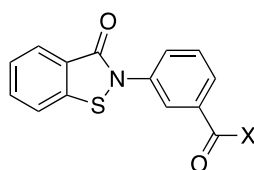


Figure 3.2. Template designed for the mono-aryl series
(where X = OH, OMe and morpholine)

Of particular interest was the morpholine amide compound, **1** (Figure 3.3), which incorporates a mono-aryl functionality along with a morpholine solubilising group in the side chain. Morpholines are at the core of many biologically active compounds and are widely distributed throughout natural products.¹ The morpholine group not only aids aqueous solubility but can also increase the binding affinity of drug molecules. This occurs through donor-acceptor type interactions via the oxygen atom.² Amide linkers are also useful in drug compounds as they can be used as a handle to introduce a vast array of diversity as well as improving aqueous solubility (as a result of the dipoles created in the carbonyl C=O and amide C-N bonds).³ Amides are also hydrolysed slowly *in vivo* and are therefore commonly used to develop drugs with longer half-lives.⁴

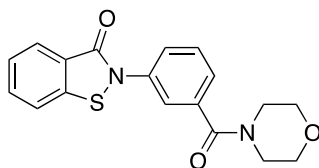
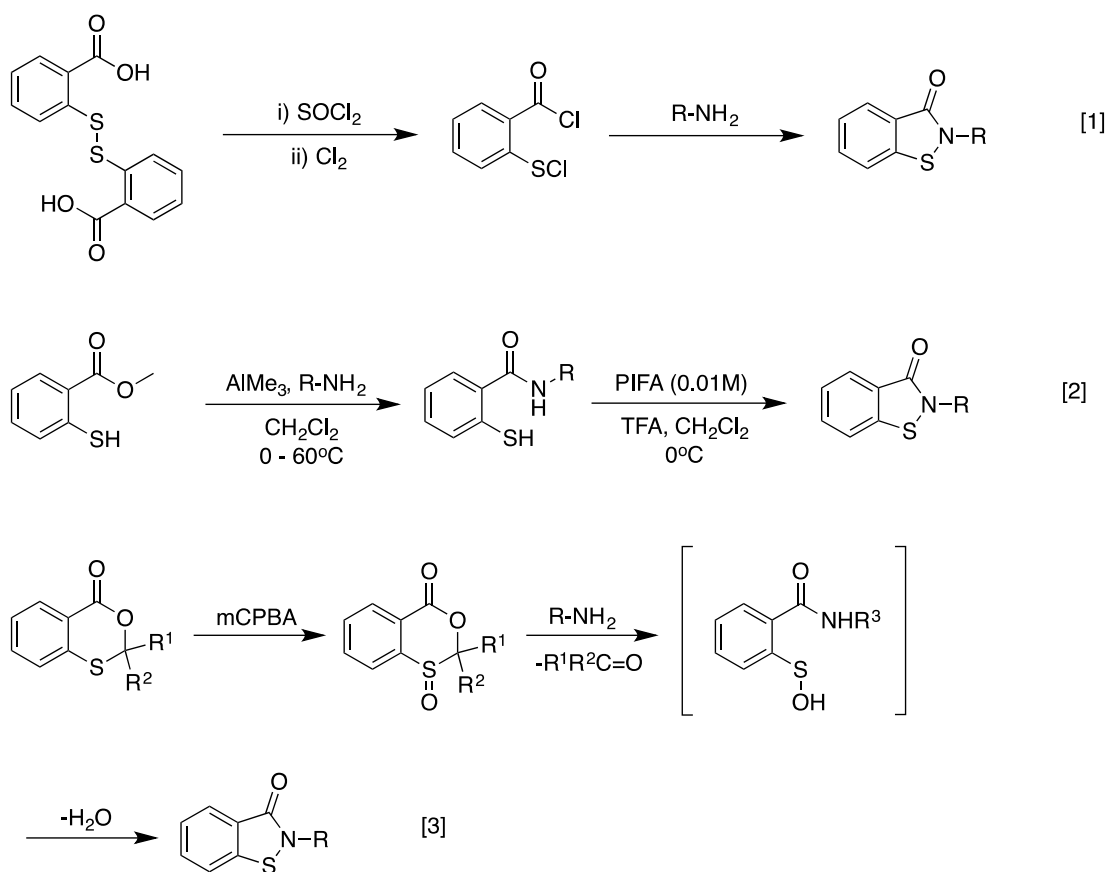


Figure 3.3. 2-(3-(Morpholine-4-carbonyl)phenyl)benzo[*d*]isothiazol-3(2*H*)-one (**1**),
the morpholine amide compound designed for this SAR

The synthesis of this first series of compounds, also allowed for the exploration of a number of routes in which to generate the benzisothiazolinone core.

3.2.2 Synthesis

The first consideration in the synthesis of these compounds was the method used to construct the benzisothiazolinone core. There are a variety of different routes to achieve this, and a number of these are outlined in Scheme 3.1.



Scheme 3.1. A number of common routes used to synthesise benzisothiazolinone compounds

A classic benzisothiazolinone synthesis [1] uses thionyl chloride and chlorine gas to generate a 2-chlorothiobenzoyl chloride intermediate from 2,2'-dithiodibenzic acid. Quenching this intermediate with the desired amine

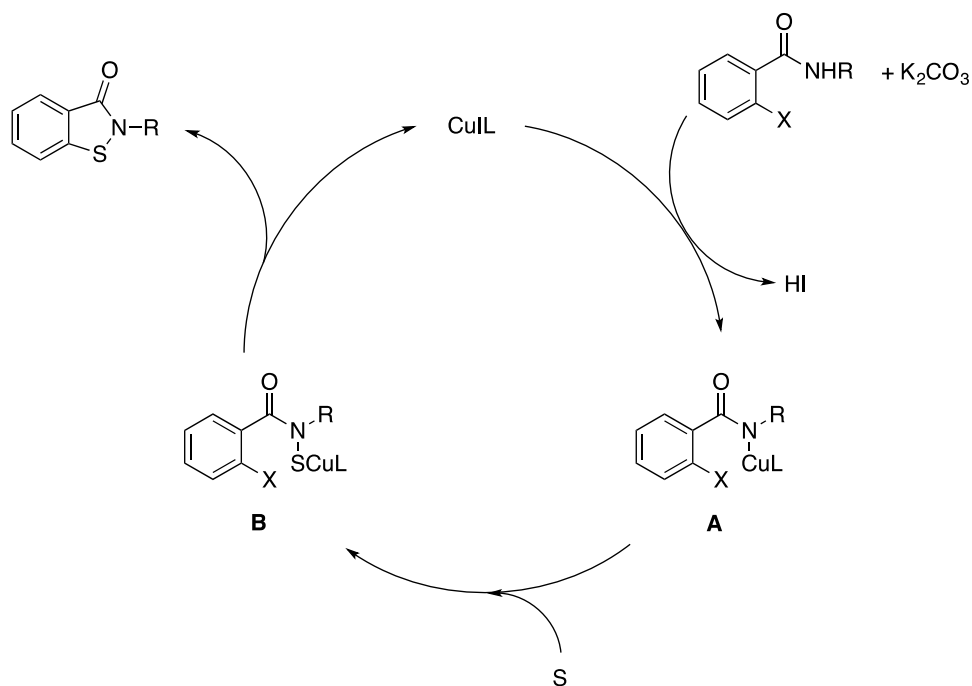
produces the ring-closed product.⁵ Similar chemistry can also be carried out using bromine as a replacement for chlorine.⁶

An alternative method [2] generates a *N*-acylnitrenium intermediate from the desired amide of methyl thiosalicylate, using a hypervalent iodine reagent – [Bis(trifluoroacetoxy)iodo]benzene (PIFA). The *N*-acylnitrenium ion is a powerful electrophile and readily undergoes intramolecular cyclisation, forming the S-N bond.⁷

Finally, 1,3-benzoxathiin-4-one 1-oxides [3] can be used to form *N*-substituted benzisothiazolinones in a multi-step ring transformation, which requires an oxidising agent, such as *m*CPBA, and an amine.⁸

The drawbacks of these methods are multi-step syntheses and the use of highly toxic and/or corrosive reagents. It was therefore decided that a copper-mediated route (Scheme 3.2), outlined by Bhakuni *et al.*, would be used in the first instance. This procedure has the advantage of using much milder reagents and is tolerant of a wide range of functional groups. Furthermore, this synthesis is carried out in a one-pot procedure, which helps to reduce both time and cost.⁹

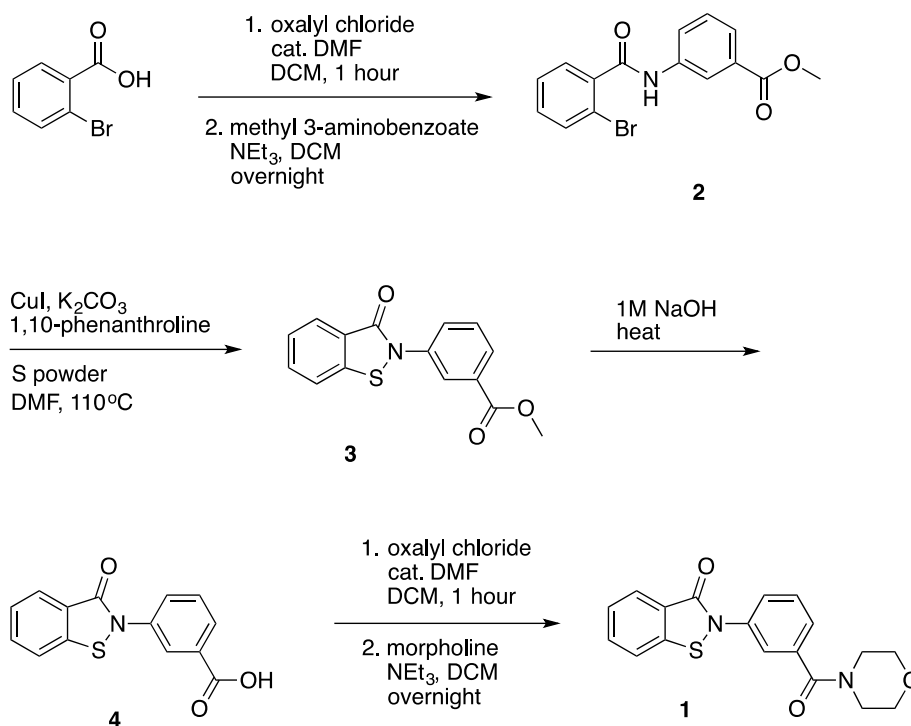
This method sees 2-halo-arylamides converted to *N*-substituted benzisothiazolinones using a copper iodide catalyst, a ligand, a base and sulfur powder. The proposed mechanism (Scheme 3.2) proceeds via a copper-amide complex. It is proposed that a base facilitates the formation of the LCu-NR amide complex **A** (where L = ligand), due to the failure of benzisothiazolinone formation in its absence. Sulfur inserts into the LCu-NR bond to give intermediate **B**. An intramolecular reaction with the *ortho*-halogen, followed by reductive elimination, result in the formation of the benzisothiazolinone core and regeneration of the CuIL complex.



Scheme 3.2. The proposed mechanism of action for the copper iodide mediated synthesis of benzisothiazolinones (X = Cl, Br, I)

Adapted from: An efficient copper-mediated synthetic methodology for benzo[*d*]isothiazol-3(2*H*)-ones and related sulfur–nitrogen heterocycles, Bhakuni *et al.*

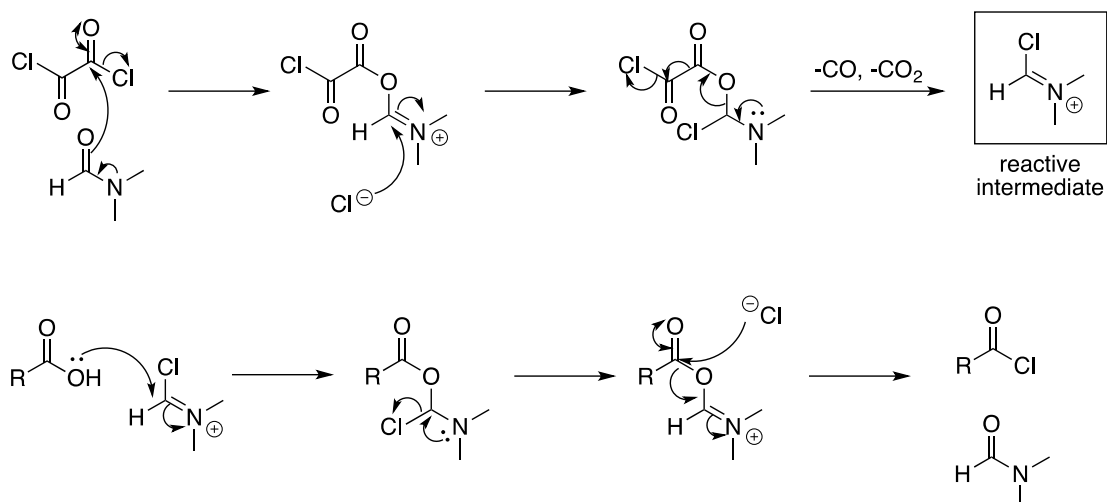
A synthetic pathway to generate the mono-aryl series was therefore devised, which utilised the copper-iodide mediated method for the key benzisothiazolinone forming step (Scheme 3.3).



Scheme 3.3. Initial pathway proposed for the synthesis of the mono-aryl series, which incorporates a copper iodide-mediated synthesis of the sulfur-nitrogen heterocycle

The first step in this pathway was the synthesis of the amide intermediate (**2**) from 2-bromobenzoic acid and methyl 3-aminobenzoate. 2-Bromobenzoic acid was first converted to a more reactive acid chloride intermediate using oxalyl chloride and a catalytic amount DMF. The acid chloride was then reacted with 3-aminobenzoate, without further purification, to give methyl 3-(2-bromobenzamido)benzoate (**2**) in an 81% yield.

Oxalyl chloride reacts with DMF to produce a highly electrophilic cationic intermediate, whilst liberating both carbon monoxide and carbon dioxide. This electrophilic intermediate reacts rapidly with a carboxylic acid, forming an acid chloride and regenerating DMF (Scheme 3.4).¹⁰



Scheme 3.4. The mechanism of acid chloride formation using oxalyl chloride and DMF
Adapted from: Organic Chemistry; Clayden, Greeves, Warren and Wothers

The copper iodide-mediated ring closure method was then employed to form the benzisothiazolinone core, using 1,10-phenanthroline as the ligand. 1,10-Phenanthroline is a popular choice of ligand in co-ordination chemistry due to its versatility in metal binding and the tightly bound complexes it forms (a result of the chelating nitrogen donors being pre-organised).¹¹ However, mass spectrometry identified the product to be the dimer of the starting material rather than the desired product (Figure 3.4).

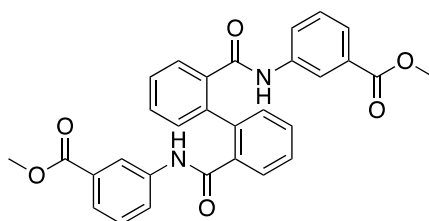
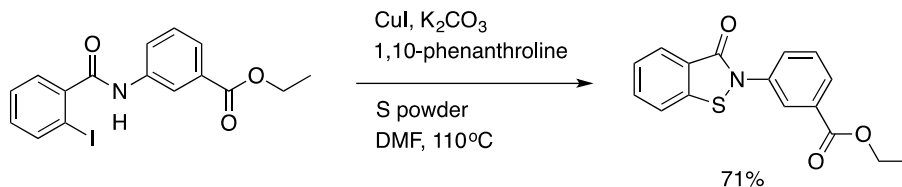


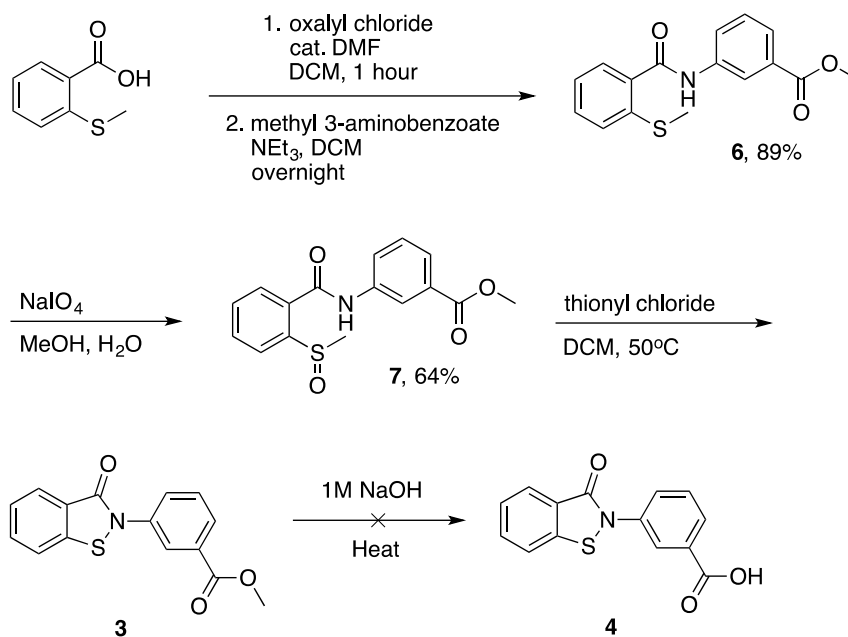
Figure 3.4. The major product obtained from the copper iodide-mediated synthesis of the benzisothiazolinone core. HRMS (CI, m/z) calculated for $[C_{15}H_{12}NO_3S]^+$ (M+H)⁺ 286.0538, found 509.5368

The original paper published by Bhakuni *et al.* quoted a 71% yield for the formation of the ethyl ester of compound **3**, using 2-iodobenzoic acid as starting material (Scheme 3.5).



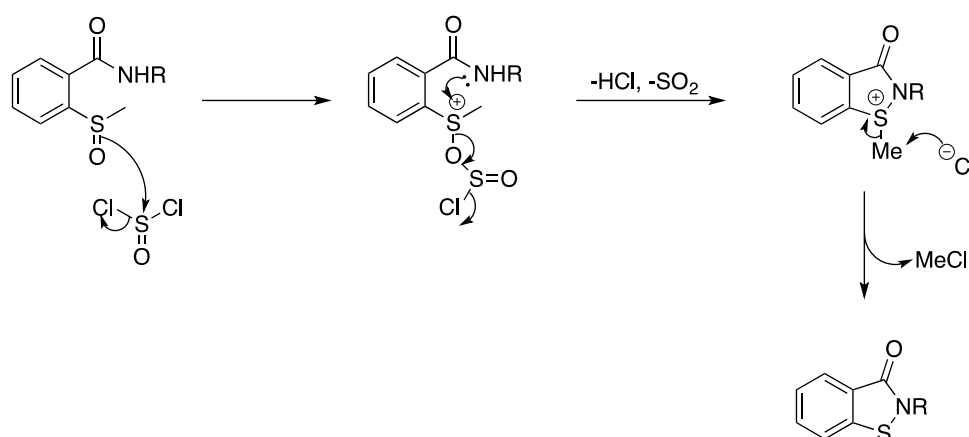
Scheme 3.5. Analogous ethyl ester synthesis by Bhakuni *et al.*

The synthesis was then repeated from 2-iodobenzoic acid in place of 2-bromobenzoic acid; however, the dimer product was obtained once more.⁹ An alternative route to generate the mono-aryl series was therefore devised from research published by Uchida and Kozuka (Scheme 3.6).



Scheme 3.6. An alternative pathway to generate the mono-aryl series of compounds, which was devised from work by Uchida and Kozuka

This research describes the synthesis of benzisothiazolinones by cyclisation of 2-(methylsulfinyl)benzamides with thionyl chloride.¹² The first step of this synthesis involved the formation of methyl 3-(2-(methylthio)benzamido)benzoate (**6**) from 2-(methylthio)benzoic acid and methyl 3-aminobenzoate. This was a straightforward amide formation and proceeded with an 89% yield. The sulfide (**6**) was then converted to the corresponding sulfoxide (**7**) using sodium periodate as the oxidising agent.¹³ Compound **7** was then treated with thionyl chloride in order to form the benzisothiazolinone core. A plausible mechanism for this transformation (Scheme 3.7) involves the formation of an acylaminosulfonium salt, before the S-methyl carbon is attacked by chloride to generate the benzisothiazolinone and chloromethane.



Scheme 3.7. The proposed mechanism for benzisothiazolinone synthesis between thionyl chloride and a sulfoxide

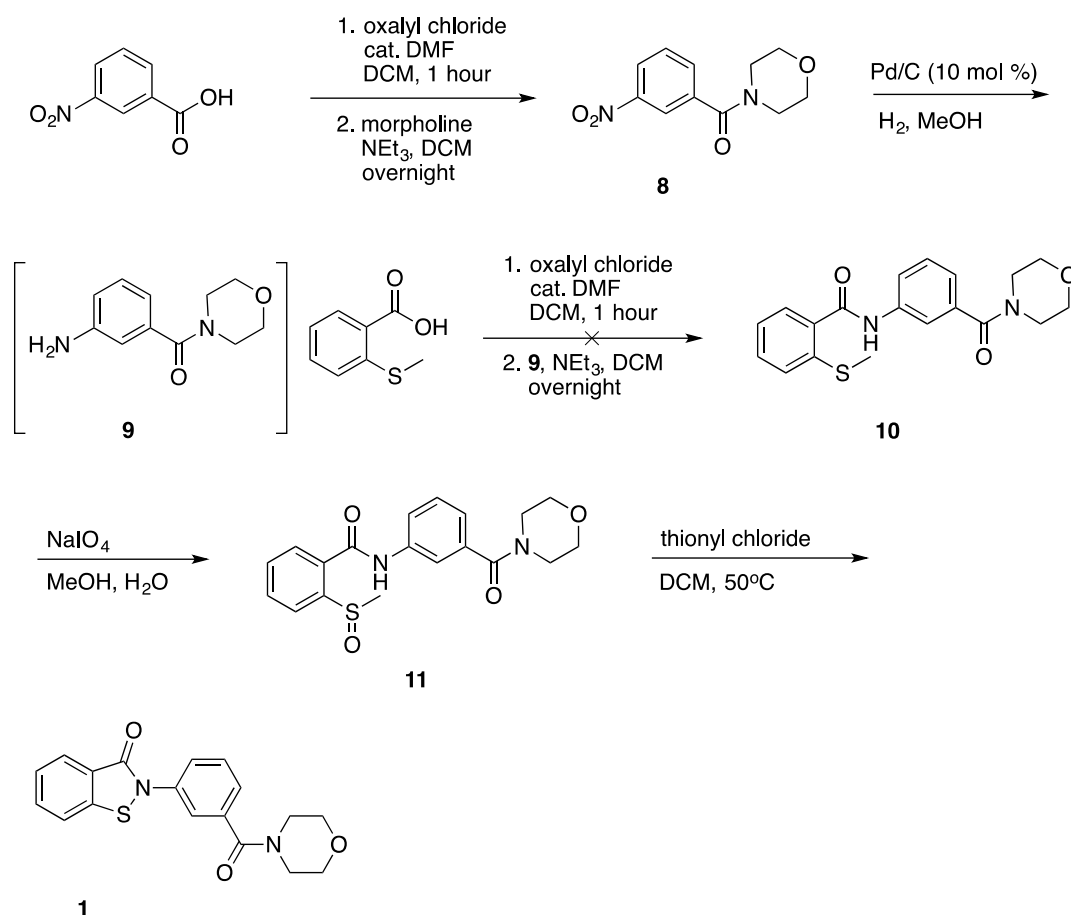
Adapted from: A Novel Route to 2-Substituted 1,2-Benzisothiazol-3(2N)-ones,
Uchida and Kozuka¹²

This step successfully formed methyl 3-(3-oxobenzod[isothiazol-2(3H)-yl)benzoate (**3**) in a 64% yield. The next step in the pathway involved hydrolysis of the ester (**3**), to the corresponding carboxylic acid (**4**). This transformation was initially carried out by warming compound **3** in 1M NaOH. Traditionally, a methyl ester is simple to hydrolyse; however, the presence of the benzisothiazolinone core complicates matters in this instance.¹⁴ Although the

ester functionality was successfully hydrolysed, the benzisothiazolinone ring was re-opened, presumably by attack of hydroxide on the sulfur atom in the ring. An acid hydrolysis was therefore carried out on the ester using concentrated hydrochloric acid at room temperature for three days; however, no reaction was observed. It was suggested that a stronger acid could be more successful, so compound **3** was heated in concentrated sulfuric acid for 7 days. Disappointingly, a poor yield of <10% of carboxylic acid **4** was achieved.

As the method used here to generate the benzisothiazolinone core was successful, another pathway was devised that incorporated this reaction but changed the method of building up the molecule (Scheme 3.8). The reason for doing this was to obtain a larger quantity of compound **1** for the purpose of biological testing.

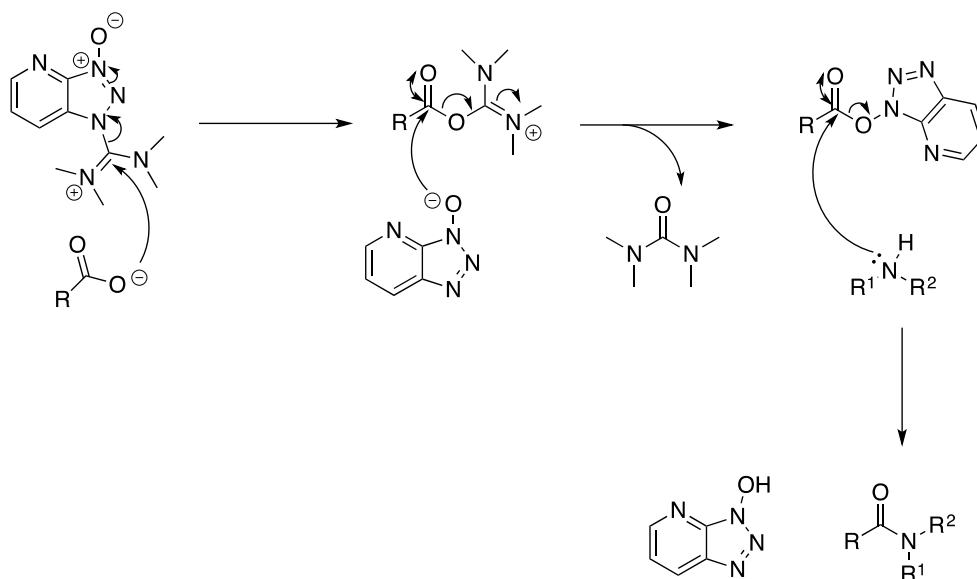
In the first step of this synthesis, morpholino(3-nitrophenyl)methanone (**8**) was formed from 3-nitrobenzoic acid and morpholine in a 93% yield. The nitro moiety of compound **8** was then reduced to an amine via catalytic hydrogenation, using palladium on carbon as the catalyst. The yield of compound **9** was 47%, which is relatively low. The conditions used for this transformation may have been too harsh and resulted in the decomposition of the morpholine ring, which could account for the loss of yield. If this step were to be repeated, an alternative method, such as iron and acetic acid, could be used. These conditions are milder and tolerant of a wider range of functional groups.¹⁵



Scheme 3.8. Rearranged pathway for the synthesis of 2-(3-(morpholine-4-carbonyl)phenyl)benzo[*d*]isothiazol-3(2*H*)-one (**1**)

Compound **9** was then coupled to 2-(methylthio)benzoic acid to form 2-(methylthio)-*N*-(3-(morpholine-4-carbonyl)phenyl)benzamide (**10**). Oxalyl chloride was initially used to form the acid chloride of 2-(methylthio)benzoic acid, before coupling with compound **9**; however, this reaction proved unsuccessful. Therefore, an alternative coupling method was investigated.

1-[Bis(dimethylamino)methylene]-1*H*-1,2,3-triazolo[4,5-*b*]pyridinium 3-oxid hexafluorophosphate (HATU) is used as a coupling agent in peptide chemistry. It is the *N*-guanidine salt of 1-hydroxy-7-azabenzotriazole (HOAt) and is used to generate an activated ester, before the addition of a nucleophile. DIPEA, or Hünig's base, is a non-nucleophilic base used to deprotonate the starting carboxylic acid. A polar solvent such as DMF is also used in these coupling reactions. The mechanism is shown below in Scheme 3.9.^{16,17}



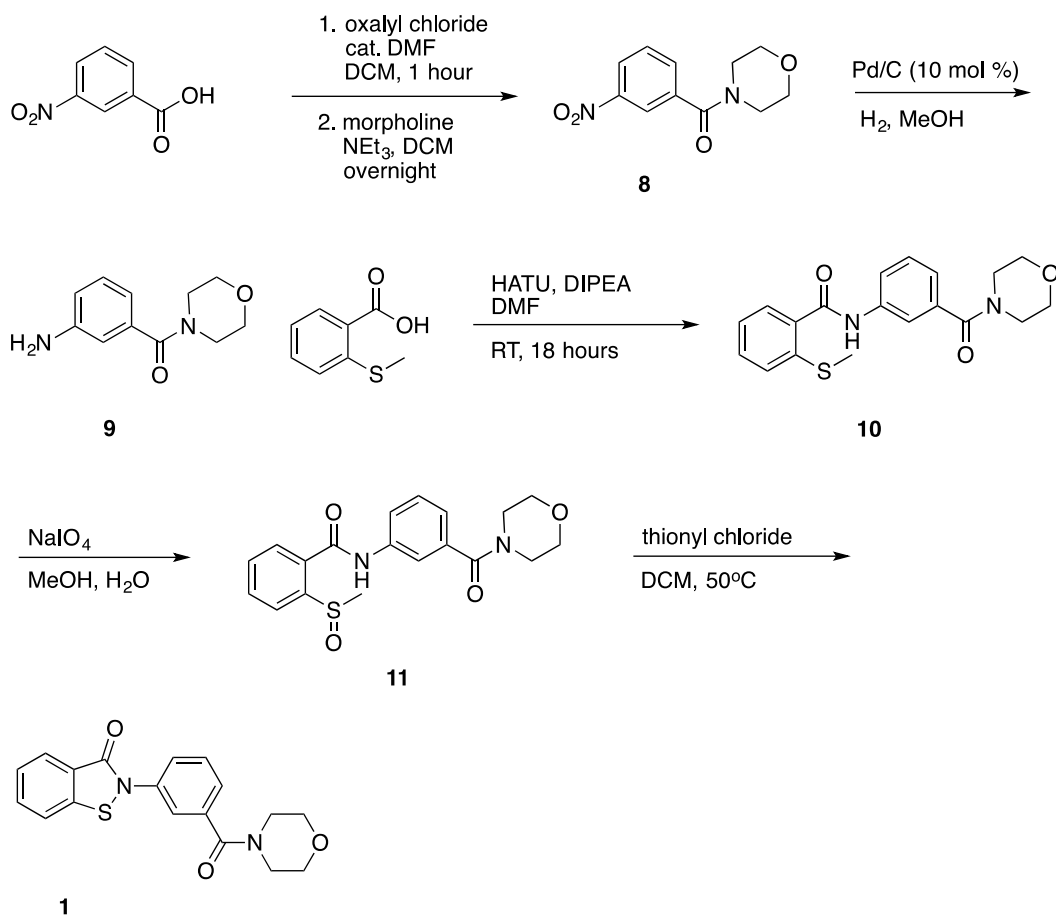
Scheme 3.9. The mechanism of HATU mediated amide synthesis:

- i) The carboxylic acid, which is deprotonated by DIPEA, attacks the electron deficient carbon of HATU forming an O-acyl(tetramethyl)isouronium salt
- ii) The HOAt anion attacks the uronium salt, generating an OAt-activated ester and liberating tetramethylurea
- iii) The amine attacks the activated ester and generates an amide product

Replacing the oxalyl chloride step with a HATU coupling produced the desired amide (**10**) in an 83% yield. The final steps in this synthesis involved the formation of sulfoxide **11**, using sodium periodate, and a thionyl chloride mediated ring closure (as discussed previously). This resulted in the production of 2-(3-(morpholine-4-carbonyl)phenyl)benzo[*d*]isothiazol-3(2*H*)-one (**1**) in a 66% yield. The final synthetic pathway used to obtain this mono-aryl analogue is shown below in Scheme 3.10.

Melting point, ^1H and ^{13}C NMR, MS, IR, and CHN analysis were carried out on compound **1**. Two strong carbonyl stretches were observed in IR (Figure 3.5), one for the benzisothiazolinone ring (1654 cm^{-1}) and one for the morpholine amide (1620 cm^{-1}). The carbonyl in the benzisothiazolinone ring has a slightly higher frequency due to the constraints of the ring system.¹⁸ The morpholine CH_2

protons did not resolve in ^1H NMR and are therefore seen as a large multiplet, around 3.77-3.57 ppm, that integrates to 8.



Scheme 3.10. Final synthetic pathway used to produce 2-(3-(morpholine-4-carbonyl)phenyl)benzo[*d*]isothiazol-3(2*H*)-one (**1**)

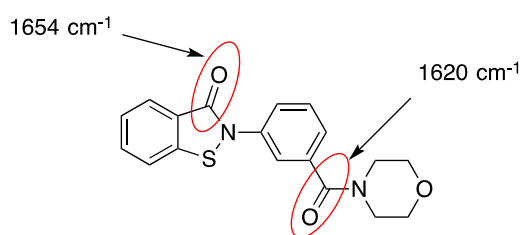


Figure 3.5. IR stretching frequencies of the two carbonyl groups in compound **1**

3.2.3 Results

All three compounds were sent for *in vitro* testing against both enzymatic and 3D7 whole cell assays. 3D7 is a chloroquine sensitive but sulfadoxine resistant strain of *P. falciparum*.¹⁹ Testing the methyl ester, carboxylic acid and amide would not only allow for comparison of the activity of each compound against the enzyme itself, but also establish how the nature of the side chain affects uptake across the apicoplast membrane and into the enzyme. The results are summarised below in Table 3.1.

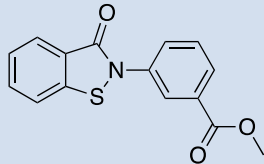
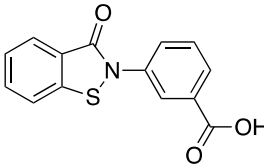
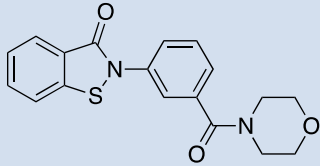
Compound	IspD (μM)	3D7 (μM)	CLogP*
 3	0.153 (n=1)	11.70 (n=1)	3.32
 4	0.483 (n=1)	>200 (n=1)	3.10
 1	0.153 (n=1)	26.08 (n=1)	1.98

Table 3.1. *In vitro* testing data and CLogP values for three compounds synthesised in this SAR: methyl ester (**3**), carboxylic acid (**4**) and morpholine amide (**1**)

*CLogP calculated using ChemDraw Professional 15

Compound **3** exhibited low micromolar activity against both the enzymatic and whole cell assays. It's calculated LogP was less than 5, which is in line with Lipinski's rules, and should result in the compound being well absorbed. However, the reactive nature of the side chain means that this compound could

be readily hydrolysed by esterases *in vivo* and as a result, could potentially undergo extensive first pass metabolism.²⁰

The carboxylic acid analogue (**4**) also had a low micromolar activity against the enzyme but activity against the whole cell was lost. Despite the CLogP being reasonable for a drug-like compound, the carboxylic acid moiety could be readily deprotonated at physiological pH. The charged carboxylate anion would not be able to cross the apicoplast membrane and therefore wouldn't be able to inhibit the enzyme.²¹

The morpholine amide compound (**1**) had low micromolar activity against both enzymatic and whole cell assays. The compound must therefore bind well to either the active site or an allosteric binding pocket of the IspD enzyme. There was no significant change in activity moving from the methyl ester (**3**) to the morpholine amide (**1**); however, the amide would be more resistant to metabolism *in vivo*, resulting in a longer half-life.²² The calculated lipophilicity (1.98) is also acceptable for a drug compound.²³

3.2.4 Conclusion

This first SAR exploration resulted in the development of a series of mono-aryl compounds that displayed low micromolar activity against the IspD enzyme. The most promising compound to emerge from this series was the morpholine amide analogue (**1**). This compound had an IC₅₀ value of 0.153 μM against the enzyme and has the greatest potential of all the mono-aryl analogues for a favourable PK profile.

A number of routes for the synthesis of the benzisothiazolinone core were explored, which could be applied to the development of further compounds in this SAR study. The final synthetic route to compound **1** (Scheme 3.10) was established in 5 steps, and each step proceeded with a good yield. If this compound were to be resynthesised, an alternative method for the reduction of the

nitro intermediate (**8**) to the corresponding amine (**9**) could be explored in order to reduce the number of side products and improve the yield.

3.3 A-ring Modification

3.3.1 Rationale

This series of compounds (Figure 3.6) was developed in order to probe the steric and electronic properties around the A-ring of the benzisothiazolinone core. A number of substituents were introduced (including both electron-donating and electron-withdrawing groups) at different positions around the ring in order to observe the effect on activity.

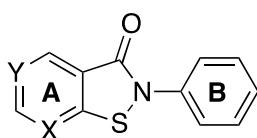


Figure 3.6. Template for the A-ring modified series

The phenyl ring was also replaced a pyridyl ring in one of the analogues of this series, in order to form a pyridoisothiazolone (compound **17**, Figure 3.7). Pyridine is one of the simplest yet most important heterocycles. It is found in many important naturally occurring compounds, such as niacin (vitamin B₃) and NADP (a cofactor used in anabolic reactions), and it is also features in many pharmaceuticals.^{24,25} Pyridoisothiazolones have found applications as anti-cancer, antibacterial and antifungal agents.^{26,27} They are generally stable, crystalline compounds that are resistant to aqueous acids but will decompose upon prolonged exposure to hydroxide solutions.

Introduction of a pyridyl moiety should assist in increasing the solubility of these isothiazolinone compounds and potentially provide another site for hydrogen bonding to occur with amino acid residues in the binding site of the enzyme.^{29,30} It was also postulated that pyridine could provide a site for metal ion

coordination, with the proposed Mg^{2+} ion in the active site of the IspD enzyme.³¹ Furthermore, incorporation of pyridine into the core could potentially affect the reactivity of the S-N bond and therefore alter the biological activity of these compounds.

3.3.2 Synthesis

A total of 6 compounds were synthesised in this series, which incorporate a variety of substituents around the benzisothiazolinone core (see Figure 3.7). The synthesis of each compound is discussed in detail below.

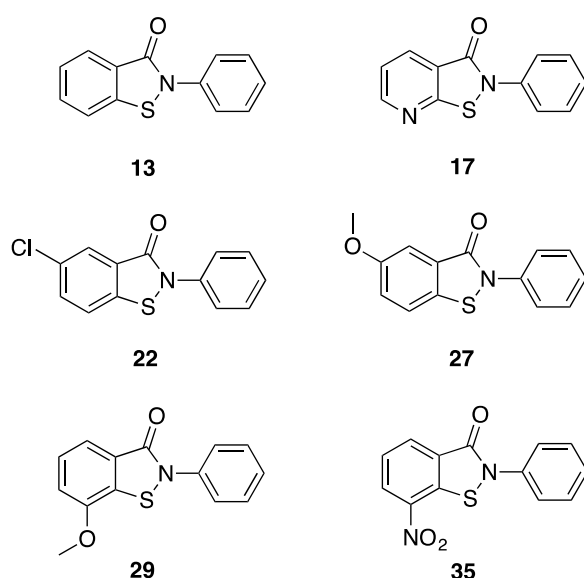


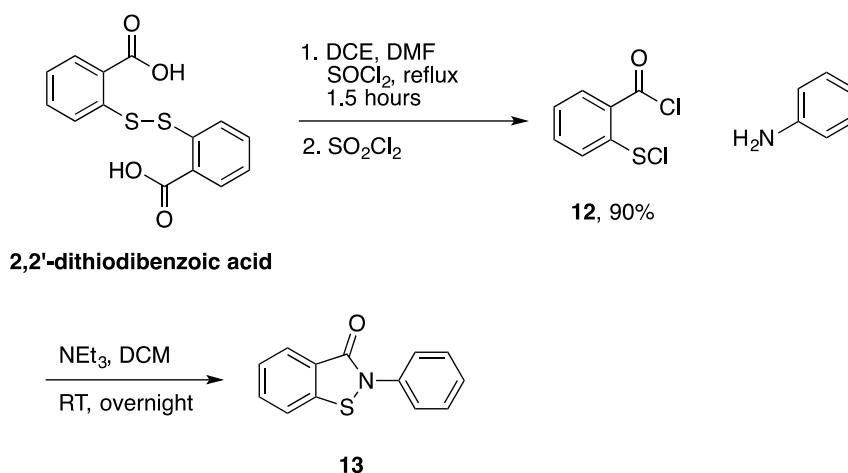
Figure 3.7. Structures of the analogues synthesised in the A-ring modified series

3.3.2.1 2-Phenylbenzo[d]isothiazol-3(2H)-one

The first compound synthesised in this series was the parent benzisothiazolinone (**13**). Although a high yield of 84% was quoted for the synthesis of this compound using the copper-iodide mediated route (Bhakuni *et al.*, Section 3.1.2), these conditions demonstrated a lack of tolerance for the side chain of the morpholine amide compound (**1**). A limited number of side chains were tested in the original paper, therefore these conditions could be selective.

An alternative route was investigated that would allow an amine side chain to be synthesised separately, before being incorporated into the benzisothiazolinone core.

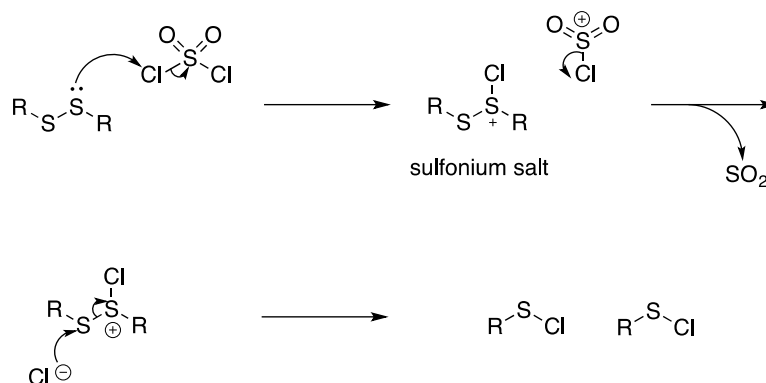
Aprile, Grosso and Grosa outlined the synthesis of a sulfenyl chloride intermediate (**12**) from 2,2'-dithiodibenzoic acid, using milder conditions than previously reported (see Section 3.2.2).³² In this synthesis, sulfonyl chloride is used to cleave the disulfide bond and generate the SCl intermediate, in place of chlorine gas. Quenching this intermediate with the required amine generates the desired benzisothiazolinone compound.³³ The planned synthesis of the parent benzisothiazolinone (**13**) is therefore shown below in Scheme 3.11.



Scheme 3.11. The synthetic pathway used to generate the parent benzisothiazolinone **13**

The first step in this synthesis was the formation of 2-chlorothiobenzoyl chloride (**12**) from 2,2'-dithiodibenzoic acid. Thionyl chloride was used to generate the acid chloride of the starting carboxylic acid before addition of sulfonyl chloride, which produced compound **12** in a 90% yield. The mechanism for this transformation is shown below in Scheme 3.12. This compound was taken forward to the next step without purification due to the moisture sensitive nature of the acid chloride. Addition of aniline in the presence of triethylamine

generated the parent compound, 2-phenylbenzo[*d*]isothiazol-3(2*H*)-one (**13**), in a 55% yield. This yield was lower than expected, and could be a consequence of carrying forward intermediate (**12**) without purification.



Scheme 3.12. The proposed mechanism of sulfenyl chloride formation

- i) One of the sulfur atoms in the disulfide bond acts as a nucleophile and attacks one of the electrophilic chlorine atoms of sulfur dichloride, generating a sulfonium salt
- ii) A chloride ion and sulphur dioxide are liberated
- iii) The chloride ion attacks the other sulfur atom of the sulfonium salt
- iv) Two molecules of RSCl are generated

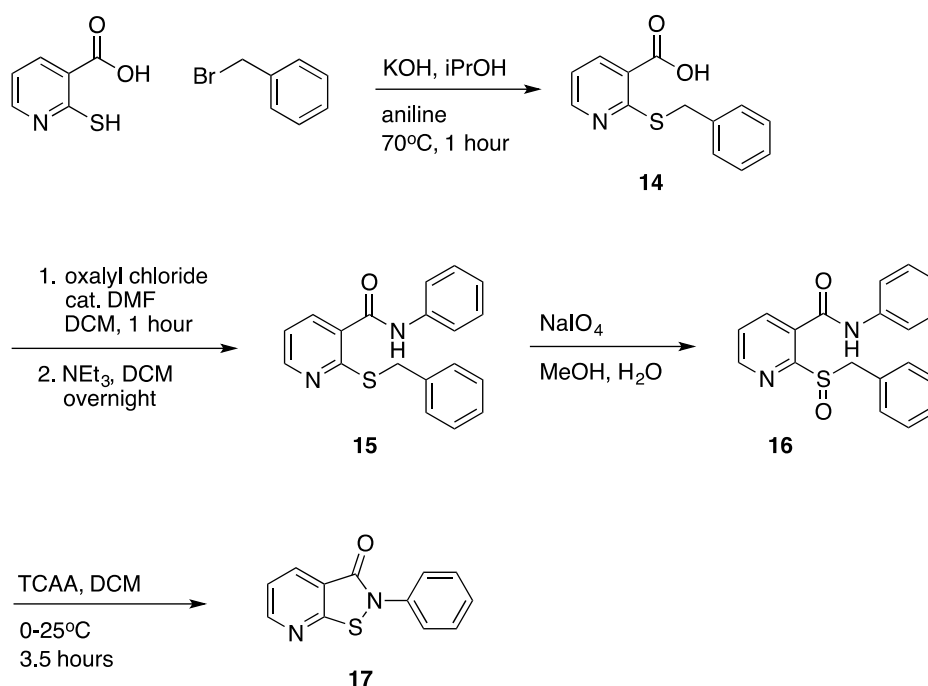
Adapted from: Organic Chemistry; Clayden, Greeves, Warren and Wothers¹⁰

These conditions provide a much simpler route into the formation of the benzisothiazolinone core than the copper iodide mediated method, which appears to be restrictive in terms of functional group tolerance. The sulfenyl chloride intermediate (**12**) could therefore be synthesised in bulk and a vast array of amine side chains could be incorporated with relative ease.

3.3.2.2 2-Phenylisothiazolo[5,4-*b*]pyridin-3(2*H*)-one

The next compound to be synthesised in this series of A-ring modified analogues was the pyridoisothiazolone **17**. This compound would be inaccessible by a number of the previous routes discussed; pyridine would poison a copper iodide catalyst and 2,2'-dithiobis(3-pyridinecarboxylic acid) is not commercially available. Therefore a novel route adapted from research by Wright *et al.* was

established. They discovered that protected thiols could be oxidatively cyclised to produce a variety of isothiazolinones in mild and high-yielding conditions.³⁴ They outlined the synthesis of compound **17** from a benzyl sulfoxide intermediate (**16**), using trichloroacetic anhydride (TCAA) to perform the ring-closing step. A synthetic pathway to the desired pyridoisothiazolone was developed as shown in Scheme 3.13.



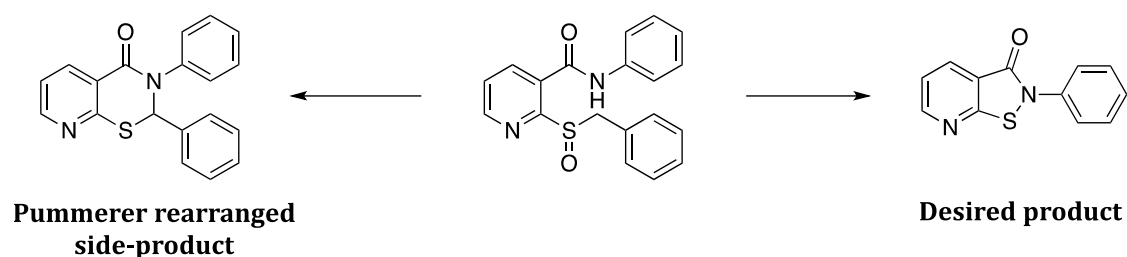
Scheme 3.13. Synthesis of 2-phenylisothiazolo[5,4-*b*]pyridin-3(2*H*)-one (**17**) via a benzyl sulfoxide intermediate

The first step involved the synthesis of 2-(benzylthio)nicotinic acid (**14**) from 2-mercaptonicotinic acid and benzyl bromide. This nucleophilic substitution proceeded with a 44% yield. Despite TLC showing complete consumption of the starting material, a large portion could have remained in the deprotonated form, which would be too polar to move from the baseline on TLC. To improve the yield for this step, the reaction time should be increased.

2-(Benzylthio)nicotinic acid (**14**) was then coupled to aniline, forming a benzyl sulfide intermediate (**15**) in a 93% yield. The benzyl sulfide intermediate (**15**)

was then oxidised to the corresponding benzyl sulfoxide (**16**) in a 66% yield, using sodium periodate as the oxidising agent. NMR data was not collected for this compound due to solubility issues. However, a downfield shift would have been expected for the CH₂ protons as the sulfide is oxidised to the sulfoxide.

The benzyl sulfoxide intermediate (**16**) then underwent a ring closure reaction using TCAA, producing 2-phenylisothiazolo[5,4-*b*]pyridin-3(2*H*)-one (**17**) in a 50% yield. This yield was not as high as quoted in the original paper (91%). Loss of product could have occurred through the formation of the Pummerer rearranged side product (see Scheme 3.14); however, the only product isolated from column chromatography was the desired pyridoisothiazolone (**17**).³⁵

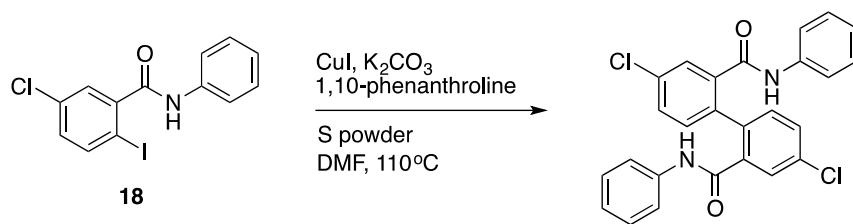


Scheme 3.14. The possible products of benzyl sulfoxide ring-closure using TCAA

This four step synthetic pathway provided a useful route for the formation of the pyridoisothiazolone and found further applications in the synthesis of the A-ring pyridyl series (see Section 3.4).

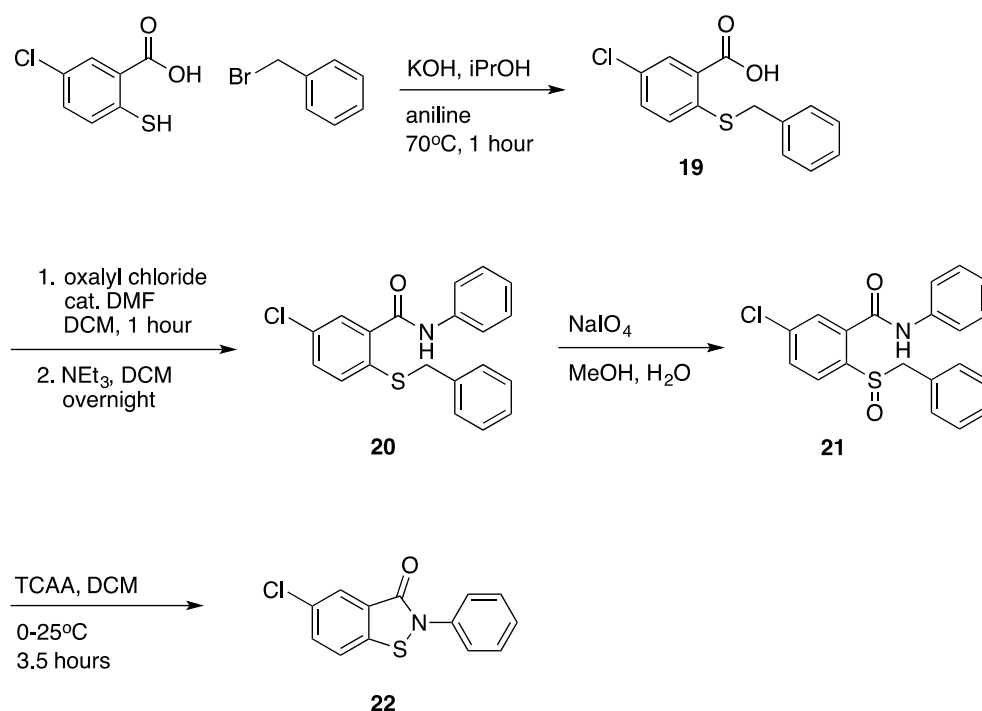
3.3.2.3 5-Chloro-2-phenylbenzo[*d*]isothiazol-3(2*H*)-one

The synthesis of this analogue was initially attempted via the copper iodide-mediated route, from 5-chloro-2-iodo-*N*-phenylbenzamide (**18**); however, this reaction proved unsuccessful and a dimer between two molecules of the starting material was formed as the main product (see Scheme 3.15).



Scheme 3.15. The dimer formed as a result of the treatment of 5-chloro-2-iodo-*N*-phenylbenzamide (**18**) with copper iodide-catalysed conditions

Due to the formation of the dimer, an alternative route was used to synthesise the 5-Cl analogue (see Scheme 3.16). This route is analogous to that used to synthesise the pyridoisothiazolone **17**. The first step generated 2-(benzylthio)-5-chlorobenzoic acid (**19**) from 5-chloro-2-mercaptobenzoic acid and benzyl bromide in a 46% yield. Aniline was then coupled to 2-(benzylthio)-5-chlorobenzoic acid to form the amide **20**, before oxidation and ring-closure steps were carried out. The final ring closure produced compound **22** in a 72% yield.



Scheme 3.16. The pathway used to successfully synthesise 5-chloro-2-phenylbenzo[*d*]isothiazol-3(*2H*)-one (**22**)

The formation of sulfoxide **21** was confirmed using ^1H and ^{13}C NMR as well as mass spectrometry. The NMR of sulfide **20** shows the CH_2 protons of the benzyl sulfide moiety as a singlet at 4.07 ppm. This is shifted further downfield than a typical aliphatic CH_2 ($\sim 1\text{-}2$ ppm), due to the de-shielding effects of the aromatic ring and sulfur. However, the NMR of sulfoxide **21** shows the two CH_2 protons as two sets of doublets (4.56 and 3.36 ppm); each integrating to one, with a large coupling constant of 12.7 Hz.

Although sulfoxides are typically represented as being analogous to a carbonyl group, the sulfur atom is in fact a stereogenic centre when the R groups are inequivalent. The oxygen and sulfur do not share a p-orbital π -bond that results in the planar confirmation observed with carbonyls. Instead, the oxygen donates electron density from a lone pair into a d-orbital on sulfur, resulting in a tetrahedral sp^3 hybridised organisation, with a lone pair of electrons on sulfur occupying the fourth position (Figure 3.8).³⁶

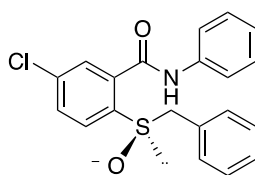


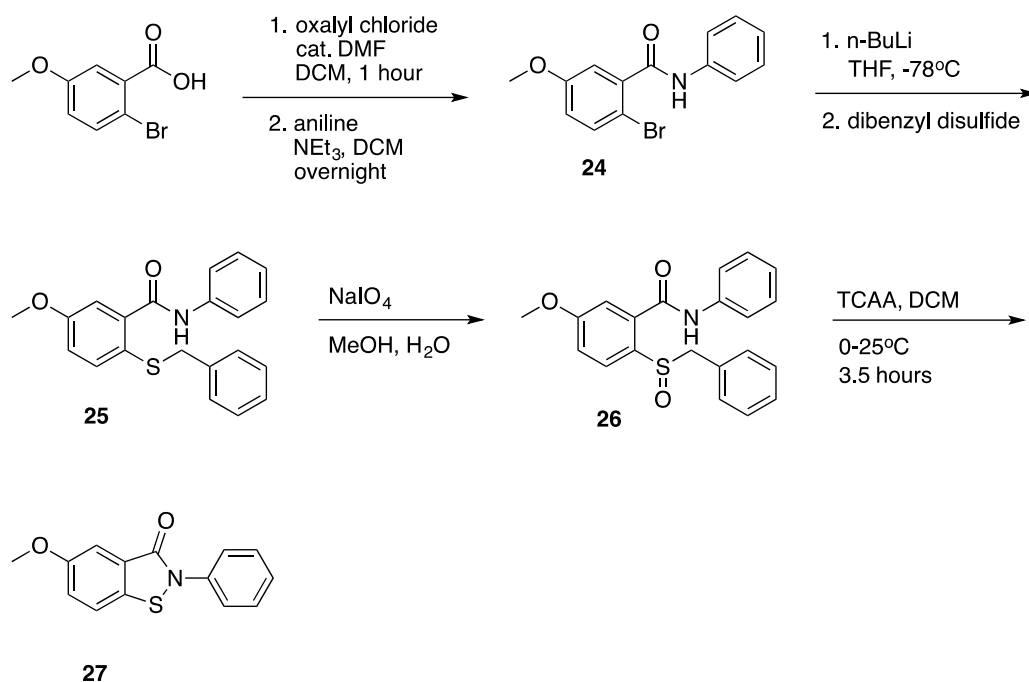
Figure 3.8. An alternate representation of sulfoxide **21**

Therefore, the two CH_2 protons are no longer equivalent as they are next to this stereogenic centre. This explains the appearance of two doublets in ^1H NMR and the large coupling constant observed between them.

3.3.2.4 5-Methoxy-2-phenylbenzo[*d*]isothiazol-3(2*H*)-one

Like the 5-Cl analogue (**22**), the copper iodide-mediated route was unsuccessful in the synthesis of the 5-OMe compound (**27**). Therefore, a TCAA ring closure route was developed. This route was slightly more complicated as a 5-OMe substituted 2-mercaptobenzoic acid was not commercially available, so an

alternative route to the benzyl protected thiol (**25**) was developed (Scheme 3.17).



Scheme 3.17. The synthesis of 5-methoxy-2-phenylbenzo[*d*]isothiazol-3(2*H*)-one (**27**) via a benzyl sulfoxide intermediate

The first step in this synthesis involved a coupling reaction between 2-bromo-5-methoxybenzoic acid and aniline using the oxalyl chloride route shown. This produced 2-bromo-5-methoxy-*N*-phenylbenzamide (**24**) in a >95% yield.

The next step involved a halogen-metal exchange reaction using *n*-butyllithium in THF at -78°C.³⁷ After stirring at -78°C for 30 minutes, the reaction mixture was warmed to 0°C for one hour. The solution was then cooled back down to -78°C before the addition of dibenzyl disulfide. TLC was used to follow the progress of this reaction, and confirmed that all of the starting material (compound **24**) had been consumed. Two new spots emerged on TLC, one with a very similar R_f value to the starting material and one that was significantly less polar. The least polar spot was isolated by column chromatography and analysed by NMR and MS. However, the structure of this product was confirmed to be a butyl analogue of the starting material (see Figure 3.9) rather than the desired benzyl sulfide

product. The other spot was therefore isolated and confirmed to be the protonated analogue of the organolithium intermediate (Figure 3.9).

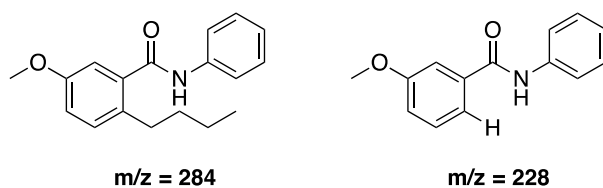


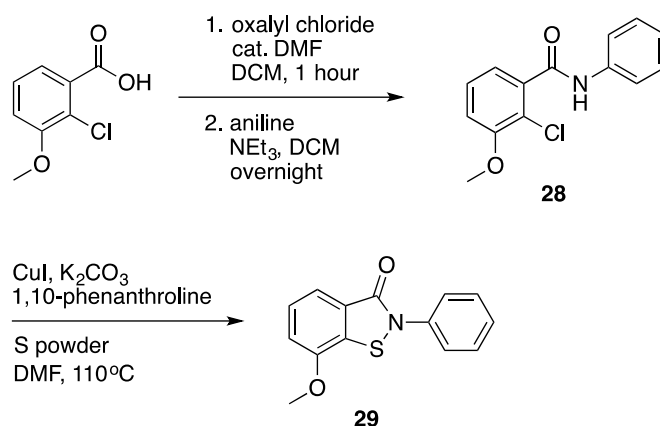
Figure 3.9. The products formed from the initial halogen-metal exchange reaction between 2-bromo-5-methoxy-*N*-phenylbenzamide and *n*-BuLi

When *n*-BuLi is used for halogen-metal exchange reactions, an electrophilic *n*-BuX is obtained as a side-product.³⁸ This alkyl halide (*n*-BuBr in this instance) can undergo an S_N2 substitution reaction, with the newly formed organolithium acting as the nucleophile. S_N2 reactions of organolithiums with alkyl halides are rather slow at low temperatures; therefore, in order to circumvent the formation of the butyl side-product, the reaction was repeated and dibenzyl disulfide was added to the stirring solution of the starting material and *n*-BuLi after just 10 minutes.³⁹ This method proved successful and 2-(benzylthio)-5-methoxy-*N*-phenylbenzamide (**25**) was formed in a >95% yield.

The final steps of the synthesis involved oxidation of compound **25** using sodium periodate to form the sulfoxide intermediate **26**, and a subsequent ring-closure using TCAA. 5-Methoxy-2-phenylbenzo[*d*]isothiazol-3(2*H*)-one (**27**) was formed in a 65% yield.

3.3.2.5 7-Methoxy-2-phenylbenzo[*d*]isothiazol-3(2*H*)-one

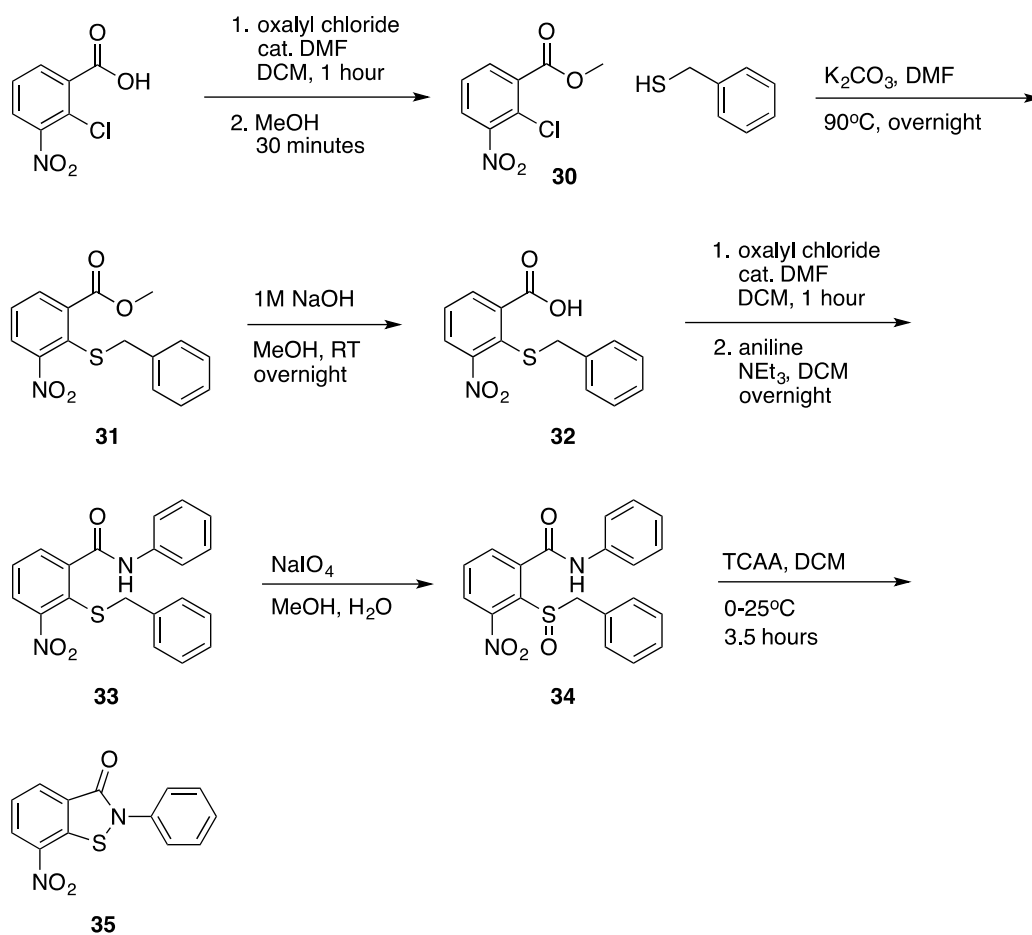
7-Methoxy-2-phenylbenzo[*d*]isothiazol-3(2*H*)-one (**29**) was synthesised in a simple two-step process from 2-chloro-3-methoxybenzoic acid (Scheme 3.18). The first step involved the coupling of the starting carboxylic acid with aniline to form the amide intermediate (**28**) in a 92% yield. The copper iodide-mediated method was then applied to form the benzisothiazolinone core. This reaction successfully formed the desired product (**29**) in a 56% yield.



Scheme 3.18. The successful 2 step synthesis of 7-methoxy-2-phenylbenzo[d]isothiazol-3(2H)-one (**29**) from 2-chloro-3-methoxybenzoic acid

3.3.2.6 7-Nitro-2-phenylbenzo[d]isothiazol-3(2H)-one

The final compound to be synthesised in this series was the 7-nitro analogue in order to observe the effect of introducing an electron withdrawing group into this position on the ring. This compound was also synthesised via a benzyl sulfoxide intermediate and TCAA ring closure; however, the formation of the benzyl-protected thiol was slightly modified to account for the availability of starting materials (see Scheme 3.19 for the synthetic pathway used).



Scheme 3.19. The pathway developed to synthesise 7-nitro-2-phenylbenzo[*d*]isothiazol-3(2*H*)-one (**35**)

The first step in this synthesis involved protection of the carboxylic acid as a methyl ester (**30**), in order for the benzyl sulfide moiety to be introduced by nucleophilic aromatic substitution. This addition-elimination reaction between the aryl halide (**30**) and benzyl mercaptan was aided by the presence of 2 electron-withdrawing groups *ortho* to the chloride leaving group, which helped to stabilise the negative charge generated in the reaction.^{10,40} Once the benzyl sulfide moiety was introduced, the methyl ester was hydrolysed back to a carboxylic acid (compound **32**) under basic conditions. Compound **32** was then coupled to aniline using the oxalyl chloride method and the oxidation and ring closure steps was carried out, as previously described, to generate 7-nitro-2-phenylbenzo[*d*]isothiazol-3(2*H*)-one (**35**).

3.3.3 Results

The 6 compounds synthesised were sent for *in vitro* testing against both enzymatic and 3D7 whole cell assays, and the results are summarised below in Table 3.2.

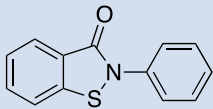
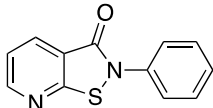
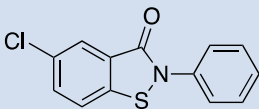
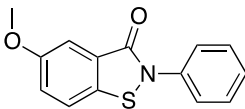
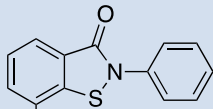
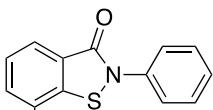
Compound	IspD (μM)	3D7 (μM)	ClogP*
 13	0.60 n=1	5.49 n=1	3.35
 17	0.26 n=1	44.16 n=1	1.86
 22	9.50 n=1	-	4.07
 27	-	-	3.27
 29	>200 n=1	35.99 n=1	3.27
 35	>200 n=1	51.38 n=1	3.10

Table 3.2. *In vitro* testing data and CLogP values for the A-ring modified compounds synthesised in this SAR

*CLogP calculated using ChemDraw Professional 15

The parent benzisothiazolinone (**13**) was synthesised in order to provide a data set that would allow for comparison with the other A-ring modified compounds. This compound had an IC₅₀ of 0.60 μM against the enzyme and 5.49 μM against the whole cell assay. Activity against the IspD enzyme was less potent than that of the most active mono-aryl compound (**1**, IC₅₀ = 0.15 μM), suggesting that modifications to the side chain are well tolerated. Whole cell data was improved (5.49 μM for compound **13** vs. 11.70 μM for compound **1**) and this could be a result of the increased lipophilicity of compound **13** (CLogP = 3.35 for compound **13** vs 1.98 for compound **1**).

Introduction of the pyridyl moiety in compound **17** resulted in an improved activity against the enzyme compared to the parent benzisothiazolinone **13** (0.26 μM vs. 0.60 μM respectively). There could be a number of reasons for this increased inhibitory activity: the pyridine nitrogen could be increasing the number of binding interactions within the active site, either through hydrogen bonding interactions with amino acids or through coordination to the Mg²⁺ ion postulated to be present. Or, the presence of the pyridyl could be increasing the reactivity of the S-N bond, which could make it more susceptible to nucleophilic attack by the proposed cysteine residue within the active site. Whole cell activity decreased (44.16 μM for **17** vs. 5.49 μM for compound **13**); however, this was to be expected due to the more polar nature of this analogue compared to the more lipophilic benzisothiazolinone.

Introduction of a chloro group into the 5-position of the A-ring (**22**) resulted in a significant drop in potency against the IspD enzyme (IC₅₀ = 9.50 μM). The introduction of a substituent into this position could have led to unfavourable steric interactions within the binding pocket, which resulted in a weaker binding interaction. Disappointingly, whole cell data is not yet available for this

compound. Both enzymatic and whole cell data are eagerly awaited for the 5-methoxy analogue (**27**) also.

Introduction of substituents into the 7-position of the ring (compounds **29** and **35**) completely abolished inhibitory activity against the IspD enzyme. This could be a result of unfavourable steric interactions within the binding site, thus preventing these compounds from adopting an orientation necessary to exert an inhibitory effect. It is less likely to be a result of electronic effects as both an electron-donating (7-OMe analogue **29**) and electron-withdrawing (7-NO₂ analogue **35**) substituents were introduced. However, a peculiar result was observed for the activity of both compounds against the whole cell assay. Both the 7-OMe and 7-NO₂ compounds showed micromolar activity (35.99 μM and 51.38 μM respectively) in the 3D7 assay. These compounds are displaying off target activity, which is an undesirable characteristic for drug compounds. It could be the case that these compounds are selectively targeting a different enzyme in the MEP pathway, and this would still be desirable. As previously discussed in Chapter II, IspD genes are tightly linked to IspF so these compounds have the potential to act as inhibitors here.⁴¹ Furthermore, a series of inhibitors developed by Diederich *et al.* to target IspD exhibited activity against IspE instead.⁴² However, these compounds could be targeting somewhere different altogether.

3.3.4 Conclusion

Testing data from the A-ring modified series showed that the most active compound against the IspD enzyme was 2-phenylisothiazolo[5,4-*b*]pyridin-3(2*H*)-one (**17**). Substitution in the 7-position resulted in complete loss of activity against the enzyme and off target activity was observed in the whole cell 3D7 assay. Despite the 5-Cl analogue exhibiting micromolar activity against the enzyme, it was not as potent as the parent benzisothiazolinone (**13**). It was decided that the optimum modification to this portion of the molecule was the pyridyl group, and this moiety would be further investigated going forward.

Despite compound **17** being the most potent inhibitor of the enzymatic assay, the whole cell activity dropped significantly in comparison to the parent benzisothiazolinone. This could be a result of the lower calculated lipophilicity for compound **17** compared to **13**; therefore, the next series of compounds to be investigated in this SAR study were a combination of the potent pyridoisothiazolone core with a lipophilic side chain (Section 3.4).

3.4 A-ring Pyridyls

3.4.1 Rationale

As previously discussed, the introduction of a pyridyl moiety into the A-ring of the benzisothiazolinone core produced some of the most potent activity against the IspD enzyme seen so far. The rationale behind this series of A-ring pyridyl analogues was to introduce a variety of side chains in order to help improve the lipophilicity of these compounds. Drug compounds need to have some degree of lipophilicity in order to cross membranes, and as a general rule, there is an ideal range of lipophilicity which corresponds to more favourable permeability (usually between 2 and 4).^{43,44}

However, if drug compounds are too non-polar they may be insoluble in the aqueous conditions found in the gastrointestinal tract and bloodstream; or, they may bind too tightly to components in food or to proteins in the blood to be available to interact with the desired target.⁴⁵ Christopher Lipinski noted that most orally bioavailable drugs on the market seemed to have logP values < 5, therefore a series of A-ring pyridyls were designed in order to increase lipophilicity whilst ensuring calculated partition-coefficients did not exceed 5 (Figure 3.10).^{46,23}

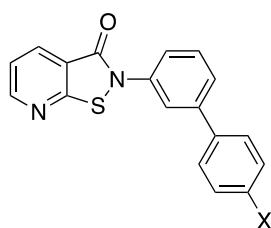
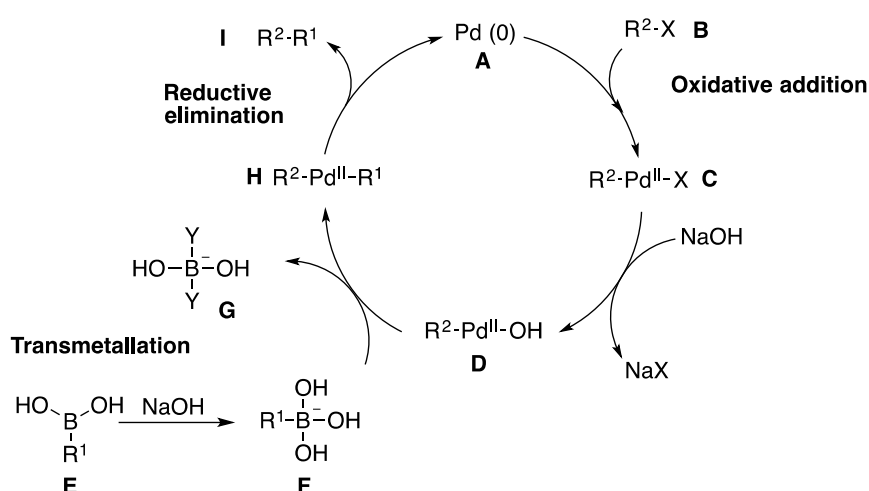


Figure 3.10. The template designed for the series of A-ring pyridyl analogues (X =Cl, OMe, CF₃)

3.4.2 Synthesis

The initial pathway involved the generation of compound **37** in bulk. This sulfoxide could then be coupled to a variety of boronic acids, before a simple ring closure completed the synthesis (Scheme 3.20).



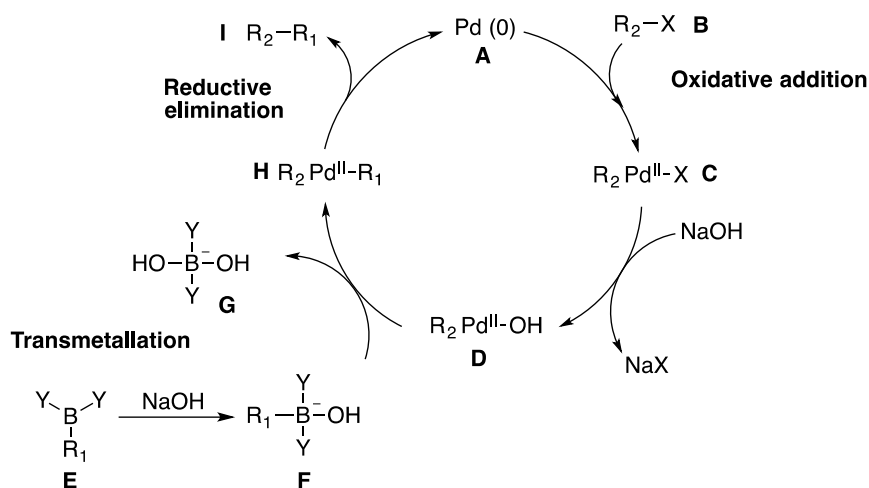
Scheme 3.20. Initial route developed for the synthesis of the A-ring pyridyl analogues

The biphenyl moiety in the side chain of these compounds was planned to be introduced by a Suzuki cross-coupling reaction. A Suzuki reaction classically forms a carbon-carbon single bond between an organoboron species and a halogen using a palladium (0) catalyst, and is widely used to synthesise polyolefins and styrenes as well as biphenyls.⁴⁷ Akira Suzuki, who first published his work on this reaction in 1979, was awarded the Nobel Prize for his efforts in palladium cross-coupling reactions in 2010.⁴⁸ The Suzuki reaction has a broad

substrate scope, which tolerates a wide variety of functional groups and sterically demanding substrates.⁴⁹

The first step in this reaction is the oxidative addition of a palladium (0) catalyst to the organohalide, which generates an organopalladium intermediate (**C**). The carbon-halide bond of the starting material is broken and palladium (0) is oxidised to palladium (II). Initially the *cis* isomer is formed, however this rapidly isomerizes to produce the *trans* isomer (**C**) shown below in Scheme 3.21.⁵⁰ The *trans* isomer reacts with base to form intermediate **D** before a transmetallation step occurs. The organoboron species (**E**) is also activated by base to facilitate the transmetallation step, which sees the R¹ group transferred from the organoboron (**F**) to the palladium (II) complex.⁵¹ In the final step, the palladium (II) complex (**H**) undergoes reductive elimination, expelling the product and regenerating the palladium (0) species.^{52,53}

Previous work within the group established that the Suzuki coupling conditions were unsuccessful in the presence of the benzisothiazolinone core; therefore, this step was introduced at the penultimate stage, where the sulfur is protected as a methyl sulfoxide (**37**).



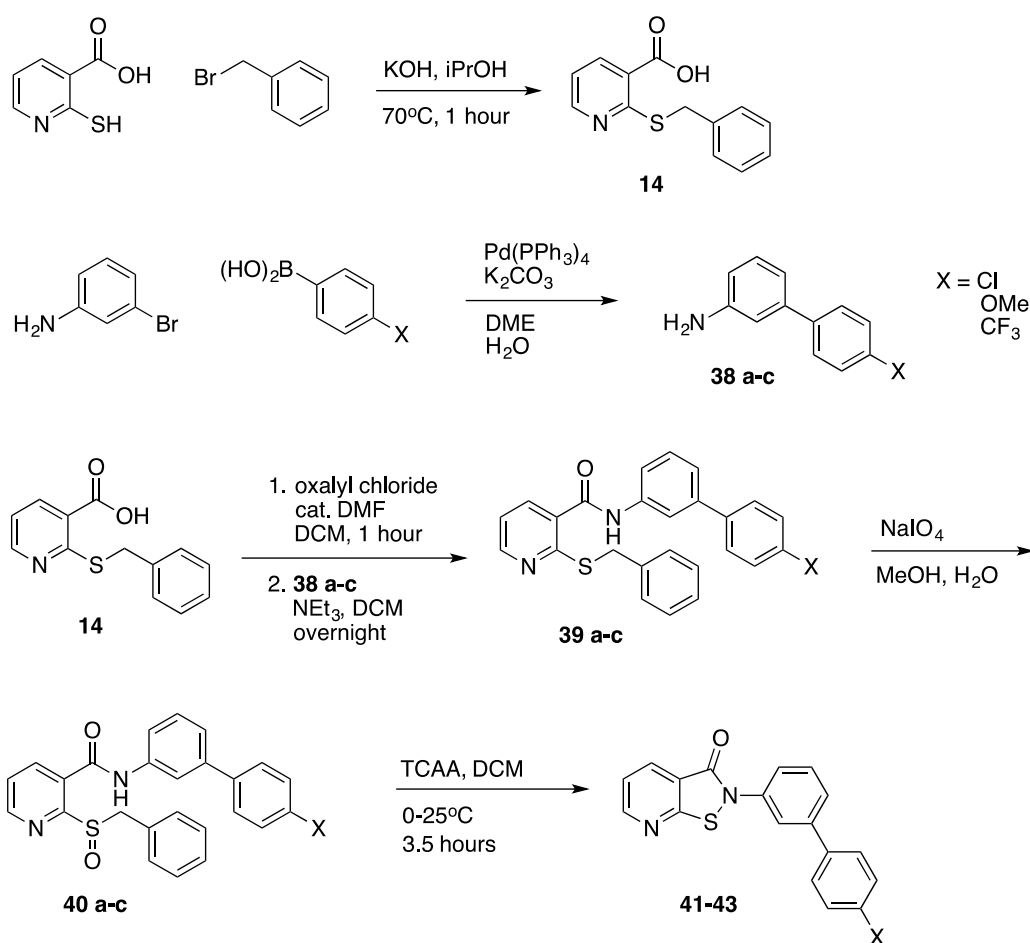
Scheme 3.21. The proposed mechanism for a Suzuki cross-coupling reaction between an organohalide and an organoborane, catalysed by a palladium (0) complex in the presence of base

Adapted from: Palladium-Catalyzed Suzuki-Miyaura Cross-coupling Reactions Employing Dialkylbiaryl Phosphine Ligands, Ruben Martin and Stephen L. Buchwald⁵⁴

The sulfoxide intermediate (**37**) was synthesised in two high yielding steps from 2-(methylthio)nicotinic acid and 3-bromoaniline. The Suzuki cross-coupling conditions were then applied to the newly generated sulfoxide with the boronic acids required for each analogue. This step proved to be unsuccessful, with a mixture of byproducts observed for each reaction and no traces of product present. This result is surprising, as aromatic heterocycles are usually well tolerated by Suzuki conditions; however, the reaction was not compatible with this system.⁴⁹ It was also discovered that the methyl sulfide route was unsuccessful in the presence of an A-ring pyridyl, so a benzyl sulfide route was employed.

Due to the lack of success with the initial route, an alternative method was proposed (Scheme 3.22). This route was developed from the synthesis of the parent pyridoisothiazolone (**17**). This method was initially avoided due to its linear nature and large number of steps.

The side chain was prepared separately, using Suzuki cross-coupling conditions, in order to avoid the issues encountered previously. The side chains (**38 a-c**) were synthesised in yields varying from 46 - 86%, and were coupled to 2-(benzylthio)nicotinic acid (**14**) in order to form the amide intermediates (**39 a-c**). The benzyl sulfide moiety of compounds **39 a-c** was then oxidised using sodium periodate, and the final ring closure step was facilitated by TCAA.



Scheme 3.22. Pathway developed for the successful synthesis of A-ring pyridyl analogues **41-43** (X =Cl, OMe, CF₃)

3.4.3 Results

The 6 compounds synthesised were tested *in vitro* for their enzymatic and phenotypic biological activity and the results are summarised below in Table 3.3.

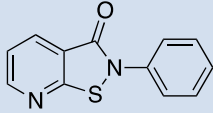
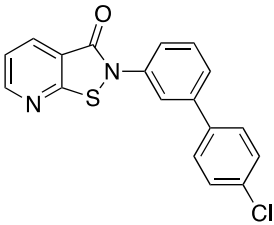
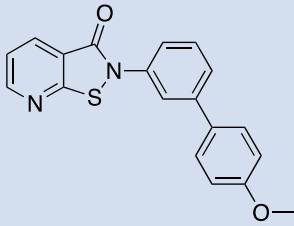
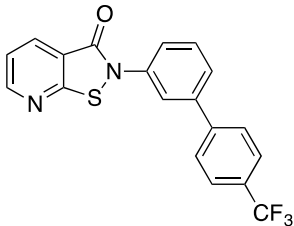
Compound	IspD (μM)	3D7 (μM)	CLogP*
 17	0.26 n=1	44.16 n=1	1.86
 41	Solubility issues	31.28 n=1 (slurry)	4.46
 42	0.79 n=1	25.75 n=1	3.66
 43	0.72 n=1	21.32 n=1	4.63

Table 3.3. *In vitro* testing data and CLogP values for the A-ring pyridyl compounds synthesised in this SAR

*CLogP calculated using ChemDraw Professional 15

Unfortunately, enzymatic data for the -Cl (**41**) analogue could not be obtained due to solubility issues with this compound. Enzymatic data obtained for the -OMe (**42**) and -CF₃ (**43**) compounds shows that low micromolar activity (0.79 μM and 0.72 μM respectively) was maintained against the enzyme, despite neither being quite as potent as the parent pyridoisothiazolone (**17**, IC₅₀ = 0.26 μM). Whole cell 3D7 data was improved for all 3 analogues compared to the parent pyridoisothiazolone (IC₅₀ = 44.16 μM vs. 3D7), with the most potent whole cell activity (21.32 μM) shown by the -CF₃ analogue, compound **43**.

3.4.4 Conclusion

The aim of this series of compounds was to maintain the low micromolar activity exhibited by 2-phenylisothiazolo[5,4-*b*]pyridin-3(2*H*)-one (**17**) against the IspD enzyme, whilst improving phenotypic activity through the introduction of a more lipophilic side chain. Despite an improvement in whole cell activity, these compounds were not as potent against IspD as compound **17**. This series represents a novel class of antimalarial compounds that inhibit IspD; however, there is still scope for further modification to improve potency. Therefore, it was decided to move the position of the pyridyl group from the A-ring to the B-ring.

3.5 B-ring Pyridyls

3.5.1 Rationale

As discussed in Section 3.2.1, there are many advantages of introducing a pyridine moiety into a potential drug compound. Previous investigations in this SAR study have involved the incorporation of a pyridyl group into the A-ring of the benzisothiazolone core. However, the effects of moving this group have yet to be explored. Therefore, this series of compounds (Figure 3.11) was designed in order to observe the effect of moving the pyridyl group into the B-ring.

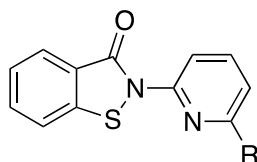
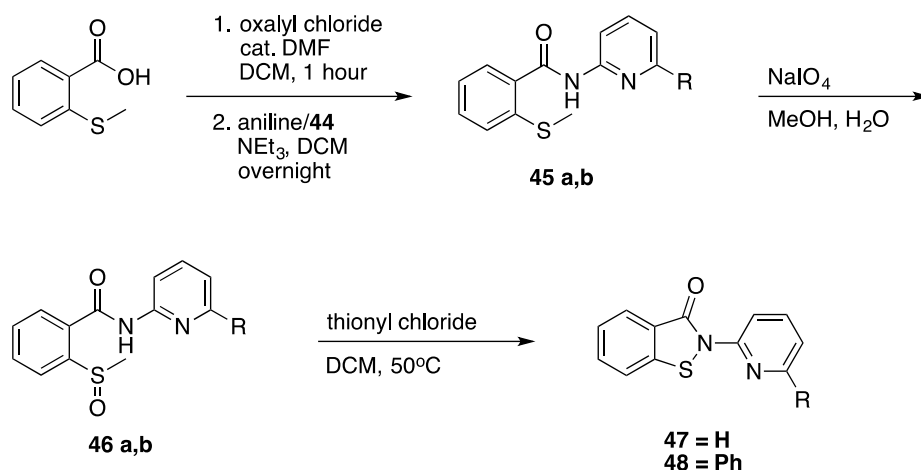


Figure 3.11. The template developed for the B-ring pyridyl series

Changing the position of the pyridyl group should have an effect on the electronics and reactivity of the S-N bond and alter the inhibitory activity of this series compared with the A-ring pyridyl series.⁵⁵ A number of solubilising groups, such as morpholine and 4-methylpiperazine, were also introduced into this series in order to avoid the solubility issues observed with the A-ring pyridyls (compound **41**).⁵⁶

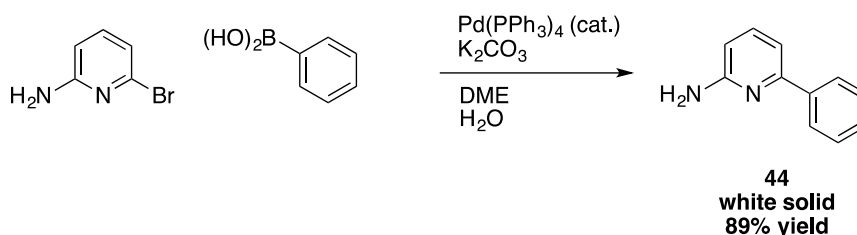
3.5.2 Synthesis

Synthesis of the first two compounds in this series (the parent B-ring pyridyl (**47**) and the bi-aryl pyridyl (**48**), Scheme 3.23) was achieved using the protected sulfur method first outlined in Section 3.2.2.



Scheme 3.23. Pathway outlining the synthesis of the first two analogues of the B-ring pyridyl series: the parent B-ring pyridyl (**47**) and the biaryl analogue (**48**)

The first step was a coupling reaction between 2-(methylthio)benzoic acid and the desired amine side chain. 2-(Methylthio)benzoic acid was then coupled to 2-aminopyridine to complete the synthesis of compound **47** in a quantitative yield. For compound **48**, the bi-aryl side chain was formed first, and this was achieved by a Suzuki cross-coupling reaction between 2-amino-6-bromopyridine and phenylboronic acid in an 89% yield (Scheme 3.24).



Scheme 3.24. The synthesis of amine side chain **44**, using Suzuki cross-coupling conditions

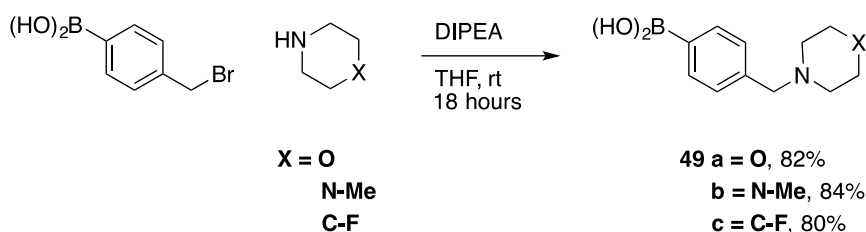
Once amide compounds **45a** and **45b** were prepared, the methyl sulfide moieties were oxidised to the corresponding sulfoxides (**46a** and **46b**) using sodium periodate as the oxidising agent. The final step in this synthetic pathway was a thionyl chloride mediated ring closure, which produced the desired compounds,

47 and **48**, in an 86% and 70% yield respectively (see Scheme 3.7 for the mechanism).

3.5.2.1 Amine solubilising groups

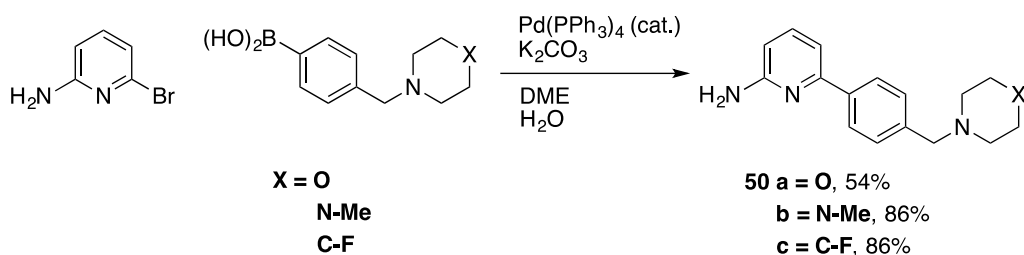
These bi-aryl side chains were designed to incorporate solubilising groups, such as morpholine and 4-fluoropiperidine, in order to help balance the increased lipophilicity.

The side chains for this group of compounds were synthesised separately, as was the case with compound **48**, before incorporation into the benzisothiazolinone core. The first step generated a series of *para*-substituted boronic acids using 4-(bromomethyl)phenylboronic with the appropriate amine in the presence of base (Scheme 3.25). DIPEA was chosen for this nucleophilic substitution as it is a good base but a poor nucleophile, so would not interfere with the substitution step.⁵⁷



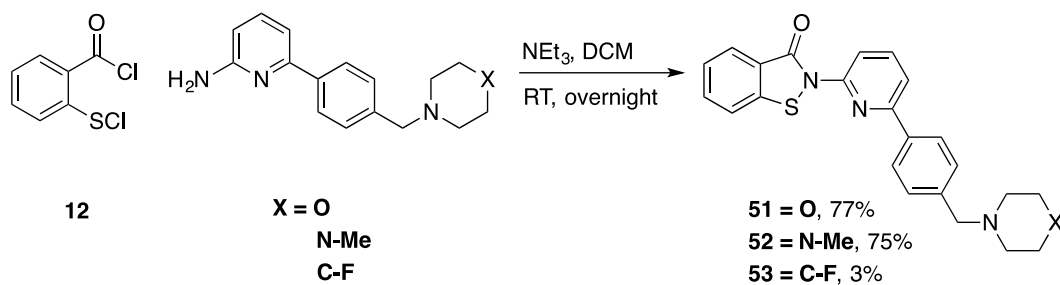
Scheme 3.25. Synthesis of substituted boronic acids with amine solubilising side chains

The substituted boronic acids (**49a-c**) were then reacted with 2-amino-6-bromopyridine using Suzuki cross-coupling conditions (Scheme 3.26) in order to form the bi-aryl side chains (**50a-c**).



Scheme 3.26. Synthesis of bi-aryl side chains **50a-c** using Suzuki cross-coupling conditions

The side chains were then coupled to 2-chlorothiobenzoyl chloride (**12**) in order to form the benzisothiazolinone core (Scheme 3.27). The resulting B-ring pyridyl analogues were generated in high yields and submitted for *in vitro* testing against both enzymatic and phenotypic assays. An S-Cl mediated ring closure (see Section 3.2.2.1) was chosen due to the reduced number of steps compared to the sulfide-sulfoxide-ring closure method used for the first two analogues of this series (**47** and **48**). The low yield for compound **53** could be explained by the difference in quality of two batches of the starting material **12**.

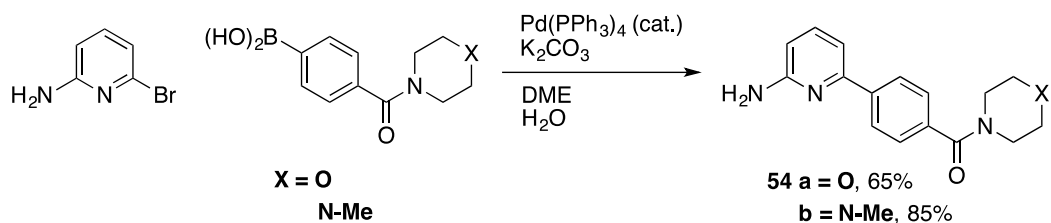


Scheme 3.27. Synthesis of final compounds using an SCl mediated ring closure

3.5.2.2 Amide solubilising side chains

The *para*-amide substituted boronic acids, (4-(morpholine-4-carbonyl)phenyl)boronic acid (Scheme 3.28, X=O) and (4-(4-methylpiperazine-1-carbonyl)phenyl)boronic acid (Scheme 3.28, X=N-Me), were commercially available and therefore used in the synthesis of these analogues.. Both compounds underwent successful Suzuki cross-coupling reactions with 2-amino-

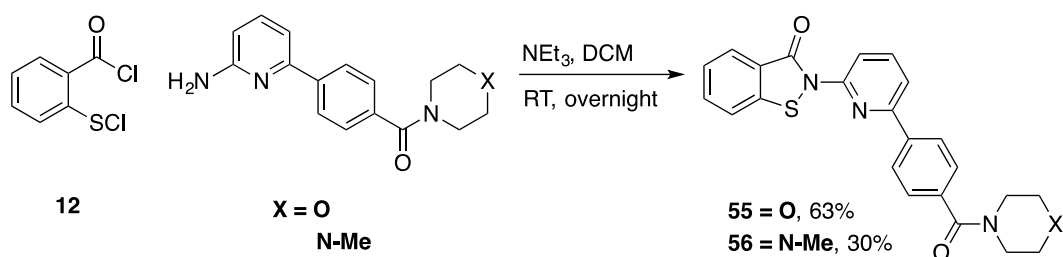
6-bromopyridine. The yield for the morpholine amide analogue (**54a**) was 65%, compared with 85% for the *N*-methyl piperazine amide (**54b**).



Scheme 3.28. Bi-aryl side chain synthesis using Suzuki cross-coupling conditions

The corresponding 4-fluoropiperidine compound, (4-(4-fluoropiperidine-1-carbonyl)phenyl)boronic acid, was not available and attempts to synthesise this compound using traditional amide formation methods proved unsuccessful; potentially due to the sensitivity of the boronic acid functionality. Therefore the 4-fluoropiperidine side-chain was not synthesised.

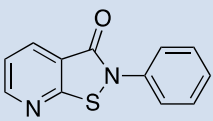
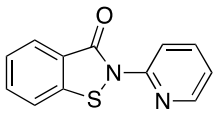
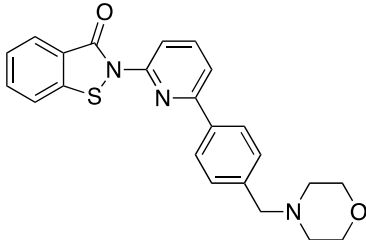
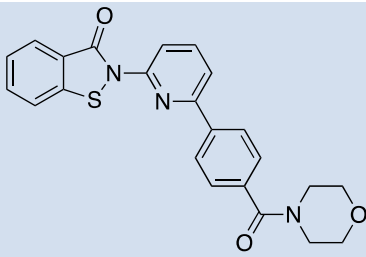
The side chains were then coupled to 2-chlorothiobenzoyl chloride (**12**) to generate the final ring-closed benzisothiazolinone compounds, **55** and **56**, in 63% and 30% yields respectively.



Scheme 3.29. Synthesis of final compounds using an SCl mediated ring closure

Results

The 7 compounds synthesised in this B ring pyridyl series were submitted for *in vitro* enzymatic and phenotypic testing. The results of the testing data are summarised below in Table 3.4.

Compound	IspD (μM)	3D7 (μM)	CLogP*
 17	0.26 n=1	44.16 n=1	1.86
 47	0.17 n=1	70.02 n=1	1.86
 48	1.07 n=1	0.90 n=1	3.95 n=1
 51	>200 n=1	0.46 \pm 0.20 n=4	3.70
 55	5.10 n=1	2.01 n=1	2.66

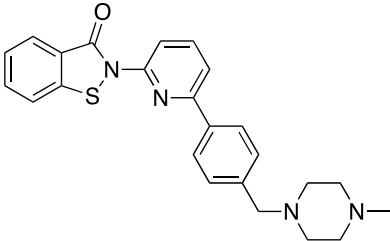
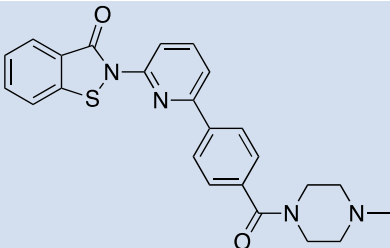
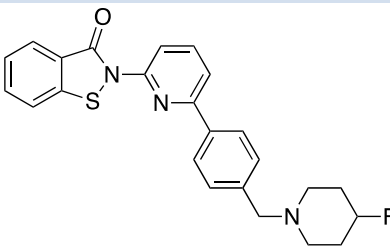
 <p style="text-align: center;">52</p>	<p>>200 n=1</p>	<p>1.07 n=1</p>	<p>4.26</p>
 <p style="text-align: center;">56</p>	<p>4.48 n=1</p>	<p>2.12 n=1</p>	<p>3.22</p>
 <p style="text-align: center;">53</p>	<p>>200 n=1</p>	<p>1.05 n=1</p>	<p>4.67</p>

Table 3.4. *In vitro* testing data and CLogP values for the B-ring pyridyl compounds synthesised in this SAR study

*CLogP calculated using ChemDraw Professional 15

The parent B-ring pyridyl analogue (**47**) exhibited inhibitory activity against the IspD enzyme that was comparable to the parent pyridoisothiazolone (**17**). Moving the pyridyl moiety from the A-ring into the B-ring appears to have little effect on the enzymatic activity of these compounds (0.17 μM vs. 0.26 μM respectively). However, whole cell activity (**47**, IC_{50} = 70.02 μM) was less potent than the A-ring pyridyl (**17**, IC_{50} = 44.16 μM).

The bi-aryl analogue, **48**, exhibited low micromolar activity (1.07 μM) against the IspD enzyme; however, this activity was an order of magnitude weaker than the parent B-ring pyridyl (**47**). On the other hand, whole cell activity was vastly improved compared with compound **47** (0.9 μM vs. 70.02 μM respectively). Compound **48** was also the first compound in this SAR exploration to exhibit equipotent activity against both enzymatic and phenotypic assays.

Amide analogues **55** and **56** displayed micromolar activity against both enzymatic and whole cell assays; however, neither were as potent as the parent B-ring pyridyl **47** or the B-ring bi-aryl **48**. The length of the side chains in these analogues could result in them being poorly accommodated within the active site and explain the decreased activity.

An unexpected set of results was observed for amine analogues **51**, **52** and **53**. Despite displaying micromolar whole cell inhibition, enzymatic activity was completely lost. A plausible explanation for this result could be that these compounds are exhibiting off-target effects due to their lipophilic nature (CLogPs >3.70).⁵⁸ These analogues could be inhibiting a different enzyme of the MEP pathway, which would be advantageous; however, the target might be something else entirely, and a lack of specificity is highly undesirable in drug compounds.⁵⁹

3.5.4 Conclusion

Despite the parent B-ring pyridyl (**47**) having an IC₅₀ of 0.17 μM against the IspD enzyme, phenotypic activity was significantly lower. A number of side chains were introduced in order to help improve whole cell activity, which was achieved; however, a drop in activity against the enzyme was also observed (**55** and **56**). The most promising compound to emerge was the bi-aryl **48**. The apparent off-target effects of the amine solubilising side chain analogues (compounds **51-53**) meant that this series of compounds was unsuitable for further development.

3.6 CH₂ Linked Compounds

3.6.1 Rationale

This series was identified using a chemoinformatic approach. Data from the original high-throughput screen was used to build a machine-learning model that could predict the activity of untested compounds. A library of 11,831 compounds, based upon the active benzisothiazolinone chemotype, was developed *in silico*. The model was then used to predict the activity of this library

of compounds and a short-list of 64 active compounds was drawn up. CH₂ linked benzisothiazolinone compounds emerged a number of times in the short-list of 64 actives; therefore, this chemotype was selected for further investigation.

The introduction of a CH₂ linker into these compounds (Figure 3.12) should allow for greater flexibility of the side chain within the binding site of the enzyme. Flexibility within the binding site could delay the development of resistance to these benzisothiazolones; particularly in the case of single amino acid mutations, which can abolish the activity of drug compounds with rigid structures.^{60,61} Conformational changes as a result of point mutations could also be offset by additional contacts formed with different amino acid residues in the binding pocket, therefore overcoming the effects of the mutation.⁶²

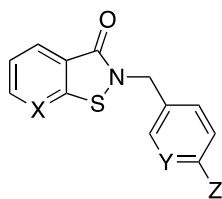
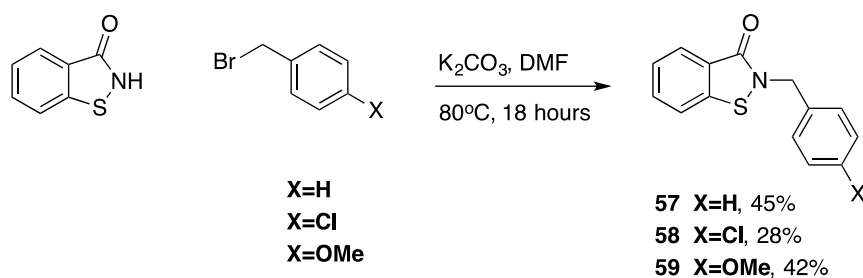


Figure 3.12. The template developed for the series of CH₂ linked compounds

3.6.2 Benzisothiazolinone CH₂ linked analogues

3.6.2.1 Synthesis

The first three analogues in this series were generated in simple one step transformations, starting from the commercially available 1,2-benzisothiazol-3(2*H*)-one (Scheme 3.30).



Scheme 3.30. The synthesis of benzisothiazolinone CH₂ linked analogues

These alkylations with substituted benzyl bromides produced the desired final compounds in yields varying from 28-45%.⁶³

One further compound was synthesised in this series, and this compound contained a pyridyl ring in the side chain (compound **60**) rather than a phenyl ring, in order to investigate whether this has an effect on enzymatic activity. A slightly modified route was used as shown below in Scheme 3.31.



Scheme 3.31. The synthesis of benzisothiazolinone CH₂ linked analogue with a pyridine side chain

This route was chosen as an alternative to the alkylation method due to the low yields that were obtained. This route gave a slightly improved yield of 50%; however, this was also lower than expected. Potentially the reactive acid chloride intermediate (**12**) had started to decompose to the corresponding carboxylic acid, as acid chlorides are highly moisture sensitive. Carboxylic acids are much less reactive and as a result this compound would not undergo the amide-forming step.

3.6.2.2 Results

The activity of each compound in this series was tested *in vitro* against both enzymatic and whole cell 3D7 assays, and the results are summarised below in Table 3.5.

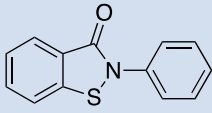
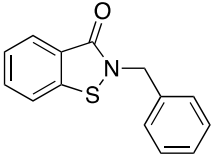
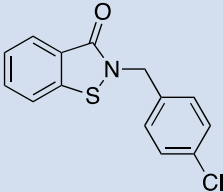
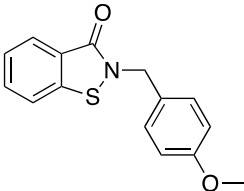
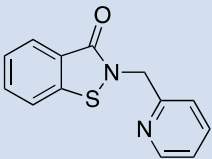
Compound	IspD (μM)	3D7 (μM)	CLogP*
 13	0.60 n=1	5.49 n=1	3.35
 57	2.43 n=1	46.45 n=1	2.90
 58	0.62 n=1	17.88 n=1	3.62
 59	1.34 n=1	67.60 n=1	2.82
 60	1.90 n=1	39.28 n=1	1.41

Table 3.5. *In vitro* testing data and CLogP values for the benzisothiazolinone CH₂ linked analogues synthesised in this SAR study

*CLogP calculated using ChemDraw Professional 15

Whilst compound **57** had low micromolar activity against the IspD enzyme (IC_{50} = 2.43 μM), it was not comparable to the original parent benzisothiazolinone

compound (**13**, $IC_{50} = 0.60 \mu\text{M}$). Introduction of a *para*-chloro substituent (**58**) resulted in vastly improved enzymatic activity ($0.62 \mu\text{M}$) but whole cell activity was still relatively weak in comparison ($17.88 \mu\text{M}$) despite the relatively lipophilic nature of this compound. Potentially the *para*-chloro substituent provides an extra handle for interactions, such as dipole-dipole and Van der Waals, with amino acids in the binding pocket. An increased number of interactions would result in a higher binding affinity and therefore a greater inhibitory effect.

Compounds **59** and **60** maintained low micromolar activity against the enzyme but whole cell data was weak. Lipophilicity does not appear to be a factor here, as the more polar compound (**60**), has better whole cell activity than the more lipophilic methoxy analogue (**59**).

3.6.3 Pyridoisothiazolone CH_2 linked analogues

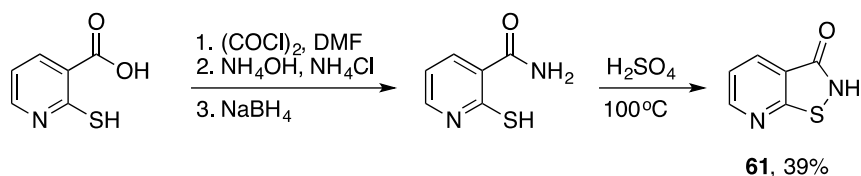
Incorporation of a pyridyl group into the A-ring of the parent benzisothiazolinone resulted in increased activity against the enzyme. A number of pyridoisothiazolone CH_2 linked analogues were created in order to see whether the same effect occurred for this series of compounds as well.

3.6.3.1 Synthesis

An analogous route to the previous CH_2 linked analogues (Scheme 3.30) was used to synthesise these compounds but isothiazolo[5,4-*b*]pyridin-3(2*H*)-one (**61**) was not commercially available and needed to be prepared first.

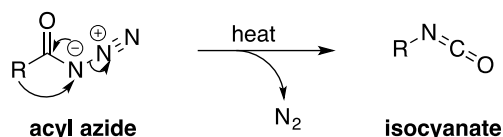
The initial route trialled is shown below in Scheme 3.32, and is adapted from work by Wright and Corbett. The first step involved converting 2-mercaptonicotinic acid to 2-mercaptonicotinamide by treatment with thionyl chloride, ammonium hydroxide and sodium borohydride. Sodium borohydride was used to reduce the disulfide. 2-Mercaptonicotinamide was then heated in

sulfuric acid in order to facilitate the ring closure, producing isothiazolo[5,4-*b*]pyridin-3(2*H*)-one. Sulfuric acid acted as both the oxidant and the solvent.⁶⁴



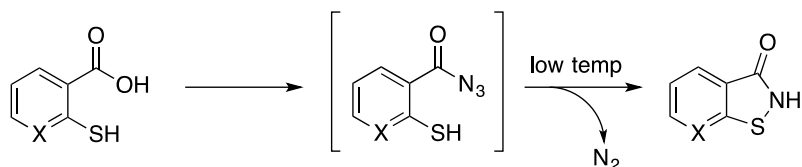
Scheme 3.32. Initial route trialled for the synthesis of isothiazolo[5,4-*b*]pyridin-3(2*H*)-one (**61**)

This route proved unsuccessful, with difficulties encountered in the work up. As a result, the desired pyridoisothiazolone was not obtained. A second method was therefore attempted, which was adapted from research by Chiyoda *et al.* This group successfully synthesised both 1,2-benzisothiazol-3(2*H*)-one (Scheme 3.30) and isothiazolo[5,4-*b*]pyridin-3(2*H*)-one (**61**) via an acyl azide intermediate.⁶⁵ Acyl azides can be used to generate a variety of functional groups such as amines, amides and carbamates via an isocyanate intermediate.^{66,67} This isocyanate intermediate is generated from the acyl azide in a thermal decomposition reaction known as the Curtius rearrangement (Scheme 3.33). Once formed, the isocyanate intermediate can be attacked with a variety of nucleophiles in order to form the desired products. The reaction is believed to be a concerted process where loss of nitrogen and migration of the R-group occur in one step.⁶⁸



Scheme 3.33. The Curtius rearrangement: thermal decomposition of an acyl azide to an isocyanate with loss of nitrogen gas

This rearrangement can be suppressed at lower temperatures and Chiyoda *et al.* discovered that this could allow for a heteroatom-nitrogen bond to be formed, with loss of nitrogen (Scheme 3.34).



Scheme 3.34. Reaction controlled at low temperature to avoid Curtius rearrangement

The acyl azide intermediate can be formed in a variety of ways. The most common involve either a two-step process, which proceeds through an acid chloride intermediate that is attacked by sodium azide, or a one-pot reaction that directly forms the acyl azide from a carboxylic acid using diphenylphosphoryl azide (DPPA) in the presence of a base (Figure 3.13).⁶⁹

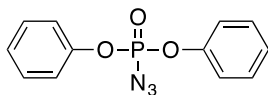


Figure 3.13. The structure of diphenylphosphoryl azide (DPPA)

This method was followed to produce isothiazolo[5,4-*b*]pyridin-3(2*H*)-one (**61**) from 2-mercaptonicotinic acid in a 39% yield. The measured ¹H NMR shifts for each proton in the pyridoisothiazolone ring are shown in Figure 3.14. Each signal is split into a doublet of doublets as each proton couples to two inequivalent protons on the ring.

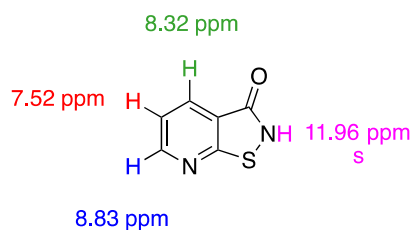


Figure 3.14 ^1H NMR shifts for isothiazolo[5,4-*b*]pyridin-3(2H)-one (**61**)

The different chemical shifts observed for each proton can be explained by resonance (Figure 3.15).

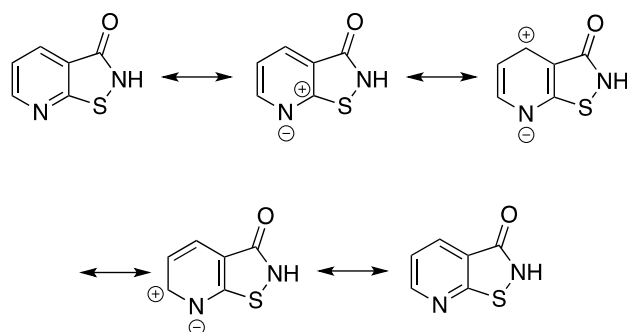
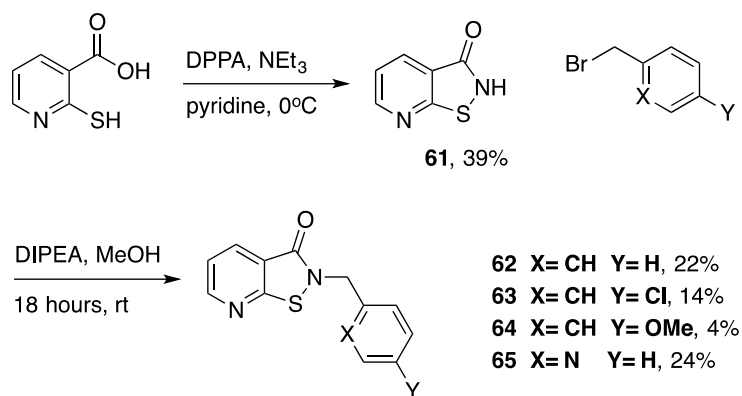


Figure 3.15. Resonance structures of isothiazolo[5,4-*b*]pyridin-3(2H)-one (**61**)

Electron density from the *ortho*- and *para*- positions can be donated via resonance to the electronegative nitrogen atom in the ring. These nuclei are therefore deshielded and feel a stronger magnetic field. As a result, their signals are shifted further downfield (8.83 and 8.32 ppm). There is no resonance form for the *meta*-position, therefore this nucleus is more shielded and its chemical shift is further upfield (7.52 ppm).⁷⁰

Compounds **62** to **65** were then formed in simple alkylation reactions using a variety of substituted benzyl and pyridyl bromides (Scheme 3.35).



Scheme 3.35. Synthesis of the pyridoisothiazolone CH₂ linked compounds

The yields for this final transformation were poor (<24%), and much lower than the corresponding CH₂ linked benzisothiazolinones. The introduction of pyridine into the ring could be affecting the nucleophilicity of the amide nitrogen, resulting in a reduced yield. If these compounds were to be re-synthesised, the benzyl sulfide-benzyl sulfoxide-pyridoisothiazolone method used for the A-ring pyridyl series could be adopted (Scheme 3.22).

3.6.3.2 Results

Each compound in this series was submitted for both enzymatic and whole cell 3D7 testing and the results are summarised below in Table 3.6.

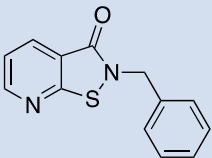
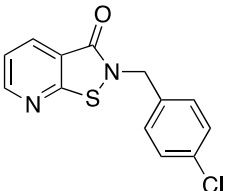
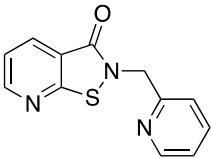
Compound	IspD (μM)	3D7 (μM)	CLogP*
 62	1.52 n=1	55.26 n=1	1.41
 63	~10 n=1	-	2.12
 64	3.31 n=1	57.24 n=1	1.32
 65	>10 n=1	-	-0.09

Table 3.6. *In vitro* testing data and CLogP values for the pyridoisothiazolone CH₂ linked analogues synthesised in this SAR study

*CLogP calculated using ChemDraw Professional 15

Introduction of a pyridyl group into the A-ring lead to an increased potency against the IspD enzyme for compound **62** compared with the benzisothiazolinone analogue **57** (1.52 μM vs. 2.43 μM respectively). However,

the introduction of *para*-substituents resulted in a decrease in potency (Figure 3.16). The most active compound of the benzisothiazolinone CH₂ linked series was the *para*-chloro analogue **58**; however, the analogous pyridoisothiazolone compound **63** had very poor activity against the IspD enzyme, and as a result whole cell data has not been measured. Compound **65**, which incorporates a pyridyl group into the B-ring as well as the A-ring, also displayed poor inhibitory activity against the enzyme.

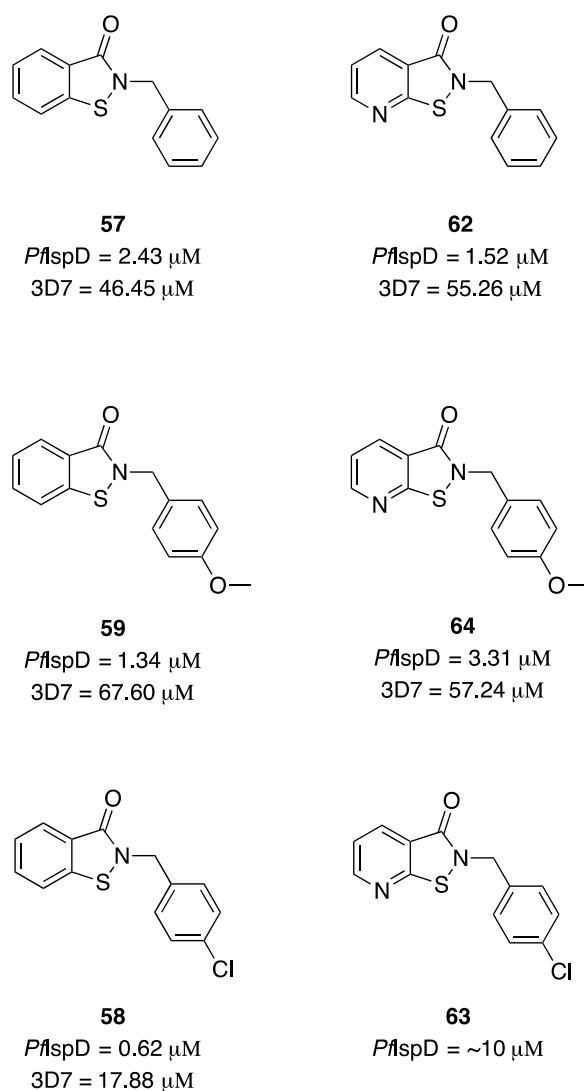


Figure 3.16. A comparison of CH₂ linked benzisothiazolinones and pyridoisothiazolones: *para*-substitution increased *Pfl*spD potency for benzisothiazolinones, in contrast to pyridoisothiazolones, where a decrease in potency was observed

Overall, the benzisothiazolinone CH₂ linked analogues displayed better inhibition profiles, therefore no further pyridyl analogues were synthesised for this series.

3.6.4 5-OMe CH₂ linked analogues

Another A-ring modification predicted to be well tolerated was the introduction of a methoxy group into the 5-position on the benzisothiazolinone ring (awaiting data). Therefore it was decided to incorporate this moiety into the CH₂ linked series (Figure 3.17). The most potent side chain from the benzisothiazolinone CH₂ linked series, a *para*-chloro substituted benzyl moiety was incorporated, as well as benzyl side chain for comparison.

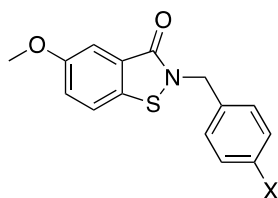
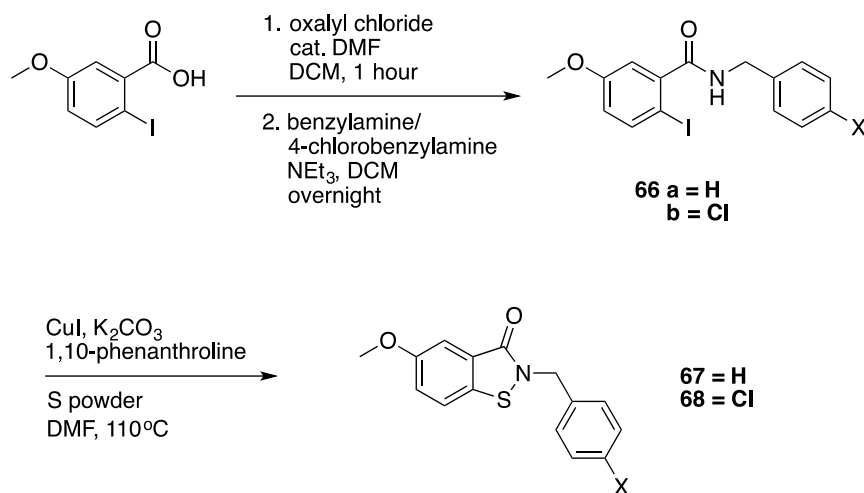


Figure 3.17. Template for the 5-OMe CH₂ linked analogues

3.6.4.1 Synthesis

The synthesis of the 5-OMe analogues is outlined below in Scheme 3.36. 2-Iodo-5-methoxybenzoic acid was coupled to both benzylamine and 4-chlorobenzyl amine in order to generate the amide intermediates **66 a** and **b**. The copper iodide-mediated route described in Section 3.2.2 was used to facilitate ring closure. The final compounds, **67** and **68**, were generated in 35% and 45% yields respectively.



Scheme 3.36. The synthesis of 5-methoxy CH₂ linked analogues

3.6.4.2 Results

The inhibitory activity of compounds **67** and **68** was measured in both enzymatic and whole cell 3D7 assays, and the results are summarised below in Table 3.7. It can be seen that the parent benzyl analogue (**67**) was not only potent against the IspD enzyme, but had the most potent whole cell activity of the CH₂ linked series.

Compound **68** had much lower inhibitory activity against the enzyme than predicted, and as a result, whole cell inhibition was not measured. It appears as though the same effect is seen here that was seen for the *para* substituted pyridoisothiazolone compounds, **63** and **64**, where substitution in this position leads to a decrease in potency.

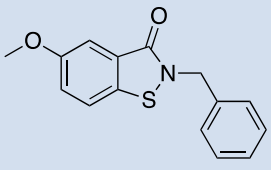
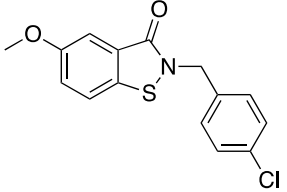
Compound	IspD (μM)	3D7 (μM)	CLogP*
 67	0.91 n=1	7.50 n=1	2.82
 68	>5 n=1	-	3.53

Table 3.7. *In vitro* testing data and CLogP values for the 5-OMe CH₂ linked analogues synthesised in this SAR study

*CLogP calculated using ChemDraw Professional 15

3.6.5 Conclusion

The two best compounds to emerge from this CH₂ linked series were the *para* chloro and 5-OMe analogues, **58** and **67** (Figure 3.18). Despite compound **58** having slightly more potent activity against the enzyme, the improved whole cell data for compound **67** make this the most promising compound to emerge from this portion of the SAR exploration and a potential candidate for further development.

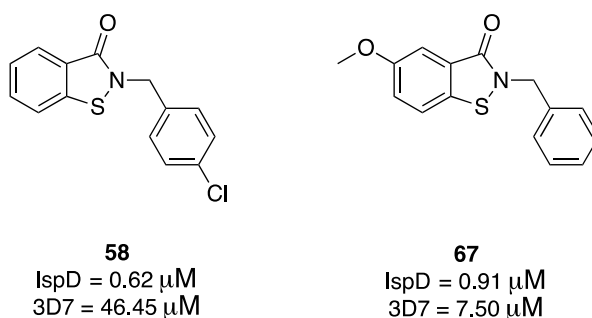


Figure 3.18. The most potent analogues to emerge from the CH₂ linked series

3.7 Selenium analogues

3.7.1 Rationale

For many years selenium was considered to be a poison and evidence of selenosis in livestock dates back to 1285.⁷¹ Nowadays it is known to be an essential trace element, and selenoproteins are known to carry out a number of important functions throughout the body, including the protection of cellular components against oxidative and free radical damage.^{72,73} Despite a number of beneficial effects associated with dietary supplementation of selenium, its use in drug compounds has been rather limited due to the fact that the dose required by many pharmaceuticals, would exceed safe levels of selenium and result in toxicity. The key to the use of selenium in drug compounds is to therefore ensure it is “tied up” in heterocycles, so that it is no longer bioavailable.⁷⁴

There are now a number of examples where sulfur has been successfully replaced by selenium in drug compounds and an increase in biological activity has been observed.⁷⁵ Despite being members of the same period, there are key differences between sulfur and selenium. Selenium for example has a much larger atomic radius and as a result is less electronegative than sulfur. Bond dissociation energies for C-Se, H-Se and Se-Se are lower than their sulfur counterparts, resulting in organoseleniums being more reactive than organosulfurs.^{76,77}

Selenium has now found uses in anti-oxidant, anti-inflammatory and anti-cancer drugs.⁷⁸ What is even more interesting for this project is the proposal that selenium can interact with cysteine thiols in proteins and therefore modulate the activity of that protein.⁷⁹

However, the principal reason behind replacing the core benzisothiazolinone with a benzisoselenazolone is one of the best-known selenium containing drug compounds, ebselen (Figure 3.19). Ebselen was designed for the treatment of acute ischaemic stroke by inhibiting lipid peroxidation through a number of

different mechanisms.^{80,81} Despite promising early trial data, it was abandoned in the final phase due to insufficient efficacy. Although the drug was abandoned for the treatment of acute ischaemic stroke, the trial data showed it was well tolerated and clinically safe; therefore, it is now being tested for a number of other illnesses including bipolar disorder and multi-drug resistant staphylococcal skin infections.^{82,83}

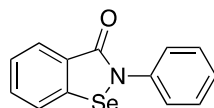
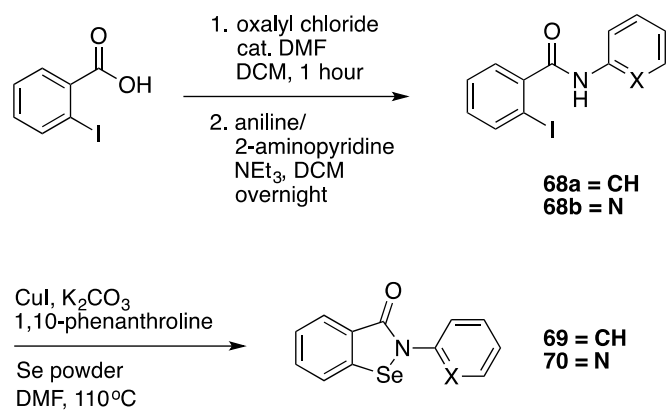


Figure 3.19. The structure of Ebselen (**70**), a benzisoselenazolone

The success of ebselen, the proposed mechanism of protein modulation and the increased biological activity observed for replacement of sulfur with selenium in drug compounds, all led to the design of this final stage of SAR exploration.

3.7.2 Synthesis

The first two compounds synthesised in this series were ebselen (**70**) and its B-ring pyridyl analogue (**71**) in order to compare their activity with the analogous sulfur compounds, **13** and **47**. Both **70** and **71** were synthesised from the same common starting material, 2-iodobenzoic acid (Scheme 3.37). The first step involved the formation of the amide intermediates (**69 a** and **b**) required for the final ring closure step, and this was achieved via an acid chloride. An analogous copper iodide-mediated ring closure can be applied to the synthesis of benzisoselenazolones as benzisothiazolinones.⁸⁴ The method outlined by Bhakuni *et al.* led to the formation of **70** and **71** in a 25% and 9% yield respectively.



Scheme 3.37. The synthetic pathway to benzisoselenazolone compounds **70** and **71**

The main side product from both reactions was identified as the dimer that is shown in Figure 3.20. The formation of this product is responsible for the main loss of yield in these copper iodide-catalysed reactions.

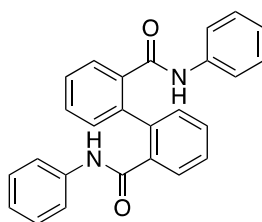


Figure 3.20. The structure of the main side product formed in the copper iodide catalysed ring closure

A preferred method would be a Se-Cl mediated ring closure, analogous to the S-Cl route utilised for the synthesis of compound **13** but the corresponding diselenide starting material, 2,2'-diselanediyldibenzoic acid (Figure 3.21) was not commercially available.⁸⁵ Many methods published regarding the synthesis of 2,2'-diselanediyldibenzoic acid involve the use of disodium diselenide (Na₂Se₂).^{86,87} A number of routes for the synthesis of disodium diselenide were investigated; however, most ran the risk of generating hydrogen selenide gas (H₂Se gas) which is highly toxic and were therefore not feasible without the use of a glovebox.^{88,89}

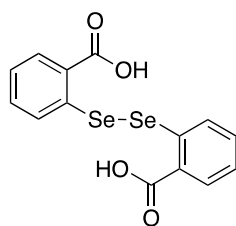
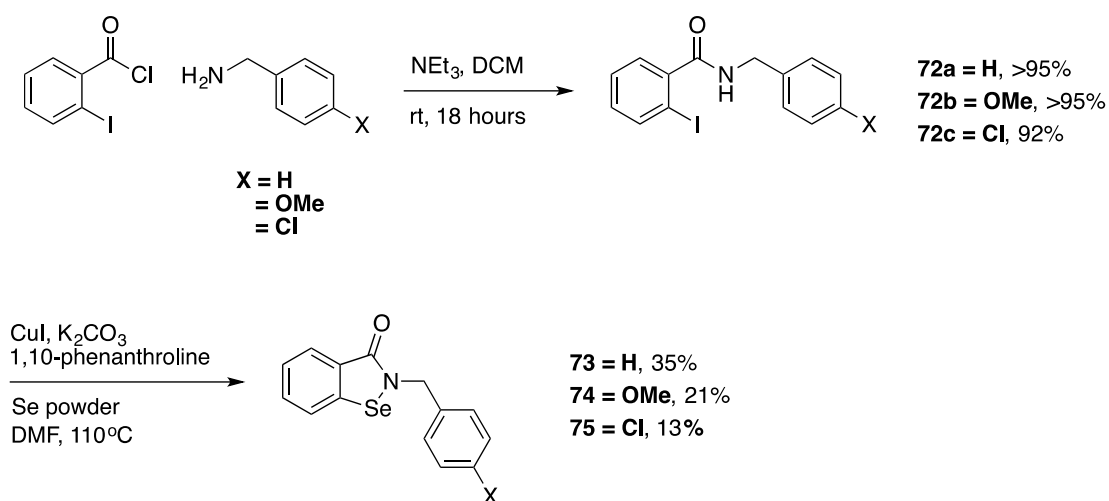


Figure 3.21. The structure of 2,2'-diselanediyldibenzoic acid

Therefore, it was decided that the copper iodide-catalysed ring closure would be utilised going forward, despite the low yields obtained. The final three compounds to be synthesised in this series were analogues of the CH₂ linked benzisothiazolinone compounds **57**, **58** and **59**.

These compounds were synthesised from 2-iodobenzoyl chloride (Scheme 3.38), as this was available to purchase for the same price as 2-iodobenzoic acid and ultimately avoids the time and cost of materials when generating the acid chloride *in situ*. Once the desired amides were synthesised (**72 a-c**) they underwent ring closure to form the final benzisoselenazolone compounds (**73-75**) in yields varying from 13-35%.



Scheme 3.38. The synthetic pathway to benzisoselenazolone CH₂ linked compounds

Again, the low yields for the copper iodide-mediated ring closure step can be accounted for by formation of the dimer shown in Figure 3.20.

3.7.3 Results

The activity of each compound in this series was tested *in vitro* against both enzymatic and whole cell 3D7 assays, and the results are summarised below in Table 3.8.

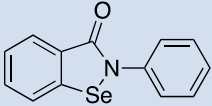
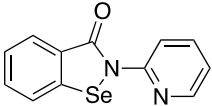
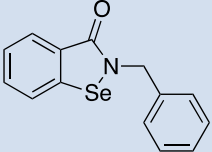
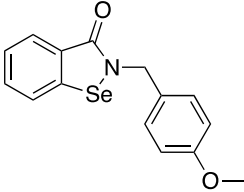
Compound	IspD (μM)	3D7 (μM)	CLogP*
 70	8.78 \pm 0.59 n=2	9.65 n=1	3.70
 71	0.76 n=1	15.77 n=1	2.21
 73	0.50 n=1	19.71 n=1	3.73
 74	0.23 n=1	23.35 n=1	3.65
 75	0.17 n=1	5.54 n=1	4.44

Table 3.8. *In vitro* testing data and CLogP values for the benzoselenazolone series of compounds

*CLogP calculated using ChemDraw Professional 15

The parent benziselenazolone **70** had micromolar activity against both enzymatic and whole cell assays ($8.78 \pm 0.59 \mu\text{M}$ and $9.65 \mu\text{M}$ respectively) but was not potent enough to be taken forward. It was however, one of the few compounds across the whole SAR study that had equipotent activity against both the IspD enzyme and whole cell.

The introduction of a pyridyl moiety into the B-ring (compound **71**) had a significant effect on the enzymatic activity, with the IC_{50} improving to $0.76 \mu\text{M}$. Despite improved inhibitory activity against the enzyme, whole cell activity decreased, potentially due to the more polar nature of the pyridyl analogue.

A comparison in Table 3.9 shows that neither compound **70** nor **71** were as potent as the analogous sulphur compounds (**13** and **47**) against the IspD enzyme, and this difference was most profound between compounds **13** and **70** ($0.60 \mu\text{M}$ vs. $8.78 \pm 0.59 \mu\text{M}$). However, the difference in whole cell activity between **13** and **70** was less marked, and benziselenazolone **71** had more potent whole cell activity than the benzisothiazolinone equivalent **47** ($70.02 \mu\text{M}$ vs. $15.77 \mu\text{M}$ respectively).

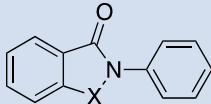
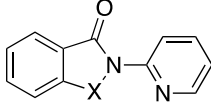
Compound	IspD (μM)	3D7 (μM)	CLogP*
 13, X = S 70, X = Se	S = 0.60 Se = 9.37	S = 5.49 Se = 9.65	S = 3.35 Se = 3.70
 47, X = S 71, X = Se	S = 0.17 Se = 0.76	S = 70.02 Se = 15.77	S = 1.86 Se = 2.21

Table 3.9. A comparison between the benzisothiazolinone and benziselenazolone phenyl and B-ring pyridyl compounds

*CLogP calculated using ChemDraw Professional 15

All three CH₂ linked analogues (**73** – **75**) had increased potency against IspD compared to the phenyl and pyridyl analogues **70** and **71**. The *para*-chloro analogue (**75**) had the most potent activity, with an IC₅₀ value of 0.17 μM against the enzyme. This analogue also had the most potent activity against the whole cell 3D7 assay, which could be a consequence of the high lipophilicity of this compound (ClogP = 4.44) compared to the other compounds in this series.

Table 3.10 compares the activity of analogous sulfur and selenium CH₂ linked compounds. The benzoselenazolone series mirrors that of the benzothiazolinones, with the least potent compounds being non-substituted benzyl analogues, and the most potent being *para*-chloro substituted analogues. Both series followed the trend that whole cell activity increased as lipophilicity increased but the benzoselenazolone CH₂ linked compounds were more potent against the whole cell.

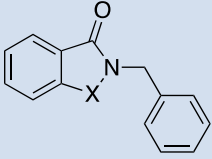
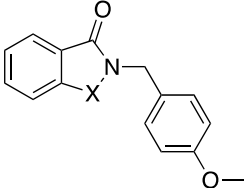
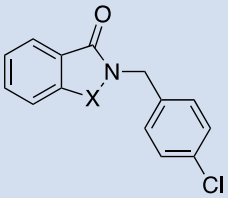
Compound	IspD (μM)	3D7 (μM)	CLogP*
 57, X = S 73, X = Se	S = 2.43 Se = 0.50	S = 46.45 Se = 19.71	S = 2.90 Se = 3.73
 59, X = S 74, X = Se	S = 1.34 Se = 0.23	S = 67.60 Se = 23.35	S = 2.82 Se = 3.65
 58, X = S 75, X = Se	S = 0.62 Se = 0.17	S = 17.88 Se = 5.54	S = 3.62 Se = 4.44

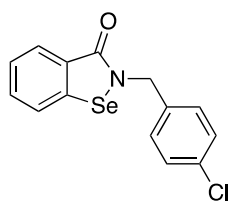
Table 3.10. A comparison between the benzisothiazolinone and benzoselenazolone CH_2 linked series

*CLogP calculated using ChemDraw Professional 15

3.7.4 Conclusion

This series of benzoselenazolone compounds, developed from ebselen, show that a Se-N heterocycle provides a good alternative to the S-N heterocycles already investigated. These selenium analogues have improved lipophilicity and the CH_2 linked compounds are more potent than their sulfur counterparts.

The most potent compound to emerge from this series was the *para*-chloro analogue **75** (Figure 3.22), which has low micromolar activity against both IspD and the whole cell, and is therefore a candidate for further development.



75
PflspD = 0.17 μ M
3D7 = 5.54 μ M

Figure 3.22. The structure of the most potent analogue from this series, the *para*-chloro analogue, **75**

The yields for the copper iodide-mediated ring closure were low (<35%); therefore, if further work were to be conducted on this series of compounds, an alternative method of forming the benziselenazolone core should be investigated.

3.8 Summary

The aim of this project was to generate a library of novel compounds designed to target the IspD enzyme and to explore structure activity relationships (SAR) around the hit template that was identified from an initial high throughput screen.

A library of over 30 compounds was therefore synthesised, and the inhibitory activity of these compounds was tested against both enzymatic (*PflspD*) and phenotypic (3D7 whole cell) *in vitro* assays. A number of different methods to synthesise the isothiazolinone core were also investigated.

Furthermore, a variety of modifications and substitutions have been introduced in order to explore structure activity relationships around the benzisothiazolinone core. The most active compounds to emerge from each drug class are summarised below in Figure 3.23.

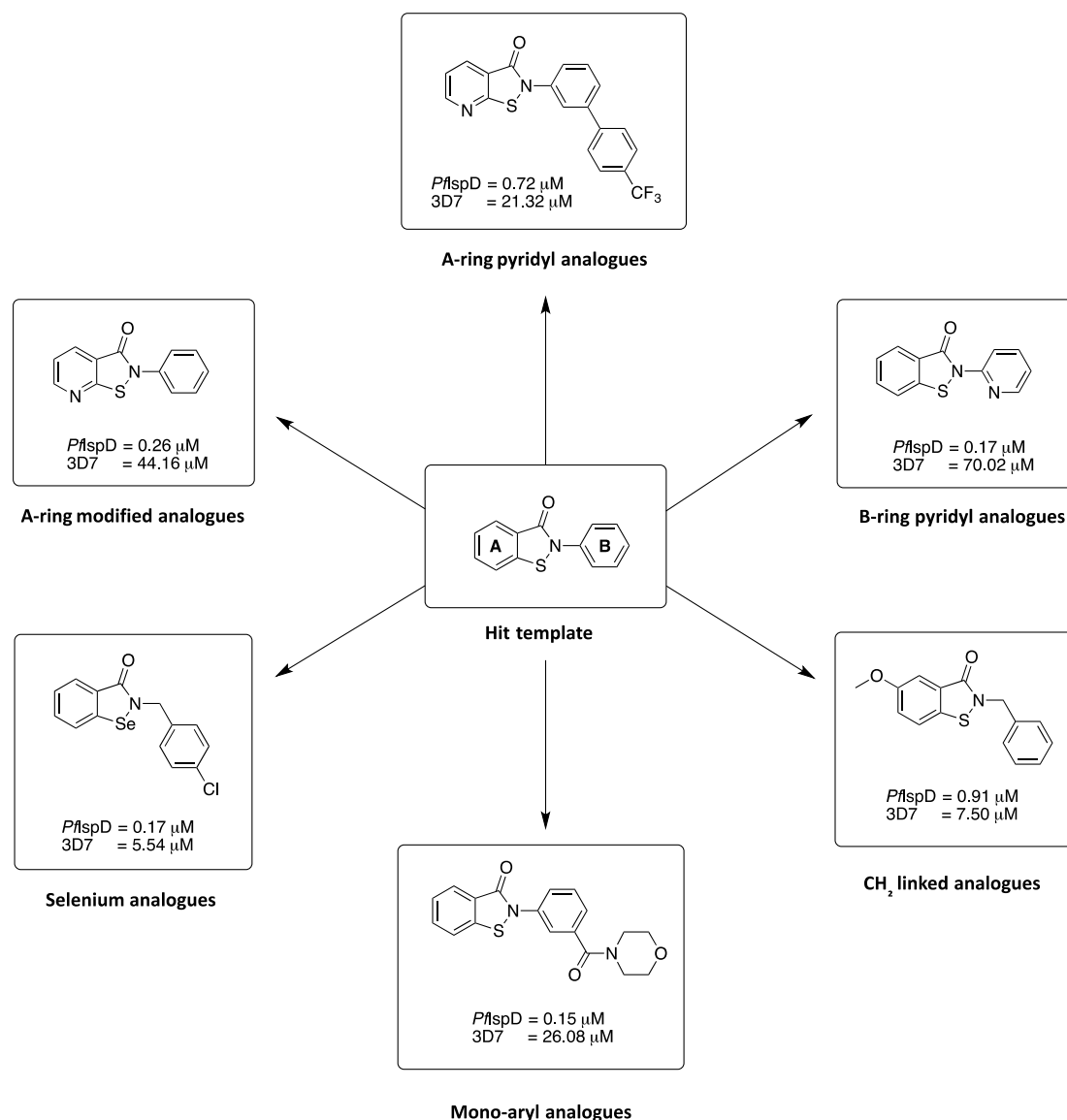
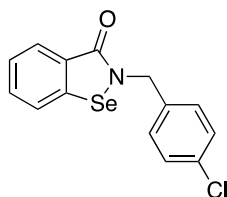


Figure 3.23. A summary of the most potent compounds identified in this SAR exploration

A number of compounds displayed low micromolar activity against *PflspD* but whole cell activity was not comparable. The lipophilicity of a number of compounds was therefore increased in order to help improve whole cell potency and this was achieved; however, a drop in inhibitory activity against the enzyme was also observed.

The most promising compound to emerge from this research was the CH₂ linked benzisoselenazolone **75**, which exhibited potent activity against both *PflspD* and

phenotypic 3D7 assays. In fact, all of the CH₂ linked benzoselenazolones displayed more potent activities than the analogous benzisothiazolinones. Compound **75** (Figure 3.24) has the greatest potential for further development as a novel drug candidate and the next steps would be to investigate the inhibitory activity of this compound and determine its pharmacokinetic profile in an *in vivo* model.



75
*Pf*spD = 0.17 μM
3D7 = 5.54 μM
CLogP = 4.44

Figure 3.24. The structure of the most promising compound to emerge from this SAR, a CH₂ linked benzoselenazolone (**75**)

This research represents the early stage development of a series of compounds designed to inhibit a novel target in antimalarial drug discovery, IspD. The following chapters will discuss the late stage development of a group of tetraoxane antimalarials, which have evolved from artemisinin, a natural product with potent antimalarial activity.

3.9 Experimental

Setting up reactions

All reactions and purifications were carried out in a fume cupboard with appropriate PPE in place. Reactions sensitive to air and moisture were carried out in oven-dried glassware sealed with rubber septa. A positive pressure of dry nitrogen or argon was achieved from manifold or balloon. Sensitive liquids and solutions were transferred via single-use syringes, free from latex and silicone oil. Reactions, which required heating, were heated in an oil bath and fitted with a reflux condenser. All reactions were stirred using a Teflon coated magnetic stirrer bar and organic solutions were concentrated using a Büchi rotary evaporator with a vacuum pump.

Purification of reagents and organic solvents

Anhydrous solvents were either obtained from commercial sources or dried and distilled immediately prior to use under constant flow of dry nitrogen. THF was distilled from sodium benzophenone and dichloromethane was distilled from calcium hydride. All reagents were purchased from Sigma Aldrich, Alfa Aesar, Apollo Scientific and Fluorochem and were used without further purification unless otherwise indicated.

Purification of products

Analytical thin layer chromatography (TLC) was carried out using Merck TLC Silica gel 60 F₂₅₄ alum inium sheets and visualized under UV or by appropriate stain. Column chromatography was carried out using Sigma Aldrich technical grade silica gel (pore size 60 Å, 230-400 mesh particle size, 40-63 µm particle size).

Analysis

¹H NMR Spectra were recorded on a Bruker AMX400 (400 MHz) or a Bruker AMX250 (250 MHz). The chemical shifts (δ) are described in parts per million (ppm) downfield from an internal standard of tetramethylsilane. Multiplicities are singlet (s), doublet (d), triplet (t), quartet (q), doublet of doublets (dd),

doublet of triplets (dt), triplet of doublets (td), doublet of doublet of doublets (ddd) and multiplet (m). Coupling values are measured in Hz. ^{13}C NMR spectra were also recorded on a Bruker AMX400 (101 MHz) and chemical shifts are reported relative to a residual solvent peak. Mass Spectra were recorded on a Micromass LCT or an Agilent QTOF 7200 Mass Spectrometer using chemical ionisation (CI) or electron spray (ES). Microanalyses (%C, %H, %N) were carried out in the University of Liverpool Microanalysis laboratory. Melting points were determined on a Gallenkamp melting point apparatus in degrees Celsius (last solvent CDCl_3).

3.9.1 General procedures

General Procedure 1: Sulfonamide synthesis

A stirring solution of the required sulfonyl chloride (1 eq) in anhydrous DCM (40 mL/g) was cooled to 0°C . Triethylamine (2 eq) and the required amine (1.25 eq) were then added and the reaction mixture stirred at room temperature for 2 hours. The reaction mixture was then washed with water (30 mL), 1M HCl solution (2x 30 mL), water (30 mL) and brine (30 mL). The organic extract was then dried over anhydrous MgSO_4 , filtered and concentrated under reduced pressure to give the crude sulfonamide product. The crude products were purified by flash chromatography.

General Procedure 2: Catalytic hydrogenation of nitro to amine

The required nitro-containing compound (1 eq) was dissolved in methanol. Palladium on activated charcoal (10 wt. % loading) was added and the reaction mixture stirred under a hydrogen atmosphere overnight. The reaction mixture was then filtered through a pad of celite and washed thoroughly with ethyl acetate before concentrating under reduced pressure to give the desired amine product. No further purification required.

General Procedure 3: Amide preparation

Step 1: To a stirring solution of the required carboxylic acid (1 eq) in anhydrous DCM (30 mL/g) was added oxalyl chloride (2 eq) and catalytic DMF (3-4 drops). The resulting reaction mixture was stirred at room temperature for 1.5 hours. The reaction mixture was then concentrated under reduced pressure and the resulting acid chloride intermediate dried thoroughly under high-vacuum.

Step 2: To a stirring solution of the acid chloride intermediate in anhydrous DCM (30 mL/g) was added the required amine (1.25 eq) and triethylamine (2 eq). The resulting reaction mixture was stirred overnight at room temperature. The reaction mixture was then washed with water (20 mL), 1M HCl (20 mL), NaHCO₃ (20 mL) and brine (20 mL). The organic extract was then dried over anhydrous MgSO₄, filtered and concentrated under reduced pressure to give the desired amide product, which was taken forward to the next step without further purification.

General Procedure 4: Oxidation of sulfide to sulfoxide

To a stirring solution of the required sulfide (1 eq) in methanol (30 mL/g) was added sodium periodate (1.3 eq) in water (10 mL/g). The resulting turbid solution was heated to 50°C for 2 hours. The reaction mixture was concentrated under reduced pressure and the resulting residue was filtered and washed with water before drying in a desiccator.

General Procedure 5: Ring closure from sulfoxide - thionyl chloride

To a stirring solution of the required sulfoxide (1 eq) in anhydrous DCM (25 mL/g) was added thionyl chloride (1.3 eq). The resulting reaction mixture was heated to 50°C for 2 hours. The reaction mixture was then concentrated under reduced pressure to give the product isothiazolinone derivative. The crude products were purified by flash chromatography.

General procedure 6: Benzisothiazolinone alkylation

To a stirring solution of benzo[*d*]isothiazol-3(2*H*)-one (1 eq) in anhydrous DMF (40 mL/g) was added potassium carbonate (2 eq) and the required substituted

benzyl bromide (1.1 eq). The resulting reaction mixture was stirred at 80°C overnight. The reaction mixture was then poured into water and extracted with ethyl acetate (3 x 20 mL). The combined organic extracts were washed with brine (20 mL), dried over Na₂SO₄ and concentrated under reduced pressure. The crude products were purified by flash chromatography.

General procedure 7: Isothiazolo-pyridin-3-one alkylation

To a stirring solution of isothiazolo[5,4-*b*]pyridin-3(2*H*)-one (1 eq) in methanol (30 mL/g) was added *N,N*-diisopropylethylamine (1.1 eq) and the required substituted benzyl bromide (1.3 eq). The resulting reaction mixture was stirred overnight at room temperature. The reaction mixture was then poured into 1M HCl and extracted with ethyl acetate (3 x 20 mL). Combined organic extracts were washed with water (2 x 20 mL) and brine (20 mL), dried over Na₂SO₄, filtered and concentrated under reduced pressure. The crude products were purified by flash chromatography.

General procedure 8: Suzuki cross-coupling

A stirring solution of the required aryl halide (1 eq) in DME (0.4 mmol/mL) and water (0.4 mmol/mL) was placed under a nitrogen atmosphere. The required boronic acid (1.2 eq) and Pd(PPh₃)₄ (0.025 eq) were added sequentially, evacuating and backfilling the flask with nitrogen after each addition. The resulting reaction mixture was then stirred at 80°C overnight. The reaction mixture was then diluted with water and extracted with ethyl acetate (3 x 20 mL). The combined organics were then washed with brine (30 mL), dried over anhydrous MgSO₄, filtered and concentrated under reduced pressure. The crude products were purified by flash chromatography.

General procedure 9: Ring closure from sulfoxide - TCAA

A stirring solution of the required sulfoxide (1 eq) in anhydrous DCM (50 mL/g) was cooled to 0°C under a nitrogen atmosphere. Trichloroacetic anhydride (1.1 eq) was added drop wise and the resulting reaction mixture was allowed to warm to room temperature and stirred for 2 hours. The reaction mixture was then basified using 2M NaOH and extracted with DCM (3 x 20 mL). The combined

organics were washed with brine (30 mL), dried over anhydrous MgSO_4 , filtered and concentrated under reduced pressure. The crude products were purified by flash chromatography.

General procedure 10: Benzisothiazolinone formation via CuI ring closure

A solution of copper iodide (0.5 eq) and 1,10-phenanthroline (0.5 eq) in DMF (30 mL/g) was stirred under nitrogen for 15 minutes (dark orange/brown solution). The required amide (1 eq), sulfur powder (1.2 eq) and potassium carbonate (1.25 eq) were then added before heating to 110°C for 60 hours under a nitrogen atmosphere. The reaction mixture was then stirred in brine for 3 hours before extracting with ethyl acetate (3 x 30mL). The combined organic extracts were then dried over anhydrous MgSO_4 , filtered and concentrated under reduced pressure. The crude products were purified by flash chromatography.

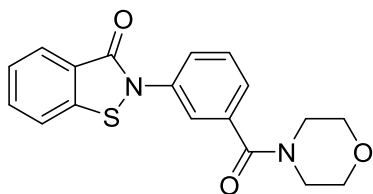
General procedure 11: SCl ring closure

To a stirring solution of the required amine side chain (1 eq) in anhydrous DCM (40 mL/g) was added 2-(chlorocarbonyl)phenyl hypochlorothioite (1.3 eq) and triethylamine (2 eq). The resulting reaction mixture was stirred at room temperature overnight under a nitrogen atmosphere. The reaction mixture was then diluted with NaHCO_3 and extracted with DCM (3 x 30 mL). The combined organics were washed with brine (30 mL), dried over Na_2SO_4 , filtered and concentrated under reduced pressure. The crude products were purified by flash chromatography.

General procedure 12: Benzisoselenazolone formation via CuI ring closure

A solution of copper iodide (0.2 eq) and 1,10-phenanthroline (0.2 eq) in DMF (30 mL/g) was stirred under nitrogen for 15 minutes (dark orange/brown solution). The required amide (1 eq), selenium (1.2 eq) and potassium carbonate (1.5 eq) were then added before heating to 110°C for 36 hours under a nitrogen atmosphere. The reaction mixture was then stirred in brine for 3 hours before extracting with ethyl acetate (3 x 30mL). The combined organic extracts were then dried over anhydrous MgSO_4 , filtered and concentrated under reduced pressure. The crude products were purified by flash chromatography.

3.9.2 Experimental for compounds 1-75



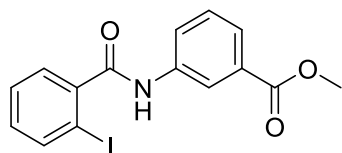
2-(3-(Morpholine-4-carbonyl)phenyl)benzo[d]isothiazol-3(2H)-one (1).

General procedure 5 was followed using 2-(methylsulfinyl)-*N*-(3-(morpholine-4-carbonyl)phenyl)benzamide to give the title compound as a white solid (108 mg, 66% yield): mp 155-157°C; ^1H NMR (400 MHz, CDCl_3) δ = 8.10 (d, J = 8 Hz, 1H), 7.85 – 7.82 (m, 1H), 7.77 (dd, J = 7, 1 Hz, 1H), 7.72 – 7.66 (m, 1H), 7.61 (d, J = 8 Hz, 1H), 7.54 (t, J = 8 Hz, 1H), 7.47 (td, J = 8, 1 Hz, 1H), 7.38 (d, J = 8 Hz, 1H), 3.77-3.57 (m, 8H) ppm; ^{13}C NMR (101 MHz, CDCl_3) δ = 169.32, 164.37, 139.85, 137.59, 136.56, 132.82, 129.94, 127.37, 126.16, 125.72, 125.64, 124.71, 123.26, 120.34, 67.02 ppm; HRMS (CI, m/z) calcd for $[\text{C}_{18}\text{H}_{17}\text{N}_2\text{O}_3\text{S}]^+$ ($\text{M}+\text{H}$) $^+$ 341.0960, found 341.0959; IR (neat) ν 2966 (w, C-H aromatic), 2858 (w, C-H aliphatic), 1654 (s, C=O amide), 1620 (s, C=O amide), 1571 (m, C-C aromatic), 1439 (m, C-H aliphatic), 1278 (s, C-O), 753 (s, S-N) cm^{-1} .



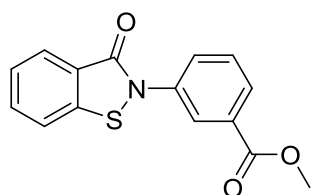
Methyl 3-(2-bromobenzamido)benzoate (2).

General procedure 3 was followed using 2-bromobenzoic acid (500 mg, 2.49 mmol) and methyl 3-aminobenzoate (0.69 mL, 2.99 mmol) to give the title compound as a pale yellow solid (775 mg, 93% yield): ^1H NMR (400 MHz, CDCl_3) δ = 8.15 (t, J = 2 Hz, 1H), 8.05 (ddd, J = 8, 2, 1 Hz, 1H), 7.94 (s, 1H), 7.86 – 7.82 (m, 1H), 7.67 – 7.62 (m, 2H), 7.46 (t, J = 8 Hz, 1H), 7.41 (td, J = 8, 1 Hz, 1H), 7.33 (td, J = 7, 2 Hz, 1H), 3.89 (s, 3H) ppm; ^{13}C NMR (101 MHz, CDCl_3) δ = 167.04, 166.05, 138.11, 137.86, 134.06, 132.18, 131.44, 130.30, 129.68, 128.29, 126.42, 124.99, 121.35, 119.72, 52.59 ppm; HRMS (ES, m/z) calcd for $[\text{C}_{15}\text{H}_{12}\text{BrNNaO}_3]^+$ ($\text{M}+\text{Na}$) $^+$ 355.9898, found 355.9897.



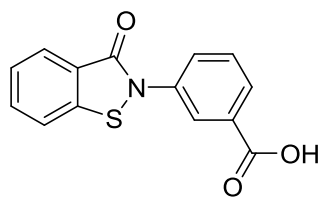
Methyl 3-(2-iodobenzamido)benzoate (2b).

General procedure 3 was followed using 2-iodobenzoic acid (1 g, 3.75 mmol) and methyl 3-aminobenzoate (709 mg, 4.69 mmol) to give the title compound as a pale brown solid (1.29 g, 92% yield): ^1H NMR (400 MHz, CDCl_3) δ = 8.15 (s, 1H), 8.07 (d, J = 8 Hz, 1H), 7.93 – 7.80 (m, 3H), 7.56 – 7.39 (m, 3H), 7.15 (dd, J = 8, 2 Hz, 1H), 3.85 (s, 3H) ppm; ^{13}C NMR (101 MHz, CDCl_3) δ = 167.55, 166.83, 141.90, 140.19, 137.94, 131.77, 131.08, 129.46, 128.68, 128.50, 126.01, 124.77, 121.06, 92.48, 52.40 ppm; HRMS (ES, m/z) calcd for $[\text{C}_{15}\text{H}_{12}\text{INaO}_3]^+$ ($\text{M}+\text{Na}$) $^+$ 403.9760, found 403.9773; Anal. Calcd for $\text{C}_{15}\text{H}_{12}\text{INO}_3$: C, 47.27; H, 3.17; N, 3.67. Found: C, 47.25; H, 3.25; N, 3.55.



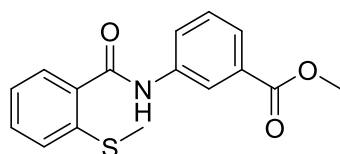
Methyl 3-(3-oxobenzothiazol-2-yl)benzoate (3).⁹⁰

General procedure 5 was followed using methyl 3-(2-(methylsulphanyl)benzamido)benzoate (2.3 g, 7.25 mmol) to give the title compound as a white solid (2.3 g, 64% yield): ^1H NMR (400 MHz, CDCl_3) δ = 8.32 – 8.30 (m, 1H), 8.13 – 8.09 (m, 1H), 8.03 – 7.97 (m, 2H), 7.68 (ddd, J = 8, 7, 1 Hz, 1H), 7.60 (dt, J = 8, 1 Hz, 1H), 7.55 (t, J = 8 Hz, 1H), 7.46 (ddd, J = 7, 5, 1 Hz, 1H), 3.94 (s, 3H) ppm; ^{13}C NMR (101 MHz, CDCl_3) δ = 166.61, 164.57, 137.96, 133.05, 131.89, 129.89, 129.20, 128.37, 127.70, 126.40, 125.62, 124.99, 120.57, 52.58 ppm; HRMS (ES, m/z) calcd for $[\text{C}_{15}\text{H}_{11}\text{NNaO}_3\text{S}]^+$ ($\text{M}+\text{Na}$) $^+$ 308.0357, found 308.0355; IR (neat) ν 3059 (m, C-H aromatic), 2962 (w, C-H aliphatic), 1726 (s, C=O ester), 1668 (s, C=O amide), 1582 (m, C-C aromatic), 1326 (s, C-O), 739 (s, S-N) cm^{-1}



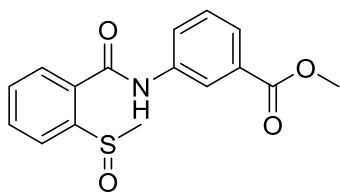
3-(3-Oxobenzo[d]isothiazol-2(3H)-yl)benzoic acid (4).⁹⁰

Methyl 3-(3-oxobenzo[d]isothiazol-2(3H)-yl)benzoate (500 mg, 1.8 mmol) was refluxed in concentrated sulphuric acid for 5 days. Water was then carefully added to the reaction mixture and the resulting precipitate was filtered and washed thoroughly with more water. After drying under reduced pressure the title compound was obtained as a white solid (50 mg, 10%): ¹H NMR (400 MHz, DMSO) δ = 9.52 (s, 1H), 8.35 (dd, J = 8, 1 Hz, 1H), 8.26 (d, J = 8 Hz, 1H), 8.15 (ddd, J = 5, 2, 1 Hz, 1H), 7.82 (dd, J = 8, 1 Hz, 1H), 7.79 – 7.73 (m, 2H), 7.56 (td, J = 8, 1 Hz, 1H), 7.06 (ddd, J = 7, 5, 1 Hz, 1H) ppm; ¹³C NMR (101 MHz, DMSO) δ = 164.76, 151.27, 149.29, 148.08, 138.75, 133.17, 131.51, 130.66, 127.01, 124.93, 120.55, 114.57, 45.08 ppm; HRMS (ES, m/z) calcd for [C₁₄H₉NNaO₃S]⁺ (M+Na)⁺ 294.0201, found 294.0204.



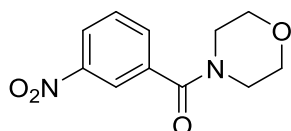
Methyl 3-(2-(methylthio)benzamido)benzoate (6).

General procedure 3 was followed using 2-(methylthio)benzoic acid (2 g, 11.9 mmol) and methyl 3-aminobenzoate (2.15 g, 14.3 mmol) to give the title compound as a white solid (3.21 g, 89% yield): ¹H NMR (400 MHz, CDCl₃) δ = 8.54 (s, 1H), 8.15 (s, 1H), 8.07 (d, J = 8 Hz, 1H), 7.82 (dt, J = 8, 1 Hz, 1H), 7.74 (dd, J = 8, 1 Hz, 1H), 7.49 – 7.42 (m, 2H), 7.38 (dd, J = 8, 1 Hz, 1H), 7.27 (td, J = 8, 1 Hz, 1H), 3.91 (s, 3H), 2.49 (s, 3H) ppm; ¹³C NMR (101 MHz, CDCl₃) δ = 166.63, 164.97, 137.46, 136.95, 136.54, 133.72, 131.98, 130.04, 128.91, 127.51, 127.06, 126.85, 126.31, 123.35, 53.62, 17.47 ppm; HRMS (ES, m/z) calcd for [C₁₆H₁₅NNaO₃S]⁺ (M+Na)⁺ 324.0670, found 324.0666



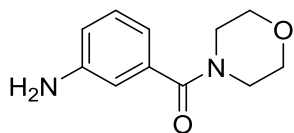
Methyl 3-(2-(methylsulphinyl)benzamido)benzoate (7).

General procedure 4 was followed using methyl 3-(2-(methylthio)benzamido)benzoate (3.37 g, 11.2 mmol) to give the title compound as a yellow solid (2.3 g, 64% yield): ^1H NMR (400 MHz, DMSO) δ = 10.83 (s, 1H), 8.43 (t, J = 2 Hz, 1H), 8.16 (dd, J = 8, 1 Hz, 1H), 8.03 (dd, J = 8, 1 Hz, 1H), 7.99 (ddd, J = 8, 2, 1 Hz, 1H), 7.88 (td, J = 8, 1 Hz, 1H), 7.75 – 7.70 (m, 2H), 7.53 (t, J = 8 Hz, 1H), 3.87 (s, 3H), 2.84 (s, 3H) ppm; ^{13}C NMR (101 MHz, DMSO) δ = 166.06, 164.85, 148.52, 139.02, 132.50, 131.87, 130.42, 130.15, 129.29, 128.15, 124.83, 123.70, 120.77, 52.30, 44.68 ppm; HRMS (ES, m/z) calcd for $[\text{C}_{16}\text{H}_{15}\text{NNaO}_4\text{S}]^+$ ($\text{M}+\text{Na}$) $^+$ 340.0619, found 340.0618.



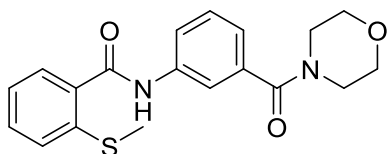
Morpholino(3-nitrophenyl)methanone (8).⁸⁸

General procedure 3 was followed using 3-nitrobenzoic acid and morpholine to give the title compound as a yellow solid (560 mg, 93% yield): ^1H NMR (400 MHz, CDCl_3) δ = 8.32 – 8.27 (m, 2H), 7.78 – 7.74 (m, 1H), 7.63 (t, J = 8 Hz, 1H), 3.90 – 3.38 (m, 8H) ppm; ^{13}C NMR (101 MHz, CDCl_3) δ = 167.87, 137.05, 133.26, 130.06, 124.84, 122.47, 66.88 ppm; HRMS (CI, m/z) calcd for $[\text{C}_{11}\text{H}_{13}\text{N}_2\text{O}_4]^+$ ($\text{M}+\text{H}$) $^+$ 237.0875, found 237.0872.



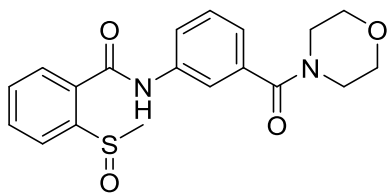
(3-Aminophenyl)(morpholino)methanone (9).

General procedure 2 was followed using morpholino(3-nitrophenyl)methanone to give the title compound as a white solid (220 mg, 47% yield): ^1H NMR (400 MHz, CDCl_3) δ = 7.19 – 7.14 (m, 1H), 6.74 – 6.69 (m, 3H), 4.12 – 3.31 (m, 10H) ppm; ^{13}C NMR (101 MHz, CDCl_3) δ = 170.74, 146.88, 136.59, 129.58, 116.89, 116.43, 113.55, 67.07 ppm; HRMS (CI, m/z) calcd for $[\text{C}_{11}\text{H}_{15}\text{N}_2\text{O}_2]^+$ (M+H) $^+$ 207.1134, found 207.1132.



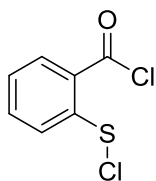
2-(Methylthio)-N-(3-(morpholine-4-carbonyl)phenyl)benzamide (10).

To a stirring solution of 2-(methylthio)benzoic acid (224 mg, 1.33 mmol) in anhydrous DMF (0.2M) was added HATU (600 mg, 1.57 mmol) and DIPEA (0.32 mL, 1.82 mmol). The resulting solution was stirred at RT for 15 mins (N_2 atmosphere). Morpholino(3-nitrophenyl)methanone (250 mg, 1.21 mmol) was then added and the resulting mixture was stirred overnight at room temperature. The reaction mixture was then diluted with ethyl acetate and washed with sodium bicarbonate (30 mL). The aqueous phase was then extracted with ethyl acetate (2 x 30 mL). Combined organics were washed with brine, dried over sodium sulfate, filtered and concentrated under reduced pressure. The crude product was purified by column chromatography (4:1 EtOAc: *n*-hexane) to yield the title compound as a white crystalline solid (356 mg, 83% yield): ^1H NMR (400 MHz, CDCl_3) δ = 8.68 (s, 1H), 7.76 (s, 1H), 7.74 – 7.70 (m, 2H), 7.47 – 7.42 (m, 1H), 7.42 – 7.37 (m, 2H), 7.27 (td, J = 8, 1 Hz, 1H), 7.16 (d, J = 8 Hz, 1H), 3.71-3.51 (m, 8H), 2.49 (s, 3H) ppm; ^{13}C NMR (101 MHz, CDCl_3) δ = 169.98, 166.28, 138.40, 137.01, 136.14, 134.92, 131.38, 129.46, 129.29, 128.06, 125.82, 123.14, 121.65, 119.16, 66.99, 17.12 ppm; HRMS (CI, m/z) calcd for $[\text{C}_{19}\text{H}_{21}\text{N}_2\text{O}_3\text{S}]^+$ (M+H) $^+$ 357.1273, found 357.1269.



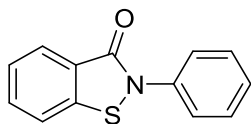
2-(Methylsulfinyl)-N-(3-(morpholine-4-carbonyl)phenyl)benzamide (11).

General procedure 4 was followed using 2-(methylthio)-N-(3-(morpholine-4-carbonyl)phenyl)benzamide to give the title compound as a shiny sand coloured powder (204 mg, 59% yield): ^1H NMR (400 MHz, DMSO) δ = 10.73 (s, 1H), 8.16 (d, J = 8 Hz, 1H), 8.00 (d, J = 8 Hz, 1H), 7.88 (t, J = 8 Hz, 1H), 7.82 (s, 1H), 7.78 (d, J = 8 Hz, 1H), 7.73 (t, J = 8 Hz, 1H), 7.45 (t, J = 8 Hz, 1H), 7.18 (d, J = 8 Hz, 1H), 3.61-3.39 (m, 8H), 2.83 (s, 3H) ppm; ^{13}C NMR (101 MHz, DMSO) δ = 168.71, 164.77, 148.42, 138.71, 135.99, 132.39, 132.00, 130.40, 128.89, 128.03, 123.67, 122.58, 121.32, 118.91, 65.86, 44.59 ppm; HRMS (ES, m/z) calcd for $[\text{C}_{19}\text{H}_{20}\text{N}_2\text{NaO}_4\text{S}]^+$ ($\text{M}+\text{Na}$) $^+$ 395.1041, found 395.1041.



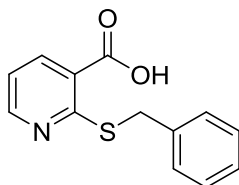
2-(Chlorocarbonyl)phenyl hypochlorothioite (12).³²

2,2'-Dithiodibenzoic acid (3 g, 9.79 mmol), DMF (25 μL) and thionyl chloride (5 mL) were added to DCE (20 mL). The resulting brown suspension was stirred at 80°C for 1.5 hours to give a clear solution. This solution was then cooled to 50°C before addition of sulfur chloride (1 mL) and further stirring for 45 minutes. The crude residue was evaporated under reduced pressure to give the title compound as a yellow solid (1.82 g, 90% yield): ^1H NMR (400 MHz, CDCl_3) δ = 8.34 (d, J = 8 Hz, 1H), 7.93 (d, J = 8 Hz, 1H), 7.77 (t, J = 8 Hz, 1H), 7.42 (t, J = 8 Hz, 1H) ppm; ^{13}C NMR (101 MHz, CDCl_3) δ = 169.65, 146.19, 135.92, 134.79, 127.54, 125.93, 124.58 ppm; Product unstable to MS conditions.



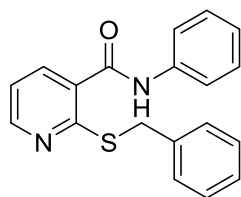
2-Phenylbenzo[d]isothiazol-3(2H)-one (13).⁸⁷

General procedure 11 was followed using 2-(chlorocarbonyl)phenyl hypochlorothioite (250 mg, 1.21 mmol) and aniline (0.14 mL, 1.51 mmol) to give the title compound as a white solid (150 mg, 55% yield): mp 136-138°C; ¹H NMR (400 MHz, CDCl₃) δ = 8.11 (d, *J* = 8 Hz, 1H), 7.71 (dt, *J* = 8, 1 Hz, 2H), 7.67 (ddd, *J* = 8, 7, 1 Hz, 1H), 7.59 (d, *J* = 8 Hz, 1H), 7.51 – 7.43 (m, 3H), 7.35 – 7.30 (m, 1H) ppm; ¹³C NMR (101 MHz, CDCl₃) δ = 164.12, 139.88, 137.25, 132.34, 129.36, 127.21, 127.05, 125.80, 124.87, 124.60, 120.08 ppm; HRMS (CI, *m/z*) calcd for [C₁₃H₁₀NOS]⁺ (M+H)⁺ 228.0483, found 228.0478; IR (neat) ν 1658 (s, C=O amide), 1591 (m, C-C aromatic), 1489 (m, C-C aromatic), 1444 (m, C-C aromatic), 1303 (m, C-N), 762 (s, S-N) cm⁻¹.



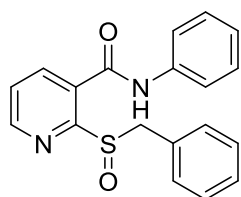
2-(Benzylthio)nicotinic acid (14).

A stirring solution of 2-mercaptonicotinic acid (2 g, 13.0 mmol) in isopropanol (40 mL) was cooled to 0°C before the addition of potassium hydroxide (1.46 g, 26.0 mmol (dissolved in the minimum amount of water)) and benzyl bromide (1.69 mL, 14.0 mmol). The resulting reaction mixture was then heated to 70°C for 45 minutes. The reaction mixture was then neutralised using 2M HCl and the resulting precipitate was filtered and dried under reduced pressure to give the title compound as a pale yellow solid (1.39 g, 44% yield): ¹H NMR (400 MHz, DMSO) δ = 8.67 (dd, *J* = 5, 2 Hz, 1H), 8.23 (dd, *J* = 8, 2 Hz, 1H), 7.43 – 7.40 (m, 5H), 7.34 – 7.23 (m, 2H), 4.37 (s, 2H) ppm; ¹³C NMR (101 MHz, DMSO) δ = 166.39, 160.66, 151.96, 139.09, 137.99, 129.24, 128.36, 126.89, 123.21, 119.13, 33.83 ppm; HRMS (CI, *m/z*) calcd for [C₁₃H₁₂NO₂S]⁺ (M+H)⁺ 246.0589, found 246.0586.



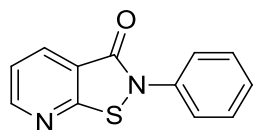
2-(Benzylthio)-*N*-phenylnicotinamide (15).²⁸

General procedure 3 was followed using 2-(benzylthio)nicotinic acid and aniline (omitting the acid wash from the work up due to the presence of pyridine) to give the title compound as a brown solid (243 mg, 93% yield): ¹H NMR (400 MHz, CDCl₃) δ = 8.57 (dd, *J* = 5, 2 Hz, 1H), 8.04 (s, 1H), 7.94 (dd, *J* = 8, 1 Hz, 1H), 7.58 (d, *J* = 8 Hz, 2H), 7.43 – 7.21 (m, 7H), 7.17 – 7.11 (m, 2H), 4.52 (s, 2H) ppm; ¹³C NMR (101 MHz, CDCl₃) δ = 156.26, 150.77, 137.56, 137.29, 136.87, 129.92, 129.23, 129.10, 128.52, 127.27, 124.94, 120.22, 119.54, 35.13 ppm; HRMS (CI, *m/z*) calcd for [C₁₉H₁₇N₂OS]⁺ (M+H)⁺ 321.1062, found 321.1062.



2-(Benzylsulfinyl)-*N*-phenylnicotinamide (16).

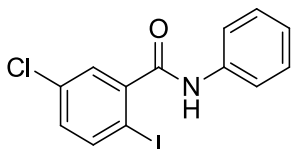
General procedure 4 was followed using 2-(benzylthio)-*N*-phenylnicotinamide (260 mg, 0.82 mmol) to give the title compound as light brown solid (180 mg, 66% yield): This intermediate was carried forward without further characterisation.



2-Phenylisothiazolo[5,4-*b*]pyridin-3(2*H*)-one (17).³⁴

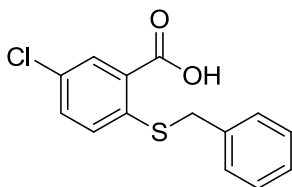
General procedure 9 was followed using 2-(benzylsulfinyl)-*N*-phenylnicotinamide to give the title compound as a flaky, pale brown solid (62 mg, 50% yield): mp 135-137°C; ¹H NMR (400 MHz, CDCl₃) δ = 8.82 (dd, *J* = 5, 1 Hz, 1H), 8.36 (dd, *J* = 8, 1 Hz, 1H), 7.70 (d, *J* = 8 Hz, 2H), 7.49 (t, *J* = 8 Hz, 2H), 7.41

(dd, $J = 8, 5$ Hz, 1H), 7.35 (t, $J = 7$ Hz, 1H) ppm; ^{13}C NMR (101 MHz, CDCl_3) $\delta = 162.63, 162.02, 154.23, 136.72, 135.44, 129.63, 127.61, 125.00, 121.15, 119.91$ ppm; HRMS (CI, m/z) calcd for $[\text{C}_{12}\text{H}_9\text{N}_2\text{OS}]^+ (\text{M}+\text{H})^+$ 229.0436, found 229.0437; Anal. Calcd for $\text{C}_{12}\text{H}_8\text{N}_2\text{OS}$: C, 63.14; H, 3.53; N, 12.27; S, 14.05. Found: C, 62.86; H, 3.65; N, 11.95; S, 13.57; IR (neat) ν 3057 (w, C-H, aromatic), 1655 (s, C=O, amide), 1587 (m, C-C, aromatic), 1562 (m, C-C, aromatic), 749 (m, S-N) cm^{-1} .



5-Chloro-2-iodo-*N*-phenylbenzamide (18).⁹¹

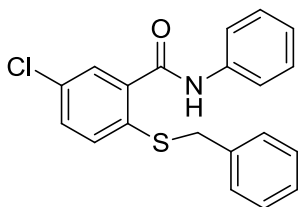
General procedure 3 was followed using 5-chloro-2-iodobenzoic acid (1 g, 3.54 mmol) and aniline (0.42 mL, 4.6 mmol) to give the title compound as a pale yellow solid (1.15 g, 90% yield): HRMS (CI, m/z) calcd for $[\text{C}_{13}\text{H}_{10}\text{ClINO}]^+ (\text{M}+\text{H})^+$ 357.9496, found 357.9504; This intermediate was carried forward without further characterisation.



2-(Benzylthio)-5-chlorobenzoic acid (19).⁹²

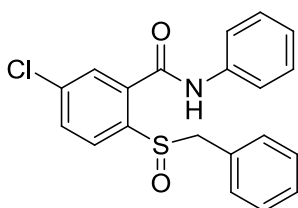
A stirring solution of 5-chloro-2-mercaptobenzoic acid (1 g, 5.3 mmol) in propan-2-ol (30 mL) was cooled to 0°C. Potassium hydroxide (0.59 g, 10.6 mmol) dissolved in water (10 mL) was added followed by the slow addition of benzyl bromide (0.69 mL, 5.83 mmol). The resulting reaction mixture was then heated to 70°C for 2 hours. The reaction mixture was then neutralised with 2M HCl and filtered to remove the resulting precipitate. The filtrate was then extracted with ethyl acetate (3 x 30 mL) and the combined organics were washed with brine (30 mL), dried over anhydrous MgSO_4 , filtered and concentrated under reduced pressure. The resulting brown residue was then purified by column chromatography (1:5 EtOAc/*n*-hexane) to give the title compound as a crystalline white solid (674 mg, 46% yield): ^1H NMR (400 MHz, CDCl_3) $\delta = 8.08$

(d, $J = 2$ Hz, 1H), 7.42 – 7.37 (m, 3H), 7.35-7.27 (m, 4H), 4.16 (s, 2H) ppm; ^{13}C NMR (101 MHz, CDCl_3) $\delta = 169.64, 141.24, 135.44, 133.17, 132.14, 130.36, 129.03, 128.78, 127.68, 127.66, 37.60$ ppm; LRMS (ES, m/z) calcd for $[\text{C}_{14}\text{H}_{10}\text{ClO}_2\text{S}]^-$ (M-H) $^-$ 277.01, found 277.0.



2-(Benzylthio)-5-chloro-*N*-phenylbenzamide (20).

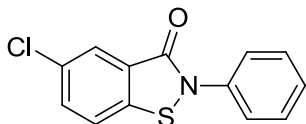
General procedure 3 was followed using 2-(benzylthio)-5-chlorobenzoic acid (674 mg, 2.42 mmol) and aniline (0.3 mL, 3.63 mmol) to give the title compound as a yellow solid (622 mg, 73% yield): ^1H NMR (400 MHz, CDCl_3) $\delta = 8.53$ (s, 1H), 7.80 (d, $J = 2$ Hz, 1H), 7.58 (d, $J = 8$ Hz, 2H), 7.40 – 7.33 (m, 4H), 7.24 – 7.20 (m, 3H), 7.18 (d, $J = 7$ Hz, 1H), 7.13 (dd, $J = 7, 3$ Hz, 2H), 4.07 (s, 2H) ppm; ^{13}C NMR (101 MHz, CDCl_3) $\delta = 164.31, 139.39, 137.72, 136.58, 135.08, 134.32, 131.16, 131.03, 130.02, 129.23, 128.95, 128.82, 127.75, 124.97, 120.32, 40.94$ ppm; HRMS (ES, m/z) calcd for $[\text{C}_{20}\text{H}_{16}\text{ClNNaOS}]^+$ (M+Na) $^+$ 376.0539, found 376.0533.



2-(Benzylsulfinyl)-5-chloro-*N*-phenylbenzamide (21).

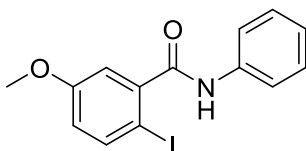
General procedure 4 was followed using 2-(benzylthio)-5-chloro-*N*-phenylbenzamide (300 mg, 0.84 mmol) to give the title compound as a sand coloured solid (314 mg, 83% yield): ^1H NMR (400 MHz, CDCl_3) $\delta = 7.95$ (s, 1H), 7.70 (s, 2H), 7.62 – 7.48 (m, 2H), 7.46 – 7.38 (m, 3H), 7.30-7.28 (m, 3H), 7.21-7.15 (m, 3H), 4.56 (d, 12.7 Hz, 1H), 3.36 (d, 12.7 Hz, 1H) ppm; ^{13}C NMR (101 MHz, CDCl_3) $\delta = 163.78, 142.62, 137.55, 136.73, 134.09, 131.37, 130.60, 129.89,$

128.85, 128.10, 127.35, 127.08, 125.01, 120.96, 120.85, 62.30 ppm; HRMS (ES, m/z) calcd for $[C_{20}H_{16}ClNNaO_2S]^+$ ($M+Na$) $^+$ 392.0488, found 392.0485.



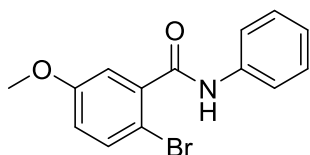
5-Chloro-2-phenylbenzo[d]isothiazol-3(2H)-one (22).⁹³

General procedure 9 was followed using 2-(benzylsulfinyl)-5-chloro-*N*-phenylbenzamide (252 mg, 0.68 mmol) to give the title compound a white solid (129 mg, 72% yield): mp 174-176°C; 1H NMR (400 MHz, $CDCl_3$) δ = 8.09 (d, J = 2 Hz, 1H), 7.7-7.67 (m, 2H), 7.63 (dd, J = 9, 2 Hz, 1H), 7.53 (d, J = 9 Hz, 1H), 7.48 (t, J = 8 Hz, 2H), 7.34 (t, J = 8 Hz, 1H) ppm; HRMS (CI, m/z) calcd for $[C_{13}H_9ClNOS]^+$ ($M+H$) $^+$ 262.0093, found 262.0089; Anal. Calcd for $C_{13}H_8ClNOS$: C, 59.66; H, 3.08; N, 5.35; S, 12.25. Found: C, 59.60; H, 3.18; N, 5.36; S, 11.80; IR (neat) ν 3063 (w, C-H aromatic), 1635 (s, C=O amide), 1591 (m, C-C aromatic), 1443 (m, C-C aromatic), 758 (s, S-N) cm^{-1} .



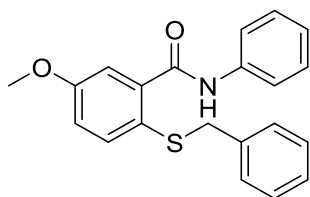
2-Iodo-5-methoxy-*N*-phenylbenzamide (23).⁹⁴

General procedure 3 was followed using 2-iodo-5-methoxybenzoic acid and aniline to give the title compound as a pale brown solid (272 mg, 86% yield): 1H NMR (400 MHz, $CDCl_3$) δ = 7.74 (d, J = 9 Hz, 1H), 7.64 (d, J = 8 Hz, 2H), 7.48 (s, 1H), 7.39 (t, J = 8 Hz, 2H), 7.18 (t, J = 7 Hz, 1H), 7.10 (d, J = 3 Hz, 1H), 6.74 (dd, J = 9, 3 Hz, 1H), 3.82 (s, 3H) ppm; ^{13}C NMR (101 MHz, $CDCl_3$) δ = 166.94, 159.92, 142.84, 140.75, 137.45, 129.18, 124.97, 120.06, 118.30, 114.35, 80.47, 55.62 ppm; HRMS (ES, m/z) calcd for $[C_{14}H_{12}INNaO_2]^+$ ($M+Na$) $^+$ 375.9810, found 375.9810.



2-Bromo-5-methoxy-*N*-phenylbenzamide (24).⁹⁵

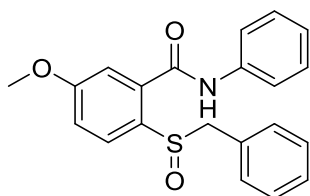
General procedure 3 was followed using 2-bromo-5-methoxy benzoic acid (1 g, 4.33 mmol) and aniline (0.51 mL, 5.63 mmol) to give the title compound as a brown solid (1.29 g, >95% yield): ¹H NMR (400 MHz, CDCl₃) δ = 7.75 (s, 1H), 7.64 (d, *J* = 7 Hz, 2H), 7.50 (d, *J* = 9 Hz, 1H), 7.38 (t, *J* = 8 Hz, 2H), 7.21 (d, *J* = 3 Hz, 1H), 7.18 (t, *J* = 7 Hz, 1H), 6.88 (dd, *J* = 9, 3 Hz, 1H), 3.82 (s, 3H) ppm; ¹³C NMR (101 MHz, CDCl₃) δ = 165.34, 159.23, 138.42, 137.59, 134.50, 129.30, 125.05, 120.19, 118.52, 115.04, 109.43, 55.84 ppm; HRMS (ES, *m/z*) calcd for [C₁₄H₁₂BrNNaO₂]⁺ (M+Na)⁺ 327.9949, found 327.9947.



2-(Benzylthio)-5-methoxy-*N*-phenylbenzamide (25).

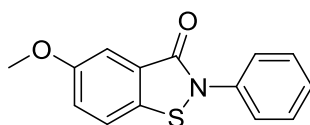
To a stirred solution of 2-bromo-5-methoxy-*N*-phenylbenzamide (200 mg, 0.65 mmol) in anhydrous THF (10 mL) was added *n*-butyllithium (0.82 mL, 1.3 mmol) at -78°C under a nitrogen atmosphere. After 10 minutes, a solution of dibenzyldisulfide (177 mg, 0.72 mmol) in anhydrous THF (5 mL) was slowly added. The reaction mixture was allowed to warm to room temperature and stirred overnight. The reaction mixture was then quenched with saturated ammonium chloride solution before extracting with EtOAc (3 x 30 mL). The combined organic layers were washed with brine (30 mL), dried over MgSO₄, filtered and concentrated under reduced pressure to give 2-(benzylthio)-5-methoxy-*N*-phenylbenzamide as a pale yellow, crystalline solid (190 mg, >95% yield): ¹H NMR (400 MHz, CDCl₃) δ = 9.18 (s, 1H), 7.59 (d, *J* = 8 Hz, 2H), 7.48 (d, *J* = 3 Hz, 1H), 7.38 – 7.33 (m, 3H), 7.19 – 7.16 (m, 3H), 7.14 (d, *J* = 7 Hz, 1H), 7.04 (dd, *J* = 6, 3 Hz, 2H), 6.89 (dd, *J* = 8, 3 Hz, 1H), 3.98 (s, 2H), 3.83 (s, 3H) ppm; ¹³C

NMR (101 MHz, CDCl₃) δ = 165.12, 160.15, 140.02, 138.06, 137.85, 137.16, 129.11, 128.94, 128.65, 127.48, 124.61, 121.86, 120.24, 117.68, 115.25, 55.67, 42.32 ppm; HRMS (CI, m/z) calcd for [C₂₁H₂₀NO₂S]⁺ (M+H)⁺ 350.1215, found 350.1224.



2-(Benzylsulfinyl)-5-methoxy-N-phenylbenzamide (26).

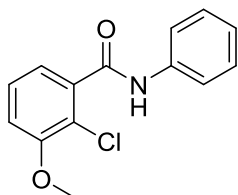
General procedure 4 was followed using 2-(benzylthio)-5-methoxy-N-phenylbenzamide (190 mg, 0.54 mmol) to give the title compound as a white solid (69 mg, 35% yield): ¹H NMR (400 MHz, CDCl₃) δ = 9.14 (s, 1H), 7.67 (d, J = 8 Hz, 2H), 7.38 (t, J = 8 Hz, 2H), 7.28-7.22 (m, 5H), 7.17 (t, J = 7 Hz, 1H), 7.11 (d, J = 6 Hz, 2H), 6.78 (dd, J = 9, 2 Hz, 1H), 4.44 (d, J = 13 Hz, 1H), 4.13 (d, J = 13 Hz, 1H), 3.82 (s, 3H) ppm; ¹³C NMR (101 MHz, CDCl₃) δ = 164.50, 161.54, 138.06, 134.99, 134.07, 130.92, 130.34, 129.24, 128.27, 128.15, 124.86, 120.26, 116.29, 113.73, 61.96, 55.98 ppm; HRMS (ES, m/z) calcd for [C₂₁H₁₉NNaO₃S]⁺ (M+Na)⁺ 388.0983, found 388.0986.



5-Methoxy-2-phenylbenzo[d]isothiazol-3(2H)-one (27).

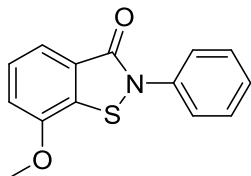
General procedure 9 was followed using 2-(benzylsulfinyl)-5-methoxy-N-phenylbenzamide to give the title compound as a white solid (31 mg, 65% yield): mp 147-149°C; ¹H NMR (400 MHz, CDCl₃) δ = 7.71 (d, J = 8 Hz, 2H), 7.55 (d, J = 2 Hz, 1H), 7.48 (t, J = 8 Hz, 3H), 7.35 – 7.28 (m, 2H), 3.91 (s, 3H) ppm; ¹³C NMR (101 MHz, CDCl₃) δ = 164.21, 158.72, 137.52, 131.89, 129.50, 127.21, 125.98, 124.74, 123.15, 121.15, 108.30, 55.96 ppm; HRMS (CI, m/z) calcd for [C₁₄H₁₂NO₂S]⁺ (M+H)⁺ 258.0589, found 258.0586; IR (neat) ν 3081 (w, C-H

aromatic), 2917 (w, C-H aliphatic), 1637 (s, C=O amide), 1466 (m, C-C aromatic), 1454 (m, C-C aromatic), 1343 (m, C-H aliphatic), 758 (s, S-N) cm^{-1} .



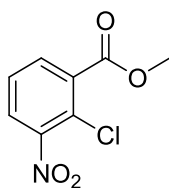
2-Chloro-3-methoxy-N-phenylbenzamide (28).⁸⁴

General procedure 3 was followed using 2-chloro-3-methoxybenzoic acid (250 mg, 1.34 mmol) and aniline (0.15 mL, 1.68 mmol) to give the title compound as a brown solid (253 mg, 92% yield): ^1H NMR (400 MHz, CDCl_3) δ = 7.84 (s, 1H), 7.66 (d, J = 8 Hz, 2H), 7.39 (t, J = 8 Hz, 2H), 7.37-7.29 (m, 2H), 7.19 (t, J = 7 Hz, 1H), 7.05 (d, J = 8 Hz, 1H), 3.96 (s, 3H) ppm; ^{13}C NMR (101 MHz, CDCl_3) δ = 164.76, 155.53, 137.73, 137.24, 129.24, 128.07, 124.94, 121.45, 120.20, 113.77, 56.66 ppm; HRMS (CI, m/z) calcd for $[\text{C}_{14}\text{H}_{13}\text{ClNO}_2]^+$ ($\text{M}+\text{H}$)⁺ 262.0635, found 262.0635.



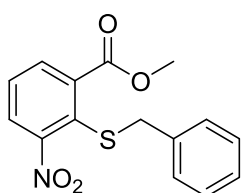
7-Methoxy-2-phenylbenzo[d]isothiazol-3(2H)-one (29).⁹

General procedure 10 was followed using 2-chloro-3-methoxy-N-phenylbenzamide to give the title compound as a white solid (164 mg, 56% yield): mp 130-132°C; ^1H NMR (400 MHz, CDCl_3) δ = 7.75-7.72 (m, 3H), 7.47 (t, J = 8 Hz, 2H), 7.41 (t, J = 8 Hz, 1H), 7.32 (t, J = 8 Hz, 1H), 7.07 (d, J = 8 Hz, 1H), 4.00 (s, 3H) ppm; ^{13}C NMR (101 MHz, CDCl_3) δ = 164.51, 152.23, 137.54, 129.47, 127.47, 127.18, 124.76, 119.10, 111.99, 56.10 ppm; HRMS (CI, m/z) calcd for $[\text{C}_{14}\text{H}_{12}\text{NO}_2\text{S}]^+$ ($\text{M}+\text{H}$)⁺ 258.0589, found 258.0593; IR (neat) ν 3047 (w, C-H aromatic), 2914 (w, C-H aliphatic), 1655 (s, C=O amide), 1590 (m, C-C aromatic), 1580 (m, C-C aromatic), 1484 (m, C-C aromatic), 1269 (s, C-O), 758 (s, S-N) cm^{-1} .



Methyl 2-chloro-3-nitrobenzoate (30).⁹⁶

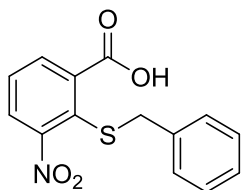
To a stirring solution of 2-chloro-3-nitrobenzoic acid (2 g, 9.92 mmol) in anhydrous DCM (30 mL) was added oxalyl chloride (1.7 mL, 19.8 mmol) and DMF (catalytic, 3 drops). The resulting yellow solution was stirred for one hour at room temperature. The solvent was then removed under reduced pressure and the acyl chloride intermediate was re-suspended in anhydrous MeOH (30 mL) and stirred for a further 30 minutes. The solvent was again removed under reduced pressure and the resulting yellow residue re-suspended in EtOAc (30 mL). The organic was then washed with NaHCO₃ (20 mL) and brine (20 mL) before being dried over MgSO₄, filtered and concentrated under reduced pressure to yield the title compound as a yellow solid (2.11 g, >95% yield): ¹H NMR (400 MHz, CDCl₃) δ = 7.95 (d, *J* = 8 Hz, 1H), 7.84 (d, *J* = 8 Hz, 1H), 7.48 (t, *J* = 8 Hz, 1H), 3.98 (s, 3H) ppm; ¹³C NMR (101 MHz, CDCl₃) δ = 164.94, 133.82, 133.44, 127.44, 127.30, 125.87, 53.25 ppm; HRMS (CI, *m/z*) calcd for [C₈H₇ClNO₄]⁺ (M+H)⁺ 216.0064, found 216.0067.



Methyl 2-(benzylthio)-3-nitrobenzoate (31).⁹⁶

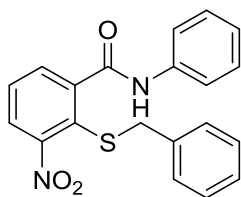
To a stirring solution of methyl 2-chloro-3-nitrobenzoate (2.1 g, 9.7 mmol) in DMF (40 mL) was added potassium carbonate (4.02 g, 29.1 mmol) and benzyl mercaptan (1.16 mL, 9.89 mmol) at 0°C. The reaction mixture was then heated to 90°C for 18 hours under a nitrogen atmosphere. The resulting reaction mixture was then diluted with water (40 mL) and extracted with EtOAc (3 x 30 mL). The combined organic extracts were washed with brine (30 mL), dried over MgSO₄, filtered and concentrated under reduced pressure to yield the title compound as

a yellow oil (2.54 g, 86% yield): ^1H NMR (400 MHz, CDCl_3) δ = 7.74 (d, J = 8 Hz, 1H), 7.70 (d, J = 8 Hz, 1H), 7.50 (t, J = 8 Hz, 1H), 7.25 – 7.19 (m, 5H), 4.14 (s, 2H), 3.95 (s, 3H) ppm; ^{13}C NMR (101 MHz, CDCl_3) δ = 166.79, 155.89, 140.65, 136.21, 131.62, 129.48, 129.20, 128.60, 127.66, 126.77, 125.34, 53.00, 42.41 ppm; HRMS (CI, m/z) calcd for $[\text{C}_{15}\text{H}_{14}\text{NO}_4\text{S}]^+$ ($\text{M}+\text{H}$) $^+$ 304.0644, found 304.0645.



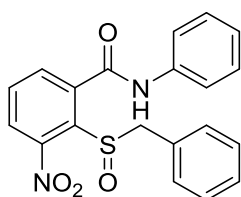
2-(Benzylthio)-3-nitrobenzoic acid (**32**).⁹⁷

To a stirring solution of methyl 2-(benzylthio)-3-nitrobenzoate (1 g, 3.3 mmol) in methanol (20 mL) was added NaOH (1M, 20 mL). The resulting turbid yellow solution was warmed to 40°C for 18 hours. The reaction mixture was then acidified using 2M HCl and the resulting yellow precipitate was filtered and dried to yield a shiny yellow solid. The filtrate was then extracted with DCM (3 x 20 mL) and the combined organic layers were washed with brine (20 mL), dried over MgSO_4 , filtered and concentrated under reduced pressure to yield a second crop of crystals. The two sets of crystals were combined to yield the title compound as a yellow solid (193 mg, 20% yield): ^1H NMR (400 MHz, CDCl_3) δ = 7.92 – 7.83 (m, 1H), 7.75 – 7.68 (m, 1H), 7.57 – 7.49 (m, 1H), 7.35-7.33 (m, 1H), 7.24 (s, 4H), 4.20 (s, 2H) ppm; ^{13}C NMR (101 MHz, CDCl_3) δ = 168.35, 155.74, 140.72, 136.25, 131.98, 129.28, 129.19, 128.52, 127.58, 126.84, 125.16, 42.18 ppm; HRMS (CI, m/z) calcd for $[\text{C}_{14}\text{H}_{12}\text{NO}_4\text{S}]^+$ ($\text{M}+\text{H}$) $^+$ 290.0487, found 290.0485.



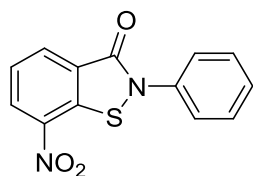
2-(Benzylthio)-3-nitro-*N*-phenylbenzamide (33).

General procedure 3 was followed using 2-(benzylthio)-3-nitrobenzoic acid and aniline to give the title compound as a yellow solid (229 mg, 91% yield): ^1H NMR (400 MHz, CDCl_3) δ = 8.37 (s, 1H), 7.94 (d, J = 8 Hz, 1H), 7.68 (d, J = 8 Hz, 1H), 7.62 (d, J = 8 Hz, 2H), 7.54 (t, J = 8 Hz, 1H), 7.41 (t, J = 8 Hz, 2H), 7.27 – 7.12 (m, 4H), 7.04 (d, J = 7 Hz, 2H), 4.08 (s, 2H) ppm; ^{13}C NMR (101 MHz, CDCl_3) δ = 164.31, 155.73, 143.07, 137.48, 135.77, 132.71, 130.01, 129.37, 129.19, 128.77, 127.94, 125.29, 125.16, 124.64, 120.27, 42.26 ppm; HRMS (CI, m/z) calcd for $[\text{C}_{20}\text{H}_{17}\text{N}_2\text{O}_3\text{S}]^+$ ($\text{M}+\text{H}$) $^+$ 365.0960, found 427.1489.



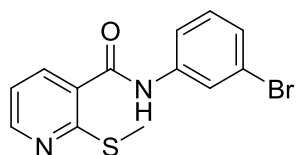
2-(Benzylsulfinyl)-3-nitro-*N*-phenylbenzamide (34).

General procedure 4 was followed using 2-(benzylthio)-3-nitro-*N*-phenylbenzamide to give the title compound as a yellow solid (96 mg, 46% yield): ^1H NMR (400 MHz, CDCl_3) δ = 10.00 (s, 1H), 8.03 (d, J = 8 Hz, 1H), 7.76 (d, J = 7 Hz, 1H), 7.56 – 7.53 (m, 3H), 7.47 (d, J = 8 Hz, 2H), 7.41 (d, J = 7 Hz, 3H), 7.03 (t, J = 8 Hz, 2H), 6.91 (t, J = 7 Hz, 1H), 5.32 (d, J = 13 Hz, 1H), 4.57 (d, J = 13 Hz, 1H) ppm; ^{13}C NMR (101 MHz, CDCl_3) δ = 164.36, 146.92, 141.49, 140.15, 138.45, 135.46, 131.72, 131.44, 131.00, 129.03, 128.95, 128.53, 125.58, 124.12, 119.80, 61.33 ppm; HRMS (ES, m/z) calcd for $[\text{C}_{20}\text{H}_{16}\text{N}_2\text{NaO}_4\text{S}]^+$ ($\text{M}+\text{Na}$) $^+$ 403.0728, found 403.0740.



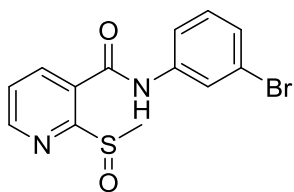
7-Nitro-2-phenylbenzo[d]isothiazol-3(2H)-one (35).³⁴

General procedure 9 was followed using 2-(benzylsulfinyl)-3-nitro-*N*-phenylbenzamide to give the title compound as an orange solid (25 mg, 38% yield): mp 149-151°C; ¹H NMR (400 MHz, CDCl₃) δ = 8.59 (d, *J* = 8 Hz, 1H), 8.48 (d, *J* = 8 Hz, 1H), 7.72 (d, *J* = 8 Hz, 2H), 7.67 (d, *J* = 8 Hz, 1H), 7.52 (t, *J* = 8 Hz, 2H), 7.38 (t, *J* = 8 Hz, 1H) ppm; ¹³C NMR (101 MHz, CDCl₃) δ = 162.56, 140.35, 137.31, 136.40, 133.79, 129.76, 128.79, 127.92, 127.90, 126.69, 124.86 ppm; HRMS (CI, *m/z*) calcd for [C₁₃H₉N₂O₃S]⁺ (M+H)⁺ 273.0334, found 273.0334; IR (neat) ν 3059 (w, C-H aromatic), 2920 (w, C-H aliphatic), 1667 (s, C=O amide), 1589 (m, C-C aromatic), 1485 (m, C-C aromatic), 1455 (m, C-H aliphatic), 753 (s, S-N) cm⁻¹.



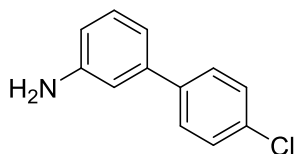
***N*-(3-Bromophenyl)-2-(methylthio)nicotinamide (36).**

General procedure 3 was followed using 2-(methylthio)nicotinic acid (3 g, 17.7 mmol) and 3-bromoaniline (2.89 mL, 26.6 mmol) (omitting the acid wash from the work up due to the presence of pyridine) to give the title compound as a fine white powder (2.3 g, 40% yield): ¹H NMR (400 MHz, Acetone) δ = 8.53 (dd, *J* = 5, 2 Hz, 1H), 7.97 (t, *J* = 2 Hz, 1H), 7.81 (dd, *J* = 8, 2 Hz, 1H), 7.58 (dt, *J* = 8, 2 Hz, 1H), 7.32 – 7.24 (m, 2H), 7.17 (dd, *J* = 8, 5 Hz, 1H), 2.54 (s, 2H) ppm; ¹³C NMR (101 MHz, Acetone) δ = 167.99, 159.67, 151.67, 141.17, 136.35, 131.62, 131.46, 128.52, 124.28, 123.32, 120.06, 119.79, 13.58 ppm; LRMS (CI, *m/z*) calcd for [C₁₃H₁₂BrN₂OS]⁺ (M+H)⁺ 324.9833, found 325.0.



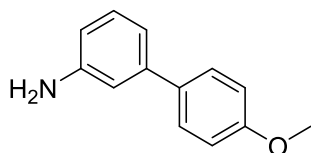
***N*-(3-Bromophenyl)-2-(methylsulfinyl)nicotinamide (37).**

General procedure 4 was followed using *N*-(3-bromophenyl)-2-(methylthio)nicotinamide (2.26 g, 7.01 mmol) to give the title compound as a white solid (2.14 g, 90% yield): ^1H NMR (400 MHz, DMSO) δ = 10.86 (s, 1H), 8.89 (dd, J = 5, 2 Hz, 1H), 8.24 (dd, J = 8, 2 Hz, 1H), 8.04 (s, 1H), 7.73 (dd, J = 8, 5 Hz, 1H), 7.66 – 7.58 (m, 1H), 7.39 – 7.30 (m, H), 2.86 (s, 3H) ppm; ^{13}C NMR (101 MHz, DMSO) δ = 164.01, 162.70, 151.45, 140.22, 137.04, 130.96, 130.84, 126.79, 125.30, 122.26, 121.53, 118.75, 40.46 ppm; Product unstable to MS conditions (Small molecular ion peak at 337.0 and peak at 277.0 (product minus sulfoxide)).



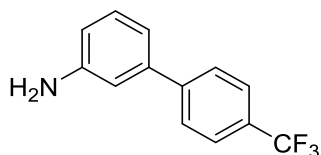
4'-Chloro-[1,1'-biphenyl]-3-amine (38a).⁹⁸

General procedure 8 was followed using 3-bromoaniline and 4-chlorophenylboronic acid to give the title compound as a pale yellow solid (109 mg, 46% yield): ^1H NMR (400 MHz, CDCl_3) δ = 7.49 (d, J = 9 Hz, 2H), 7.38 (d, J = 9 Hz, 2H), 7.23 (t, J = 8 Hz, 1H), 6.95 (d, J = 8 Hz, 1H), 6.86 (s, 1H), 6.69 (dd, J = 8, 2 Hz, 1H), 3.76 (s, 2H) ppm; ^{13}C NMR (101 MHz, CDCl_3) δ = 146.94, 141.32, 139.95, 133.37, 129.96, 128.90, 128.47, 117.58, 114.50, 113.75 ppm; HRMS (CI, m/z) calcd for $[\text{C}_{12}\text{H}_{11}\text{ClN}]^+$ ($\text{M}+\text{H}$) $^+$ 204.0580, found 204.0572.



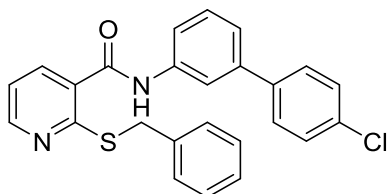
4'-Methoxy-[1,1'-biphenyl]-3-amine (38b).⁹⁹

General procedure 8 was followed using 3-bromoaniline (200 mg, 1.16 mmol) and (4-methoxyphenyl)boronic acid (212 mg, 1.4 mmol) to give the title compound as a yellow solid (194 mg, 84% yield): ¹H NMR (400 MHz, CDCl₃) δ = 7.54 – 7.48 (m, 2H), 7.21 (t, *J* = 8 Hz, 1H), 6.98 – 6.94 (m, 3H), 6.87 (t, *J* = 2 Hz, 1H), 6.65 (ddd, *J* = 8, 2, 1 Hz, 1H), 3.85 (s, 3H), 3.75 (br, s, 2H) ppm; ¹³C NMR (101 MHz, CDCl₃) δ = 159.21, 146.82, 142.15, 134.05, 129.77, 128.22, 117.44, 114.19, 113.69, 113.65, 55.46 ppm; HRMS (CI, *m/z*) calcd for [C₁₃H₁₄NO]⁺ (M+H)⁺ 200.1075, found 200.1069.



4'-(Trifluoromethyl)-[1,1'-biphenyl]-3-amine (38c).⁹⁹

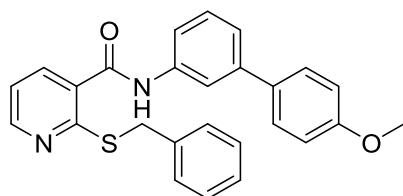
General procedure 8 was followed using 3-bromoaniline and 4-(trifluoromethyl)phenylboronic acid to give the title compound as a pale yellow solid (236 mg, 86% yield): ¹H NMR (400 MHz, CDCl₃) δ = 7.65 (s, 4H), 7.25 (t, *J* = 8 Hz, 1H), 6.98 (d, *J* = 8 Hz, 1H), 6.89 (s, 1H), 6.75 – 6.70 (m, 1H), 3.76 (s, 2H) ppm; ¹³C NMR (101 MHz, CDCl₃) δ = 147.03, 145.06, 141.10, 130.06, 129.55, 129.23, 127.49, 125.73, 125.69, 123.12, 117.83, 115.05, 113.98 ppm; HRMS (CI, *m/z*) calcd for [C₁₃H₁₁F₃N]⁺ (M+H)⁺ 238.0844, found 238.0836.



2-(Benzylthio)-N-(4'-chloro-[1,1'-biphenyl]-3-yl)nicotinamide (39a).

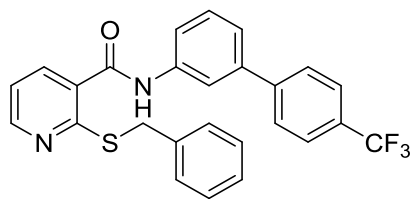
General procedure 3 was followed using 2-(benzylthio)nicotinic acid and 4'-chloro-[1,1'-biphenyl]-3-amine (omitting the acid wash from the work up due to

the presence of pyridine) to give the title compound as a yellow solid (127 mg, 80% yield): ^1H NMR (400 MHz, CDCl_3) δ = 8.59 (dd, J = 5, 2 Hz, 1H), 8.14 (s, 1H), 7.95 (dd, J = 8, 2 Hz, 1H), 7.86 (s, 1H), 7.54 – 7.49 (m, 3H), 7.44 – 7.38 (m, 5H), 7.35 – 7.32 (m, 1H), 7.31 – 7.27 (m, 2H), 7.26 – 7.21 (m, 1H), 7.14 (dd, J = 8, 5 Hz, 1H), 4.53 (s, 2H) ppm; ^{13}C NMR (101 MHz, CDCl_3) δ = 164.60, 156.43, 151.02, 141.17, 139.14, 138.07, 137.68, 137.00, 133.82, 129.90, 129.73, 129.35, 129.05, 128.67, 128.61, 127.44, 123.66, 119.72, 119.38, 118.91, 35.28 ppm; HRMS (ES, m/z) calcd for $[\text{C}_{25}\text{H}_{19}\text{ClN}_2\text{NaOS}]^+$ ($\text{M}+\text{Na}$) $^+$ 453.0804, found 453.0805; Anal. Calcd for $\text{C}_{25}\text{H}_{19}\text{ClN}_2\text{OS}$: C, 69.68; H, 4.44; N, 6.50; S, 7.44. Found: C, 69.70; H, 4.56; N, 6.50; S, 7.84.



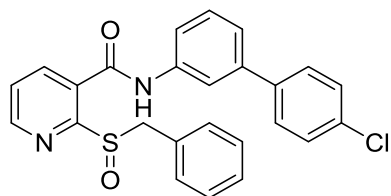
2-(Benzylthio)-N-(4'-methoxy-[1,1'-biphenyl]-3-yl)nicotinamide (39b).

General procedure 3 was followed using 2-(benzylthio)nicotinic acid and 4'-methoxy-[1,1'-biphenyl]-3-amine (omitting the acid wash from the work up due to the presence of pyridine) to give the title compound as a white solid (303 mg, 85% yield): ^1H NMR (400 MHz, CDCl_3) δ = 8.58 (dd, J = 5, 1 Hz, 1H), 8.09 (s, 1H), 7.95 (d, J = 8 Hz, 1H), 7.79 (s, 1H), 7.54-7.50 (m, 3H), 7.45 – 7.38 (m, 3H), 7.35 (t, J = 8 Hz, 1H), 7.29 (t, J = 7 Hz, 2H), 7.26 – 7.21 (m, 1H), 7.14 (dd, J = 8, 5 Hz, 1H), 6.97 (d, J = 9 Hz, 2H), 4.53 (s, 2H), 3.85 (s, 3H) ppm; ^{13}C NMR (101 MHz, CDCl_3) δ = 164.53, 159.50, 156.42, 150.95, 142.01, 137.93, 137.73, 136.99, 133.22, 130.09, 129.57, 129.36, 128.66, 128.40, 127.41, 123.46, 119.72, 118.63, 114.33, 55.50, 35.28 ppm; HRMS (CI, m/z) calcd for $[\text{C}_{26}\text{H}_{23}\text{N}_2\text{O}_2\text{S}]^+$ ($\text{M}+\text{H}$) $^+$ 427.1480, found 427.1489.



2-(Benzylthio)-N-(4'-(trifluoromethyl)-[1,1'-biphenyl]-3-yl)nicotinamide (39c).

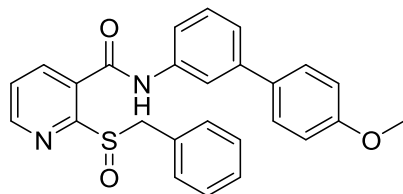
General procedure 3 was followed using 2-(benzylthio)nicotinic acid and 4'-(trifluoromethyl)-[1,1'-biphenyl]-3-amine (omitting the acid wash from the work up due to the presence of pyridine) to give the title compound as a cream coloured solid (242 mg, 74% yield): $^1\text{H NMR}$ (250 MHz, CDCl_3) δ = 8.59 (dd, J = 5, 2 Hz, 1H), 8.18 (s, 1H), 7.99 – 7.87 (m, 2H), 7.69 (s, 4H), 7.55 (d, J = 8 Hz, 1H), 7.50 – 7.34 (m, 4H), 7.34 – 7.23 (m, 3H), 7.14 (dd, J = 8, 5 Hz, 1H), 4.53 (s, 2H) ppm; $^{13}\text{C NMR}$ (63 MHz, CDCl_3) δ = 164.66, 156.45, 153.83, 151.05, 144.18, 140.93, 138.16, 137.66, 137.01, 129.83, 129.36, 128.68, 127.66, 127.45, 125.88, 125.81, 123.93, 119.93, 119.72, 119.21, 35.28 ppm; HRMS (ES, m/z) calcd for $[\text{C}_{26}\text{H}_{19}\text{F}_3\text{N}_2\text{NaOS}]^+$ ($\text{M}+\text{Na}$) $^+$ 487.1068, found 487.1063.



2-(Benzylsulfinyl)-N-(4'-chloro-[1,1'-biphenyl]-3-yl)nicotinamide (40a).

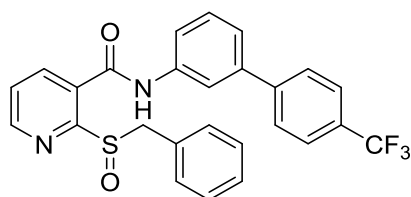
General procedure 4 was followed using 2-(benzylthio)-N-(4'-chloro-[1,1'-biphenyl]-3-yl)nicotinamide to give the title compound as a cream coloured solid (78 mg, 71% yield): $^1\text{H NMR}$ (400 MHz, DMSO) δ = 10.81 (s, 1H), 8.87 (d, J = 5 Hz, 1H), 8.30 (d, J = 8 Hz, 1H), 7.99 (s, 1H), 7.74 (dd, J = 8, 5 Hz, 2H), 7.65 (d, J = 9 Hz, 2H), 7.55 (d, J = 9 Hz, 2H), 7.48 (t, J = 8 Hz, 1H), 7.44 (d, J = 8 Hz, 1H), 7.33 – 7.25 (m, 5H), 4.47 (d, J = 13 Hz, 1H), 4.15 (d, J = 13 Hz, 1H) ppm; $^{13}\text{C NMR}$ (101 MHz, DMSO) δ = 163.86, 161.87, 151.44, 139.49, 139.23, 138.80, 137.12, 132.59, 131.97, 131.26, 130.27, 129.65, 129.07, 128.53, 128.42, 127.94, 125.38, 122.63,

119.53, 118.34, 60.53 ppm; HRMS (ES, m/z) calcd for $[\text{C}_{25}\text{H}_{19}\text{ClN}_2\text{NaO}_2\text{S}]^+$ ($\text{M}+\text{Na}$) $^+$ 469.0753, found 469.0744.



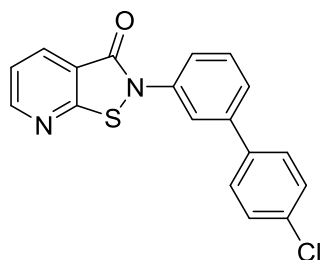
2-(Benzylsulfinyl)-*N*-(4'-methoxy-[1,1'-biphenyl]-3-yl)nicotinamide (40b).

General procedure 4 was followed using 2-(benzylthio)-*N*-(4'-methoxy-[1,1'-biphenyl]-3-yl)nicotinamide to give the title compound as a fluffy white solid (290 mg, >95% yield): HRMS (ES, m/z) calcd for $[\text{C}_{26}\text{H}_{22}\text{N}_2\text{NaO}_3\text{S}]^+$ ($\text{M}+\text{Na}$) $^+$ 465.1249, found 465.1259; This intermediate was taken forward to the next step without further characterisation.



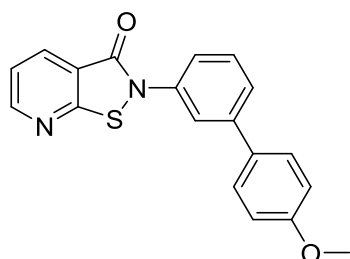
2-(Benzylsulfinyl)-*N*-(4'-(trifluoromethyl)-[1,1'-biphenyl]-3-yl)nicotinamide (40c).

General procedure 4 was followed using 2-(benzylthio)-*N*-(4'-(trifluoromethyl)-[1,1'-biphenyl]-3-yl)nicotinamide to give the title compound as a fluffy white solid (185 mg, 89% yield): ^1H NMR (400 MHz, DMSO) δ = 10.88 (s, 1H), 8.90 (dd, J = 5, 1 Hz, 1H), 8.33 (d, J = 8 Hz, 1H), 8.08 (s, 1H), 7.87 (s, 4H), 7.82 – 7.74 (m, 2H), 7.57 – 7.52 (m, 2H), 7.37 – 7.26 (m, 5H), 4.49 (d, J = 13 Hz, 1H), 4.18 (d, J = 13 Hz, 1H) ppm; ^{13}C NMR (101 MHz, DMSO) δ = 163.92, 161.87, 151.47, 144.00, 139.35, 139.26, 137.16, 131.96, 131.27, 130.29, 129.80, 128.55, 127.96, 127.49, 126.03, 125.41, 123.02, 120.14, 118.67, 60.52 ppm; HRMS (ES, m/z) calcd for $[\text{C}_{26}\text{H}_{19}\text{F}_3\text{N}_2\text{NaO}_2\text{S}]^+$ ($\text{M}+\text{Na}$) $^+$ 503.1017, found 503.1025.



2-(4'-Chloro-[1,1'-biphenyl]-3-yl)isothiazolo[5,4-*b*]pyridin-3(2*H*)-one (41).

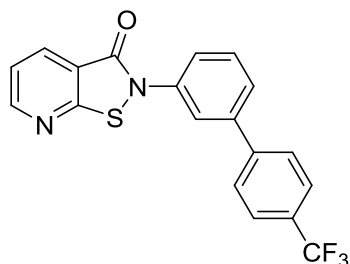
General procedure 9 was followed using 2-(benzylsulfinyl)-*N*-(4'-chloro-[1,1'-biphenyl]-3-yl)nicotinamide to give the title compound as a white solid (50 mg, 86% yield): mp 189-191°C (white solid to brown liquid); ¹H NMR (400 MHz, CDCl₃) δ = 8.83 (s, 1H), 8.37 (d, *J* = 8 Hz, 1H), 7.92 (s, 1H), 7.66 (d, *J* = 7 Hz, 1H), 7.60 – 7.50 (m, 4H), 7.43 (d, *J* = 8 Hz, 3H) ppm; ¹³C NMR (101 MHz, CDCl₃) δ = 162.75, 161.98, 154.35, 141.68, 138.54, 137.31, 135.49, 134.22, 130.16, 129.23, 128.66, 126.16, 123.93, 123.64, 121.27 ppm; HRMS (CI, *m/z*) calcd for [C₁₈H₁₂ClN₂OS]⁺ (M+H)⁺ 339.0359, found 339.0359; IR (neat) ν 1665 (s, C=O amide), 1562 (m, C-C aromatic), 1459 (m, C-C aromatic), 1394 (m, C-H aliphatic), 752 (s, S-N) cm⁻¹.



2-(4'-Methoxy-[1,1'-biphenyl]-3-yl)isothiazolo[5,4-*b*]pyridin-3(2*H*)-one (42).

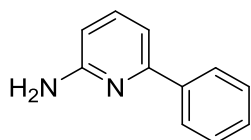
General procedure 9 was followed using 2-(benzylsulfinyl)-*N*-(4'-methoxy-[1,1'-biphenyl]-3-yl)nicotinamide to give the title compound as a white solid (148 mg, 68% yield): mp 170-172°C; ¹H NMR (400 MHz, CDCl₃) δ = 8.82 (dd, *J* = 5, 1 Hz, 1H), 8.37 (dd, *J* = 8, 2 Hz, 1H), 7.91 – 7.86 (m, 1H), 7.66 – 7.59 (m, 1H), 7.59 – 7.51 (m, 4H), 7.42 (dd, *J* = 8, 5 Hz, 1H), 7.03 – 6.97 (m, 2H), 3.86 (s, 3H) ppm; ¹³C NMR (101 MHz, CDCl₃) δ 162.68, 162.03, 159.76, 154.15, 142.56, 137.16, 135.50, 132.61, 129.95, 128.47, 125.96, 123.36, 123.11, 121.18, 120.01, 114.49, 55.52; HRMS (CI, *m/z*) calcd for [C₁₉H₁₅N₂O₂S]⁺ (M+H)⁺ 335.0854, found 335.0851;

Anal. Calcd for C₁₉H₁₄N₂O₂S: C, 68.24; H, 4.22; N, 8.38; S, 9.59. Found: C, 67.80; H, 4.36; N, 8.18; S, 9.48; IR (neat) ν 3057 (w, C-H aromatic), 2961 (w, C-H aliphatic), 1673 (s, C=O amide), 1567 (m, C-C aromatic), 1518 (m, C-C aromatic), 1396 (m, C-H aliphatic), 1238 (s, C-O), 758 (m, S-N) cm⁻¹.



2-(4'-(Trifluoromethyl)-[1,1'-biphenyl]-3-yl)isothiazolo[5,4-*b*]pyridin-3(2*H*)-one (43).

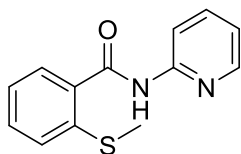
General procedure 9 was followed using 2-(benzylsulfinyl)-*N*-(4'-(trifluoromethyl)-[1,1'-biphenyl]-3-yl)nicotinamide to give the title compound as a cream coloured solid (73 mg, 97% yield): ¹H NMR (400 MHz, CDCl₃) δ = 8.84 (dd, *J* = 5, 2 Hz, 1H), 8.38 (dd, *J* = 8, 2 Hz, 1H), 7.98-7.96 (m, 1H), 7.73 (s, 4H), 7.58-7.57 (m, 1H), 7.58 (s, 1H), 7.42 – 7.39 (m, 3H) ppm; ¹³C NMR (101 MHz, CDCl₃) δ 162.78, 161.95, 154.41, 143.59, 141.43, 137.43, 135.52, 133.87, 130.28, 129.18, 128.93, 128.46, 127.75, 126.42, 126.03, 125.99, 124.45, 123.90, 121.31, 119.81, 70.85 ppm; LRMS (CI, *m/z*) calcd for [C₁₉H₁₂F₃N₂OS]⁺ (M+H)⁺ 373.0622, found 373.1; IR (neat) ν 1672 (s, C=O amide), 1560 (m, C-C aromatic), 1459 (m, C-C aromatic), 1392 (m, C-H aliphatic), 752 (s, S-N) cm⁻¹.



6-Phenylpyridin-2-amine (44).⁸⁹

General procedure 8 was followed using 2-amino-6-bromopyridine and phenylboronic acid to give the title compound as an off white solid (220 mg, 89% yield): ¹H NMR (400 MHz, CDCl₃) δ = 7.93 (d, *J* = 8 Hz, 2H), 7.49 (t, *J* = 8 Hz, 1H), 7.43 (t, *J* = 7 Hz, 2H), 7.39 – 7.34 (m, 1H), 7.08 (d, *J* = 7 Hz, 1H), 6.44 (d, *J* = 8 Hz, 1H), 4.54 (s, 2H) ppm; ¹³C NMR (101 MHz, CDCl₃) δ = 158.37, 156.24, 139.78,

138.52, 128.70, 128.67, 126.94, 111.08, 107.23 ppm; HRMS (CI, m/z) calcd for $[C_{11}H_{11}N_2]^+$ ($M+H$)⁺ 171.0922, found 171.0917.



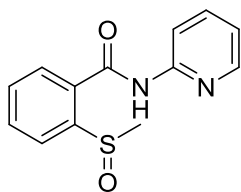
2-(Methylthio)-*N*-(pyridin-2-yl)benzamide (45a).

General procedure 3 was followed using 2-(methylthio)benzoic acid (1 g, 5.9 mmol) and 2-aminopyridine (0.7 g, 7.1 mmol) (omitting the acid wash from the work up due to the presence of pyridine) to give the title compound as a pale yellow solid (1.4 g, >95% yield): ¹H NMR (400 MHz, CDCl₃) δ = 8.49 (ddd, J = 5, 2, 1 Hz, 1H), 7.78 – 7.73 (m, 1H), 7.64 (dd, J = 8, 1 Hz, 1H), 7.48 – 7.44 (m, 1H), 7.23 (ddd, J = 7, 2, 1 Hz, 1H), 7.21 – 7.18 (m, 1H), 7.12 – 7.08 (m, 1H), 7.03 (td, J = 8, 1 Hz, 1H), 2.37 (s, 3H) ppm; ¹³C NMR (101 MHz, CDCl₃) δ = 173.15, 154.93, 151.34, 141.67, 139.98, 136.58, 132.87, 131.24, 128.27, 126.20, 124.68, 124.60, 18.26 ppm.



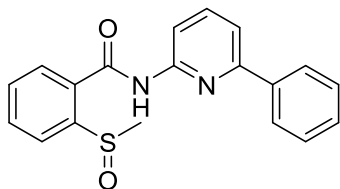
2-(Methylthio)-*N*-(6-phenylpyridin-2-yl)benzamide (45b).

General procedure 3 was followed using 2-(methylthio)benzoic acid and 6-phenylpyridin-2-amine (omitting the acid wash from the work up due to the presence of pyridine) to give the title compound as a colourless oil (162 mg, 39% yield): ¹H NMR (400 MHz, CDCl₃) δ = 8.82 (s, 1H), 8.34 (d, J = 8 Hz, 1H), 7.98 – 7.92 (m, 2H), 7.83 (t, J = 8 Hz, 1H), 7.69 (d, J = 8 Hz, 1H), 7.52 (d, J = 8 Hz, 1H), 7.49 – 7.40 (m, 4H), 7.37 (d, J = 8 Hz, 1H), 2.50 (s, 3H) ppm; ¹³C NMR (101 MHz, CDCl₃) δ = 166.57, 151.29, 131.44, 129.27, 128.86, 128.50, 127.27, 126.96, 125.27, 116.82, 112.72, 16.72 ppm; HRMS (CI, m/z) calcd for $[C_{19}H_{16}N_2OS]^+$ ($M+H$)⁺ 321.1062, found 321.1065.



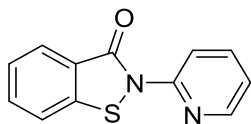
2-(Methylsulfinyl)-N-(pyridin-2-yl)benzamide (46a).

General procedure 4 was followed using 2-(methylthio)-N-(pyridin-2-yl)benzamide (1.4 g, 5.73 mmol) to give the title compound as an off-white fine powder (484 mg, 33% yield): ^1H NMR (400 MHz, CDCl_3) δ = 9.39 (s, 1H), 8.35 (dd, J = 8, 1 Hz, 1H), 8.27 (d, J = 8 Hz, 1H), 8.18 (ddd, J = 5, 2, 1 Hz, 1H), 7.83 (dd, J = 8, 1 Hz, 1H), 7.80 – 7.72 (m, 2H), 7.57 (td, J = 8, 1 Hz, 1H), 7.07 (ddd, J = 7, 5, 1 Hz, 1H), 2.95 (s, 3H) ppm; ^{13}C NMR (101 MHz, CDCl_3) δ = 164.98, 151.52, 149.66, 148.40, 139.04, 133.49, 131.75, 130.97, 127.20, 125.26, 120.86, 114.82, 45.51 ppm; HRMS (ES, m/z) calcd for $[\text{C}_{13}\text{H}_{12}\text{N}_2\text{NaO}_2\text{S}]^+$ ($\text{M}+\text{Na}$) $^+$ 283.0517, found 283.0518.



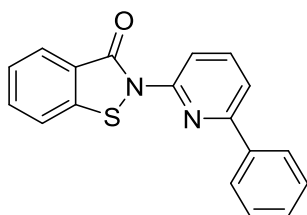
2-(Methylsulfinyl)-N-(6-phenylpyridin-2-yl)benzamide (46b).

General procedure 4 was followed using 2-(methylthio)-N-(6-phenylpyridin-2-yl)benzamide to give the title compound as a shiny white solid (97 mg, 62% yield): ^1H NMR (400 MHz, CDCl_3) δ = 8.89 (s, 1H), 8.39 (d, J = 8 Hz, 1H), 8.23 (d, J = 8 Hz, 1H), 7.97 – 7.92 (m, 2H), 7.89 – 7.78 (m, 3H), 7.61 (td, J = 8, 1 Hz, 1H), 7.55 (d, J = 8 Hz, 1H), 7.50 – 7.40 (m, 3H), 2.97 (s, 3H) ppm; ^{13}C NMR (101 MHz, CDCl_3) δ = 164.41, 156.24, 150.66, 149.56, 139.49, 133.18, 131.26, 130.53, 129.38, 128.83, 126.85, 126.51, 124.96, 117.28, 112.46, 45.08 ppm; HRMS (CI, m/z) calcd for $[\text{C}_{19}\text{H}_{15}\text{N}_2\text{OS}]^+$ ($\text{M}-\text{H}_2\text{O}$) 319.0905, found 319.0905.



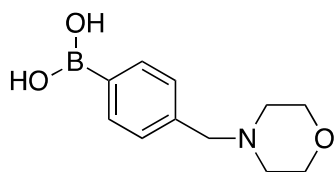
2-(Pyridin-2-yl)benzo[d]isothiazol-3(2H)-one (47).¹⁰⁰

General procedure 5 was followed using 2-(methylsulfinyl)-*N*-(pyridin-2-yl)benzamide (450 mg, 1.73 mmol) to give the title compound as a pale yellow solid (395 mg, 86% yield): mp 194-196°C; ¹H NMR (400 MHz, CDCl₃) δ = 8.74 (d, *J* = 8 Hz, 1H), 8.41 (dd, *J* = 5, 1 Hz, 1H), 8.06 (d, *J* = 8 Hz, 1H), 7.86 – 7.76 (m, 1H), 7.69 – 7.61 (m, 1H), 7.58 (d, *J* = 8 Hz, 1H), 7.45 – 7.33 (m, 1H), 7.14 (ddd, *J* = 7, 5, 1 Hz, 1H) ppm; ¹³C NMR (101 MHz, CDCl₃) δ = 164.18, 150.53, 147.74, 141.13, 138.54, 132.95, 126.92, 126.73, 125.66, 120.83, 120.44, 114.59 ppm; LRMS (CI, *m/z*) calcd for [C₁₂H₉N₂OS]⁺ (M+H)⁺ 229.0436, found 229.0; IR (neat) ν 3059 (m, C-H aromatic), 1668 (s, C=O amide), 1581 (m, C-C aromatic), 735 (s, S-N) cm⁻¹.



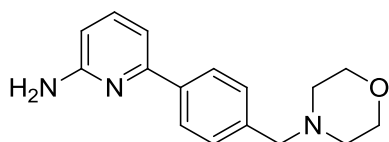
2-(6-Phenylpyridin-2-yl)benzo[d]isothiazol-3(2H)-one (48).

General procedure 5 was followed using 2-(methylsulfinyl)-*N*-(6-phenylpyridin-2-yl)benzamide to give the title compound as a white solid (55 mg, 70% yield): mp 168-170°C; ¹H NMR (400 MHz, CDCl₃) δ = 8.66 (d, *J* = 8 Hz, 1H), 8.12 (d, *J* = 7 Hz, 2H), 8.08 (d, *J* = 8 Hz, 1H), 7.87 (t, *J* = 8 Hz, 1H), 7.68-7.58 (m, 3H), 7.54-7.50 (m, 2H), 7.48 – 7.39 (m, 1H) ppm; ¹³C NMR (101 MHz, CDCl₃) δ = 164.18, 155.37, 150.04, 141.43, 139.47, 137.91, 132.92, 129.64, 128.96, 126.95, 125.60, 120.42, 116.88, 112.76 ppm; HRMS (CI, *m/z*) calcd for [C₁₈H₁₃N₂OS]⁺ (M+H)⁺ 305.0749, found 305.0746; IR (neat) ν 3059 (w, C-H aromatic), 2921 (w, C-H aliphatic), 1673 (s, C=O amide), 1583 (m, C-C aromatic), 1561 (m, C-C aromatic), 1443 (m, C-H aromatic), 763 (s, S-N) cm⁻¹.



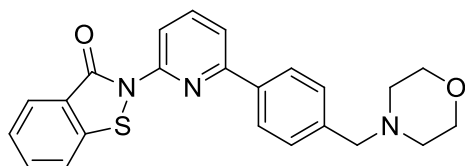
4-(Morpholinomethyl)phenyl boronic acid (49a).¹⁰¹

To a stirring solution of 4-bromomethylbenzene boronic acid (250 mg, 1.16 mmol) in anhydrous THF (10 mL) was added morpholine (0.25 mL, 2.91 mmol) and DIPEA (0.41 mL, 2.33 mmol). The resulting reaction mixture was stirred at room temperature for 18 hours under a nitrogen atmosphere. The reaction mixture was then diluted with brine and extracted with ethyl acetate (3 x 15 mL). The combined organics were dried over sodium sulphate, filtered and concentrated under reduced pressure to give the title compound as a white solid (261 mg, 82% yield): ¹H NMR (400 MHz, CDCl₃) δ = 7.96 (d, *J* = 7 Hz, 2H), 7.35 (d, *J* = 7 Hz, 2H), 3.72-3.70 (m, 4H), 3.53 (s, 2H), 2.46 (s, 4H) ppm; ¹³C NMR (100 MHz, CDCl₃) δ = 136.94, 133.77, 134.04, 128.52, 67.03, 63.61, 53.65 ppm; HRMS (CI, *m/z*) calcd for [C₁₁H₁₆BNO₃]⁺ (M+H)⁺ 222.1301, found 178.1234 ([C₁₁H₁₅NO]+H)⁺, which corresponds to (M-B(OH)₂).



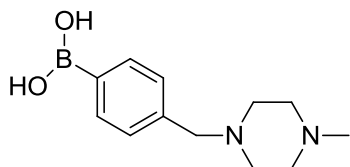
6-(4-(Morpholinomethyl)phenyl)pyridin-2-amine (50a).

General procedure 8 was followed using 4-(morpholinomethyl)phenyl boronic acid and 2-amino-6-bromopyridine to give the title compound as a yellow oil (94 mg, 45% yield): ¹H NMR (400 MHz, CDCl₃) δ = 7.86 (d, *J* = 8 Hz, 2H), 7.49 (t, *J* = 8 Hz, 1H), 7.39 (d, *J* = 8 Hz, 2H), 7.06 (d, *J* = 8 Hz, 1H), 6.44 (d, *J* = 8 Hz, 1H), 3.72-3.70 (m, 4H), 3.54 (s, 2H), 2.48-2.45 (m, 4H) ppm; ¹³C NMR (100 MHz, CDCl₃) δ = 158.39, 156.05, 138.79, 138.54, 138.17, 129.59, 126.91, 111.02, 107.22, 67.06, 63.22, 53.67 ppm; HRMS (CI, *m/z*) calcd for [C₁₆H₂₀N₃O]⁺ (M+H)⁺ 270.1606, found 270.1607.



2-(6-(4-(Morpholinomethyl)phenyl)pyridin-2-yl)benzo[d]isothiazol-3(2H)-one (51).

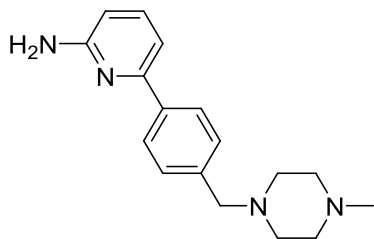
General procedure 11 was followed using 2-(chlorocarbonyl)phenyl hypochlorothioite and 6-(4-(morpholinomethyl)phenyl)pyridin-2-amine to give the title compound as yellow solid (109 mg, 77% yield): mp 149-151°C; ¹H NMR (400 MHz, CDCl₃) δ = 8.65 (d, *J* = 8 Hz, 1H), 8.07 (dd, *J* = 8, 2 Hz, 3H), 7.86 (t, *J* = 8 Hz, 1H), 7.66 (t, *J* = 8 Hz, 1H), 7.60 (d, *J* = 8 Hz, 2H), 7.48 (d, *J* = 8 Hz, 2H), 7.41 (t, *J* = 7 Hz, 1H), 3.80 – 3.69 (m, 4H), 3.58 (s, 2H), 2.50 (s, 4H) ppm; ¹³C NMR (101 MHz, CDCl₃) δ = 164.05, 155.06, 149.89, 141.31, 139.34, 136.81, 132.81, 129.64, 126.77, 125.49, 120.29, 116.66, 112.54, 67.03, 63.13, 53.67 ppm; HRMS (CI, *m/z*) calcd for [C₂₃H₂₂N₃O₂S]⁺ (M+H)⁺ 404.1433, found 404.1427; IR (neat) ν 3060 (w, C-H, aromatic), 2815 (w, C-H, aliphatic), 1681 (s, C=O, amide), 1582 (m, C-C, aromatic), 1563 (m, C-C, aromatic), 1444 (m, C-H, aliphatic), 742 (m, S-N) cm⁻¹.



(4-((4-Methylpiperazin-1-yl)methyl)phenyl)boronic acid (49b).

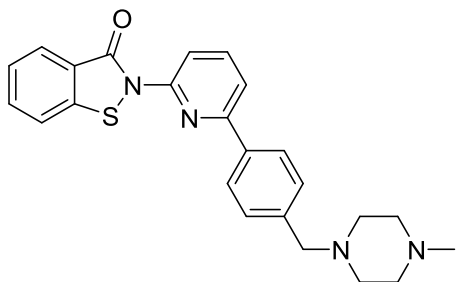
To a stirring solution of 4-bromomethylbenzene boronic acid (500 mg, 2.3 mmol) in anhydrous THF (10 mL) was added N-methylpiperazine (0.64 mL, 5.83 mmol) and DIPEA (0.81 mL, 4.7 mmol). The resulting reaction mixture was stirred at room temperature for 48 hours under a nitrogen atmosphere. The reaction mixture was then diluted with brine and extracted with ethyl acetate (3 x 15 mL). The combined organics were dried over sodium sulfate, filtered and concentrated under reduced pressure to give the title compound as a yellow oil (457 mg, 84% yield): ¹H NMR (400 MHz, CDCl₃) δ = 7.94 (d, *J* = 8 Hz, 2H), 7.32 (d, *J* = 8 Hz, 2H), 3.53 (s, 2H), 3.17 – 2.98 (m, 2H), 2.49 (br s, 8H), 2.31 (s, 3H) ppm; (Boronic acid moiety too sensitive for ms conditions however peak present for

title compound minus boronic acid) HRMS (CI, m/z) calcd for $[C_{12}H_{19}N]^+$ ($M(-B(OH)_2)+H$) $^+$ 194.1548, found 191.1547.



6-(4-((4-Methylpiperazin-1-yl)methyl)phenyl)pyridin-2-amine (50b).

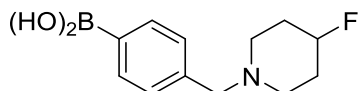
General procedure 8 was followed using (4-((4-methylpiperazin-1-yl)methyl)phenyl)boronic acid and 2-amino-6-bromopyridine to give the title compound as a pale yellow solid (388 mg, 86% yield): 1H NMR (400 MHz, $CDCl_3$) δ = 2.24 (s, 3H), 2.4-2.5 (m, 8H), 3.49 (s, 2H), 4.66 (bs, 2H), 6.36 (d, J = 8 Hz, 1H), 7.00 (d, J = 7 Hz, 1H), 7.34 (m, 2H), 7.41 (t, J = 8 Hz, 1H), 7.81 (m, 2H) ppm; ^{13}C NMR (101 MHz, $CDCl_3$) δ = 46.0, 53.0, 55.1, 62.7, 107.0, 110.7, 126.7, 129.4, 138.3, 138.6, 156.0, 158.4 ppm; HRMS (ES, m/z) calcd for $[C_{17}H_{23}N_4]^+$ ($M+H$) $^+$ 283.1923, found 283.1922.



2-(6-(4-((4-Methylpiperazin-1-yl)methyl)phenyl)pyridin-2-yl)benzo[d]isothiazol-3(2H)-one (52).

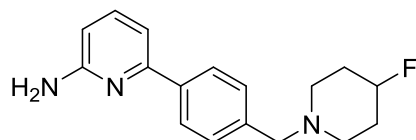
General procedure 11 was followed using 2-(chlorocarbonyl)phenyl hypochlorothioite and 6-(4-((4-methylpiperazin-1-yl)methyl)phenyl)pyridin-2-amine to give the title compound as a yellow solid (472 mg, 75% yield): mp 176-178°C; 1H NMR (400 MHz, $CDCl_3$) δ = 8.64 (d, J = 8 Hz, 1H), 8.07 (t, J = 7 Hz, 3H), 7.86 (t, J = 8 Hz, 1H), 7.69 - 7.63 (m, 1H), 7.60 (d, J = 8 Hz, 2H), 7.47 (d, J = 8 Hz, 2H), 7.41 (t, J = 8 Hz, 1H), 3.59 (s, 2H), 2.49 (s, 8H), 2.30 (s, 3H) ppm; ^{13}C NMR (101 MHz, $CDCl_3$) δ = 164.05, 155.17, 149.88, 141.30, 139.93, 139.30, 136.66,

132.78, 129.59, 126.86, 126.80, 126.70, 125.46, 120.29, 116.64, 112.48, 62.73, 55.18, 53.18, 46.06 ppm; HRMS (CI, m/z) calcd for $[C_{24}H_{25}N_4OS]^+$ (M+H)⁺ 417.1749, found 417.1746; IR (neat) ν 2980 (w, C-H aliphatic), 1679 (s, C=O amide), 1561 (m, C-C aromatic), 1444 (m, C-C aromatic), 1325 (m, C-H aliphatic), 738 (s, S-N) cm^{-1} .



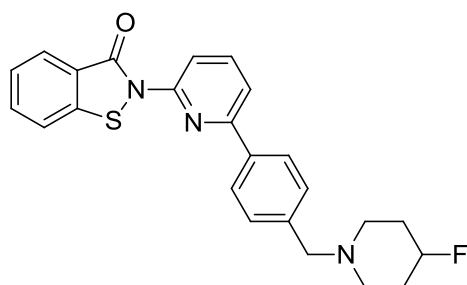
(4-((4-Fluoropiperidin-1-yl)methyl)phenyl)boronic acid (49c).

To a stirring solution of 4-bromomethylbenzene boronic acid (300 mg, 1.4 mmol) in anhydrous THF (10 mL) was added 4-fluoropiperidine hydrochloride (389 mg, 2.79 mmol) and DIPEA (1.2 mL, 6.98 mmol). The resulting reaction mixture was stirred at room temperature for 18 hours under a nitrogen atmosphere. The reaction mixture was then diluted with brine and extracted with ethyl acetate (3 x 15 mL). The combined organics were dried over sodium sulphate, filtered and concentrated under reduced pressure to give the title compound as a white, foam-like solid (266 mg, 80% yield): ¹H NMR (400 MHz, CDCl₃) δ = 7.95 (d, J = 7 Hz, 2H), 7.33 (d, J = 7 Hz, 2H), 4.66 (d, J = 49 Hz, 1H), 3.54 (s, J = 13 Hz, 2H), 3.14 (br s, 2H), 2.60-2.41 (m, 4H), 1.94-1.85 (m, 4H) ppm; ¹³C NMR (101 MHz, CDCl₃) δ = 133.97, 128.51, 63.01, 49.37, 31.30, 18.45 ppm; (Boronic acid moiety too sensitive for ms conditions however peak present for title compound minus boronic acid) HRMS (CI, m/z) calcd for $[C_{12}H_{12}FN]^+$ (M(-B(OH)₂)+H)⁺ 194.1345, found 194.1346.



6-(4-((4-Fluoropiperidin-1-yl)methyl)phenyl)pyridin-2-amine (50c).

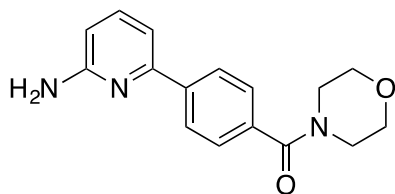
General procedure 8 was followed using (4-((4-fluoropiperidin-1-yl)methyl)phenyl)boronic acid and 2-amino-6-bromopyridine to give the title compound as a white solid (292 mg, 86% yield): ^1H NMR (400 MHz, CDCl_3) δ = 7.86 (d, J = 8 Hz, 2H), 7.50-7.46 (m, 1H), 7.37 (d, J = 8 Hz, 2H), 7.09-7.06 (m, 1H), 6.44 (d, J = 8 Hz, 1H), 4.77 – 4.57 (m, 1H), 4.53 (s, 1H), 3.54 (s, 1H), 2.59-2.58 (m, 2H), 2.42 – 2.33 (m, 2H), 1.99 – 1.81 (m, 4H) ppm; ^{13}C NMR (101 MHz, CDCl_3) δ = 158.26, 156.04, 138.80, 138.64, 138.40, 129.36, 126.74, 110.91, 107.05, 62.70, 49.46, 31.61, 31.42 ppm; HRMS (CI, m/z) calcd for $[\text{C}_{17}\text{H}_{21}\text{FN}_3]^+$ ($\text{M}+\text{H}$) $^+$ 286.1720, found 286.1720.



2-(6-(4-((4-Fluoropiperidin-1-yl)methyl)phenyl)pyridin-2-yl)benzo[d]isothiazol-3(2H)-one (53).

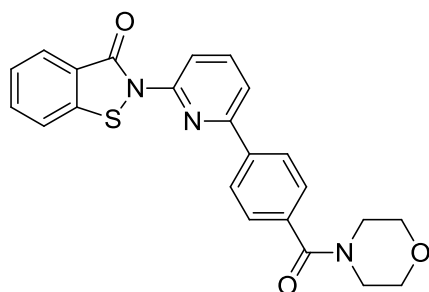
General procedure 11 was followed using 2-(chlorocarbonyl)phenyl hypochlorothioite and 6-(4-((4-fluoropiperidin-1-yl)methyl)phenyl)pyridin-2-amine to give the title compound as a pale yellow solid (14 mg, 3% yield): mp 148-150°C; ^1H NMR (400 MHz, CDCl_3) δ = 8.65 (d, J = 8 Hz, 1H), 8.06 (d, J = 5 Hz, 3H), 7.86 (t, J = 8 Hz, 1H), 7.66 (t, J = 7 Hz, 1H), 7.60 (d, J = 8 Hz, 2H), 7.46 (d, J = 7 Hz, 2H), 7.41 (t, J = 7 Hz, 1H), 4.70 (d, J = 49 Hz, 1H), 3.59 (s, 2H), 2.63 (s, 2H), 2.43 (s, 2H), 1.91 (m, 4H) ppm; ^{13}C NMR (101 MHz, CDCl_3) δ = 164.07, 155.11, 155.11, 149.87, 141.28, 139.95, 139.34, 136.70, 132.81, 129.52, 126.85, 126.81, 126.75, 125.49, 120.30, 116.67, 112.51, 89.49, 62.65, 49.51, 31.62, 31.43; HRMS (ES, m/z) calcd for $[\text{C}_{24}\text{H}_{23}\text{FN}_3\text{OS}]^+$ ($\text{M}+\text{H}$) $^+$ 420.1546, found 420.1538; IR (neat) ν

2953 (w, aromatic C-H), 2811 (m, C-H aliphatic), 1676 (s, C=O amide), 1444 (m, C-C aromatic), 1292 (m, C-N amine aromatic), 760 (s, S-N) cm^{-1} .



(4-(6-Aminopyridin-2-yl)phenyl)(morpholino)methanone (54a).

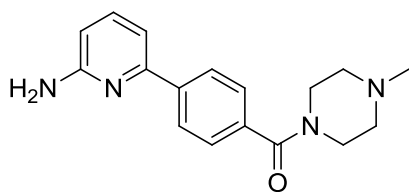
General procedure 8 was followed using (4-(morpholine-4-carbonyl)phenyl)boronic acid and 2-amino-6-bromopyridine to give the title compound as a colourless oil (324 mg, 65% yield): ^1H NMR (400 MHz, CDCl_3) δ = 7.86 (d, J = 8 Hz, 2H), 7.37-7.33 (m, 3H), 6.94 (d, J = 7 Hz, 1H), 6.34 (d, J = 8 Hz, 1H), 4.72 (s, 2H), 3.65-3.53 (m, 8H) ppm; ^{13}C NMR (101 MHz, CDCl_3) δ = 170.15, 158.50, 154.61, 141.14, 138.24, 134.91, 127.27, 126.79, 110.61, 107.66, 66.68 ppm; HRMS (CI, m/z) calcd for $[\text{C}_{16}\text{H}_{17}\text{N}_3\text{O}_2]^+$ (M+H) $^+$ 284.1399, found 284.1403.



2-(6-(4-(Morpholine-4-carbonyl)phenyl)pyridin-2-yl)benzo[d]isothiazol-3(2H)-one (55).

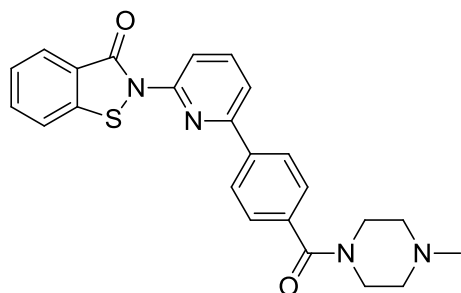
General procedure 11 was followed using 2-(chlorocarbonyl)phenyl hypochlorothioite and (4-(6-aminopyridin-2-yl)phenyl)(morpholino)methanone to give the title compound as a fluffy, yellow solid (300 mg, 63% yield): mp 230-232°C; ^1H NMR (400 MHz, CDCl_3) δ = 8.71 (d, J = 8 Hz, 1H), 8.16 (d, J = 8 Hz, 2H), 8.08 (d, J = 8 Hz, 1H), 7.90 (t, J = 8 Hz, 1H), 7.69 – 7.54 (m, 5H), 7.42 (t, J = 8 Hz, 1H), 3.91 – 3.46 (m, 8H) ppm; ^{13}C NMR (101 MHz, CDCl_3) δ = 170.16, 164.24, 154.26, 150.23, 141.30, 139.65, 139.40, 136.26, 133.07, 127.86, 127.13, 127.00,

126.86, 125.71, 120.43, 117.07, 113.39, 67.06 ppm; HRMS (ES, m/z) calcd for $[C_{23}H_{20}N_3O_3S]^+$ ($M+H$) $^+$ 418.1225, found 418.1213; Anal. Calcd for $C_{23}H_{19}N_3O_3S$: C, 66.17; H, 4.59; N, 10.07; S, 7.68. Found: C, 66.12; H, 4.62; N, 9.68; S, 7.54; IR 2974, 2899, 1672, 1624, 1578, 1560, 1429, 672, 548 cm^{-1} ; IR (neat) ν 2974 (w, C-H, aromatic), 2899 (w, C-H, aliphatic), 1672 (s, C=O, amide), 1624 (s, C=O, amide), 1578 (m, C-C, aromatic), 1560 (m, C-C, aromatic), 1429 (m, C-H, aliphatic) cm^{-1} .



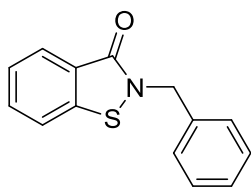
**(4-(6-Aminopyridin-2-yl)phenyl)(4-methylpiperazin-1-yl)methanone
(54b).**

General procedure 8 was followed using (4-(4-methylpiperazine-1-carbonyl)phenyl)boronic acid and 2-amino-6-bromopyridine to give the title compound as a yellow oil (202 mg, 85% yield): 1H NMR (400 MHz, $CDCl_3$) δ = 7.95 (d, J = 8 Hz, 1H), 7.49 (dd, J = 9, 5 Hz, 2H), 7.45 (dd, J = 9, 5 Hz, 1H), 7.08 (d, J = 8 Hz, 2H), 6.47 (d, J = 8 Hz, 1H), 4.55 (br s, 2H), 3.87 – 3.42 (m, 4H), 2.48 - 2.33 (m, 4H), 2.31 (d, J = 5 Hz, 3H) ppm; ^{13}C NMR (101 MHz, $CDCl_3$) δ = 170.22, 158.35, 155.12, 141.05, 139.75, 138.48, 135.69, 129.68, 128.48, 127.39, 127.04, 126.90, 111.11, 107.65, 106.73, 46.03 ppm; HRMS (CI, m/z) calcd for $[C_{17}H_{21}N_4O]^+$ ($M+H$) $^+$ 297.1715, found 297.1715.



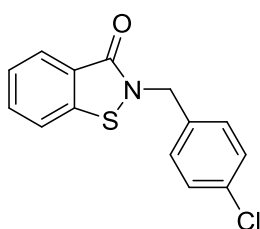
2-(6-(4-(4-Methylpiperazine-1-carbonyl)phenyl)pyridin-2-yl)benzo[d]isothiazol-3(2H)-one (56).

General procedure 11 was followed using (4-(6-aminopyridin-2-yl)phenyl)(4-methylpiperazin-1-yl)methanone and 2-(chlorocarbonyl)phenyl hypochlorothioite to give the title compound as a yellow foam (102 mg, 30% yield): mp 146-148°C; ¹H NMR (400 MHz, CDCl₃) δ = 8.71 (d, *J* = 8 Hz, 1H), 8.16 (d, *J* = 8 Hz, 2H), 8.08 (d, *J* = 8 Hz, 1H), 7.90 (t, *J* = 8 Hz, 1H), 7.67 (t, *J* = 8 Hz, 1H), 7.64 – 7.60 (m, 2H), 7.56 (d, *J* = 8 Hz, 2H), 7.45 – 7.41 (m, 1H), 3.86-3.55 (m, 4H), 2.56-2.44 (m, 4H), 2.37 (s, 3H) ppm; ¹³C NMR (101 MHz, CDCl₃) δ = 170.07, 164.25, 154.36, 150.23, 141.34, 139.65, 139.26, 136.68, 133.06, 129.88, 128.64, 127.83, 127.20, 127.08, 127.01, 126.89, 125.71, 120.44, 117.08, 113.35, 46.02 ppm; HRMS (ES, *m/z*) calcd for [C₂₄H₂₃N₄O₂S]⁺ (M+H)⁺431.1542, found 431.1533; Unable to duplicate CHN readings; IR (neat) ν 3080 (w, aromatic C-H), 2791 (m, C-H aliphatic), 1669 (s, C=O amide (benzisothiazolone ring)), 1620 (s, C=O amide (piperazine)), 1442 (m, C-C aromatic), 1333 (m, C-N amine aromatic), 1138 (m, C-N amine aliphatic), 763 (s, S-N) cm⁻¹.



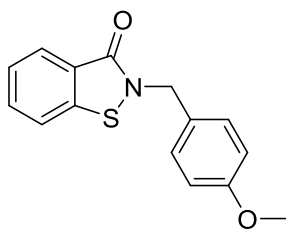
2-Benzylbenzo[d]isothiazol-3(2H)-one (57).⁹

General procedure 6 was followed using benzo[d]isothiazol-3(2H)-one (250 mg, 1.65 mmol) and benzyl bromide (0.22 mL, 1.82 mmol) to give the title compound as an off-white solid (177 mg, 45% yield): mp 81-83°C; ¹H NMR (400 MHz, CDCl₃) δ = 8.07 (d, *J* = 8 Hz, 1H), 7.59 (ddd, *J* = 8, 7, 2 Hz, 1H), 7.49 (d, *J* = 8 Hz, 1H), 7.43 – 7.38 (m, 1H), 7.38 – 7.34 (m, 5H), 5.06 (s, 2H) ppm; ¹³C NMR (101 MHz, CDCl₃) δ = 165.76, 140.80, 136.58, 132.26, 129.25, 128.86, 128.71, 127.24, 125.92, 120.80, 47.98 ppm; HRMS (CI, *m/z*) calcd for [C₁₄H₁₂NOS]⁺ (M+H)⁺ 242.0640, found 242.0629; IR (neat) ν 3077 (m, C-H aromatic), 2923 (w, C-H aliphatic), 1655 (s, C=O amide), 1591 (m, C=C aromatic), 1444 (m, C-H aliphatic), 746 (s, S-N) cm⁻¹.



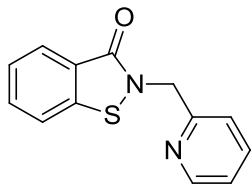
2-(4-Chlorobenzyl)benzo[d]isothiazol-3(2H)-one (58).¹⁰²

General procedure 6 was followed using benzo[d]isothiazol-3(2H)-one (250 mg, 1.65 mmol) and 4-chlorobenzyl bromide (374 mg, 1.82 mmol) to give the title compound as an off-white solid (140 mg, 28% yield): mp 86-88°C; ¹H NMR (400 MHz, CDCl₃) δ = 8.07 (d, *J* = 8 Hz, 1H), 7.63 – 7.58 (m, 1H), 7.51 (d, *J* = 8 Hz, 1H), 7.42 (t, *J* = 8 Hz, 1H), 7.36 – 7.25 (m, 4H), 5.02 (s, 2H) ppm; ¹³C NMR (101 MHz, CDCl₃) δ = 165.82, 165.77, 140.69, 135.14, 134.63, 132.43, 130.16, 129.44, 127.28, 126.05, 124.69, 120.86, 47.07 ppm; HRMS (CI, *m/z*) calcd for [C₁₄H₁₁ClNOS]⁺ (M+H)⁺ 276.0250, found 276.0244; Anal. Calcd for C₁₄H₁₀ClNOS: C, 60.98; H, 3.66; N, 5.08; S, 11.63. Found: C, 60.85; H, 3.73; N, 5.05; S, 11.29; IR (neat) ν 3056 (m, C-H aromatic), 2928 (w, C-H aliphatic), 1656 (s, C=O amide), 1594 (m, C=C aromatic), 1459 (m, C-H aliphatic), 736 (s, S-N) cm⁻¹.



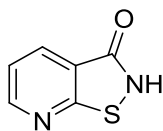
2-(4-Methoxybenzyl)benzo[d]isothiazol-3(2H)-one (59).¹⁰²

General procedure 6 was followed using benzo[d]isothiazol-3(2H)-one (250 mg, 1.65 mmol) and 4-methoxybenzyl bromide (0.27 mL, 1.82 mmol) to give the title compound as an off-white solid (190 mg, 42% yield): mp 72-74°C; ¹H NMR (400 MHz, CDCl₃) δ = 8.06 (d, *J* = 8 Hz, 1H), 7.60 – 7.55 (m, 1H), 7.48 (d, *J* = 8 Hz, 1H), 7.39 (t, *J* = 8 Hz, 1H), 7.30 (d, *J* = 8 Hz, 2H), 6.90 – 6.87 (m, 2H), 4.99 (s, 2H), 3.80 (s, 3H) ppm; ¹³C NMR (101 MHz, CDCl₃) δ = 165.37, 159.79, 140.54, 131.88, 130.15, 128.40, 126.89, 125.58, 124.85, 120.52, 114.33, 55.42, 47.25 ppm; HRMS (CI, *m/z*) calcd for [C₁₅H₁₄NO₂S]⁺ (M+H)⁺ 272.0745, found 272.0736; IR (neat) ν 3059 (m, C-H aromatic), 2930 (w, C-H aliphatic), 1645 (s, C=O amide), 1609 (m, C-C aromatic), 1459 (m, C-H aliphatic), 1246 (m, C-O), 736 (s, S-N) cm⁻¹.



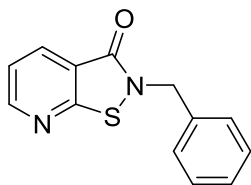
2-(Pyridin-2-ylmethyl)benzo[d]isothiazol-3(2H)-one (60).

General procedure 10 was followed using 2-iodo-*N*-(pyridin-2-ylmethyl)benzamide to give the title compound as a white solid (337 mg, 50% yield): mp 126-128°C; ¹H NMR (400 MHz, CDCl₃) δ = 8.60 (d, *J* = 5 Hz, 1H), 8.07 (d, *J* = 8 Hz, 1H), 7.66 (td, *J* = 8, 2 Hz, 1H), 7.63 – 7.58 (m, 1H), 7.53 (d, *J* = 8 Hz, 1H), 7.43 – 7.38 (m, 1H), 7.32 (d, *J* = 8 Hz, 1H), 7.25 – 7.20 (m, 1H), 5.18 (s, 2H) ppm; ¹³C NMR (101 MHz, CDCl₃) δ = 165.59, 156.02, 149.65, 140.87, 137.24, 132.11, 127.01, 125.65, 124.27, 123.09, 122.71, 120.55, 49.32 ppm; HRMS (CI, *m/z*) calcd for [C₁₃H₁₁N₂OS]⁺ (M+H)⁺ 243.0592, found 243.0595; IR (neat) ν 3056 (w, C-H aromatic), 2938 (w, C-H aliphatic), 1636 (s, C=O amide), 1590 (m, C-C aromatic), 1441 (m, C-H aliphatic) cm⁻¹.



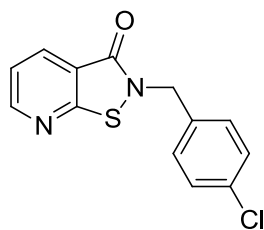
Isothiazolo[5,4-*b*]pyridin-3(2*H*)-one (61).⁸⁷

A solution of 2-mercaptonicotinic acid (1 g, 6.4 mmol) in pyridine (20 mL) was added dropwise to a solution of diphenylphosphoryl azide (1.38 mL, 6.4 mmol) in triethylamine (1.5 mL, 11.0 mmol) at 0°C. The reaction mixture was stirred at room temperature overnight. The reaction mixture was then concentrated under reduced pressure to yield a thick, orange oil. Ethanol (10 mL) was then added at 30°C to the crude product and a yellow precipitate was formed that was filtered and dried to give the title compound as a yellow solid (337 mg, 39% yield): ¹H NMR (400 MHz, DMSO) δ = 11.96 (s, 1H), 8.83 (dd, *J* = 5, 2 Hz, 1H), 8.32 (dd, *J* = 8, 2 Hz, 1H), 7.52 (dd, *J* = 8, 5 Hz, 1H) ppm; ¹³C NMR (101 MHz, DMSO) δ = 163.00, 152.56, 133.16, 120.39, 118.54 ppm; HRMS (CI, *m/z*) calcd for [C₆H₅N₂OS]⁺ (M+H)⁺ 153.0123, found 153.0124.



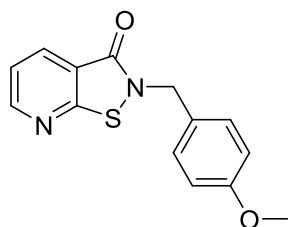
2-Benzylisothiazolo[5,4-*b*]pyridin-3(2*H*)-one (62).²

General procedure 7 was followed using isothiazolo[5,4-*b*]pyridin-3(2*H*)-one (170 mg, 1.12 mmol) and benzyl bromide (0.17 mL, 1.45 mmol) to give the title compound as a white solid (61 mg, 22% yield): mp 78-80°C; ¹H NMR (400 MHz, CDCl₃) δ = 8.73 (dd, *J* = 5, 2 Hz, 1H), 8.30 (dd, *J* = 8, 2 Hz, 1H), 7.41 – 7.31 (m, 6H), 5.08 (s, 2H) ppm; ¹³C NMR (101 MHz, CDCl₃) δ = 163.79, 162.52, 153.76, 135.84, 135.04, 129.08, 128.63, 120.84, 119.45, 47.61 ppm; HRMS (CI, *m/z*) calcd for [C₁₃H₁₁N₂OS]⁺ (M+H)⁺ 243.0592, found 243.0587; Anal. Calcd for C₁₃H₁₀N₂OS: C, 64.44; H, 4.16; N, 11.56; S, 13.23. Found: C, 64.64; H, 4.35; N, 11.16; S, 12.84; IR (neat) ν 3046 (m, C-H aromatic), 2933 (w, C-H aliphatic), 1652 (s, C=O amide), 1584 (m, C=C aromatic), 1453 (m, C-H aliphatic), 757 (s, S-N) cm⁻¹.



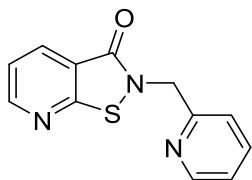
2-(4-Chlorobenzyl)isothiazolo[5,4-*b*]pyridin-3(2*H*)-one (63).²

General procedure 7 was followed using isothiazolo[5,4-*b*]pyridin-3(2*H*)-one (200 mg, 1.3 mmol) and 4-chlorobenzyl bromide (350 mg, 1.7 mmol) to give the title compound as a white crystalline solid (50 mg, 14% yield): mp 156-158°C; ¹H NMR (400 MHz, CDCl₃) δ = 8.75 (dd, *J* = 5, 2 Hz, 1H), 8.30 (dd, *J* = 8, 2 Hz, 1H), 7.37 (dd, *J* = 8, 5 Hz, 1H), 7.35 – 7.29 (m, 4H), 5.04 (s, 2H) ppm; ¹³C NMR (101 MHz, CDCl₃) δ = 163.83, 162.44, 153.93, 135.10, 134.58, 134.38, 129.96, 129.29, 120.97, 119.30, 46.90 ppm; HRMS (CI, *m/z*) calcd for [C₁₃H₁₀ClN₂OS]⁺ (M+H)⁺ 277.0202, found 277.0208; Anal. Calcd for C₁₃H₉ClN₂OS: C, 56.42; H, 3.28; N, 10.12; S, 11.58. Found: C, 56.50; H, 3.38; N, 9.91; S, 11.36; IR (neat) ν 3064 (w, C-H aromatic), 2918 (w, C-H aliphatic), 1668 (s, C=O amide), 1489 (m, C-C aromatic), 1392 (m, C-H aliphatic), 758 (s, S-N) cm⁻¹.



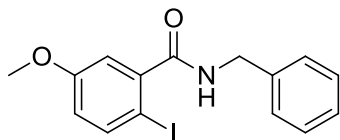
2-(4-Methoxybenzyl)isothiazolo[5,4-*b*]pyridin-3(2*H*)-one (64).

General procedure 7 was followed using isothiazolo[5,4-*b*]pyridin-3(2*H*)-one (220 mg, 1.5 mmol) and 4-methoxybenzyl bromide (378 mg, 1.88 mmol) to give the title compound as a white solid (16 mg, 4% yield): mp 96-98°C; ¹H NMR (400 MHz, CDCl₃) δ = 8.72 (dd, *J* = 5, 2 Hz, 1H), 8.29 (dd, *J* = 8, 2 Hz, 1H), 7.35 (dd, *J* = 8, 5 Hz, 1H), 7.33 – 7.29 (m, 2H), 6.93 – 6.86 (m, 2H), 5.01 (s, 2H), 3.81 (s, 3H) ppm; ¹³C NMR (101 MHz, CDCl₃) δ = 164.00, 162.76, 160.17, 154.06, 135.18, 130.43, 128.17, 121.10, 119.72, 114.72, 55.84, 47.38 ppm; HRMS (CI, *m/z*) calcd for [C₁₄H₁₂N₂O₂S]⁺ (M+H)⁺ 273.0698, found 273.0687; IR (neat) ν 3051 (m, C-H aromatic), 2918 (w, C-H aliphatic), 1651 (s, C=O amide), 1609 (m, C=C aromatic), 1460 (m, C-H aliphatic), 1248 (m, C-O), 756 (s, S-N) cm⁻¹.



2-(Pyridin-2-ylmethyl)isothiazolo[5,4-*b*]pyridin-3(2*H*)-one (65).¹⁰³

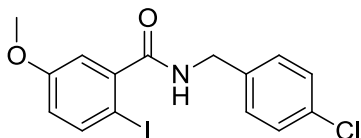
To a stirred solution of isothiazolo[5,4-*b*]pyridin-3(2*H*)-one (177 mg, 1.16 mmol) in anhydrous methanol (12 mL) was added 2-(bromoethyl)pyridine hydrobromide (382 mg, 1.51 mmol) and *N,N*-Diisopropylethylamine (0.5 mL, 2.9 mmol). The resulting orange solution was stirred for 12 hours under a nitrogen atmosphere. The reaction mixture was then neutralised by addition of 1M HCl before extraction with ethyl acetate (3 x 20 mL). The combined organic layers were washed with brine (30 mL), dried over anhydrous sodium sulfate, filtered and concentrated under reduced pressure. The resulting orange solid was purified by column chromatography (DCM: MeOH (49:1)) to afford 2-(pyridin-2-ylmethyl)isothiazolo[5,4-*b*]pyridin-3(2*H*)-one as a pale yellow solid (68 mg, 24% yield): mp 109-111°C; ¹H NMR (500 MHz, CDCl₃) δ = 8.75 (dd, *J* = 5, 2 Hz, 1H), 8.62 – 8.60 (m, 1H), 8.31 (dd, *J* = 8, 2 Hz, 1H), 7.68 (td, *J* = 8, 2 Hz, 1H), 7.36 (dd, *J* = 8, 5 Hz, 1H), 7.34 (d, *J* = 6 Hz, 1H), 7.24 (ddd, *J* = 8, 5, 1 Hz, 1H), 5.20 (s, 2H) ppm; ¹³C NMR (101 MHz, CDCl₃) δ = 163.95, 162.86, 155.47, 153.91, 149.81, 137.30, 135.07, 123.25, 122.73, 120.82, 119.11, 49.11 ppm; HRMS (ES, *m/z*) calcd for [C₁₂H₉N₃NaOS]⁺ (*M*+Na)⁺ 266.0361, found 266.0364; IR (neat) ν 1644 (s, C=O amide), 1590 (m, C-C aromatic), 1575 (m, C-C aromatic), 1398 (m, C-H aliphatic), 758 (s, S-N) cm⁻¹.



***N*-Benzyl-2-iodo-5-methoxybenzamide (66a).**

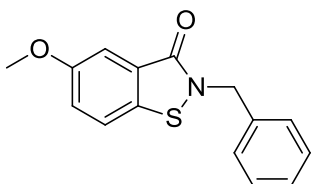
General procedure 3 was followed using 2-iodo-5-methoxybenzoic acid (250 mg, 0.89 mmol) and benzylamine (0.12 mL, 1.12 mmol) to give the title compound as a brown solid (320 mg, >95% yield): ¹H NMR (400 MHz, CDCl₃) δ = 7.69 (d, *J* = 9 Hz, 1H), 7.42-7.34 (m, 4H), 7.33 – 7.27 (m, 2H), 6.68 (dd, *J* = 9, 3 Hz, 1H), 4.64 (d, *J* = 6 Hz, 1H), 3.79 (s, 2H) ppm; ¹³C NMR (101 MHz, CDCl₃) δ = 168.90, 159.80,

142.81, 140.61, 137.46, 128.94, 128.79, 128.22, 127.78, 127.57, 117.75, 114.32, 55.56, 44.31 ppm; HRMS (CI, m/z) calcd for $[C_{15}H_{15}INO_2]^+$ (M+H)⁺ 368.0147, found 368.0157.



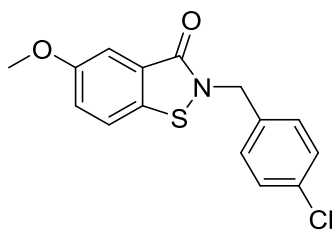
***N*-(4-Chlorobenzyl)-2-iodo-5-methoxybenzamide (66b).**

General procedure 3 was followed using 2-iodo-5-methoxybenzoic acid (250 mg, 0.89 mmol) and 4-chlorobenzylamine (0.14 mL, 1.17 mmol) to give the title compound as a white solid (246 mg, 68% yield): ¹H NMR (400 MHz, CDCl₃) δ = 7.69 (d, J = 9 Hz, 1H), 7.38 – 7.30 (m, 4H), 6.98 (d, J = 3 Hz, 1H), 6.69 (dd, J = 9, 3 Hz, 1H), 6.07 (s, 1H), 4.61 (d, J = 6 Hz, 2H), 3.79 (s, 3H) ppm; ¹³C NMR (101 MHz, CDCl₃) δ = 169.09, 159.95, 142.69, 140.79, 136.18, 133.72, 129.71, 129.04, 117.97, 114.49, 80.66, 55.71, 43.67 ppm; HRMS (CI, m/z) calcd for $[C_{15}H_{14}ClINO_2]^+$ (M+H)⁺ 401.9758, found 401.9768.



2-Benzyl-5-methoxybenzo[*d*]isothiazol-3(2*H*)-one (67).⁹

General procedure 10 was followed using *N*-benzyl-2-iodo-5-methoxybenzamide (320 mg, 0.98 mmol) to give the title compound as a white solid (94 mg, 35% yield): mp 107-109°C; ¹H NMR (400 MHz, CDCl₃) δ = 7.51 (d, J = 2 Hz, 1H), 7.39 – 7.33 (m, 6H), 7.22 (dd, J = 9, 2 Hz, 1H), 5.05 (s, 2H), 3.88 (s, 3H) ppm; ¹³C NMR (101 MHz, CDCl₃) δ = 165.43, 158.51, 136.36, 132.41, 128.96, 128.56, 128.41, 125.63, 122.63, 121.42, 108.04, 55.90, 47.89 ppm; HRMS (CI, m/z) calcd for $[C_{15}H_{14}NO_2S]^+$ (M+H)⁺ 272.0745, found 272.0745; Anal. Calcd for C₁₅H₁₃NO₂S: C, 66.40; H, 4.83; N, 5.16; S, 11.82. Found: C, 66.60; H, 4.92; N, 5.23; S, 11.59; IR (neat) ν 2919 (w, C-H aliphatic), 1628 (s, C=O amide), 1466 (m, C-C aromatic), 1427 (m, C-C aromatic), 1347 (m, C-H aliphatic), 1029 (s, C-O), 758 (s, S-N) cm⁻¹.



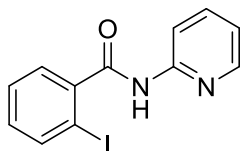
2-(4-Chlorobenzyl)-5-methoxybenzo[d]isothiazol-3(2H)-one (68).

General procedure 10 was followed using *N*-(4-chlorobenzyl)-2-iodo-5-methoxybenzamide (235 mg, 0.59 mmol) to give the title compound as a yellow solid (80 mg, 45% yield): mp 111-113°C; ¹H NMR (400 MHz, CDCl₃) δ = 7.51 (d, *J* = 3 Hz, 1H), 7.38 (d, *J* = 9 Hz, 1H), 7.34-7.27 (m, 4H), 7.25 (td, *J* = 9, 3 Hz, 1H), 5.01 (s, 2H), 3.88 (s, 3H) ppm; ¹³C NMR (101 MHz, CDCl₃) δ = 165.43, 158.57, 134.85, 134.31, 132.25, 129.85, 129.14, 125.41, 122.79, 121.46, 108.03, 55.90, 47.14 ppm; HRMS (ES, *m/z*) calcd for [C₁₅H₁₂NNaO₂S]⁺ (M+Na)⁺ 328.0175, found 328.0166; IR (neat) ν 2917 (m, C-H aliphatic), 1629 (s, C=O amide), 1488 (m, C-C aromatic), 1351 (m, C-H aliphatic), 1029 (s, C-O), 757 (s, S-N) cm⁻¹.



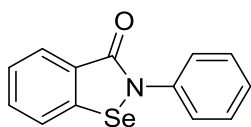
2-Iodo-*N*-phenylbenzamide (69a).¹⁰⁴

General procedure 3 was followed using 2-iodobenzoic acid and aniline to give the title compound as a pale yellow solid (2.23 g, 86% yield): ¹H NMR (400 MHz, CDCl₃) δ = 7.91 (d, *J* = 8 Hz, 1H), 7.64 (d, *J* = 8 Hz, 2H), 7.52 (dd, *J* = 8, 2 Hz, 2H), 7.47 – 7.35 (m, 3H), 7.16 (ddd, *J* = 9, 8, 5 Hz, 2H) ppm; ¹³C NMR (101 MHz, CDCl₃) δ = 167.34, 142.26, 140.19, 137.64, 131.65, 129.29, 128.69, 128.50, 125.07, 120.23, 92.49 ppm; HRMS (CI, *m/z*) calcd for [C₁₃H₁₁INO]⁺ (M+H)⁺ 323.9885, found 323.9887.



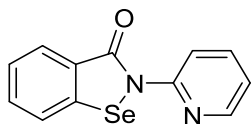
2-Iodo-*N*-(pyridin-2-yl)benzamide (69b).

General procedure 3 was followed using 2-iodobenzoic acid and 2-aminopyridine (omitting the acid wash from the work up due to the presence of pyridine) to give the title compound as a yellow oil (1.06 g, 81% yield): ^1H NMR (400 MHz, CDCl_3) δ = 8.47 (dd, J = 5, 2 Hz, 1H), 7.80 – 7.74 (m, 2H), 7.60 – 7.56 (m, 2H), 7.31 (t, J = 8 Hz, 2H), 7.00 (td, J = 8, 2 Hz, 2H) ppm; ^{13}C NMR (101 MHz, CDCl_3) δ = 171.03, 152.14, 149.63, 147.89, 140.80, 140.45, 140.26, 138.87, 138.28, 131.91, 131.50, 129.36, 128.49, 127.95, 123.52, 123.43, 120.44, 114.51, 93.54 ppm; HRMS (CI, m/z) calcd for $[\text{C}_{12}\text{H}_{10}\text{IN}_2\text{O}]^+$ ($\text{M}+\text{H}$) $^+$ 324.9838, found 324.9843.



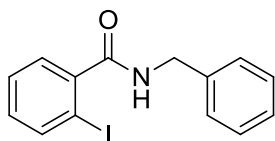
2-Phenylbenzo[*d*][1,2]selenazol-3(2*H*)-one (70).⁸⁴

General procedure 12 was followed using 2-iodo-*N*-phenylbenzamide to give the title compound as a white solid (323 mg, 25% yield): mp 179-181°C, ^1H NMR (400 MHz, CDCl_3) δ = 8.12 (d, J = 7 Hz, 1H), 7.66-7.62 (m, 4H), 7.49-7.42 (m, 3H), 7.29 (d, J = 7 Hz, 1H) ppm; ^{13}C NMR (101 MHz, CDCl_3) δ = 165.84, 139.26, 138.45, 137.74, 129.56, 129.48, 127.71, 126.89, 126.70, 125.56, 123.86 ppm; HRMS (ES, m/z) calcd for $[\text{C}_{13}\text{H}_9\text{NNaOSe}]^+$ ($\text{M}+\text{Na}$) $^+$ 297.9747, found 297.9737; Anal. Calcd for $\text{C}_{13}\text{H}_9\text{NOSe}$: C, 56.95; H, 3.31; N, 5.11. Found: C, 57.10; H, 3.46; N, 4.99; IR (neat) ν 3080 (w, aromatic C-H), 1643 (w, C=O amide), 1587 (m, C-C aromatic), 1486 (m, C-C aromatic), 1442 (m, C-C aromatic), 1307 (m, C-N amine) cm^{-1} .



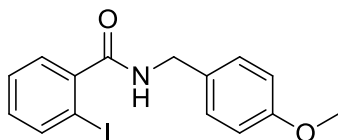
2-(Pyridin-2-yl)benzo[d][1,2]selenazol-3(2H)-one (71).¹⁰⁵

General procedure 12 was followed using 2-iodo-*N*-(pyridin-2-yl)benzamide to give the title compound as an off-white solid (80 mg, 9% yield): mp 233-234°C; ¹H NMR (400 MHz, CDCl₃) δ = 8.71 (d, *J* = 8 Hz, 1H), 8.34 (dd, *J* = 5, 1 Hz, 1H), 8.07 (d, *J* = 8 Hz, 1H), 7.80 – 7.73 (m, 1H), 7.68 – 7.60 (m, 2H), 7.42 (ddd, *J* = 8, 7, 2 Hz, 1H), 7.10 (ddd, *J* = 7, 5, 1 Hz, 1H) ppm; ¹³C NMR (101 MHz, CDCl₃) δ = 165.13, 151.56, 147.62, 138.86, 138.39, 132.86, 130.38, 126.17, 123.86, 120.38, 114.48 ppm; HRMS (CI, *m/z*) calcd for [C₁₂H₉N₂OSe]⁺ (M+H)⁺ 276.9880, found 276.9876; IR (neat) ν 2921 (w, aromatic C-H), 2851 (m, C-H aliphatic), 1606 (s, C=O amide), 1444 (s, C-C aromatic), 1427 (s, C-C aromatic), 1308 (m, C-N amine aromatic) cm⁻¹.



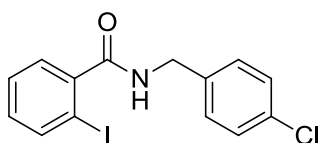
***N*-Benzyl-2-iodobenzamide (72a).**¹⁰⁶

General procedure 3 was followed using 2-iodobenzoyl chloride and benzylamine to give the title compound as a white solid (623 mg, >95% yield): ¹H NMR (400 MHz, CDCl₃) δ = 7.86 (dd, *J* = 8, 1 Hz, 1H), 7.44 – 7.28 (m, 7H), 7.09 (td, *J* = 8, 2 Hz, 1H), 6.05 (br s, 1H), 4.64 (d, *J* = 6 Hz, 2H) ppm; ¹³C NMR (101 MHz, CDCl₃) δ = 169.32, 142.21, 140.06, 137.67, 131.32, 128.91, 128.44, 128.32, 127.89, 92.57, 44.40 ppm; HRMS (CI, *m/z*) calcd for [C₁₄H₁₃INO]⁺ (M+H)⁺ 338.0042, found 338.0047.



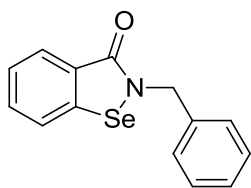
2-Iodo-N-(4-methoxybenzyl)benzamide (72b).

General procedure 3 was followed using 2-iodobenzoic acid and 4-methoxybenzylamine to give the title compound as a yellow solid (679 mg, >95% yield): ¹H NMR (400 MHz, CDCl₃) δ = 7.84 (d, *J* = 8 Hz, 1H), 7.41 – 7.36 (m, 1H), 7.36 (d, *J* = 7 Hz, 1H), 7.32 (d, *J* = 9 Hz, 2H), 7.08 (td, *J* = 8, 2 Hz, 1H), 6.88 (d, *J* = 9 Hz, 2H), 6.01 (s, 1H), 4.56 (d, *J* = 6 Hz, 2H), 3.80 (s, 3H) ppm; ¹³C NMR (101 MHz, CDCl₃) δ = 168.88, 158.97, 141.91, 139.66, 130.91, 129.41, 129.34, 128.06, 127.93, 113.91, 92.30, 55.06, 43.51 ppm; HRMS (CI, *m/z*) calcd for [C₁₅H₁₅INO₂]⁺ (M+H)⁺ 368.0147, found 368.0156.



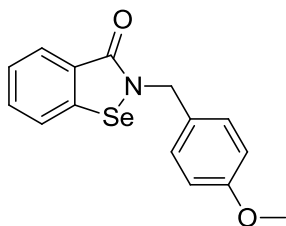
N-(4-Chlorobenzyl)-2-iodobenzamide (72c).¹⁰⁷

General procedure 3 was followed using 2-iodobenzoic acid and 4-chlorobenzylamine to give the title compound as a white solid (644 mg, 92% yield): ¹H NMR (400 MHz, CDCl₃) δ = 7.86 (d, *J* = 8 Hz, 1H), 7.42 – 7.30 (m, 6H), 7.10 (td, *J* = 8, 2 Hz, 1H), 6.07 (s, 1H), 4.61 (d, *J* = 6 Hz, 1H) ppm; ¹³C NMR (101 MHz, CDCl₃) δ = 169.37, 141.99, 140.11, 136.27, 133.72, 131.45, 129.68, 129.05, 128.47, 128.37, 92.51, 43.64 ppm; HRMS (CI, *m/z*) calcd for [C₁₄H₁₂ClINO]⁺ (M+H)⁺ 371.9652, found 371.9657.



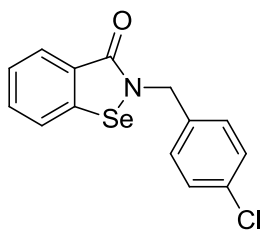
2-Benzylbenzo[d][1,2]selenazol-3(2H)-one (73).⁸⁴

General procedure 12 was followed using *N*-benzyl-2-iodobenzamide to give the title compound as a white solid (185 mg, 35% yield): mp 124-126°C; ¹H NMR (400 MHz, CDCl₃) δ = 8.08 (d, *J* = 8 Hz, 1H), 7.59 – 7.55 (m, 2H), 7.45 – 7.40 (m, 1H), 7.39 – 7.31 (m, 5H), 5.04 – 5.00 (s, 2H) ppm; ¹³C NMR (101 MHz, CDCl₃) δ = 167.31, 138.19, 137.37, 132.15, 129.10, 129.00, 128.69, 128.47, 126.37, 124.10, 48.81 ppm; HRMS (CI, *m/z*) calcd for [C₁₄H₁₂NOSe]⁺ (M+H)⁺ 290.0084, found 290.0086; IR (neat) ν 3055 (w, C-H aromatic), 2980 (w, C-H aliphatic), 1624 (s, C=O amide), 1556 (m, C-C aromatic), 1454 (m, C-C aromatic), 1440 (m, C-H aliphatic) cm⁻¹.



2-(4-Methoxybenzyl)benzo[d][1,2]selenazol-3(2H)-one (74).¹⁰⁸

General procedure 12 was followed using 2-iodo-*N*-(4-methoxybenzyl)benzamide to give the title compound as a pale yellow solid (117 mg, 21% yield): mp 128-130°C; ¹H NMR (400 MHz, CDCl₃) δ = 8.07 (d, *J* = 8 Hz, 1H), 7.55 (d, *J* = 4 Hz, 2H), 7.44 – 7.39 (m, 1H), 7.30 (d, *J* = 9 Hz, 2H), 6.89 (d, *J* = 9 Hz, 2H), 4.94 (s, 2H), 3.81 (s, 3H) ppm; ¹³C NMR (101 MHz, CDCl₃) δ = 167.16, 159.85, 138.27, 132.03, 130.27, 129.49, 128.98, 127.89, 126.31, 124.07, 114.34, 55.44, 48.36 ppm; HRMS (CI, *m/z*) calcd for [C₁₅H₁₄NO₂Se]⁺ (M+H)⁺ 320.0190, found 320.0190; Anal. Calcd for C₁₅H₁₃NO₂Se: C, 56.61; H, 4.12; N, 4.40. Found: C, 56.83; H, 4.09; N, 4.45; IR (neat) ν 3033 (w, C-H aromatic), 2980 (w, C-H aliphatic), 1586 (s, C=O amide), 1557 (m, C-C aromatic), 1440 (m, C-H aliphatic), 1244 (s, C-O) cm⁻¹.



2-(4-Chlorobenzyl)benzo[d][1,2]selenazol-3(2H)-one (75).

General procedure 12 was followed using *N*-(4-chlorobenzyl)-2-iodobenzamide to give the title compound as a white solid (75 mg, 13% yield): mp 118-120°C; ¹H NMR (400 MHz, CDCl₃) δ = 8.07 (d, *J* = 8 Hz, 1H), 7.59 (d, *J* = 4 Hz, 2H), 7.46 – 7.41 (m, 1H), 7.35 – 7.27 (m, 4H), 4.98 (s, 2H) ppm; ¹³C NMR (101 MHz, CDCl₃) δ = 167.37, 166.57, 138.03, 135.83, 134.35, 132.34, 129.94, 129.37, 129.19, 129.05, 126.51, 124.17, 48.04 ppm; HRMS (CI, *m/z*) calcd for [C₁₄H₁₁ClNOSe]⁺ (M+H)⁺ 323.9694, found 323.9689; Anal. Calcd for C₁₄H₁₀ClNOSe: C, 52.12; H, 3.12; N, 4.34. Found: C, 52.22; H, 3.07; N, 4.21; IR (neat) ν 3052 (m, C-H aromatic), 2908 (m, C-H aliphatic), 1634 (s, C=O amide), 1586 (s, C-C aromatic), 1443 (m, C-H aliphatic) cm⁻¹.

3.9 References

- 1 S. Rizzo, V. Wakchaure and H. Waldmann, in *Natural Products in Medicinal Chemistry*, ed. S. Hanessian, Wiley-VCH, Weinheim, 2013, vol. 60, ch. 2, pp. 43–81.
- 2 K. Valko, in *Physicochemical and Biomimetic Properties in Drug Discovery: Chromatographic Techniques for Lead Optimization*, Wiley, Hoboken, 1st edn, 2014, ch. 6, pp. 112–150.
- 3 H. Sigel and R. B. Martin, *Chem. Rev.*, 1982, **82**, 385–426.
- 4 B. Testa and J. M. Mayer, *Hydrolysis in Drug and Prodrug Metabolism*, VHCA and Wiley-VCH, Zürich and Weinheim, 2003, ch. 4, pp. 81–163.
- 5 M. Pietka-Ottlik, P. Potaczek, E. Piasecki and J. Mlochowski, *Molecules*, 2010, **15**, 8214–8228.
- 6 J. C. Grivas, *J. Org. Chem.*, 1975, **40**, 2029–2032.
- 7 A. Correa, I. Tellitu, E. Domínguez and R. SanMartin, *Org. Lett.*, 2006, **8**, 4811–4813.
- 8 M. Shimizu, T. Shimazaki, T. Yoshida, W. Ando and T. Konakahara, *Tetrahedron*, 2012, **68**, 3932–3936.
- 9 B. S. Bhakuni, S. J. Balkrishna, A. Kumar and S. Kumar, *Tetrahedron Lett.*, 2012, **53**, 1354–1357.
- 10 J. Clayden, N. Greeves and S. Warren, *Organic Chemistry*, OUP Oxford, 2012.
- 11 A. Bencini and V. Lippolis, *Coord. Chem. Rev.*, 2010, **254**, 2096–2180.
- 12 Y. Uchida and S. Kozuka, *J. Chem. Soc. Chem. Commun.*, 1981, 510–511.
- 13 F. Ruff and A. Kucsman, *J. Chem. Soc., Perkin Trans. 2*, 1985, **11**, 683–687.
- 14 B. Dayal, G. Salen, B. Toome, G. S. Tint, S. Shefer and J. Padia, *Steroids*, 1990, **55**, 233–237.
- 15 S. R. Sandler and W. Karo, *Sourcebook of Advanced Organic Laboratory Preparations*, Academic Press, Inc., San Diego, 2012, ch. 13, pp. 118–136.
- 16 C. A. G. N. Montalbetti and V. Falque, *Tetrahedron*, 2005, **61**, 10827–10852.
- 17 T. I. Al-Warhi, H. M. A. Al-Hazimi and A. El-Faham, *J. Saudi Chem. Soc.*, 2012, **16**, 97–116.
- 18 D. W. Mayo, in *Course Notes on the Interpretation of Infrared and Raman Spectra*, ed. D. W. Mayo, F. A. Miller and R. W. Hannah, Wiley, Hoboken,

- 2004, ch. 7, pp. 179–205..
- 19 A. Nzila, *J. Antimicrob. Chemother.*, 2006, **57**, 1043–1054.
- 20 Y. N. Gavhane and A. V. Yadav, *Saudi Pharm. J.*, 2012, **20**, 331–344.
- 21 G. M. Cooper, *The Cell: A Molecular Approach*, ASM Press, Washington, 2000.
- 22 H. P. Rang and M. M. Dale, *Rang and Dale's Pharmacology*, Elsevier/Churchill Livingstone, London, 2012.
- 23 C. A. Lipinski, F. Lombardo, B. W. Dominy and P. J. Feeney, *Adv. Drug Deliv. Rev.*, 2001, **46**, 3–26.
- 24 A. A. Altaf, A. Shahzad, Z. Gul, N. Rasool, A. Badshah, B. Lal and E. Khan, *J. Drug Des. Med. Chem.*, 2015, **1**, 1–11.
- 25 M. Baumann and I. R. Baxendale, *Beilstein J. Org. Chem.*, 2013, **9**, 2265–2319.
- 26 S. D. Furdas, S. Shekfeh, E.-M. Bissinger, J. M. Wagner, S. Schlimme, V. Valkov, M. Hendzel, M. Jung and W. Sippl, *Bioorg. Med. Chem.*, 2011, **19**, 3678–3689.
- 27 F. Clerici, M. L. Gelmi, S. Pellegrino and D. Pocar, *Top. Heterocycl. Chem.*, 2007, **9**, 179–264.
- 28 S. W. Wright, J. J. Petraitis, M. M. Abelman, D. G. Batt, L. L. Bostrom, R. L. Corbett, C. P. Decicco, S. V. Di Meo and B. Freimark, *J. Med. Chem.*, 1994, **37**, 3071–3078.
- 29 C. Bissantz, B. Kuhn and M. Stahl, *J. Med. Chem.*, 2010, **53**, 5061–5084.
- 30 W. Adam, A. Grimison, R. Hoffmann and C. Zuazaga de Ortiz, *J. Am. Chem. Soc.*, 1968, **90**, 1509–1516.
- 31 P. Tomasik and Z. Ratajewicz, *The Chemistry of Heterocyclic Compounds: Pyridine-Metal Complexes*, ed. G. R. Newkome and L. Strekowski, John Wiley & Sons, Hoboken, 1985.
- 32 S. Aprile, E. Del Grosso and G. Grosa, *Xenobiotica*, 2011, **41**, 212–225.
- 33 M. Pietka-Ottlik, P. Potaczek, E. Piasecki and J. Mlochowski, *Molecules*, 2010, **15**, 8214–8228.
- 34 S. W. Wright, M. M. Abelman, L. L. Bostrom and R. L. Corbett, *Tetrahedron Lett.*, 1992, **33**, 153–156.
- 35 C. R. Johnson, J. C. Sharp and W. G. Phillips, *Tetrahedron Lett.*, 1967, **8**,

- 5299–5302.
- 36 D. G. Morris, *Stereochemistry*, Royal Society of Chemistry, Cambridge, 2001.
- 37 W. F. Bailey and J. J. Patricia, *J. Organomet. Chem.*, 1988, **352**, 1–46.
- 38 D. Seyferth, *Organometallics*, 2006, **25**, 2–24.
- 39 R. B. Grossman, *The Art of Writing Reasonable Organic Reaction Mechanisms*, Springer New York, 2007.
- 40 M. R. Crampton, in *Organic Reaction Mechanisms*, ed. A. C. Knipe, Wiley, Chichester, 2013, ch. 5, pp. 217–273.
- 41 H. Lüttgen, F. Rohdich, S. Herz, J. Wungsintaweekul, S. Hecht, C. A. Schuhr, M. Fellermeier, S. Sagner, M. H. Zenk, A. Bacher and W. Eisenreich, *Proc. Natl. Acad. Sci.*, 2000, **97**, 1062–1067.
- 42 C. M. Crane, A. K. H. Hirsch, M. S. Alphey, T. Sgraja, S. Lauw, V. Illarionova, F. Rohdich, W. Eisenreich, W. N. Hunter, A. Bacher and F. Diederich, *ChemMedChem*, 2008, **3**, 91–101.
- 43 J. M. Berg, J. L. Tymoczko and L. Stryer, *Biochemistry*, W. H. Freeman Publishers, New York, 2002.
- 44 P. K. Anthony, *Pharmacology Secrets*, Hanley & Belfus, Philadelphia, 2002.
- 45 G. L. Patrick, *An Introduction to Drug Synthesis*, Oxford University Press, Oxford, 2015.
- 46 P. Leeson, *Nature*, 2012, **481**, 455–456.
- 47 N. Miyaura, K. Yamada and A. Suzuki, *Tetrahedron Lett.*, 1979, **20**, 3437–3440.
- 48 T. J. Colacot, *Platinum Metals Rev.*, 2011, **55**, 84–90.
- 49 A. J. J. Lennox and G. C. Lloyd-Jones, *Chem. Soc. Rev.*, 2014, **43**, 412–443.
- 50 I. Maluenda and O. Navarro, *Molecules*, 2015, **20**, 7528–7557.
- 51 K. Matos and J. A. Soderquist, *J. Org. Chem.*, 1998, **63**, 461–470.
- 52 N. Miyaura, T. Yanagi and A. Suzuki, *Synth. Commun.*, 1981, **11**, 513–519.
- 53 G. B. Smith, G. C. Dezeny, D. L. Hughes, A. O. King and T. R. Verhoeven, *J. Org. Chem.*, 1994, **59**, 8151–8156
- 54 R. Martin and S. L. Buchwald, *Acc. Chem. Res.*, 2008, **41**, 1461–1473.
- 55 E. Pop, D. C. Oniciu, M. E. Pape and C. T. Cramer, 2004, **77**, 301–306.
- 56 G. Thomas, *Medicinal Chemistry: An Introduction*, Wiley, Chichester, 2nd edn, 2011.

- 57 K. L. Sorgi, *Encyclopedia of Reagents for Organic Synthesis*, John Wiley & Sons, Hoboken, 2001.
- 58 A. L. Hopkins, in *The Practice of Medicinal Chemistry*, ed. C. G. Wermuth, D. Aldous, P. Raboisson and D. Rognan, Elsevier Science, Amsterdam, 4th edn, 2015, ch. 16, pp. 395–407.
- 59 H. K. Han and G. L. Amidon, *AAPS PharmSci*, 2000, **2**, 48–58.
- 60 P. Ollario, *Pharmacol. Ther.*, 2001, **89**, 207–219.
- 61 F. Ding and C. Simmerling, in *Drug Design: Structure- and Ligand-Based Approaches*, ed. K. M. Merz, D. Ringe and C. H. Reynolds, Cambridge University Press, New York, 2010, ch. 6, pp. 87–98.
- 62 Y. Hsiou, K. Das, J. Ding, A. D. Clark, J.-P. Kleim, M. Rösner, I. Winkler, G. Riess, S. H. Hughes and E. Arnold, *J. Mol. Biol.*, 1998, **284**, 313–323.
- 63 R. N. Salvatore, C. H. Yoon and K. W. Jung, *Tetrahedron*, 2001, **57**, 7785–7811.
- 64 S. W. Wright and R. L. Corbett, *Org. Prep. Proced. Int.*, 1993, **25**, 247–249.
- 65 T. Chiyoda, K. Iida, K. Takatori and M. Kajiwara, *Synlett*, 2000, **10**, 1427–1428.
- 66 S. Bräse, C. Gil, K. Knepper and V. Zimmermann, *Angew. Chemie Int. Ed.*, 2005, **44**, 5188–5240.
- 67 T. L. Capson and C. D. Poulter, *Tetrahedron Lett.*, 1984, **25**, 3515–3518.
- 68 A. R. Katritzky, O. Meth-Cohn, C. J. Moody and C. W. Rees, *Comprehensive Organic Functional Group Transformations*, Pergamon, 1995.
- 69 E. F. V Scriven and K. Turnbull, *Chem. Rev.*, 1988, **88**, 297–368.
- 70 R. J. Abraham and M. Reid, *J. Chem. Soc.*, 2002, **6**, 1081–1091.
- 71 S. Santoro, J. B. Azeredo, V. Nascimento, L. Sancineto, A. L. Braga and C. Santi, *RSC Adv.*, 2014, **4**, 31521–31535.
- 72 S. W. May, *Expert Opin. Investig. Drugs*, 1999, **8**, 1017–1030.
- 73 C. Santi, C. Tidei, C. Scalera, M. Piroddi and F. Galli, *Curr. Chem. Biol.*, 2013, **7**, 25–36.
- 74 D. R. Garud, M. Koketsu and H. Ishihara, *Molecules*, 2007, **12**, 504–535.
- 75 U. Tinggi, *Environ. Health Prev. Med.*, 2008, **13**, 102–108.
- 76 A. Ogawa, in *Main Group Metals in Organic Synthesis*, ed. H. Yamamoto and K. Oshima, Wiley-VCH, Weinheim, 2004, ch. 15 pp. 813–867.

- 77 S. W. May, in *Atypical Elements in Drug Design*, ed. J. Schwarz, Springer International Publishing, Switzerland, 2016, ch. 4, pp. 87–118.
- 78 H. Tapiero, D. M. Townsend and K. D. Tew, *Biomed. Pharmacother.*, 2003, **57**, 134–144.
- 79 G. N. Schrauzer, *Selenium: Present Status and Perspectives in Biology and Medicine*, Springer Science & Business Media, New York City, 2012.
- 80 N. R. Gonzales and J. C. Grotta in *Stroke: Pathophysiology, Diagnosis, and Management*, Elsevier Health Sciences, Amsterdam, 6th edn, 2015, ch. 55, pp. 916–937.
- 81 T. Yamaguchi, K. Sano, K. Takakura, I. Saito, Y. Shinohara, T. Asano and H. Yasuhara, *Stroke*, 1998, **29**, 12–17.
- 82 N. Singh, A. C. Halliday, J. M. Thomas, O. V Kuznetsova, R. Baldwin, E. C. Y. Woon, P. K. Aley, I. Antoniadou, T. Sharp, S. R. Vasudevan and G. C. Churchill, *Nat. Commun.*, 2013, **4**, 1332.
- 83 S. Thangamani, W. Younis and M. N. Seleem, *Sci. Rep.*, 2015, **5**, DOI: 10.1038/srep11596.
- 84 S. J. Balkrishna, B. S. Bhakuni and S. Kumar, *Tetrahedron*, 2011, **67**, 9565–9575.
- 85 M. Piętka-Ottlik, H. Wójtowicz-Młochowska, K. Kołodziejczyk, E. Piasecki and J. Młochowski, *Chem. Pharm. Bull. (Tokyo)*, 2008, **56**, 1423–1427.
- 86 K. P. Bhabak and G. Muges, *Chem. Eur. J.*, 2007, **13**, 4594–4601.
- 87 J. He, D. Li, K. Xiong, Y. Ge, H. Jin, G. Zhang, M. Hong, Y. Tian, J. Yin and H. Zeng, *Bioorg. Med. Chem.*, 2012, **20**, 3816–3827.
- 88 K. K. Bhasin, E. Arora, A. S. Grover, Jyoti, H. Singh, S. K. Mehta, A. K. K. Bhasin and C. Jacob, *J. Organomet. Chem.*, 2013, **732**, 137–141.
- 89 A. Choudhury, L. A. Polyakova, S. Strobel and P. K. Dorhout, *J. Solid State Chem.*, 2007, **180**, 1381–1389.
- 90 Y. Bravo, P. Teriete, R.-P. Dhanya, R. Dahl, P. S. Lee, T. Kiffer-Moreira, R. Santhi, E. Sergienko, L. H. Smith, C. Farquharson, J. L. Millan and N. D. P. Cosford, *Bioorg. Med. Chem. Lett.*, 2014, **24**, 4308–4311.
- 91 G. F. Dregval, *Sov. Prog. Chem.*, 1977, **43**, 384–387.
- 92 H. Hikawa and Y. Yokoyama, *Org. Biomol. Chem.*, 2012, **10**, 2942–2945.
- 93 F. S. Fowkes and E. W. McClelland, *J. Chem. Soc.*, 1945, **1**, 405–407.

- 94 S. D. Gawande, V. Kavala, M. R. Zanwar, C.-W. Kuo, W.-C. Huang, T.-S. Kuo, H.-N. Huang, C.-H. He and C.-F. Yao, *Adv. Synth. Catal.*, 2014, **356**, 2599–2608.
- 95 P. Cheng, J. Zhou, Z. Qing, W. Kang, S. Liu, W. Liu, H. Xie and J. Zeng, *Bioorg. Med. Chem. Lett.*, 2014, **24**, 2712–2716.
- 96 K. Aso, M. Mochizuki, T. Kojima, K. Kobayashi, S. A. Pratt and A. C. Gyorkos, WO Pat., 2008/051533 A2, 2008.
- 97 R. Schurter, W. Kunz and R. Nyfeler, US Pat. 4 931 581, 1990.
- 98 M. Szabo, M. Agostino, D. T. Malone, E. Yuriev and B. Capuano, *Bioorg. Med. Chem. Lett.*, 2011, **21**, 6782–6787.
- 99 C. A. Parrish, N. D. Adams, K. R. Auger, J. L. Burgess, J. D. Carson, A. M. Chaudhar, R. A. Copeland, M. A. Diamond, C. A. Donatelli, K. J. Duffy, L. F. Faucette, J. T. Finer, W. F. Huffman, E. D. Hugger, J. R. Jackson, S. D. Knight, L. Luo, M. L. Moore, K. A. Newlander, L. H. Ridgers, R. Sakowicz, A. N. Shaw, C.-M. Sung, D. Sutton, K. W. Wood, S.-Y. Zhang, M. N. Zimmerman and D. Dhanak, *J. Med. Chem.*, 2007, **50**, 4939–4952.
- 100 H. X. Ngo, S. K. Shrestha, K. D. Green and S. Garneau-Tsodikova, *Bioorg. Med. Chem.*, 2016, **24**, 6298–6306.
- 101 M. Gravel, K. A. Thompson, M. Zak, C. Berube and D. G. Hall, *J. Org. Chem.*, 2002, **67**, 3–15.
- 102 M. Shimizu, Y. Sugano, T. Konakahara, Y. Gama and I. Shibuya, *Tetrahedron*, 2002, **58**, 3779–3783.
- 103 S. W. Wright, J. J. Petratis, D. G. Batt, R. L. Corbett, S. V. Di Meo, B. Freimark, J. V. Giannaras, M. J. Orwat, D. J. Pinto, M. A. Pratta, S. R. Sherk, H. F. Stampfli, J. M. Williams, R. L. Magolda and E. C. Arner, *Bioorg. Med. Chem.*, 1995, **3**, 227–234.
- 104 Y. Nishiyama, M. Nakamura, T. Misawa, M. Nakagoni, M. Makishima and M. Ishikawa, *Bioorg. Med. Chem.*, 2014, **22**, 2799–2808.
- 105 H. Wojtowicz, K. Kloc, I. Maliszewska, J. Mlochowski, M. Pietka and E. Piasecki, *Il Farmaco*, 2004, **59**, 863–868.
- 106 B. Yao, Q. Wang and J. Zhu, *Angew. Chem. Int. Ed.*, 2013, **52**, 12992–12996.
- 107 W. Khan and A. F. G. M. Reza, *Tetrahedron*, 2005, **61**, 11204–11210.
- 108 T.-C. Chang, M.-L. Huang, W.-L. Hsu, J.-M. Hwang and L.-Y. Hsu, *Chem.*

Pharm. Bull., 2003, **51**, 1413–1416.

Chapter IV

A Review of Endoperoxide Antimalarials

Table of Contents

4.1 The Proposed Mechanism of Action of Artemisinin	213
4.1.1 Bioactivation of artemisinin	213
4.1.1.1 Reductive scission model	214
Formation of a Primary Carbon-Centred Radical	215
Formation of a Secondary Carbon-Centred Radical	216
4.1.1.2 Open peroxide model	217
4.1.2 Proposed molecular targets	219
4.2 Artemisinin Resistance	223
4.3 Fully Synthetic Endoperoxides	225
4.3.1 1,2,4-Trioxolanes	225
4.3.2 1,2,4,5-Tetraoxanes	231
4.4 Aim	235
4.5 References	236

4.1 The Proposed Mechanism of Action of Artemisinin

Artemisinin (**1**, Figure 4.1) and its semi-synthetic analogues are one of the most important classes of antimalarial drugs to be developed and artemisinin-based combination therapies (ACTs) are the most effective drug therapies available today.¹ Like the 4-aminoquinolines e.g. chloroquine, amodiaquine and piperaquine, artemisinin and its derivatives are potent schizonticides, acting upon the parasite within an infected erythrocyte.² However, the fact that these trioxane compounds can be used against multi-drug resistant strains suggests that their mechanism of action must be very different.³ A number of plausible theories have been put forward; however, the exact mechanism of action of these compounds is still the subject of much debate.⁴ Understanding the mechanism of action of trioxane antimalarials will aid the targeted design of future antimalarials and also help to predict potential resistance mechanisms.⁵

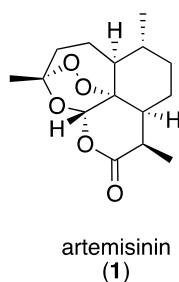


Figure 4.1. The chemical structure of the trioxane antimalarial, artemisinin (**1**)

4.1.1 Bioactivation of artemisinin

In the early 1990s Meshnick *et al.* proposed that bioactivation of artemisinin was triggered by iron (II).⁶ Labelling studies using ¹⁴C showed high selectivity of artemisinin for parasite-infected red blood cells, with little to no drug detected in uninfected erythrocytes. It is well known that heme is present in large quantities in malaria parasites as a result of hemoglobin degradation (see Chapter 1, Section 1.2.2) and heme is known to act as a catalyst for organic peroxide degradation.⁷ It was therefore suggested that artemisinin has an affinity for this

iron (II) complex and an artemisinin-heme adduct was indeed isolated from these studies. This adduct was not harmful to the parasite on its own, but a mixture of artemisinin and heme was, therefore suggesting that reactive oxygen species could be generated as a by-product of this adduct formation.⁸ This proposal is further supported by the fact that the peroxide bridge is necessary for the antimalarial activity of these compounds and that free radical scavengers reduce the antimalarial effect of artemisinin.^{9,10}

Since these initial findings, two different models of bioactivation have been proposed: A reductive scission model (Section 4.1.1.1) and an open peroxide model (Section 4.1.1.2).

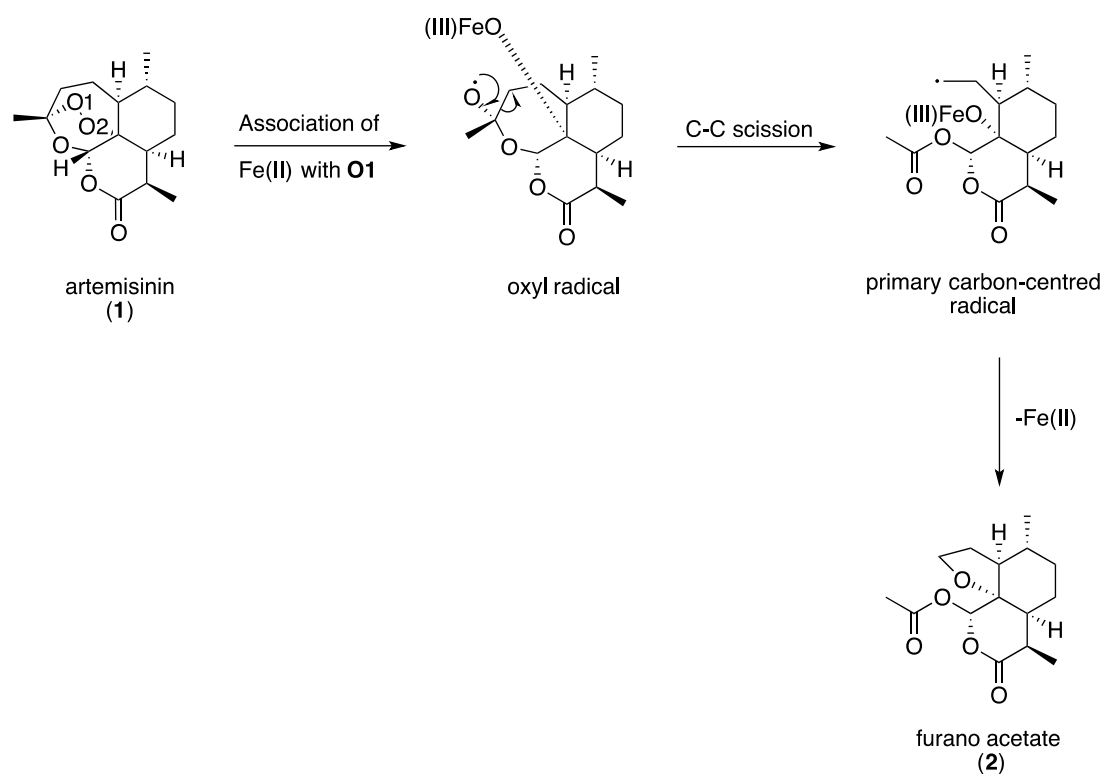
4.1.1.1 Reductive scission model

Posner *et al.* proposed that the reactive oxygen radicals initially formed through interaction with heme, undergo a subsequent rearrangement to form carbon centred radicals.¹¹ They used regiospecific ¹⁸O-labelling studies to support this theory by analysing the degradation products of a simple 1,2,4-trioxane in the presence of ferrous iron.¹² The products obtained were typical of the metabolites formed from artemisinin in the presence of rat liver microsomes. Jefford *et al.* also isolated the same products after stirring artemisinin (**1**) with iron (II) chloride in acetonitrile at 25°C for just 15 minutes.¹³

The products formed in each case were the furano acetate (**2**, Scheme 4.1) and the hydroxy-deoxy product (**3**, Scheme 4.2). It was suggested that two different products were formed as a result of the unsymmetrical nature of the endoperoxide bridge, allowing the possibility of forming both a primary and secondary carbon-centred radical following cleavage of the endoperoxide bond.¹⁴

Formation of a Primary Carbon-Centred Radical

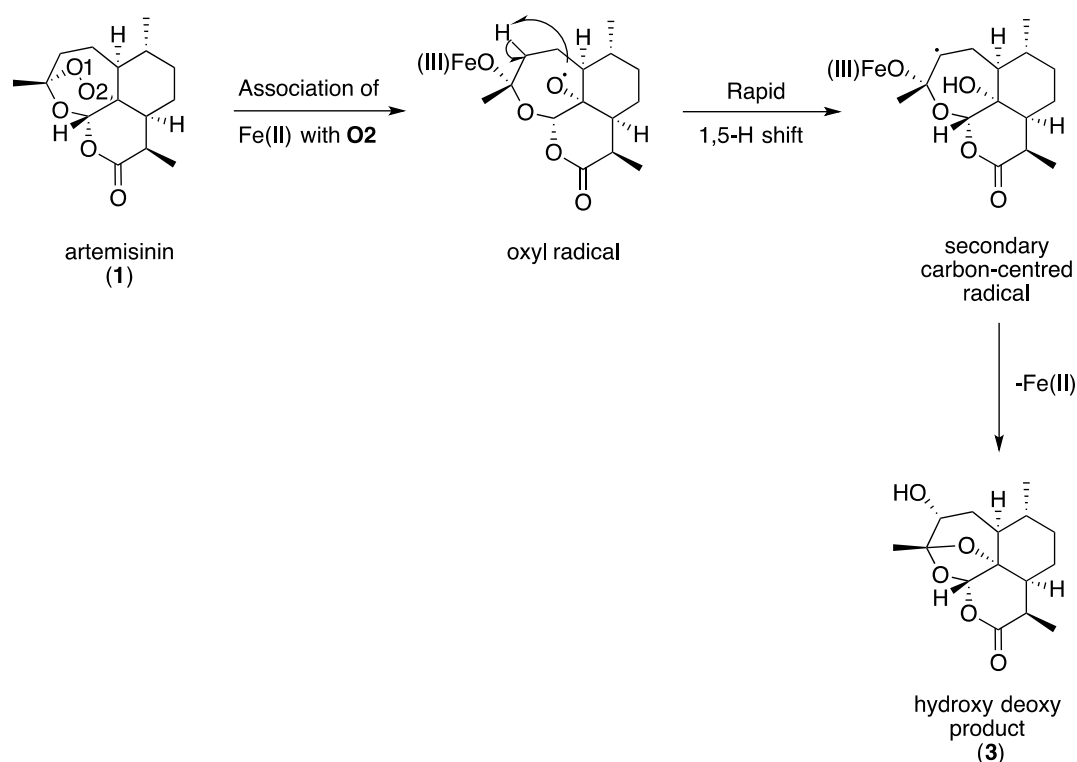
This reactive species is formed when peroxide oxygen **O1** (see Scheme 4.1) interacts with ferrous iron or heme. The oxyl radical initially produced is very short lived and rearranges through carbon-carbon bond scission to give a primary carbon-centred radical. This radical could go on to form an adduct with heme in an infected erythrocyte, thereby preventing hemazoin formation; or it could alkylate important parasite proteins. In the absence of a target protein, rearrangement can occur, forming the acetate product (**2**).¹⁵



Scheme 4.1. Formation of a primary carbon-centred radical through association of **O1** with ferrous iron

Formation of a Secondary Carbon-Centred Radical

This reactive species is formed when peroxide oxygen **O2** (see Scheme 4.2) interacts with ferrous iron or heme. The initial oxyl radical can abstract a hydrogen atom from the same face of the ring system and undergo a 1,5-hydrogen shift. The resulting secondary carbon-centred radical could rearrange to form the hydroxyl product (**3**) or, as with the primary radical, could alkylate vital parasite proteins.¹⁵



Scheme 4.2: Formation of a secondary carbon-centred radical through association of **O2** with ferrous iron

Posner *et al.* provided further evidence to support this model with a series of 4-methylated trioxanes that were structurally similar to artemisinin (Figure 4.2). The analogues that blocked the possibility of a 1,5-hydrogen shift occurring were inactive as antimalarials, illustrating the importance of a carbon-centred radical to the mechanism of action of these compounds.¹⁶

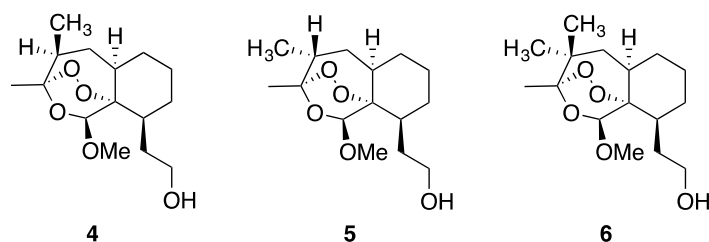


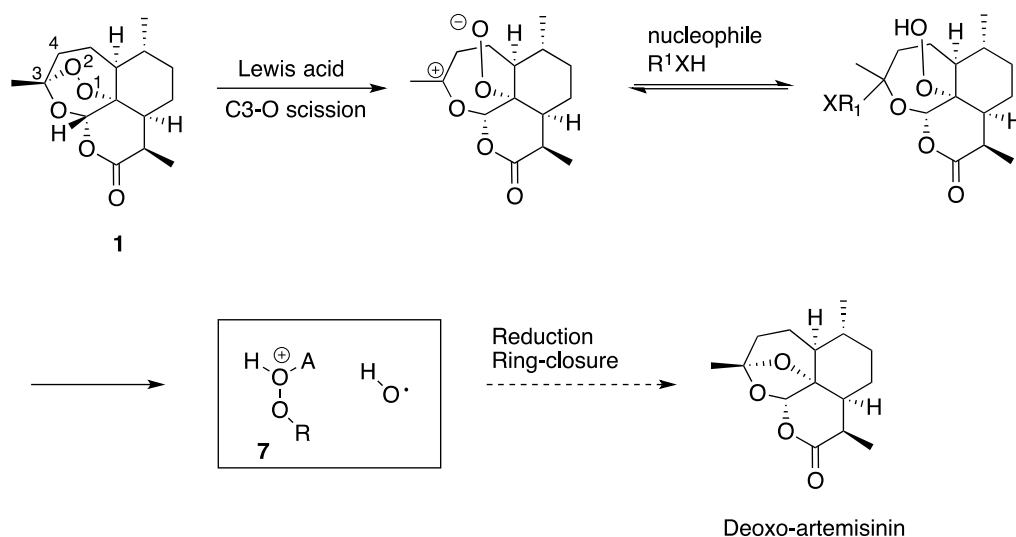
Figure 4.2. The structures of the 4-methylated trioxanes synthesised by Posner *et al.*

The 4β-methylated trioxane (**4**) has potent antimalarial activity (2.2 ng/mL vs. *P. falciparum* NF54) and allows for a 1,5-H shift to take place. The 4α-methylated trioxane (**5**) and the gem-dimethylated analogue (**6**) do not allow for the 1,5-H shift to occur and have no antimalarial activity.

4.1.1.2 Open peroxide model

Haynes *et al.* suggested that the antimalarial activity of artemisinin compounds is a result of the trioxane unit acting as a protected source of hydroperoxide.¹⁷ An open hydroperoxide intermediate can be formed through binding to a protein surface, which results in scission of the C3-O bond (Scheme 4.3).¹⁸

The open peroxide can then produce an electrophilic oxygenating species (carbocation **7**) via protonation or association with a Lewis acid. Further degradation of the hydroperoxide by reductive cleavage with exogenous iron (II) or other reducing agents, produces a hydroxyl radical that can oxidise target amino acid residues.¹⁹



Scheme 4.3. Proposed bioactivation of trioxanes, such as artemisinin, by an open peroxide model: Association of the trioxane with a protein surface causes scission of the **C3-O** bond, generating an open hydroperoxide. This hydroperoxide can produce a cationic oxygenating species (**7**, where A = a proton or a Lewis acid and R = artemisinyl residue) and further degradation produces a hydroxyl radical.

Adapted from: Ring Opening of Artemisinin (Qinghaosu) and Dihydroartemisinin and Interception of the Open Hydroperoxides with Formation of *N*-Oxides - A Chemical Model for Antimalarial Mode of Action, Haynes *et al*, 1999.²⁰

Further evidence to support this theory comes from the discovery that the proposed hydroperoxide can be trapped via reaction with tertiary alkylamines, to generate an *N*-oxide. The group also proposed that a primary carbon-centred radical would be too short lived to migrate away from heme to alkylate biomolecules. Furthermore, the generation of carbon-centred radicals is common in reductive cleavage of endoperoxides and many such compounds are inactive against malaria.²⁰

4.1.2 Proposed molecular targets

The *in vitro* formation of heme-drug adducts has been well documented and provides a possible mechanism of action for parasite death.²¹ Alkylation of heme would prevent the formation of hematin. Inhibition of this crucial detoxification pathway, plus the resulting accumulation of heme, would prove lethal to the parasite.²² Heme-artemisinin adducts have also been detected in the spleen and urine of *P. vinckei* infected mice treated with artemisinin.²³

Much of the data supporting this theory is however based on biomimetic chemistry and these models can only mimic the processes that occur within the parasite. More evidence is therefore required to definitively confirm this theory.^{24,25}

Radiolabelled artemisinin has been shown to covalently bind to a number of hemoproteins such as catalase, cytochrome *c* and haemoglobin.²⁶ Meshnick *et al.* also reported the *in vitro* covalent reaction of artemisinin with human albumin, the most abundant protein in human blood plasma, further demonstrating the potential of this drug to alkylate proteins other than heme.²⁷

The sarco/endoplasmic reticulum membrane calcium ATPase or SERCA transports Ca^{2+} from the cytosol of the cell to the lumen of the sarcoplasmic reticulum and is critical to the survival of the cell. *P. falciparum* parasites possess an orthologue of SERCA, known as *PfATP6*.²⁸ Studies show that *PfATP6* is inhibited by artemisinin but not by quinine or chloroquine. Further evidence to support this molecular target comes from thapsigargin (**8**, Figure 4.3), another sesquiterpene lactone and highly specific SERCA inhibitor that antagonises the activity of artemisinin.²⁹

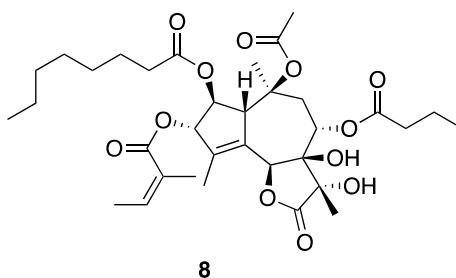


Figure 4.3. The structure of thapsigargin (**8**), a potent and selective SERCA inhibitor

Other studies suggest that *Pf*ATP6 is not a target of artemisinin as its morphology is unaffected, whereas thapsigargin has a marked impact on the structure of SERCA.³⁰

More recently, O'Neill *et al.* described a chemical proteomic approach to identify key proteins that are targeted by artemisinin. They designed a number of click chemistry compatible activity-based probes, which incorporated the endoperoxide scaffold of artemisinin as a warhead to alkylate molecular targets. Once the warhead had achieved its biological effects, reporter tags were introduced using click chemistry conditions. This allowed for purification and identification of alkylated parasite proteins. A number of inactive, non-peroxide control compounds were also employed for definitive identification of tagged proteins, so active probe alkylation products could be compared with the non-peroxide equivalents. The development of these probes is shown in Figure 4.4.

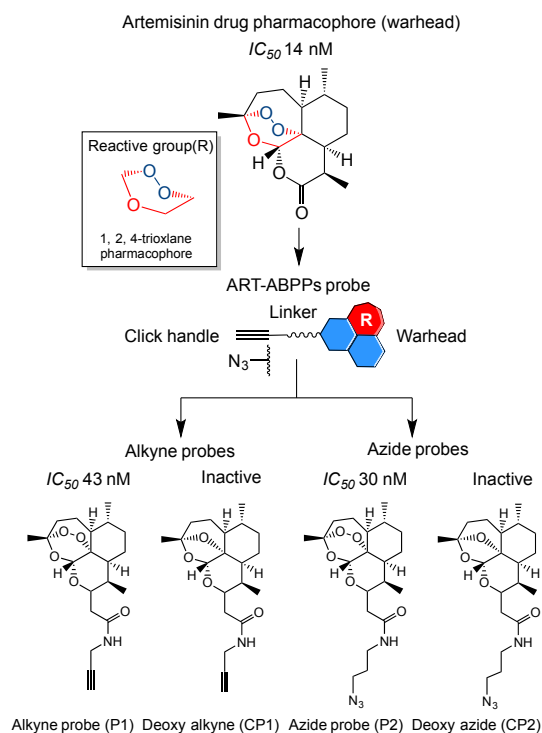


Figure 4.4. The development of activity-based probes by O'Neill *et al.*

IC_{50} values measured in vitro against *P. falciparum* 3D7*

A summary of the copper-catalysed and copper free methods used to facilitate the click-chemistry approach is shown below in Figure 4.5. Following purification, LC-MS/MS was used to identify protein targets.

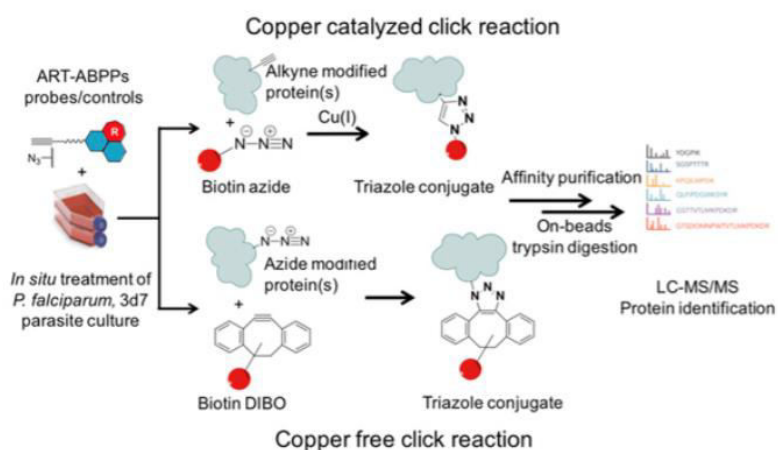


Figure 4.5. A click chemistry approach, under copper-catalysed and copper free conditions, used to identify parasite protein targets*

*Figure 4.4 and 4.5 taken from “Artemisinin activity-based probes identify multiple molecular targets within the asexual stage of the malaria parasites *Plasmodium falciparum* 3D7” by O’Neill *et al.*

LC-MS/MS identified 42 proteins targeted by both the alkyne probe (P1) and azide probe (P2). A substantial number of these proteins were identified as proteases in the parasite’s digestive food vacuole, including plasmepsin-2. It was also found that these artemisinin activity-based probes interacted with the parasite’s antioxidant defence systems, glycolysis pathway and nucleic acid and protein biosynthesis pathways. The probes also identified a number of chaperone and transport proteins as targets of artemisinin; however, PfATP6 was only detected by P1 and with low yields and low confidence.³¹

It is therefore still unclear as to the exact mechanisms of bioactivation of artemisinin and its molecular targets; however, more and more evidence is growing. A greater understanding of these processes will allow for improved drug design and identification of potential mechanisms of resistance.³²

4.2 Artemisinin Resistance

As previously discussed in Chapter 1, artemisinin-based combination therapies are recommended as the first-line of treatment for uncomplicated *P. falciparum* malaria.³³ Replacing previous failing treatments with ACTs has significantly reduced morbidity and mortality (mortality has been reduced by 33% in Africa) associated with the disease, and artesunate has successfully replaced quinine for the treatment of severe malaria.^{34,35}

However, in 2009 it was reported that resistance was beginning to emerge to artesunate on the Thai-Cambodian border, a site where resistance to previous front-line therapies has also emerged.³⁶ Resistance to chloroquine emerged in this region in the late 1950s and rapidly spread across Asia and Africa, contributing to millions of deaths.³⁷

One study published in the *New England Journal of Medicine* showed that parasites from infected patients in areas of Western Cambodia had reduced susceptibility to artesunate, resulting in slower clearance times.³⁸ This has since spread across Cambodia and to other areas of South-East Asia including eastern Myanmar, southern Vietnam and Laos (see Figure 4.6).³⁹ Sub-optimal use of artemisinin compounds, coupled with the propensity for parasites in this region to develop advantageous mutations against antimalarial agents, could have contributed towards the development of resistance in this region.⁴⁰

A number of studies suggest that slower parasite clearance times are a result of the reduced susceptibility of ring-stage parasites, which leads to the longer half-lives observed *in vivo*. Resistance has recently been linked to a mutation in the propeller domain of a *P. falciparum* Kelch protein.^{41,42} This single nucleotide polymorphism, C508Y, has strong correlations to reduced clearance times and is now used as a molecular marker for large-scale surveillance efforts to contain artemisinin resistance and prevent its global spread.^{43,44}

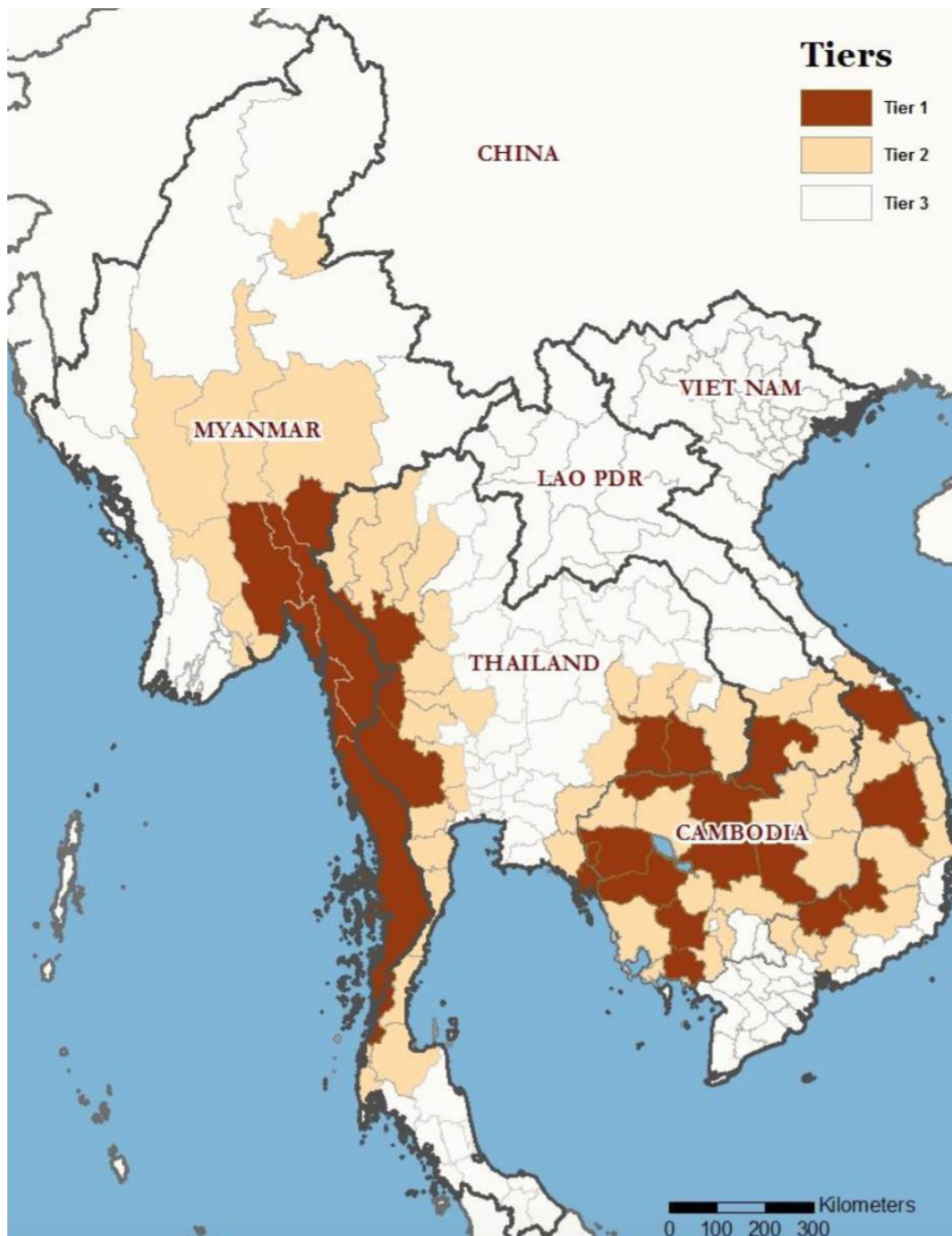


Figure 4.6. The incidence of artemisinin resistance across Southeast Asia, characterised in three tiers:

- Tier 1 – areas for which there is credible evidence of artemisinin resistance
- Tier 2 – areas with significant inflows of populations from Tier 1 areas
- Tier 3 – *P. falciparum* endemic areas which have no evidence of artemisinin resistance

Taken from: Status Report on Artemisinin Resistance, WHO, 2014 ⁴⁵

4.3 Fully Synthetic Endoperoxides

The impact of resistance towards artemisinin-based compounds spreading to other areas, including Africa, could be devastating to the control and eradication of malaria. Coupled with the high cost of synthesis for these compounds, their limiting pharmacokinetics and long treatment regimens, it is obvious to see that there is an ever increasing need to develop novel antimalarial compounds.^{46,47}

4.3.1 1,2,4-Trioxolanes

Vennerstrom *et al.* investigated the antimalarial activity of a class of fully synthetic endoperoxides, the 1,2,4-trioxolanes.⁴⁸ Like the artemisinins, these compounds contain a peroxide pharmacophore that is essential to their antimalarial activity. A number of essential properties were required for this novel group of antimalarial agents:

- Simple, low-cost synthesis
- Potential for a single-dose cure
- High potency
- Low toxicity
- Good pharmacokinetic profile⁴⁹

The first compound they synthesised was the fundamental trioxolane unit (**9**, Figure 4.7), which was completely inactive against *P. falciparum in vitro*, potentially due to the peroxide bond being too unstable. A bulky and sterically hindering adamantyl group was then incorporated into either side of the peroxide (**10**) in order to protect this sensitive moiety, but this too was inactive, potentially due to the oxygen atoms now being inaccessible. A combination of the two groups however proved successful and compound **11** (Figure 4.7) has activity against *P. falciparum in vitro* and *P. berghei in vivo* comparable to that of artesunate and artemether.⁵⁰

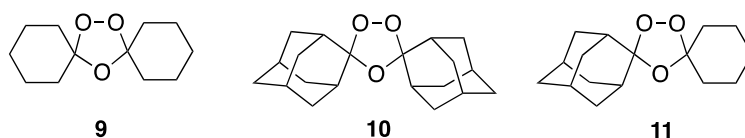
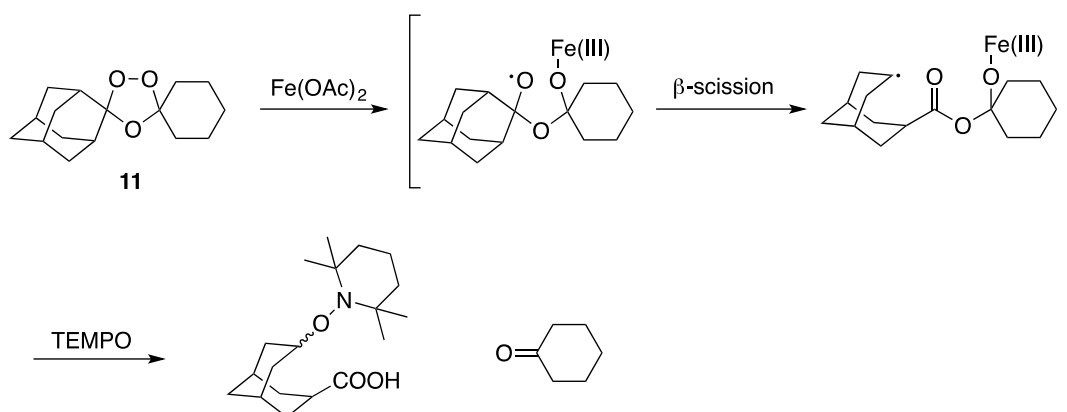


Figure 4.7. The structure of the fundamental trioxolane units synthesised by Vennerstrom *et al.* Compounds **9** and **10** are inactive as antimalarials, whereas compound **11** has antimalarial activity comparable to artemether and artesunate

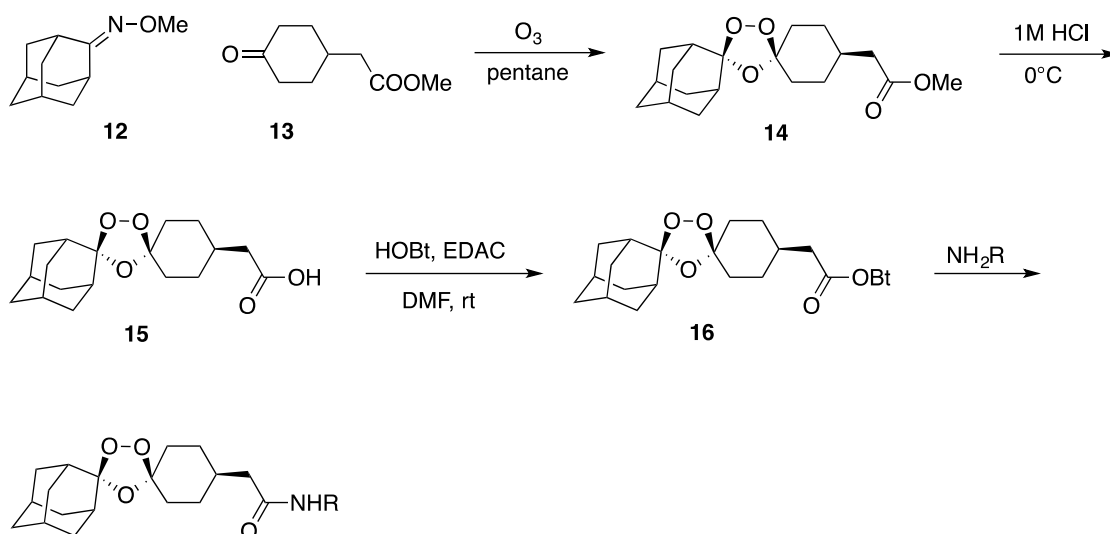
Trapping studies using 2,2,6,6-tetramethyl-1-piperidine-1-oxyl (TEMPO) revealed that a carbon-centred radical is formed through β -scission of the adamantyl carbon-carbon bond adjacent to the peroxide (see Scheme 4.4). This carbon-centred radical can potentially go on to alkylate vital parasite proteins, including the ATPase *Pf*ATP6, which may be crucial to parasite survival (see Section 4.1.2).⁵¹



Scheme 4.4. The TEMPO trapped product obtained following treatment of **11** with iron (II) and proposed mechanism of bioactivation

A number of analogues were then synthesised by the group that incorporated the basic subunit of **11**, with a variety of amide and amino amide side chains in order to generate a more drug-like compound. A hydroxybenzotriazole-activated ester (**16**) was prepared as a common intermediate to allow for the synthesis of these tetraoxane analogues.

The synthesis began with a Griesbaum co-ozonolysis between *O*-methyl-2-adamantanone oxime (**12**, Scheme 4.5) and methyl 4-oxocyclohexyl acetate (**13**). The resulting ozonide ester (**14**) was hydrolysed to the carboxylic acid (**15**) before treatment with HOBt and EDAC to form the activated ester (**16**). Reaction of **16** with a variety of amines and diamines resulted in the formation of a series of novel trioxolane analogues.⁵²



Scheme 4.5. The synthesis, devised by Vennerstrom *et al.*, for the first series of trioxolane antimalarials

The most potent compound to emerge from this study was OZ277 or arterolane (**17**, Figure 4.8), which was more active than the comparative drugs artesunate, artemether, chloroquine and mefloquine with a single 3 mgkg^{-1} oral dose against *P. berghei*. Furthermore, after $3 \times 10\text{ mg/kg}$ doses, OZ277 cured 67% of infected mice, compared to 0% for all of the comparative drugs.⁵³ OZ277 also displayed improved half-life and bioavailability profiles compared to the semi-synthetic artemisinins; therefore OZ277 was selected for candidate development.⁵⁴

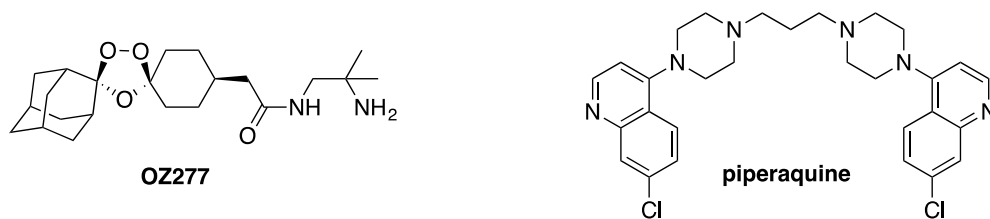


Figure 4.8. The structures of OZ277 (**17**), the most potent antimalarial to emerge from the first trioxolane series created by Vennerstrom *et al.*, and piperazine; a combination approved for the treatment of uncomplicated *P. falciparum*

The development of OZ277 was a significant breakthrough in antimalarial drug discovery and clinical development began in 2003.⁵⁵ A combination of OZ277 with piperazine showed an additive therapeutic effect in early Phase II clinical trials, with rapid parasite clearance times and fast relief of malaria related symptoms.^{56,57} This drug combination was advanced to Phase III trials in order to obtain a definitive assessment of its effectiveness, before being approved for the treatment of uncomplicated *P. falciparum* malaria in 2011.⁵⁸

Despite the promising activity of OZ277, there are a number of drawbacks associated with the drug. The half-life was still too short (only 2 to 3-fold longer than dihydroartemisinin (DHA)) and, when used in monotherapy, the drug displays reduced plasma exposure in malaria patients compared to healthy volunteers.⁵⁹ Therefore, in order to move towards a single dose cure, both the *in vivo* half-life and blood exposure profile needed to be improved.⁵³

Further studies revealed that the rapid clearance of OZ277 could be a result of reactions with endogenous iron (II) sources in the blood and tissues, resulting in the production of inactive adamantanone lactone and cyclohexanone cleavage products (Figure 4.9).⁶⁰ Therefore, Vennerstrom *et al.* devised a plan to stabilise the peroxide moiety to prevent such reactions occurring whilst maintaining potent activity against the parasite.

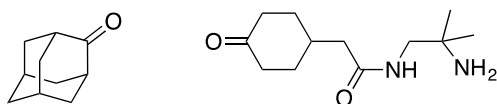


Figure 4.9. Inactive cleavage products of OZ277

A series of second generation trioxolanes were synthesised that incorporated a *cis*-8'-phenyl moiety to further protect the peroxide group through steric interactions. This strategy proved successful. These novel compounds were >50-fold more stable to iron (II) degradation than the corresponding first generation *cis*-8'-alkyl analogues, such as OZ277, and maintained heme alkylating properties.⁶¹

The lead compound to emerge from this second generation of trioxolane antimalarials was OZ439 (**18**, Figure 4.10), which displayed enhanced blood stability in both infected and non-infected patients, most probably as a result of the increased stability of the peroxide bond to iron (II).⁶² Significantly increased clearance times and an improved volume of distribution contributed towards a vastly improved half-life of greater than 20 hours following oral dosing in rats. OZ439 also had a rapid onset of action plus activity against all asexual stages of the parasite.⁶³ Most importantly, OZ439 meets the criteria for a peroxide antimalarial suitable for development as a single dose cure, with 100% of infected mice surviving for more than 30 days following a single 30 mg/kg oral dose.^{61,64}

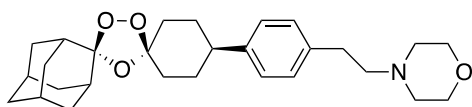
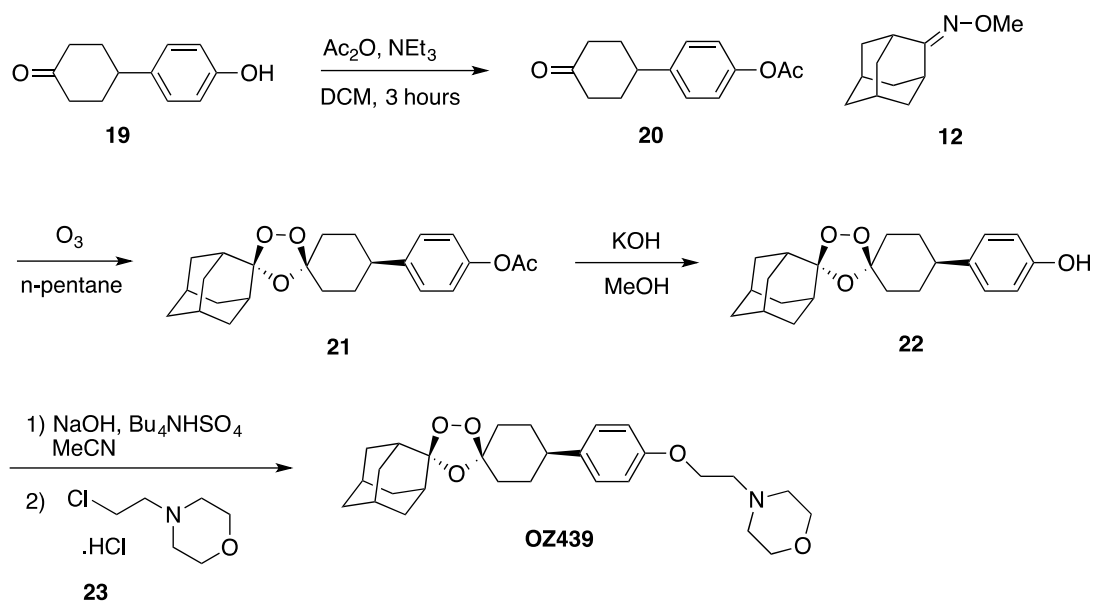


Figure 4.10. Structure of the lead compound to emerge from the second generation of trioxolane antimalarials designed by Vennerstrom *et al.*, OZ439 (**18**)

OZ439 successfully passed phase I clinical trials and has now entered phase IIa due to its exceptional antimalarial and pharmacokinetic profiles.⁶⁵ The synthesis of this compound is outlined below in Scheme 4.6. In the first step, 4-(4-hydroxyphenyl)cyclohexanol (**19**) is converted to the corresponding acetate (**20**) by reaction with acetic anhydride. Compound **20** then undergoes a

Griesbaum co-ozonolysis with *O*-methyl-2-adamantanone oxime (**12**) to form the trioxolane moiety (**21**).⁶⁶ The trioxolane acetate (**21**) can be deprotected using sodium hydroxide to give the corresponding phenol (**22**), which undergoes a nucleophilic substitution reaction with 4-(2-chloroethyl)morpholine hydrochloride (**23**) to form OZ439.



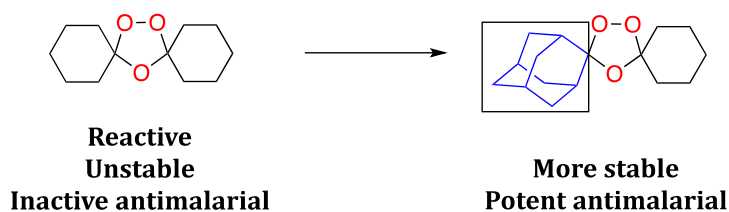
Scheme 4.6. The synthesis of OZ439 from 4-(4-hydroxyphenyl)cyclohexanone using Griesbaum co-ozonolysis to form the trioxolane moiety

Despite the promising activity of OZ439 there are a number of issues with the synthesis that need to be addressed for the large-scale production of such a compound. The Griesbaum co-ozonolysis uses large volumes of *n*-pentane as the solvent, which is harmful if inhaled or ingested and toxic to aquatic wildlife with long lasting effects. The starting material (**19**) is expensive and 4-(2-chloroethyl)morpholine hydrochloride (**23**) is acutely toxic.^{67,68}

4.3.2 1,2,4,5-Tetraoxanes

Although the plasma stability of OZ439 was improved compared to OZ277, the half-life of OZ439 is still relatively short when compared to other antimalarial agents such as chloroquine and amodiaquine (1-2 months and 1-3 weeks respectively).⁶⁹ Therefore, the O'Neill group looked at ways in which to develop these endoperoxide compounds into more stable agents, with slower clearance times and longer half-lives.⁷⁰ One way in which the activity and stability of these endoperoxide compounds could be improved would be to move from a trioxolane to a tetraoxane pharmacophore. As discussed previously (Section 4.3.1) and as Figure 4.11 below shows, the dispiro trioxolane unit is unstable and possesses no antimalarial activity until an adamantane moiety is introduced to stabilise the endoperoxide.⁵⁰

1,2,4-Trioxolane



1,2,4,5-Tetraoxane

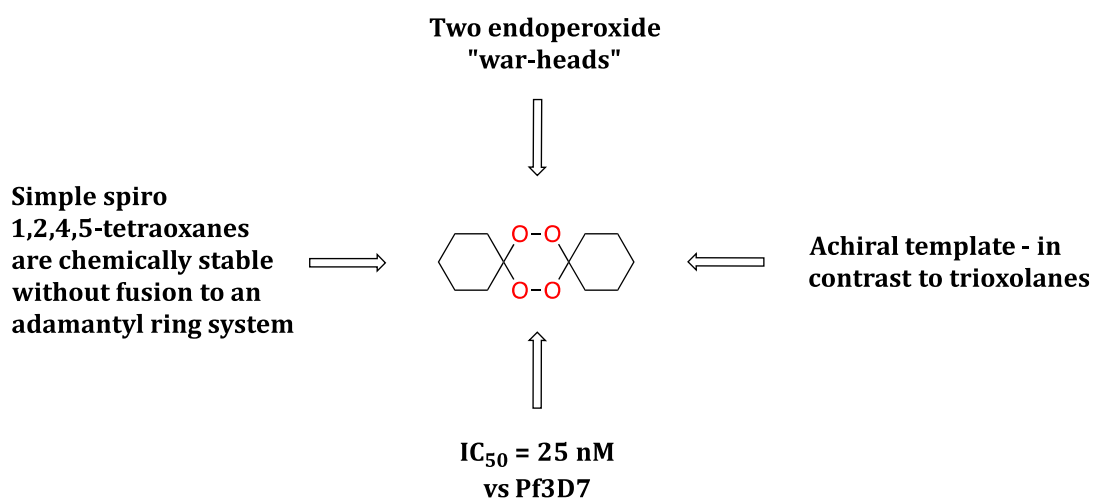


Figure 4.11. The basic unit of a trioxolane vs. a tetraoxane

In contrast, Figure 4.11 shows that the elementary tetraoxane unit is chemically quite stable; this at first glance seems slightly unusual. One might presume that the presence of two peroxide groups in a 6-membered ring would lead to a very unstable functional group, however molecular modelling research that was recently published by Gomes *et al.*, explains why this is not the case.⁷¹

Bis-peroxides actually benefit from a stabilising effect that the two peroxide groups exert on one another. This stabilisation is a result of strong $n_{\text{O}} \rightarrow \sigma^*_{\text{C-O}}$ interactions that are not found in mono-peroxides (explaining the lack of stability shown by the basic trioxolane unit). This anomeric effect means that the two peroxides can in fact be viewed as two acetals (Figure 4.12). This effect is further amplified by the structural constraints of ring systems, explaining the unexpected stability of the basic dispiro tetraoxane unit.^{72,73}

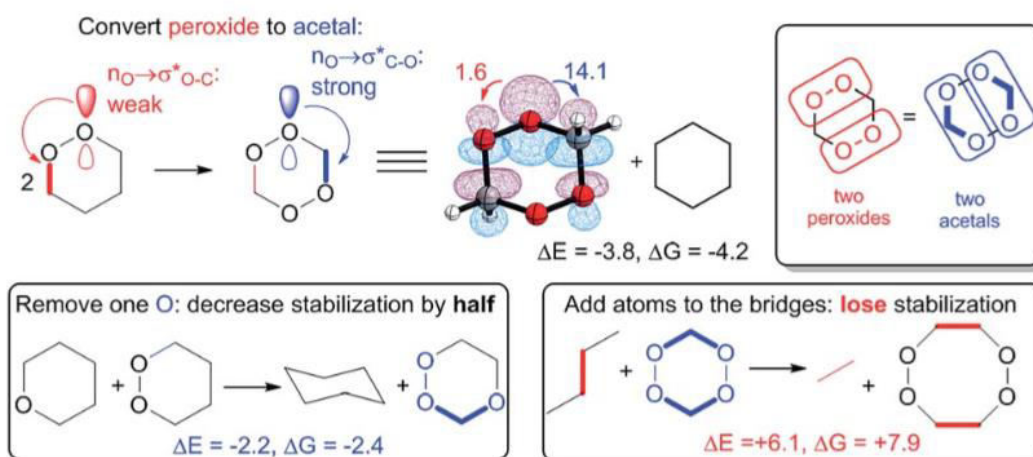


Figure 4.12. An explanation for the unexpected stability of bis-peroxides, such as 1,2,4,5-tetraoxanes.

Incorporation of a second peroxide moiety is favoured as it results in negative values for both ΔE and ΔG , showing that the bis-peroxide is thermodynamically more stable than a single peroxide. Removing one oxygen atom results in decreased stabilization, with both ΔE and ΔG becoming more positive. The largest loss in stabilization is observed when atoms are added to the bridges; this molecule is now a true bis-peroxide rather than a bis-acetal system. This is highly unfavoured as ΔE and ΔG are both positive.

Taken from: Stereoelectronic source of the anomalous stability of the bis-peroxides, Gomes *et al.*, 2015⁷¹

The O'Neill group deemed it logical to explore a novel series of tetraoxane antimalarials that incorporate an adamantane moiety as an enhanced endoperoxide stabilising motif (**24**, Figure 4.13).

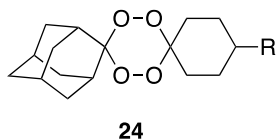


Figure 4.13. The basic tetraoxane template developed by O'Neill *et al.* for the synthesis of a novel group of antimalarial compounds (where R = CH₂CONR₁R₂)

A variety of side chains were introduced in order to aid solubility and to improve the stability and pharmacokinetic profiles of these compounds. Over 150 compounds were synthesised and subjected to rigorous *in vitro*, *in vivo* and DMPK studies in order to identify the optimal side chain. The lead compound to emerge from these studies was RKA182 (**25**, Figure 4.14).

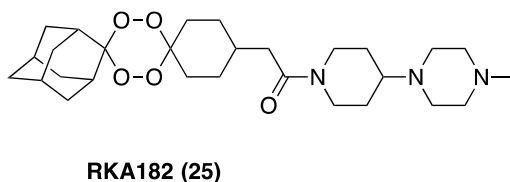
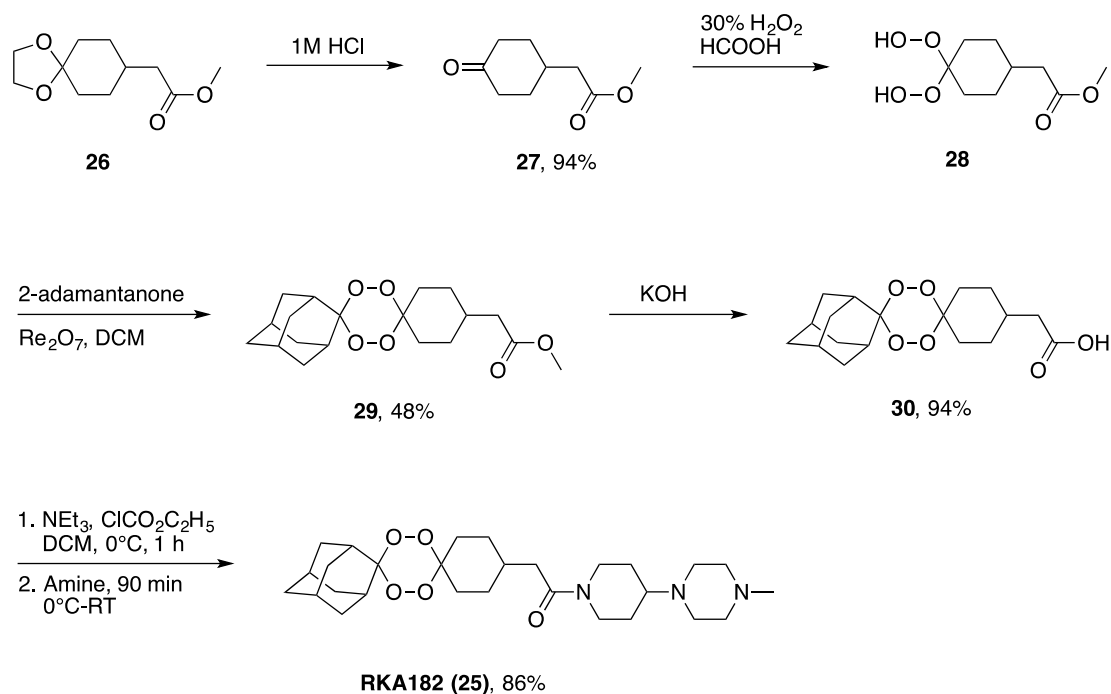


Figure 4.14. The structure of RKA182, the lead tetraoxane compound to emerge from studies by O'Neill *et al.*

The synthesis of RKA182 was carried out in a series of five, high-yielding steps (Scheme 4.7). The intermediate ketone (**27**) was prepared by hydrolysis of the protected 1,4-dispiro[4.5]decane (**26**), before formation of the bis hydroperoxide (**28**) using hydrogen peroxide.⁷⁴ The tetraoxane (**29**) was formed using a rhenium catalyst in a cyclocondensation reaction with 2-adamantanone.⁷⁵ The methyl ester was then hydrolysed to the carboxylic acid (**30**) before ethyl chloroformate was used to generate a mixed anhydride.⁷⁶ The

mixed anhydride was then stirred with the corresponding amine to form RKA182 (**25**).



Scheme 4.7. The synthesis of RKA182 ⁷⁷

RKA182 proved to be a highly potent antimalarial with an IC_{50} value of 0.87 nM against *P. falciparum* 3D7. This novel tetraoxane also displayed an excellent solubility profile of >40 mg/mL in water and infected mice survived for an average of 22 days following 3×10 mg/kg doses.⁷⁷ The main drawback of this compound is a short half-life of only 2.38 hours in the rat following a 10 mg/kg oral dose; this means that RKA182 is really only suitable for a three day dosing regimen rather than a single dose cure.⁷⁸

TEMPO spin-trapping studies with iron(II) bromide intercepted both a primary and secondary carbon-centred radical species from RKA182, compared with only the secondary carbon-centred radical formed with 1,2,4-trioxolanes; thus distinguishing the unique behaviour of 1,2,4,5-tetraoxanes from 1,2,4-trioxolanes.

4.4 Aim

Despite the impressive activity and solubility profiles displayed by RKA182, there is a demand for novel endoperoxide compounds that can achieve a single dose cure.⁷⁹ The aim of this project was to synthesise a 1,2,4,5-tetraoxane with the optimal, metabolically stable side chain, which would maintain the potency and solubility of RKA182 whilst increasing stability, in order to move towards a single dose cure.

A number of parameters were established for the desired target product profile:

- Simple, achiral synthesis
- Short number of steps in the synthetic pathway (≤ 5)
- Aqueous solubility > 5 mg/mL
- $IC_{50} < 10$ nM
- Long single dose mouse survival i.e. > 20 days survival of an infected mouse following a single 30 mg/kg dose

4.5 References

- 1 WHO | Overview of Malaria Treatment, <http://www.who.int/malaria/areas/treatment/overview/en/>, (accessed December 2016).
- 2 S. D. Seth and V. Seth, *Textbook Of Pharmacology*, Elsevier, India, 2009.
- 3 A. U. Rahman, *Studies in Natural Products Chemistry: Structure and Chemistry (Part F)*, Elsevier Science, 1998.
- 4 C. Weiyuan, *Bull. World Health Organ.*, 2009, **87**, 743–744.
- 5 P. M. O'Neill, V. E. Barton and S. A. Ward, *Molecules*, 2010, **15**, 1705–1721.
- 6 S. R. Meshnick, A. Thomas, A. Ranz, C.-M. Xu and H.-Z. Pan, *Mol. Biochem. Parasitol.*, 1991, **49**, 181–189.
- 7 B. Halliwell, *Plant Physiol.*, 2006, **141**, 312–322.
- 8 C. Loup, J. Lelievre, F. Benoit-Vical and B. Meunier, *Antimicrob. Agents Chemother.*, 2007, **51**, 3768–3770.
- 9 S. R. Krungkrai and Y. Yuthavong, *Trans. R. Soc. Trop. Med. Hyg.*, 1987, **81**, 710–714.
- 10 A. Brossi, B. Venugopalan, L. Dominguez Gerpe, H. J. C. Yeh, J. L. Flippen-Anderson, P. Buchs, X. D. Luo, W. Milhous and W. Peters, *J. Med. Chem.*, 1988, **31**, 645–650.
- 11 G. H. Posner, C. H. Oh, D. Wang, L. Gerena, W. K. Milhous, S. R. Meshnick and W. Asawamahasadka, *J. Med. Chem.*, 1994, **37**, 1256–1258.
- 12 G. H. Posner and C. H. Oh, *J. Am. Chem. Soc.*, 1992, **114**, 8328–8329.
- 13 C. W. Jefford, M. G. H. Vicente, Y. Jacquier, F. Favarger, J. Mareda, P. Millasson-Schmidt, C. Brunner and U. Burger, *Helv. Chim. Acta*, 1996, **79**, 1475–1487.
- 14 P. G. Bray, S. A. Ward and P. M. O'Neill, *Curr. Top. Microbiol. Immunol.*, 2005, **295**, 3–38.
- 15 G. H. Posner and P. M. O'Neill, *Acc. Chem. Res.*, 2004, **37**, 397–404.
- 16 G. H. Posner, D. Wang, J. N. Cumming, C. H. Oh, A. N. French, A. L. Bodley and T. A. Shapiro, *J. Med. Chem.*, 1995, **38**, 2273–2275.
- 17 R. K. Haynes and S. C. Vonwiller, *Tetrahedron Lett.*, 1996, **37**, 253–256.
- 18 R. K. Haynes and S. C. Vonwiller, *Tetrahedron Lett.*, 1996, **37**, 257–260.

- 19 R. K. Haynes, W. C. Chan, C.-M. Lung, A.-C. Uhlemann, U. Eckstein, D. Taramelli, S. Parapini, D. Monti and S. Krishna, *ChemMedChem*, 2007, **2**, 1480–1497.
- 20 R. K. Haynes, H. H.-O. Pai and A. Voerste, *Tetrahedron Lett.*, 1999, **40**, 4715–4718.
- 21 Y. Ying-Zi, B. Little and S. R. Meshnick, *Biochem. Pharmacol.*, 1994, **48**, 569–573.
- 22 S. R. Meshnick, Y. Z. Yang, V. Lima, F. Kuypers, S. Kamchonwongpaisan and Y. Yuthavong, *Antimicrob. Agents Chemother.*, 1993, **37**, 1108–1114.
- 23 A. Robert, F. Benoit-Vical, C. Claparols and B. Meunier, *Proc. Natl. Acad. Sci. U.S.A.*, 2005, **102**, 13676–13680.
- 24 Y. Wu, *Acc. Chem. Res.*, 2002, **35**, 255–259.
- 25 G. H. Posner and S. R. Meshnick, *Trends Parasitol.*, 2016, **17**, 266–267.
- 26 Y.-Z. Yang, B. Little and S. R. Meshnick, *Biochem. Pharmacol.*, 1994, **48**, 569–573.
- 27 Y. Ying-Zi, W. Asawamahasadka and S. R. Meshnick, *Biochem. Pharmacol.*, 1993, **46**, 336–339.
- 28 U. Eckstein-Ludwig, R. J. Webb, I. D. A. van Goethem, J. M. East, A. G. Lee, M. Kimura, P. M. O’Neill, P. G. Bray, S. A. Ward and S. Krishna, *Nature*, 2003, **424**, 957–961.
- 29 A.-C. Uhlemann, S. Wittlin, H. Matile, L. Y. Bustamante and S. Krishna, *Antimicrob. Agents Chemother.*, 2007, **51**, 667–672.
- 30 M. del Pilar Crespo, T. D. Avery, E. Hanssen, E. Fox, T. V Robinson, P. Valente, D. K. Taylor and L. Tilley, *Antimicrob. Agents Chemother.*, 2008, **52**, 98–109.
- 31 H. M. Ismail, V. Barton, M. Phanchana, S. Charoensutthivarakul, M. H. L. Wong, J. Hemingway, G. A. Biagini, P. M. O’Neill and S. A. Ward, *Proc. Natl. Acad. Sci. U. S. A.*, 2016, **113**, 2080–2085.
- 32 A. D. W. Boran and R. Iyengar, *Curr. Opin. Drug Discov. Devel.*, 2010, **13**, 297–309.
- 33 WHO | Q&A on artemisinin resistance, http://who.int/malaria/media/artemisinin_resistance_qa/en/, (accessed December 2016).

- 34 B. Davis, J. Ladner, K. Sams, E. Tekinturhan, D. de Korte and J. Saba, *Malar. J.*, 2013, **12**, 1–9.
- 35 A. M. Dondorp, C. I. Fanello, I. C. E. Hendriksen, E. Gomes, A. Seni and K. D. Chhaganlal, *Lancet*, 2010, **376**, 1647–1657.
- 36 A. M. Dondorp, S. Yeung, L. White, C. Nguon, N. P. J. Day, D. Socheat and L. von Seidlein, *Nat. Rev. Micro.*, 2010, **8**, 272–280.
- 37 D. Payne, *Parasitol. Today*, 1987, **3**, 241–246.
- 38 A. M. Dondorp, F. Nosten, P. Yi, D. Das, A. P. Phyto, J. Tarning, K. M. Lwin, F. Ariey, W. Hanpithakpong, S. J. Lee, P. Ringwald, K. Silamut, M. Imwong, K. Chotivanich, P. Lim, T. Herdman, S. S. An, S. Yeung, P. Singhasivanon, N. P. J. Day, N. Lindegardh, D. Socheat and N. J. White, *N. Engl. J. Med.*, 2009, **361**, 455–467.
- 39 E. A. Ashley, M. Dhorda, R. M. Fairhurst, C. Amaratunga, P. Lim and S. Suon, *N. Engl. J. Med.*, 2014, **371**, 411–23.
- 40 J. G. Beeson, P. Boeuf and F. J. Fowkes, *BMC Med.*, 2015, **13**, DOI: 10.1186/s12916-015-0349-9
- 41 T. Mita, S.-I. Tachibana, M. Hashimoto and M. Hirai, *Expert Rev. Anti. Infect. Ther.*, 2016, **14**, 125–135.
- 42 N. Mishra, S. K. Prajapati, K. Kaitholia, R. S. Bharti, B. Srivastava, S. Phookan, A. R. Anvikar, V. Dev, G. S. Sonal, A. C. Dhariwal, N. J. White and N. Valecha, *Antimicrob. Agents Chemother.*, 2015, **59**, 2548–2553.
- 43 F. Ariey, B. Witkowski, C. Amaratunga, J. Beghain, A.-C. Langlois, N. Khim, S. Kim, V. Duru, C. Bouchier, L. Ma, P. Lim, R. Leang, S. Duong, S. Sreng, S. Suon, C. M. Chuor, D. M. Bout, S. Ménard, W. O. Rogers, B. Genton, T. Fandeur, O. Miotto, P. Ringwald, J. Le Bras, A. Berry, J.-C. Barale, R. M. Fairhurst, F. Benoit-Vical, O. Mercereau-Puijalon and D. Ménard, *Nature*, 2013, **505**, 50–55.
- 44 I. H. Cheeseman, B. A. Miller, S. Nair, S. Nkhoma, A. Tan, J. C. Tan, S. Al Saai, A. P. Phyto, C. L. Moo, K. M. Lwin, R. McGready, E. Ashley, M. Imwong, K. Stepniewska, P. Yi, A. M. Dondorp, M. Mayxay, P. N. Newton, N. J. White, F. Nosten, M. T. Ferdig and T. J. C. Anderson, *Science*, 2012, **336**, 79–82.
- 45 WHO | Status Report on Artemisinin Resistance,
http://www.who.int/malaria/publications/atoz/status_rep_artemisinin_r

- esistance_sep2014.pdf?ua=1, (accessed December 2016)
- 46 WHO | Emergence and spread of artemisinin resistance calls for intensified efforts to withdraw oral artemisinin-based monotherapy from the market, <http://www.who.int/malaria/publications/atoz/oral-artemisinin-based-monotherapies-1may2014.pdf?ua=1>, (accessed December 2016).
- 47 A. Alam, M. Goyal, M. S. Iqbal, C. Pal, S. Dey, S. Bindu, P. Maity and U. Bandyopadhyay, *Expert Rev. Clin. Pharmacol.*, 2009, **2**, 469–489.
- 48 Y. Dong, J. Chollet, H. Matile, S. A. Charman, F. C. K. Chiu, W. N. Charman, B. Scorneaux, H. Urwyler, J. Santo Tomas, C. Scheurer, C. Snyder, A. Dorn, X. Wang, J. M. Karle, Y. Tang, S. Wittlin, R. Brun and J. L. Vennerstrom, *J. Med. Chem.*, 2005, **48**, 4953–4961.
- 49 P. J. Rosenthal, *Antimalarial Chemotherapy: Mechanisms of Action, Resistance, and New Directions in Drug Discovery*, Humana Press, New York, 2001.
- 50 J. L. Vennerstrom, S. Arbe-Barnes, R. Brun, S. A. Charman, F. C. K. Chiu, J. Chollet, Y. Dong, A. Dorn, D. Hunziker, H. Matile, K. McIntosh, M. Padmanilayam, J. Santo Tomas, C. Scheurer, B. Scorneaux, Y. Tang, H. Urwyler, S. Wittlin and W. N. Charman, *Nature*, 2004, **430**, 900–904.
- 51 C. L. Hartwig, E. M. W. Lauterwasser, S. S. Mahajan, J. M. Hoke, R. A. Cooper and A. R. Renslo, *J. Med. Chem.*, 2011, **54**, 8207–8213.
- 52 Y. Dong, S. Wittlin, K. Sriraghavan, J. Chollet, S. A. Charman, W. N. Charman, C. Scheurer, H. Urwyler, J. Santo Tomas, C. Snyder, D. J. Creek, J. Morizzi, M. Koltun, H. Matile, X. Wang, M. Padmanilayam, Y. Tang, A. Dorn, R. Brun and J. L. Vennerstrom, *J. Med. Chem.*, 2010, **53**, 481–491.
- 53 H. M. Staines and S. Krishna, *Treatment and Prevention of Malaria: Antimalarial Drug Chemistry, Action and Use*, Springer Basel, 2012.
- 54 M. A. Biamonte, J. Wanner and K. G. Le Roch, *Bioorg. Med. Chem. Lett.*, 2013, **23**, 2829–2843.
- 55 K. M. Muraleedharan and M. A. Avery, *Drug Discov. Today*, 2009, **14**, 793–803.
- 56 C. Snyder, J. Chollet, J. Santo-Tomas, C. Scheurer and S. Wittlin, *Exp. Parasitol.*, 2007, **115**, 296–300.
- 57 N. Valecha, S. Krudsood, N. Tangpukdee, S. Mohanty, S. K. Sharma, P. K.

- Tyagi, A. Anvikar, R. Mohanty, B. S. Rao, A. C. Jha, B. Shahi, J. P. N. Singh, A. Roy, P. Kaur, M. Kothari, S. Mehta, A. Gautam, J. K. Paliwal, S. Arora and N. Saha, *Clin. Infect. Dis.*, 2012, **55**, 663–671.
- 58 C. Patil, S. Katare, M. Baig and S. Doifode, *Ann. Med. Health Sci. Res.*, 2014, **4**, 466–471.
- 59 P. Olliaro and T. N. C. Wells, *Clin. Pharmacol. Ther.*, 2009, **85**, 584–595.
- 60 R. K. Bhamidipati, *Basis for the Dose-dependent Systemic Clearance of a Novel 1,2,4-trioxolane Antimalarial, OZ277, in Rats*, Monash University, 2009.
- 61 S. A. Charman, S. Arbe-Barnes, I. C. Bathurst, R. Brun, M. Campbell, W. N. Charman, F. C. K. Chiu, J. Chollet, J. C. Craft, D. J. Creek, Y. Dong, H. Matile, M. Maurer, J. Morizzi, T. Nguyen, P. Papastogiannidis, C. Scheurer, D. M. Shackleford, K. Sriraghavan, L. Stingelin, Y. Tang, H. Urwyler, X. Wang, K. L. White, S. Wittlin, L. Zhou and J. L. Vennerstrom, *Proc. Natl. Acad. Sci. U.S.A.*, 2011, **108**, 4400–4405.
- 62 J. J. Moehrle, S. Duparc, C. Siethoff, P. L. M. van Giersbergen, J. C. Craft, S. Arbe-Barnes, S. A. Charman, M. Gutierrez, S. Wittlin and J. L. Vennerstrom, *Br. J. Clin. Pharmacol.*, 2013, **75**, 524–537.
- 63 X. Wang, Y. Dong, S. Wittlin, S. A. Charman, F. C. K. Chiu, J. Chollet, K. Katneni, J. Mannila, J. Morizzi, E. Ryan, C. Scheurer, J. Steuten, J. Santo Tomas, C. Snyder and J. L. Vennerstrom, *J. Med. Chem.*, 2013, **56**, 2547–2555.
- 64 MMV | Developing next-generation medicines,
<http://www.mmv.org/research-development/developing-next-generation-medicines-address-drug-resistance-and-improve>, (accessed December 2016).
- 65 A. P. Phyto, P. Jittamala, F. H. Nosten, S. Pukrittayakamee, M. Imwong, N. J. White, S. Duparc, F. Macintyre, M. Baker and J. J. Möhrle, *Lancet Infect. Dis.*, 2016, **16**, 61–69.
- 66 S. D. Fontaine, A. G. DiPasquale and A. R. Renslo, *Org. Lett.*, 2014, **16**, 5776–5779.
- 67 Sigma-Aldrich | Pentane SDS,
<http://www.sigmaaldrich.com/catalog/product/sial/236705?lang=en&re>

- gion=GB, (accessed December 2016).
- 68 S.-H. Lau, A. Galván, R. R. Merchant, C. Battilocchio, J. A. Souto, M. B. Berry and S. V. Ley, *Org. Lett.*, 2015, **17**, 3218–3221.
- 69 S. Krishna and N. J. White, *Clin. Pharmacokinet.*, 1996, **30**, 263–299.
- 70 R. Amewu, A. V Stachulski, S. A. Ward, N. G. Berry, P. G. Bray, J. Davies, G. Labat, L. Vivas and P. M. O'Neill, *Org. Biomol. Chem.*, 2006, **4**, 4431–4436.
- 71 G. dos Passos Gomes, V. Vil', A. Terent'ev and I. V Alabugin, *Chem. Sci.*, 2015, **6**, 6783–6791.
- 72 G. L. Ellis, R. Amewu, S. Sabbani, P. A. Stocks, A. Shone, D. Stanford, P. Gibbons, J. Davies, L. Vivas, S. Charnaud, E. Bongard, C. Hall, K. Rimmer, S. Lozanom, M. Jesús, D. Gargallo, S. A. Ward and P. M. O'Neill, *J. Med. Chem.*, 2008, **51**, 2170–2177.
- 73 I. Opsenica, D. Opsenica, K. S. Smith, W. K. Milhous and B. A. Šolaja, *J. Med. Chem.*, 2008, **51**, 2261–2266.
- 74 E. H. Cordes and H. G. Bull, *Chem. Rev.*, 1974, **74**, 581–603.
- 75 H.-S. Kim, K. Tsuchiya, Y. Shibata, Y. Wataya, Y. Ushigoe and A. Masuyama, *J. Chem. Soc. Perkin Trans. 1*, 1999, **27**, 1867–1870.
- 76 A. Cynthia, B. E. Maryanoff, M. M. Joullié and K. M. Lassen, *ARKIVOC*, **2010**, 189–250.
- 77 P. M. O'Neill, R. K. Amewu, G. L. Nixon, F. Bousejra ElGarah, M. Mungthin, J. Chadwick, A. E. Shone, L. Vivas, H. Lander, V. Barton, S. Muangnoicharoen, P. G. Bray, J. Davies, B. K. Park, S. Wittlin, R. Brun, M. Preschel, K. Zhang and S. A. Ward, *Angew. Chemie Int. Ed.*, 2010, **49**, 5693–5697.
- 78 M. A. Biamonte, J. Wanner and K. G. Le Roch, *Bioorg. Med. Chem. Lett.*, 2013, **23**, 2829–2843.
- 79 MMV | Developing a single-dose malaria cure,
<http://www.mmv.org/newsroom/interviews/developing-single-dose-malaria-cure>, (accessed December 2016).

Chapter V

Novel Tetraoxane Antimalarials

Table of Contents

5.1 A Second Generation of Tetraoxane Analogues: N205	246
5.1.1 Synthesis	246
5.1.2 Testing data	253
5.1.3 Conclusion	258
5.2 A Third Generation of Tetraoxane Analogues: E209	259
5.2.1 Background	259
5.2.1.1 Original Synthesis of E209	263
5.2.2 E209 vs. N205	266
5.2.3 Aim	267
5.2.4 Alternative Strategy 1	268
5.2.5 Alternative Strategy 2	273
5.2.5.1 Zinc acetate/triethoxysilane reduction	275
5.2.5.2 Lithium aluminium hydride reduction	277
5.2.5.3 Triflic anhydride/sodium borohydride reduction	278
5.2.6 Alternative Strategy 3	282
5.2.7 Improving the yield of the tetraoxane-forming step	284
5.2.8 Alternative Strategy 4	286
5.2.9 Conclusion	288
5.3 Back-up Compound	290
5.3.1 Synthesis	292
5.3.2 Conclusion	294
5.4 Experimental	295
5.4.1 General Background	295
5.4.1.1 Handling peroxides	295
5.4.1.2 Setting up reactions	295
5.4.1.3 Purification of reagents and organic solvents	296
5.4.1.4 Purification of products	296
5.4.1.5 Analysis	296
5.4.2 General Procedures	297
5.4.2.1 General procedure A: Amine formation	297
	244

5.4.2.2 General Procedure B: A one-pot hydrolysis and alkylation of the tetraoxane acetate unit	297
5.4.3 Experimental	298
5.5 References	313

5.1 A Second Generation of Tetraoxane Analogues: N205

This series was designed to replace the amide side chain of RKA182 with a benzylamino functionality in order to increase lipophilicity and enhance blood stability (Figure 5.1). An increased CLogP should increase cell membrane penetration; and as these compounds are basic, this should also result in an increased volume of distribution.¹ However, a certain degree of plasma protein binding may be beneficial for these compounds as this could reduce peroxide turnover resulting from interactions with endogenous sources of Fe (II).²

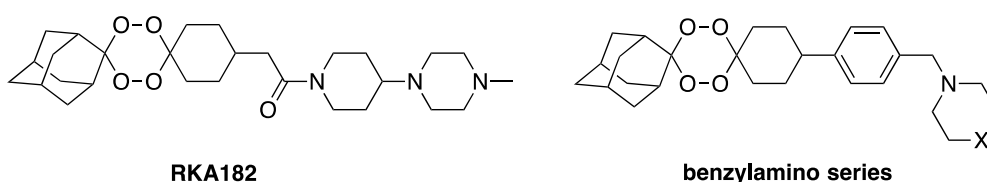
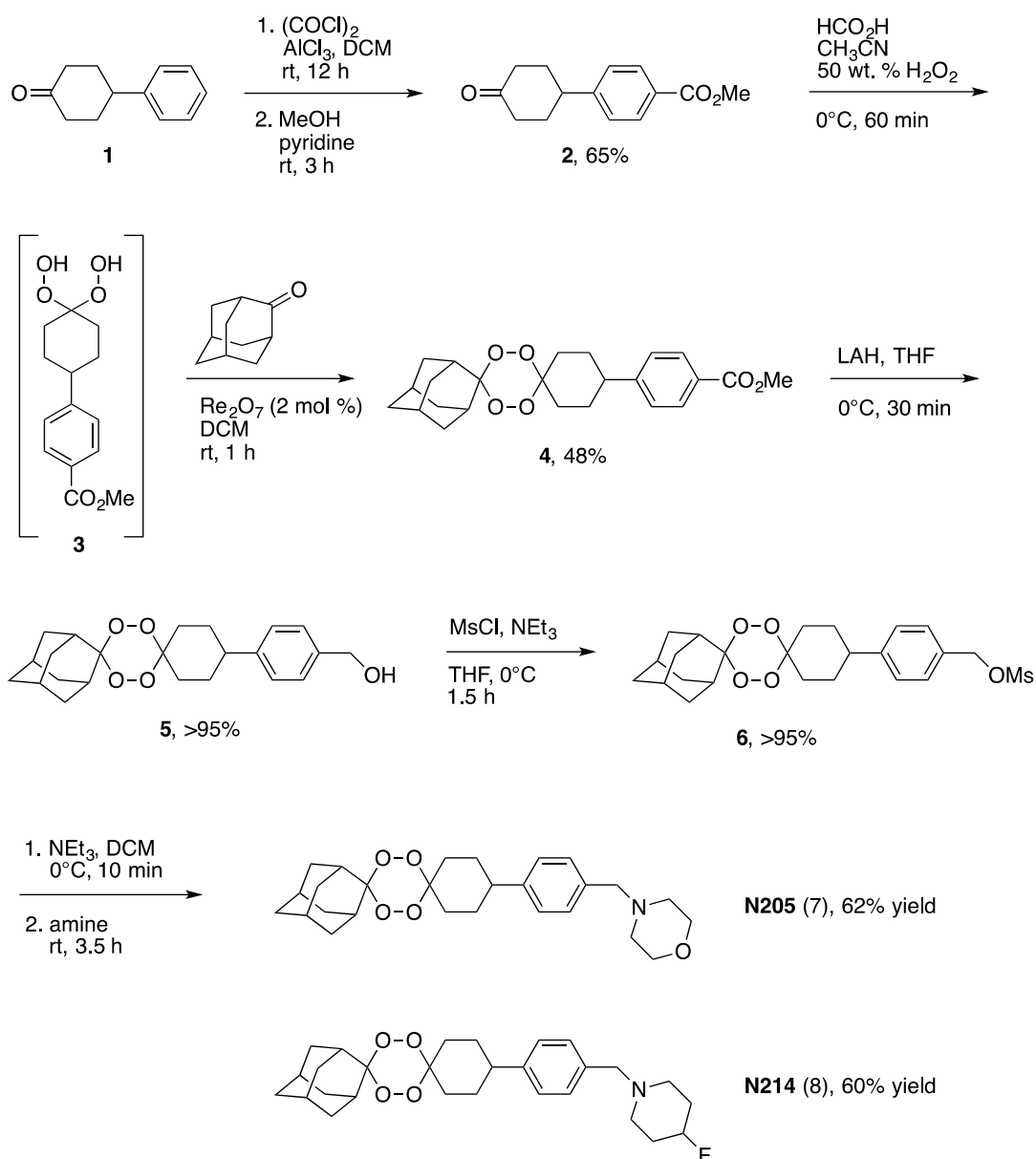


Figure 5.1. The structures of RKA182 and the template designed for the benzylamino series of tetraoxane antimalarials, where X= O and C-F

The benzyl moiety should increase the lipophilicity of these compounds compared to RKA182, whilst the inclusion of solubilising amine side chains should maintain a good level of aqueous solubility, which is important for ease of formulation and administration.^{3,4}

5.1.1 Synthesis

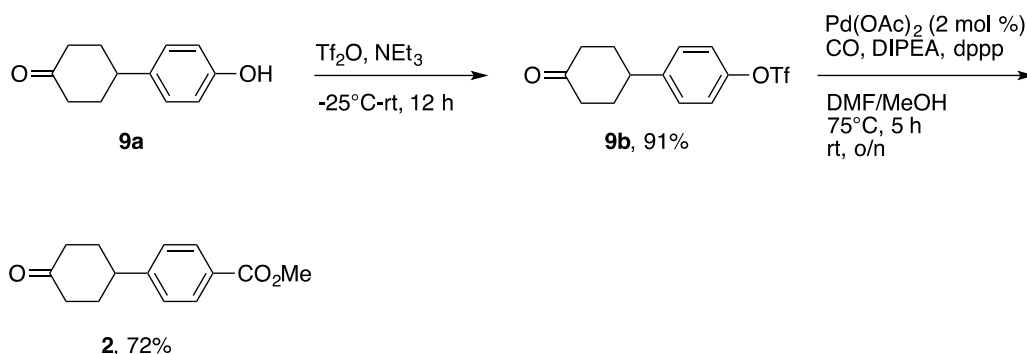
The preparation of this series of compounds is outlined below in Scheme 5.1. The synthesis consisted of five high-yielding steps (compound **3** is an intermediate in one transformation), with the last step being a point at which diversity could be introduced. This allowed for the intermediate mesylate **6** to be generated in bulk, before coupling with a range of amines in the final step. A divergent synthesis improves efficiency, thus reducing costs and labour time.⁵



Scheme 5.1. Synthetic route used to synthesise benzylamino analogues

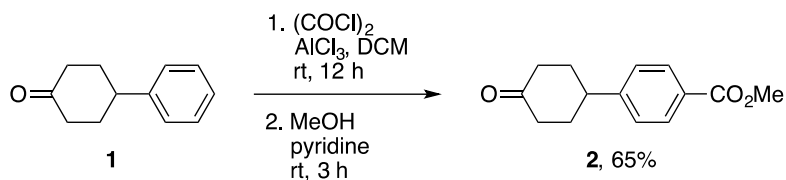
Two different routes were explored for the synthesis of the ester intermediate **2**. The initial pathway converted 4-(4-hydroxyphenyl)cyclohexanone (**9a**, see Scheme 5.2a) to the corresponding triflate (**9b**) using triflic anhydride in the presence of base. The triflate (**9b**) was then subjected to a palladium catalysed carbonylation reaction in the presence of methanol to produce the methyl ester (**2**). This reaction was first described more than 40 years ago by Richard Heck

and is a very convenient method for the synthesis of carbonyl-containing compounds.^{6,7}



Scheme 5.2a. Original synthesis of methyl ester intermediate **2**

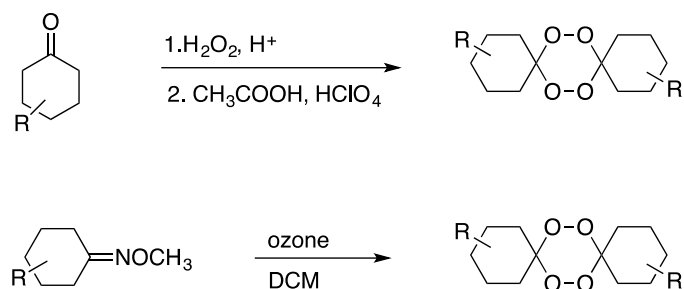
This method produced the desired ester in two high yielding steps, however an alternative route was ultimately developed that allowed for easier scale up and a reduced number of steps. This route is shown in Scheme 5.2b. 4-Phenylcyclohexan-1-one (**1**) was directly converted to methyl ester (**2**) using a modified Friedel-Crafts procedure. Acyl chlorides can be formed from aromatic compounds using oxalyl chloride in the presence of aluminium chloride.⁸ The acyl chloride intermediate was then stirred in methanol to form the desired product. Compound **2** was produced in a 65% yield, an improvement of 10% over literature.⁹



Scheme 5.2b. Alternative synthesis of methyl ester intermediate **2**

The next step involved the introduction of the adamantyl moiety and formation of the tetraoxane unit. The synthesis of functionalised tetraoxanes still remains problematic, with many procedures utilising very harsh conditions that are

incompatible with a large number of functional groups. Sanderson *et al.* outlined the synthesis of symmetrical tetraoxanes using acidic hydrogen peroxide conditions, and Vennerstrom & Dong reported the synthesis of similar compounds through ozonolysis of *O*-methyl oximes (Scheme 5.3).^{10,11} However these conditions are not applicable for the formation of the unsymmetrical structure required here.



Scheme 5.3. Synthetic routes to symmetrical tetraoxanes

Previous work in the O'Neill group led to the synthesis of a variety of dispiro-1,2,4,5-tetraoxanes using one-pot reactions. An intermediate dihydroperoxide was first formed from a ketone using hydrogen peroxide in the presence of methyltrioxorhenium(VII) (MTO) (Scheme 5.4). HBF₄ was then added, along with adamantanone, in order to catalyse the cyclocondensation step.¹² Fluoroboric acid is a strong acid, and as a result, these conditions are incompatible with many functional groups.¹³ Furthermore, these conditions can lead to decomposition of the intermediate dihydroperoxide and the product tetraoxane.

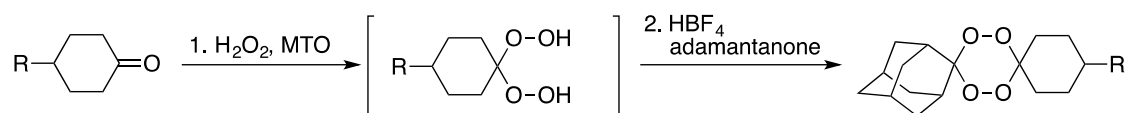
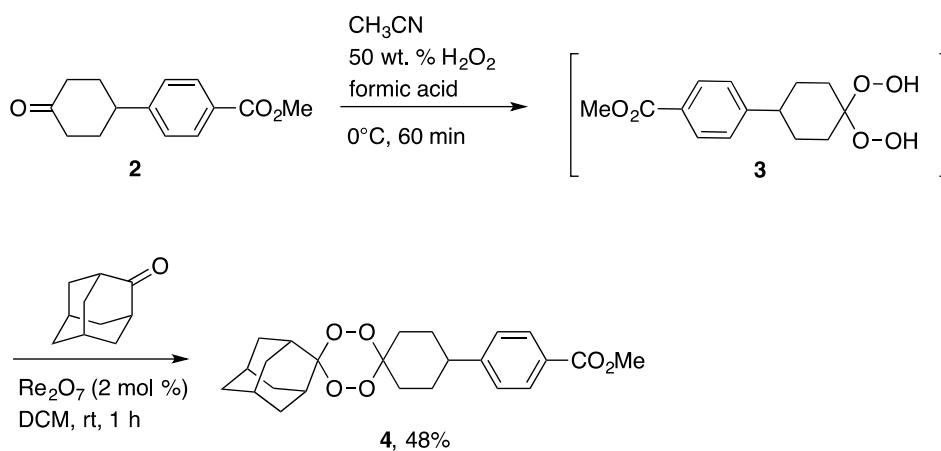


Figure 5.4. Synthesis of dispiro-1,2,4,5-tetraoxanes outlined by O'Neill *et al.*

In 2008, Ghorai and Dussault reported a method for the synthesis of unsymmetrical tetraoxanes based on a Re(VII) promoted condensation of 1,1-

dihydroperoxides and carbonyls. This procedure uses milder conditions than those described previously, and is tolerant of a wide variety of side chains.¹⁴ Therefore, these conditions were applied to the synthesis of tetraoxane **4** (Scheme 5.5) from the dihydroperoxide intermediate **3**. The rhenium (VII) oxide catalyst can also be used to generate the dihydroperoxide **3** in the first step but this catalyst is expensive, which is not ideal for the synthesis of an antimalarial drug compound.¹⁵ Acidified hydrogen peroxide was used to carry out this transformation instead, with minimal effect on the final yield of **4**.



Scheme 5.5. Tetraoxane generation using a rhenium(VII) oxide catalysed method adapted from Ghorai and Dussault

The dihydroperoxide **3** was not subjected to purification and analysis due to the hazardous nature of peroxide compounds.¹⁶ This intermediate underwent a small aqueous work-up to remove all traces of hydrogen peroxide before undergoing the rhenium-catalysed cyclocondensation. The cyclocondensation proceeded rapidly and resulted in a 48% yield of compound **4**.¹⁷ A large number of side products were observed during this step and the two main side products (see Figure 5.2) were identified to be the starting ketone (**2**) and the symmetrical tetraoxane (**10**).

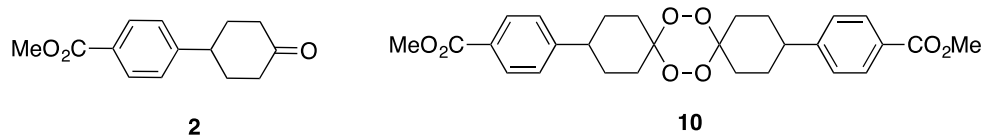
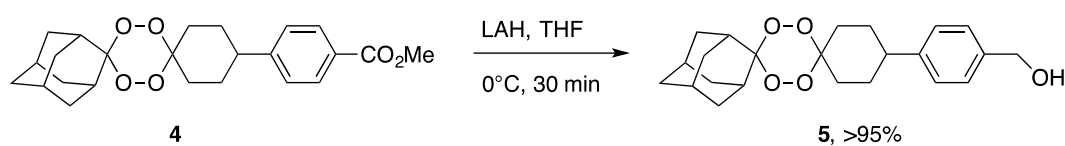


Figure 5.2. The major side products generated during the tetraoxane formation step

Despite literature quoting the preparation of these compounds on a large scale, this preparation was limited to a scale of 10 mmol for the starting ketone (**2**) due to the potentially explosive nature of peroxide compounds.¹⁸ However, once formed, the tetraoxane product is stable (see Chapter 4 Section 4.3.2) and multiple batches were combined and used for the following steps on a larger scale.

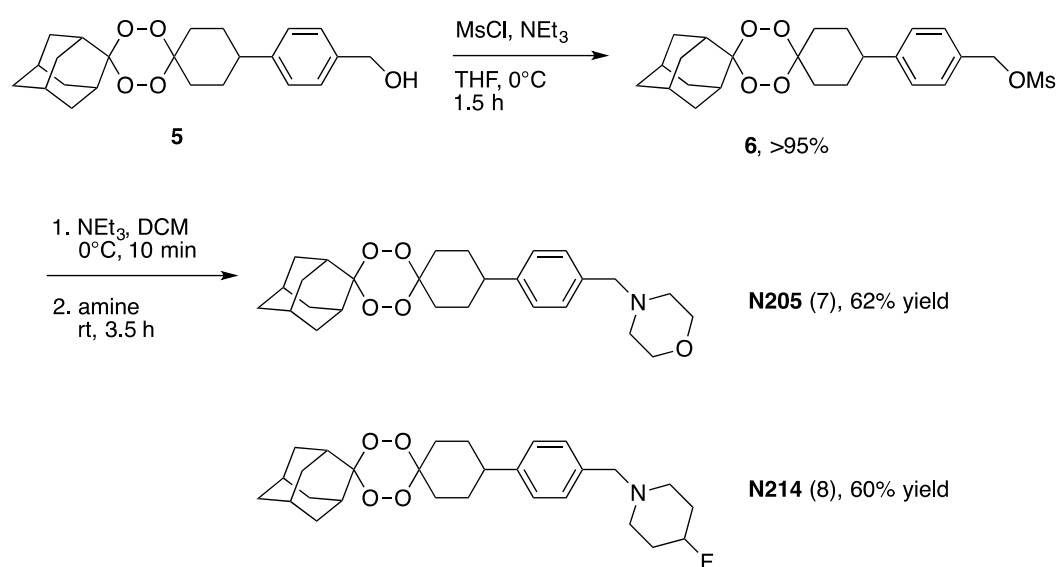
There is still much to understand about the mechanism for the tetraoxane forming steps, however it almost certainly begins with the reversible addition of dihydroperoxide to the starting ketone.¹⁴ The mechanism for the rhenium(VII) oxide catalysed step remains unclear; however, there is evidence to support the theory that the catalyst works by activating the carbonyl moiety of adamantanone, similar to a Lewis acid catalyst.¹⁹

The next step in this pathway involved the reduction of methyl ester **4** to the corresponding benzyl alcohol **5**. This was achieved in excellent yields using lithium aluminium hydride (LAH) (see Scheme 5.6). The reaction time was kept short (30 minutes) in order to minimise the risk of decomposition of the tetraoxane, as LAH is a powerful reducing agent. The first equivalent of this reagent reduced the ester to an aldehyde, which in turn is reduced by another equivalent of LAH to the corresponding alcohol.²⁰



Scheme 5.6. Conversion of methyl ester **4** into the benzyl alcohol **5**

The alcohol was then converted to a better leaving group using mesyl chloride. Mesylate is a good leaving group due to its ability to stabilise an incipient negative charge in nucleophilic substitution reactions compared with the hydroxyl group, which is a very poor leaving group.²¹ The resulting mesylate **6** then underwent nucleophilic substitution reactions with morpholine and 4-fluoropiperidine to produce the final compounds (**N205** and **N214**) (Scheme 5.7).



Scheme 5.7. The final steps in the synthesis of the benzylamino series

5.1.2 Testing data

The morpholine (N205) and 4-fluoropiperidine (N214) analogues were sent for extensive *in vitro* and *in vivo* studies. Table 5.1 highlights *in vitro* inhibitory against *P. falciparum* 3D7, calculated logD, solubility and measured logP values for these compounds, in comparison to the lead trioxolane antimalarial (OZ439).

LogD is the distribution coefficient and was calculated for each compound at physiological pH (7.4). This can give a more accurate description of the lipophilicity of a molecule, as it takes ionisable groups into account. Many drugs are likely to be charged at physiological pH and logP only accounts for neutral compounds.^{22,23} This can be valuable when considering absorption in different regions of the alimentary canal, as pH varies significantly.²⁴

Compound	IC ₅₀ (nM)	LogD _{7.4}	Solubility (mg/mL)	LogP
7 (N205)	1.3 ± 0.1	4.42	0.076	4.50 ± 0.82
8 (N214)	4.2 ± 0.4	5.02	0.025	5.36 ± 0.86
OZ439	8.0 ± 0.3	4.83	0.55	4.63 ± 0.70

Table 5.1. *In vitro* IC₅₀, calculated logD, solubility and experimentally measured logP data for the two benzylamino tetraoxane analogues vs. OZ439.

As Table 5.1 shows, N205 has potent nanomolar activity against *P. falciparum* 3D7 and is more active than the lead trioxolane OZ439. Both N205 and N214 have poor solubility profiles compared to OZ439 (0.076 mg/mL and 0.025 mg/mL respectively vs. 0.55 mg/mL). The solubility of a drug compound is an important factor as it can impact on bioavailability, and a poorly soluble orally administered drug will have limited absorption from the gastro-intestinal tract.²⁵

Salt formation is a useful approach for the optimisation of physicochemical, biopharmaceutical and processing properties of ionisable drug compounds, and it has been estimated that approximately half of all active pharmaceutical substances were progressed as salts.^{26,27} Mesylate salts in particular, allow for ease of formulation and processing and tend to be highly soluble.²⁸ Therefore the benzylamino analogues were formulated as mesylate salts in order to improve their solubility profiles. This was achieved by stirring each analogue in anhydrous diethyl ether and methanesulfonic acid. The resulting precipitate was washed with diethyl ether and dried to yield the desired salt.

Both the free base of N205 and the mesylate salts of N205 and N214 were then tested for the average survival time (in days) of *Plasmodium berghei* infected mice following a single 30 mg/kg dose. The data are summarised in Table 5.2, along with RKA182 and OZ439 for comparison.

Compound	Average mouse survival following a single 30 mg/kg dose (days)
N214 mesylate	13 (12, 13, 14)
N205	26.3 (16, 30, 30)
N205 mesylate	25.0 (15, 30, 30)
RKA182	11.4 (14, 15, 7, 7, 14)
OZ439	30 (30, 30, 30)

Table 5.2. Average survival time of *Plasmodium berghei* infected mice following a single 30 mg/kg oral dose

Table 5.2 shows that the average survival for the mesylate salt of N214 (**7a**) was 13 days and this is comparable to the lead tetraoxane RKA182. These data

suggest that N214 would be better suited for a three day dosing regimen rather than a single dose, which is a current priority for the Medicines for Malaria Venture (MMV).²⁹ N205 (**7**) performed much better in this study and an average survival of 26.3 days was observed (66% cure rate). This figure is almost comparable to that of OZ439, which gave an average survival of 30 days (100% cure rate). Based on the success of this data, N205 was selected as the lead compound for further profiling.

The solubility of the mesylate salt of N205 (**7a**) was tested in both water and an acidic buffer at 37°C, and the results are summarised below in Table 5.3. Formulation of N205 as a mesylate salt gave a vastly improved solubility profile, which was comparable to that of the OZ439 mesylate. Although not comparable to RKA182 (>40 mg/mL, see Chapter 4 Section 4.3.2), it fulfilled the solubility criteria for the desired target product (>5 mg/mL).

Compound	Solubility in water (mg/mL)	Solubility in pH 2.0 buffer (mg/mL)
N205 mesylate	>9	>9
OZ439 mesylate	6.8	>8

Table 5.3. The solubility profiles for the mesylate salts of N205 and OZ439 in water and an acidic buffer, measured at 37°C

The final important factor to consider was the blood stability of N205; as the first generation of tetraoxanes developed by O'Neill *et al.* (including RKA182) exhibited improved blood stability over OZ277. *In vitro* blood stability was measured for both N205 and OZ439 in human and rat blood, and pharmacokinetics were measured in male Sprague Dawley rats. The results are summarised below in Table 5.4.

Property	N205 mesylate	OZ439 mesylate
<i>In vitro</i> blood stability:		
T_{1/2} (h) in rat blood	~8	>15
T_{1/2} (h) in human blood	~10% loss after 4 h	No degradation detected after 4 h
Rat PK:		
CL_{plasma} (mL/min/kg)	77	40
Vd_{ss} (L/kg)	11	18
IV T_{1/2} (h, estimated)	6.3	32
BA (%)	52	~100

Table 5.4. Human/rat blood stability and rat pharmacokinetics for N205 and OZ439

As Table 5.4 shows, both N205 and OZ439 were relatively stable in human blood with only a 10% loss of N205 observed after 4 hours and no degradation observed for OZ439. There was a significant difference between these two compounds in rat blood, with N205 exhibiting an *in vitro* half-life of approximately 8 hours, compared with over 15 hours for OZ439. There was also a marked difference in the pharmacokinetic behaviour of these two compounds in the rat model. N205 was cleared at nearly twice the rate of OZ439 and had a lower volume of distribution, suggesting it may bind more tightly to plasma proteins in rat blood than OZ439.³⁰ The estimated half-life of N205 following intravenous administration was only 6.2 hours compared with 32 hours for OZ439, and bioavailability was almost half that of OZ439. These data indicate that, whilst the profile for N205 is good, it does not match OZ439.³¹

In order to obtain a clearer picture of the therapeutic efficacy of N205, the dose required to reduce parasitemia by 90% (ED₉₀) was calculated in a SCID mouse model.³² SCID mice are homozygous for the severe combined immune deficiency mutation, Prkdc^{SCID}.³³ This is characterised by the failure of the adaptive immune system to elicit or sustain an immune response, usually due to an

impaired ability to generate B and T cells. Human blood cells can therefore be transplanted into a SCID mouse and they will be accepted relatively easily due to the lack of host immunity.³⁴ The resulting humanised mouse provides a useful model for *in vivo* testing of drug compounds on human cells and tissues without putting individuals at risk.^{35,36}

Figure 5.3 shows how the percentage of parasitemia varied as the dose increased in the SCID mouse model. The single dose ED₉₀ for N205 against *P. falciparum* can be measured from this graph and was found to be 8.6 mg/kg. This confirmed the excellent antimalarial activity of N205, which is comparable to OZ439 (single dose ED₉₀ = 6.2 mg/kg). Most importantly, this data indicates that single dose applications of trioxolanes and tetraoxanes surpass multiple-doses of semi-synthetic artemisinins, such as artesunate, which has an ED₉₀ of 10 mg/kg following 4 doses.³⁷

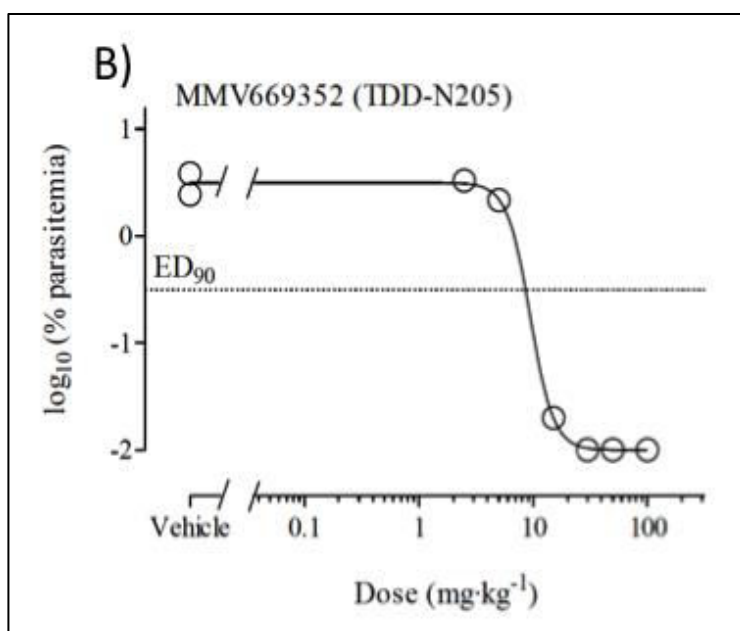


Figure 5.3. Graph to show how percentage parasitemia changed with the dose of N205 in *P. falciparum* infected humanised (SCID) mice

5.1.3 Conclusion

N205 (7) met all of the criteria set out for the target product profile. The synthesis of this novel antimalarial compound was short, achiral and simple. The aqueous solubility was greater than 5 mg/mL and potent *in vitro* antimalarial activity was observed at doses below 10 nM. Furthermore, the average mouse survival was 26.3 days following a single 30 mg/kg dose. Figure 6.4 compares the profile of N205 to RKA182. IC₅₀ data shows that N205 is not only a more potent antimalarial than RKA182 but also better suited for a single dose cure due to the greatly improved mouse survival times. Although the estimated half-life of N205 could not compare to that of OZ439, it is still a significant improvement on RKA182 (2.38 hours) and the other first generation tetraoxane analogues.

	RKA182	N205
Simple synthesis	yes	yes
Short number of steps	4	5
Aqueous solubility	>40 mg/mL	>9 mg/mL
Activity IC ₅₀ <10 nM	4.9 nM	1.3 nM
Single dose mouse survival	11.4 days	26.3 days

Figure 5.4. A comparison between the product profile of RKA182 and N205

N205 met part of the aim for this project; however, the drawbacks of N205 lie in the less than optimal stability profile observed in the rat model. Therefore, further optimisation of the side chain was necessary in order to find a potent tetraoxane with an enhanced blood stability profile.

5.2 A Third Generation of Tetraoxane Analogues: E209

5.2.1 Background

Whilst working on the benzylamino series, a third generation of 1,2,4,5-tetraoxanes were being developed in the O'Neill group (see Figure 5.5). The aim of this series of compounds was to increase lipophilicity through modifications to the side chain, in order to improve blood stability and *in vivo* rat pharmacokinetic profiles.

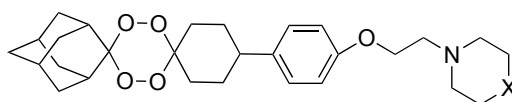


Figure 5.5. The template for the series of 3rd generation tetraoxane analogues

As Figure 5.5 shows, the benzyl amino group of the second generation of tetraoxane analogues was substituted for a phenyl ether moiety, and the chain was also extended in order to increase lipophilicity. Furthermore, a variety of amine solubilisers were incorporated in order to counterbalance the increased lipophilicity imparted by the side chain.³⁸

A number of analogues were synthesised and sent for initial *in vitro* IC₅₀ testing versus *P. falciparum* 3D7. These compounds were also subjected to *in vivo* testing on *P. berghei* infected mice and the average number of days the infected mice survived following a single 30 mg/kg dose was measured. The results, along with calculated logP values for each analogue, are summarised below in Table 5.5.

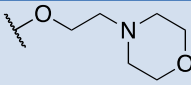
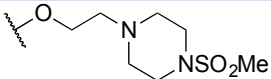
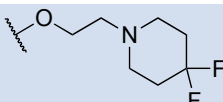
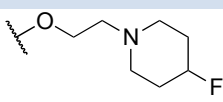
Side Chain	ClogP	IC ₅₀ (nM)	Average mouse survival (days)*
 11	5.6	10 ± 1	7.3
 12	5.6	3.5 ± 0.2	19
 13	6.1	8.5 ± 0.6	8
 14	6.4	5.1 ± 0.81	26.3

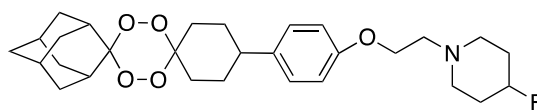
Table 5.5. The results of initial *in vitro* and *in vivo* testing. ClogP values were calculated using ChemDraw Professional 15.1 and IC₅₀ values were calculated *in vitro* against *P. falciparum* 3D7. *The average mouse survival was measured in *P. berghei* infected mice following a single 30 mg/kg dose

As Table 5.5 shows, all four of the third generation analogues had a calculated logP higher than the measured logP for N205 (4.5 ± 0.82), showing that this series was indeed more lipophilic.

All but one compound, **11**, met the original criteria for the target product; an IC₅₀ value <10 nM. Interestingly, compound **11** is the tetraoxane analogue of OZ439, however these two compounds have very different profiles *in vitro* and *in vivo*. Both compounds exhibit similar potencies *in vitro* against *P. falciparum* 3D7 (**11** = 10 nM vs. OZ439 = 8 nM), however the average mouse survival was only 7.3 days for compound **11**, compared to 30 days for OZ439.

Despite compound **12** exhibiting the most potent activity *in vitro*, the average mouse survival was only 19 days. Therefore, compound **14** known as E209 (see

Figure 5.6) was selected for further head to head testing with OZ439 due to its excellent potency and long mouse survival times following a single 30 mg/kg dose.



E209

Figure 5.6. The chemical structure of E209 (**14**); the lead compound to emerge from this series

The main drawback of N205 was a moderate stability profile in the rat model; therefore the degradation, half-life and *in vitro* clearance times were measured for E209 in both human and rat microsomes, to allow for comparison with N205 and OZ439 (Table 5.6).

Compound	Species	Degradation half-life (min)	<i>In vitro</i> Cl _{int} (μL/min/mg protein)
N205	Human	43	41
	Rat	20	89
E209	Human	76	23
	Rat	54	32
OZ439	Human	66	27
	Rat	141	16

Table 5.6. Metabolic stability parameters for N205, E209 and OZ439 based on NADPH-dependant degradation profiles in human and rat liver microsomes

**Data is presented as mean values of two independent experiments at a substrate concentration of 5 μM*

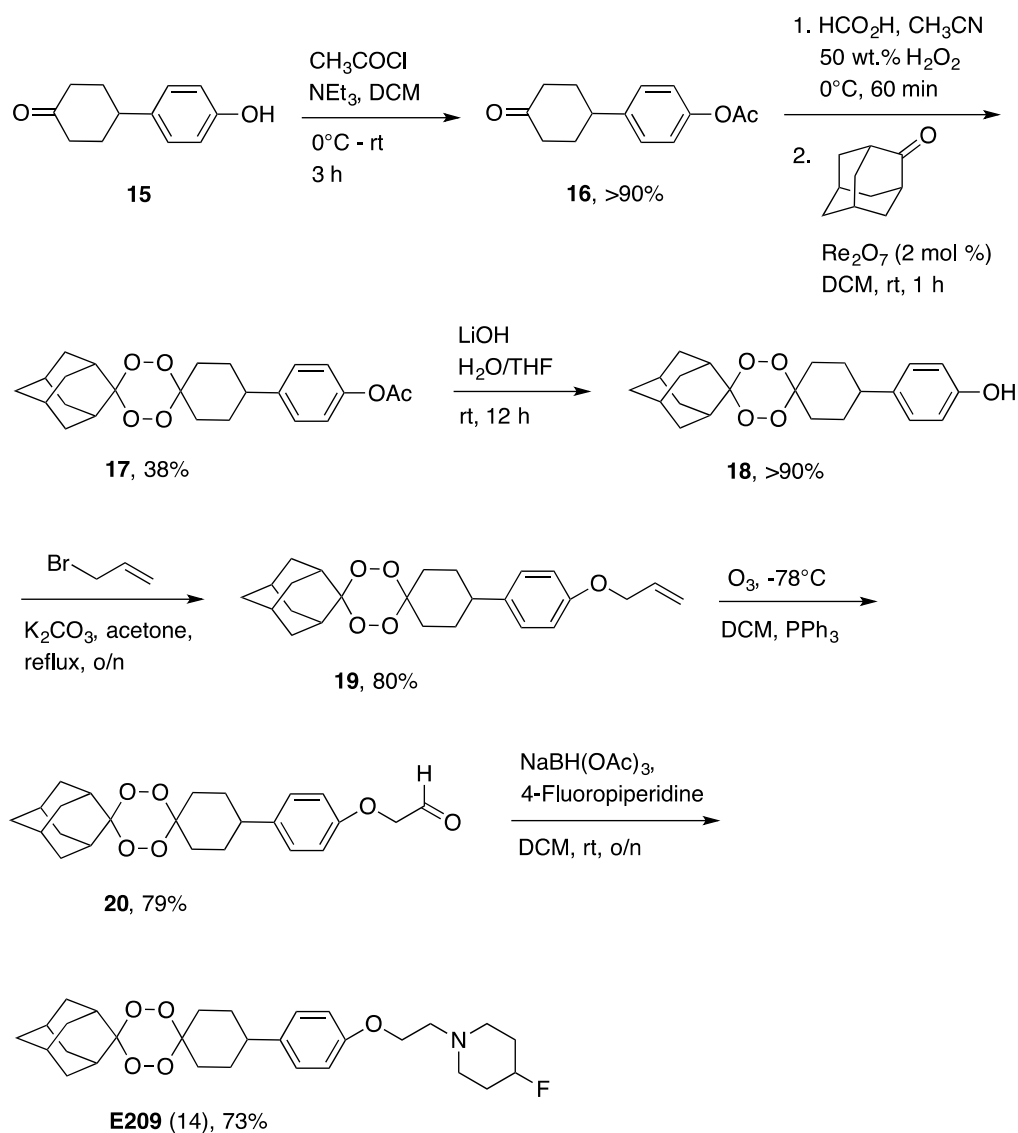
As Table 5.6 shows, E209 had a significantly improved stability profile in both human and rat microsomes. Degradation half-life in human liver microsomes was increased from 43 minutes for N205 to 76 minutes for E209, and in rat liver microsomes the half-life increased from just 20 minutes for N205 to 54 minutes for E209. Although E209 had a relatively short degradation half-life in rat liver microsomes compared with OZ439 (54 min vs. 141 min respectively), it was a significant improvement on N205. Furthermore, the degradation half-life of E209 in human liver microsomes surpassed that of OZ439 by 10 minutes, showing that this novel tetraoxane was comparable to the lead trioxolane compound.

Also of importance were the *in vitro* clearance times observed for the three compounds. N205 underwent clearance in rat liver microsomes at a rate of 89 $\mu\text{L}/\text{min}/\text{mg}$ protein compared with just 16 $\mu\text{L}/\text{min}/\text{mg}$ protein for OZ439. E209 also displayed vastly improved clearance rates in both human and rat liver microsomes, which were comparable to OZ439.

The original aims of this series of tetraoxane compounds were met; the lipophilicity of these compounds was increased in comparison to the benzylamino series and, as a result, a notable improvement in the stability profile of the best performing compound (E209) was observed. Therefore E209 was selected as the lead tetraoxane analogue for further development.

5.2.1.1 Original Synthesis of E209

The original synthesis of E209 is shown below in Scheme 5.8. It was a series of six high-yielding steps that include a crucial ozonolysis reaction to introduce an aldehyde moiety into the side chain.



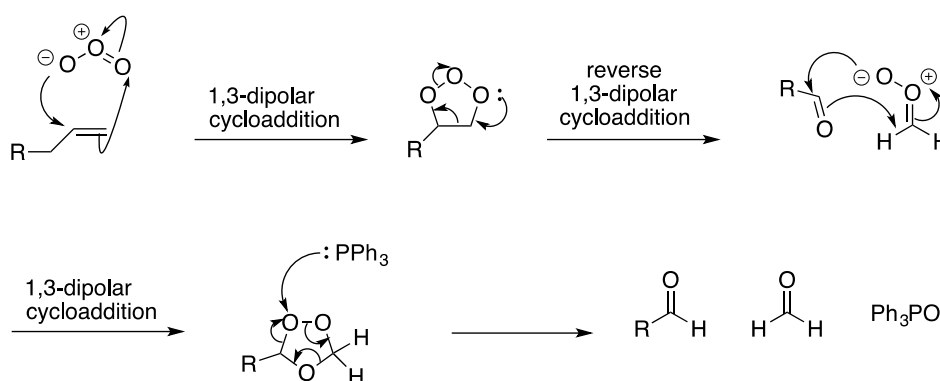
Scheme 5.8. Original synthetic route to E209

The synthesis began with the conversion of 4-(4-hydroxyphenyl)cyclohexan-1-one (**15**) to the corresponding acetyl (**16**), using acetyl chloride in the presence of a base. This extra step was introduced in order to improve the yield for the rhenium catalysed tetraoxane reaction. The phenol was poorly soluble in the

reaction solvents used for the tetraoxane-forming step, which resulted in poor yields. The corresponding acetyl was more soluble and gave higher yields for this important step. Once the tetraoxane (**17**) was formed (same conditions as N205, Section 5.1.1) the acetyl was removed by treatment with lithium hydroxide.³⁹

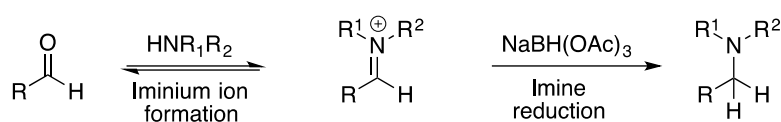
The next step was a nucleophilic substitution reaction between compound **18** and 3-bromoprop-1-ene, using potassium carbonate as a base. The resulting alkene (**19**) was then converted to the desired aldehyde (**20**) using an ozonolysis reaction. This reaction was carried out in the presence of ozone and resulted in the oxidative cleavage of the alkene π bond, producing two carbonyl products.⁴⁰

The mechanism for this reaction is shown below in Scheme 5.9 and begins with a 1,3-dipolar cycloaddition. The cyclic intermediate, a primary ozonide, contains two rather unstable O-O single bonds, which undergo immediate decomposition by a reverse 1,3-dipolar cycloaddition.⁴¹ The products are an aldehyde and a carbonyl oxide. This carbonyl oxide also contains a 1,3-dipole, like ozone, and therefore adds into the aldehyde by a second 1,3-dipolar cycloaddition.²⁰ The resulting secondary ozonide (which is more stable than the primary ozonide but still poses an explosion hazard) is then decomposed using triphenylphosphine to produce the desired tetraoxane aldehyde (**20**), as well as formaldehyde and triphenylphosphine oxide as by-products.⁴² This mechanism was first proposed by Criegee in 1975 and was later confirmed using ¹⁷O NMR spectroscopy.^{43,44}



Scheme 5.9. The mechanism for the ozonolysis of a terminal alkene

The aldehyde (**20**) then underwent a reductive amination with 4-fluoropiperidine in the presence of sodium triacetoxyborohydride to form the final product, E209 (**14**). Reductive aminations are one of the most useful routes for the synthesis of amines and they proceed via an imine intermediate (see Scheme 5.10).^{20,45} Sodium triacetoxyborohydride is commonly used as the reducing agent for these transformations owing to the fact that it is much milder than sodium borohydride, which would reduce the starting aldehyde.⁴⁶ Furthermore, using NaBH(OAc)₃ avoids the build up of toxic side-products generated by sodium cyanoborohydride.⁴⁷



Scheme 5.10. Reductive amination with a secondary amine

5.2.2 E209 vs. N205

As Figure 5.7 below shows, E209 and N205 have similar profiles; they are both potent antimalarials with good aqueous solubility and a long mouse survival time of 26 days following a single 30 mg/kg dose. However, the key difference between these two compounds is their performance in the rat model. The *in vitro* half-life observed in rat blood was significantly improved from approximately 8 hours for N205 to 13 hours for E209, and *in vitro* human and rat liver microsomal stability also increased.

	N205	E209
Simple synthesis	yes	no
Short number of steps	5	6
Aqueous solubility	>9 mg/mL	>8 mg/mL
Activity IC ₅₀ <10 nM	1.3 nM	5.1 nM
Single dose mouse survival	26.3 days	26 days
Rat blood stability/T _{1/2}	8 hours	13 hours

Figure 5.7. A comparison between the product profile of N205 and E209

Despite improvements to the stability and pharmacokinetic profiles for E209, the synthesis was longer than that of N205 and also included an ozonolysis step. This is acceptable for small-scale synthetic procedures; however, it is not suitable for scale-up reactions. Ozone is a highly toxic and irritating gas and is extremely explosive in liquid form.⁴⁸ This powerful oxidising agent also generates potentially explosive ozonide intermediates during the course of the reaction; therefore it is better suited to smaller scale reactions, where the risk of these hazards is reduced.⁴⁹

5.2.3 Aim

E209 met many of the aims of the target product profile (see Figure 5.8) but the synthetic pathway is not suitable for scale-up reactions due to the high costs associated with a large number of steps and also the hazards associated with an ozonolysis reaction.

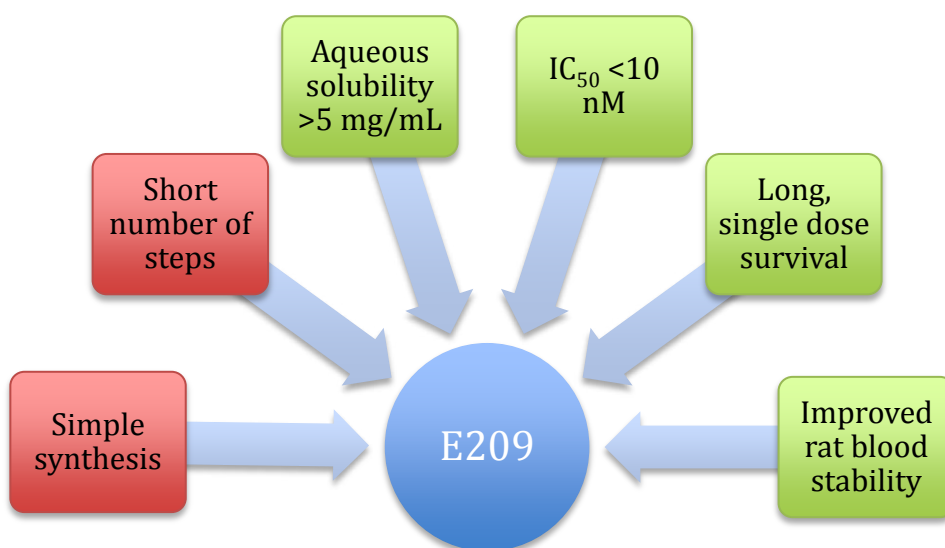
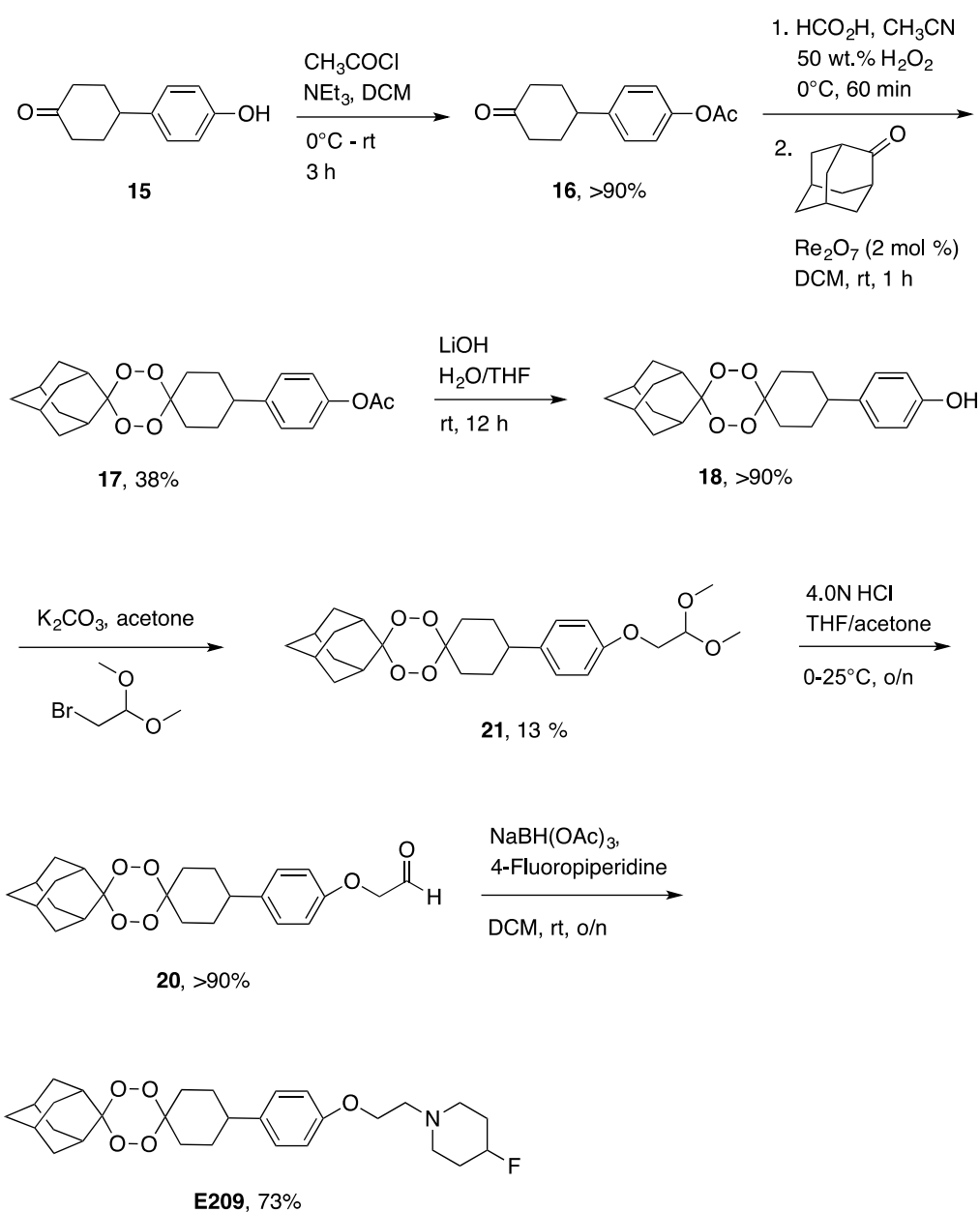


Figure 5.8. The product profile of E209

The aim of this project was to therefore establish an alternative synthetic pathway to generate E209, which could be completed in a reduced number of steps and avoided the use of an ozonolysis reaction.

5.2.4 Alternative Strategy 1

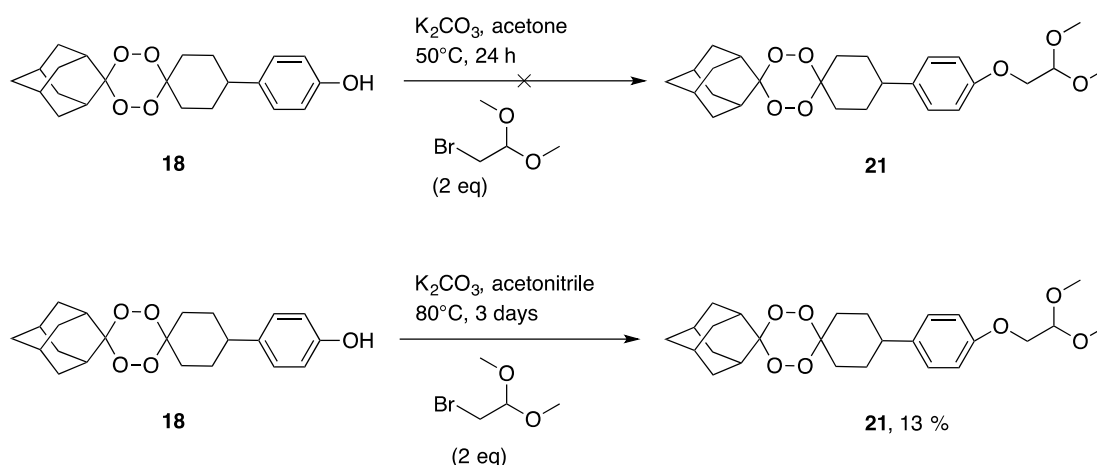
This first strategy investigated an alternative method of generating the important aldehyde functionality. The route is summarised below in Scheme 5.11 and involved the introduction of the aldehyde protected as an acetal, before subsequent hydrolysis and reductive amination steps to produce the product.⁵⁰



Scheme 5.11. Alternative strategy for the synthesis of E209

The first two steps of the synthesis were identical to that of the original route, which involved the conversion of 4-(4-hydroxyphenyl)cyclohexan-1-one (**15**) to the corresponding acetyl (**16**) before forming the tetraoxane.

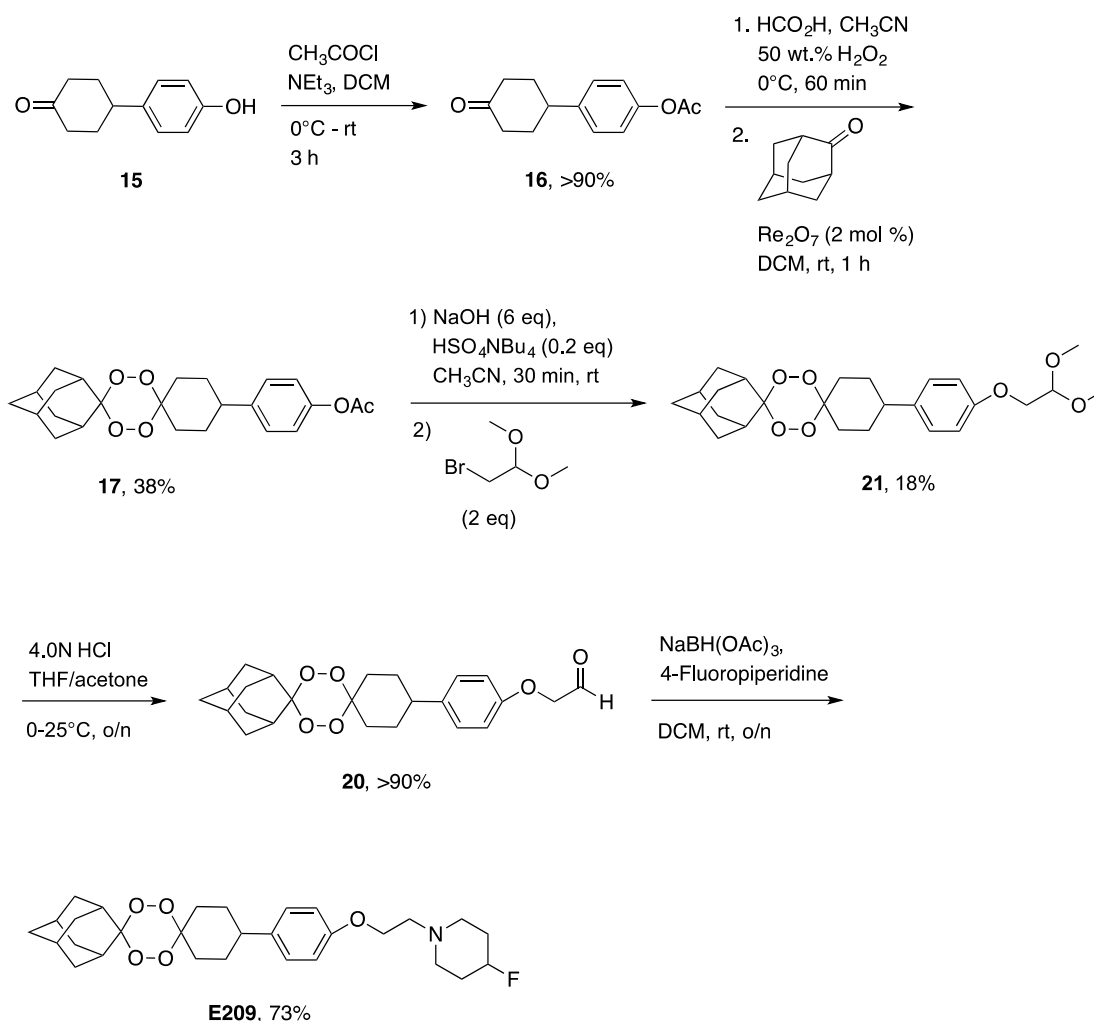
Once the acetyl was removed, the phenol (**18**) was subjected to an alkylation reaction with 2-bromo-1,1-dimethoxyethane. This procedure was first trialed using potassium carbonate and acetone at 50°C; however, no reaction was observed after 24 hours. The poor solubility of the phenol could have been a determining factor in the failure of this step, therefore the reaction was repeated with potassium carbonate in acetonitrile, and heated to 80°C for 3 days (see Scheme 5.12).⁵¹



Scheme 5.12. Alkylation of the tetraoxane phenol (**18**) with 2-bromo-1,1-dimethoxyethane

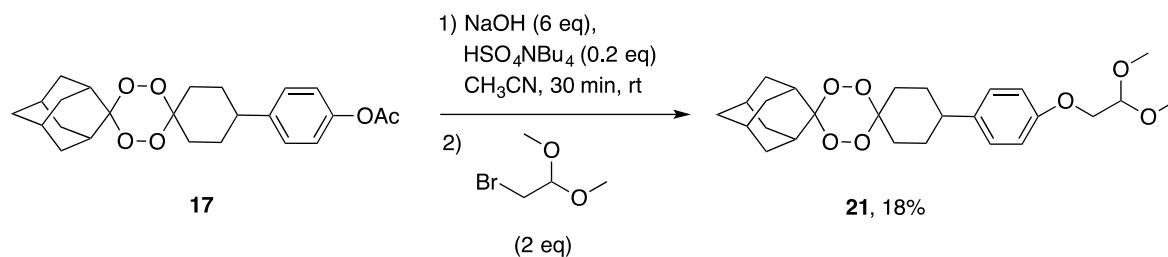
Despite some product being obtained (acetal **21**) the yield for this step was still low, even after 3 days of heating in an excess of base (4 eq.) and 2-bromo-1,1-dimethoxyethane (3 eq.). Alternative routes could have been explored for this transformation, such as the use of potassium iodide; however, the total number of steps to generate E209 was still higher than desired.⁵² Therefore an alternative procedure was developed, which was adapted from the flow

chemistry approach to the synthesis of OZ439 by Steven Ley *et al.*⁵³ This procedure is summarised below in Scheme 5.13.



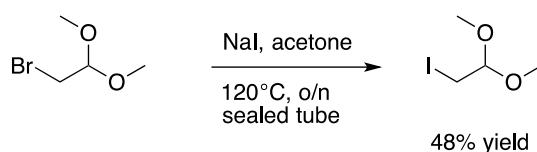
Scheme 5.13. An alternative method for introducing the acetal into the side chain

This method involved a one-pot synthesis of the tetraoxane acetal (**21**) directly from the acetate (**17**), rather than two separate steps. Sodium hydroxide was first used to remove the acetate and tetrabutylammonium hydrogensulfate was employed as a phase transfer catalyst in order to keep the resulting phenol soluble in the organic solvent. 2-bromo-1,1-dimethoxyethane was then added after one hour and the resulting mixture was stirred at 60°C overnight (Scheme 5.14).⁵⁴



Scheme 5.14. A one-pot hydrolysis and alkylation of the tetraoxane acetate (**17**)

Following work-up and purification, the yield for this transformation was still low, at only 18%. It was suggested that a better leaving group for the alkyl halide may improve the yield; therefore 2-iodo-1,1-dimethoxyethane was synthesised from 2-bromo-1,1-dimethoxyethane (Scheme 5.15). The Finkelstein reaction is driven forward by the solubility of halide salts. Sodium iodide is soluble in acetone whereas the resulting sodium bromide is not; therefore, once formed, the reaction is not reversed.⁵⁵



Scheme 5.15. Conversion of bromo to iodio, in order to create a better leaving group for the alkylation step

This reaction proceeded with a 48% yield and the product, 2-iodo-1,1-dimethoxyethane, was subjected to the one-pot hydrolysis and alkylation procedure. Despite creating a better leaving group, acetal **21** was only generated in 14% yield.

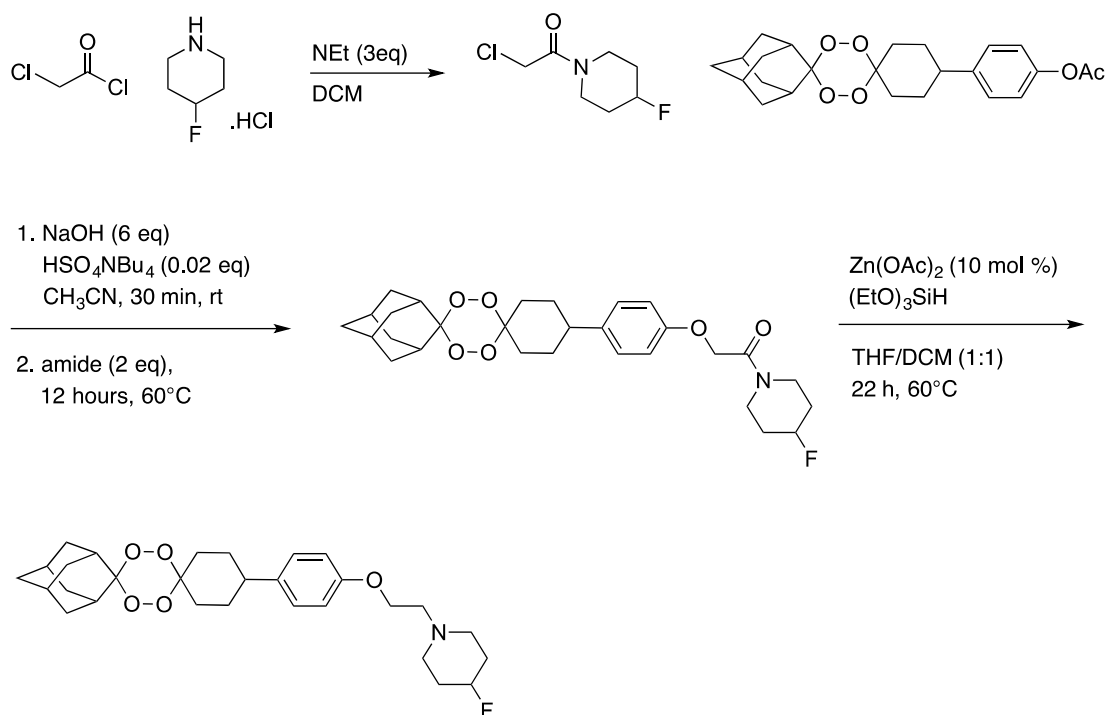
TLC was used to monitor these reactions and they all showed complete consumption of starting materials the generation of a new product spot, as well as a small amount of the tetraoxane phenol (**18**). Potentially the product acetal (**21**) could have been too unstable, and as a result decomposed rapidly after formation. However, this seems rather unlikely due to the harsh conditions that

were required to hydrolyse the small amount of acetal product to the aldehyde. Alternatively, the bulk of the starting material could have precipitated as the sodium salt of the phenol (**18**) and remained unreacted in the slurry at the bottom of the reaction vessel. This could help to explain the appearance of the TLCs during the course of the reaction and also explain why the yield obtained was so poor (14-18%).

The total number of steps for this procedure were reduced compared to the original synthesis of E209, and the ozonolysis reaction was replaced; however, the yield for the acetal-forming step was too low to consider this a viable replacement. Therefore another strategy was required.

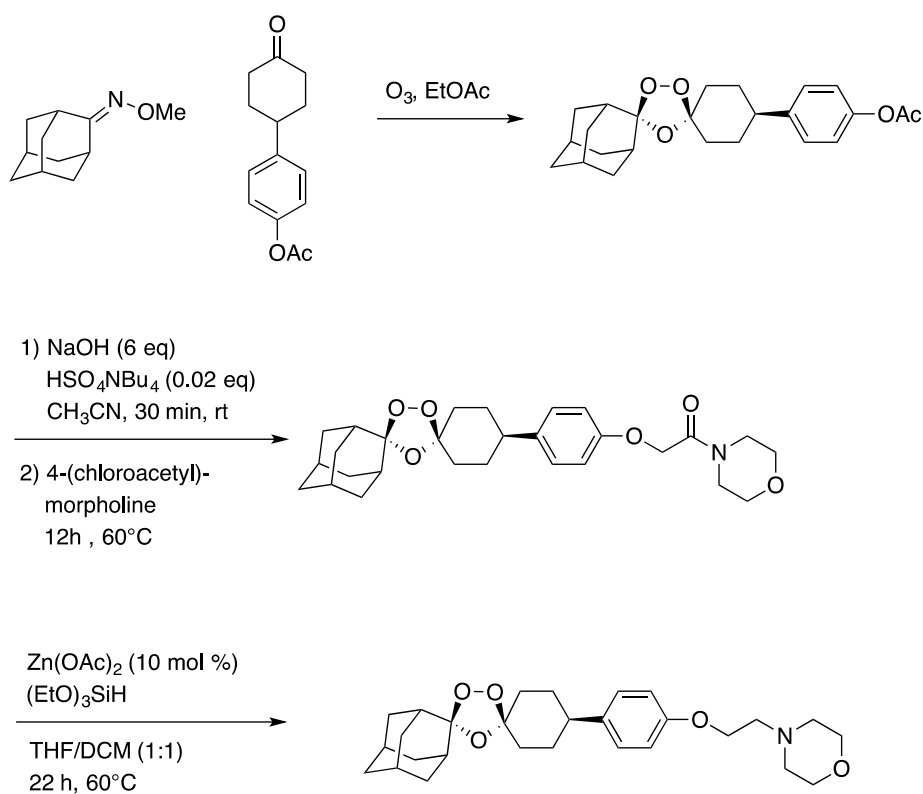
5.2.5 Alternative Strategy 2

The next line of thought was to introduce an amide group into the side chain, rather than an aldehyde, and reduce it to the product amine. The basic plan for this procedure is shown below (Scheme 5.16).



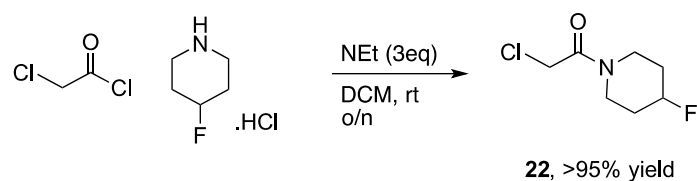
Scheme 5.16. Initial plan for the amide route to E209

This method was adapted for the synthesis of E209 from a flow-based preparation of OZ439 by Steven Ley *et al.* The original synthesis from this paper is shown in Scheme 5.17.⁵³



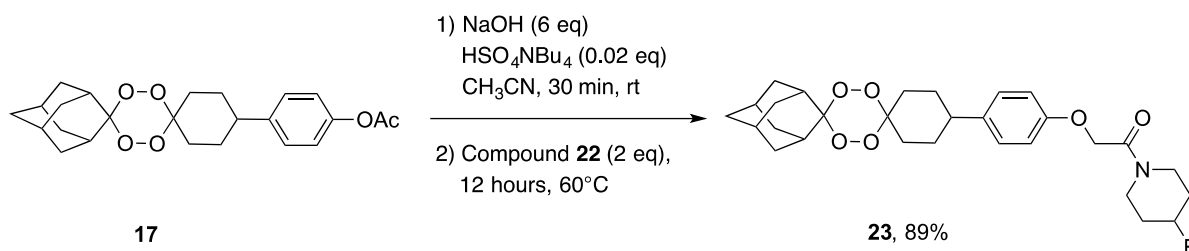
Scheme 5.17. The flow-based preparation of OZ439 that influenced this strategy⁵³

The key steps of interest in this procedure are the nucleophilic substitution of the *in situ* generated phenolate anion (from the starting trioxolane acetate) in the presence of commercially available 4-(chloroacetyl)morpholine, and subsequent selective reduction of the amide in the presence of zinc acetate and triethoxysilane.⁵⁶ An extra step was required to generate 2-chloro-1-(4-fluoropiperidin-1-yl)ethan-1-one (**22**) in the first step of the E209 synthesis. This was a straightforward, high-yielding reaction between chloroacetyl chloride and 4-fluoropiperidine hydrochloride, using triethylamine as base (Scheme 5.18).



Scheme 5.18. The synthesis of 2-chloro-1-(4-fluoropiperidin-1-yl)ethan-1-one (**22**)

Once formed, 2-chloro-1-(4-fluoropiperidin-1-yl)ethan-1-one (**22**) was coupled to the tetraoxane acetate (**17**) in an 89% yield (Scheme 5.19).



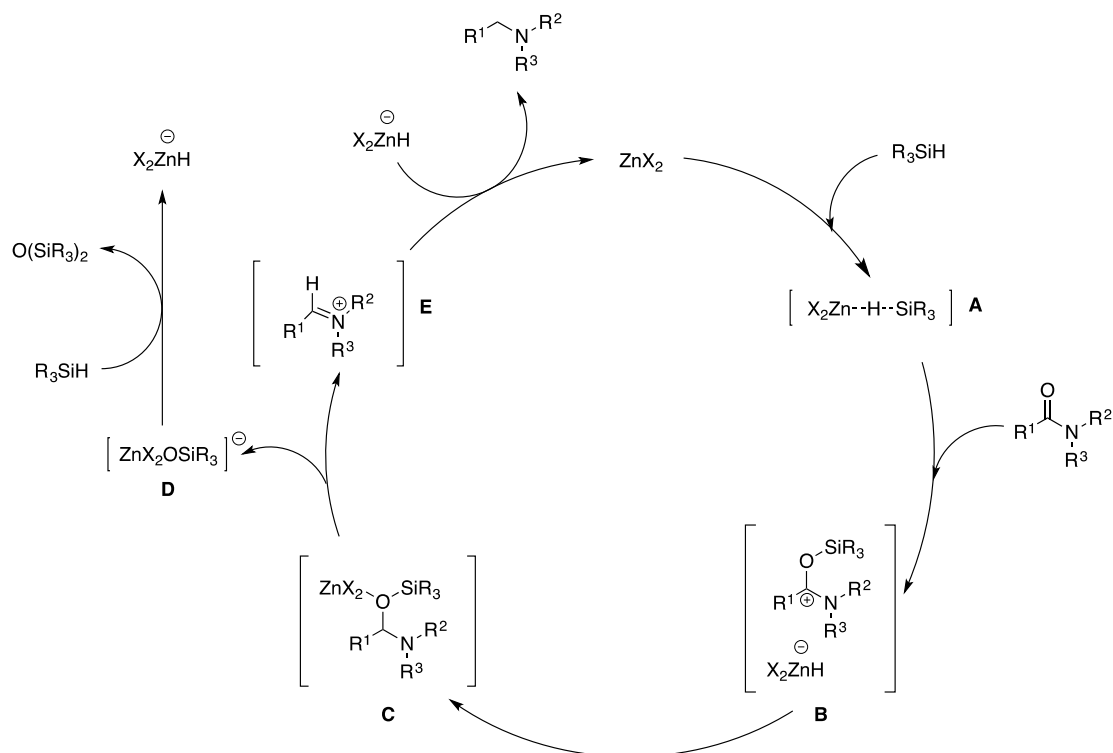
Scheme 5.19. Generation of the amide side chain from tetraoxane acetate **17** and 2-chloro-1-(4-fluoropiperidin-1-yl)ethan-1-one (**22**)

5.2.5.1 Zinc acetate/triethoxysilane reduction

The next step in the synthesis involved a selective reduction of the amide moiety to an amine. The catalytic reduction of amides to amines under mild conditions, with inexpensive and environmentally friendly reagents, is an area of high interest in organic synthesis.^{57,58} The flow-based preparation of OZ439 uses a zinc acetate-catalysed method first outlined by Beller *et al.*⁵⁹

Beller *et al.* investigated a number of zinc catalysts for the reduction of amides in the presence of triethoxysilane. They observed excellent chemoselectivity and unique functional group tolerance when using zinc acetate. This method was successful for a variety of aromatic, aliphatic, alicyclic and heterocyclic amides and showed selectivity in the presence of ester, ether, nitro, cyano and azo substituents.⁵⁹

Mechanistic studies showed that zinc acetate activates the silane, rather than the carbonyl, producing the activated species **A**. Co-ordination of an amide to the metal centre generates *N,O*-acetal **C**, via **B**. Anionic zinc ether **D** is then released, resulting in the formation of iminium species **E**, which can be reduced in the final step by another equivalent of triethoxysilane (Scheme 5.20).



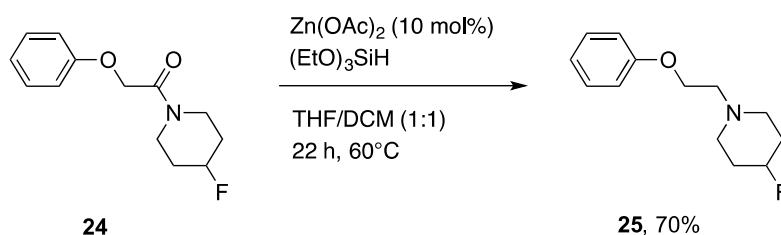
Scheme 5.20. The catalytic generation of amine from amide using zinc salts
 Adapted from: Zinc-Catalysed Reduction of Amides: Unprecedented Selectivity and
 Functional Group Tolerance, Beller *et al.*, 2010⁵⁹

This method was selected for the flow-based synthesis of OZ439 as a number of other common reducing agents, such as NaBH₄, LiAlH₄, BH₃.THF and Tf₂O/NaBH₄, resulted in both the reduction of the amide and cleavage of the trioxolane ring.⁵³ The zinc acetate conditions resulted in successful formation of OZ439 in an 86% yield.

In order to generate E209, this transformation must exhibit selectivity for the amide moiety and also show tolerance for the tetraoxane functionality. When these conditions were applied to compound **23**, no reaction was observed. The reaction was repeated in pure THF rather than a 1:1 mixture of DCM/THF due to the temperature required for this step (60°C); however, the same result was observed. It was then suggested that the tetraoxane could be co-ordinating to the zinc acetate, preventing the desired reaction from taking place. As a result, the

reaction was repeated with an increased catalyst loading of 30 mol%. However, no reaction was observed after 48 hours of heating.

The original paper stresses the use of strictly anhydrous conditions and an inert argon atmosphere due to the moisture sensitivity of zinc acetate. In order to assess whether the conditions utilised here were sufficient for this reaction to be successful, the reaction was repeated on a model substrate (**24**, Scheme 5.21).

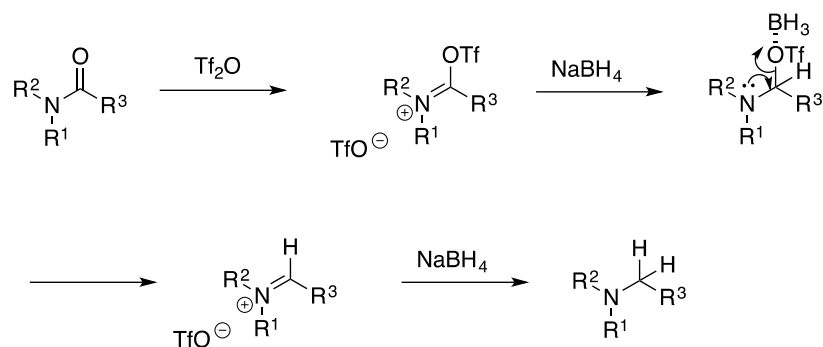


Scheme 5.21. Test reaction: Amide reduction on a model substrate (**24**), using zinc acetate in the presence of triethoxysilane

This reaction proved successful, demonstrating that the conditions used were suitable and suggesting that the tetraoxane functionality contributes towards the failure of this reaction for compound **23**. This observation further highlights the differences in stability and reactivity of trioxolane ring systems to tetraoxanes.⁶⁰

5.2.5.2 Lithium aluminium hydride reduction

Lithium aluminium hydride was previously employed in the presence of a tetraoxane moiety during the synthesis on N205, where an ester was reduced to an alcohol (see Section 5.1.1). The low temperature used and short reaction time left the tetraoxane moiety unaffected, even in the presence of this harsh reducing agent.⁶¹ Therefore it was decided to trial this reagent for the reduction of amide **23** (Scheme 5.22).

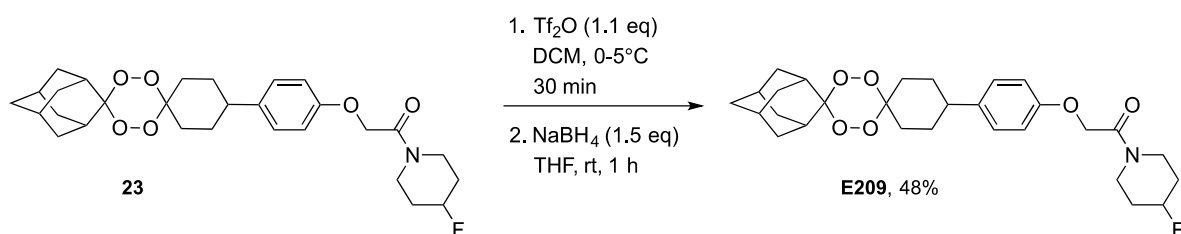


Scheme 5.23. The proposed mechanism of action for amide reductions using triflic anhydride and sodium borohydride

Adapted from: Amide Activation by Tf_2O : Reduction of Amides to Amines using NaBH_4 under Mild Conditions, Huang *et al.*, 2010⁶⁵

Despite these conditions proving too harsh for the flow-based preparation of OZ439, key differences between the trioxolane and tetraoxane ring towards reducing agents has already been observed; therefore this method was applied to the reduction of amide **23**.

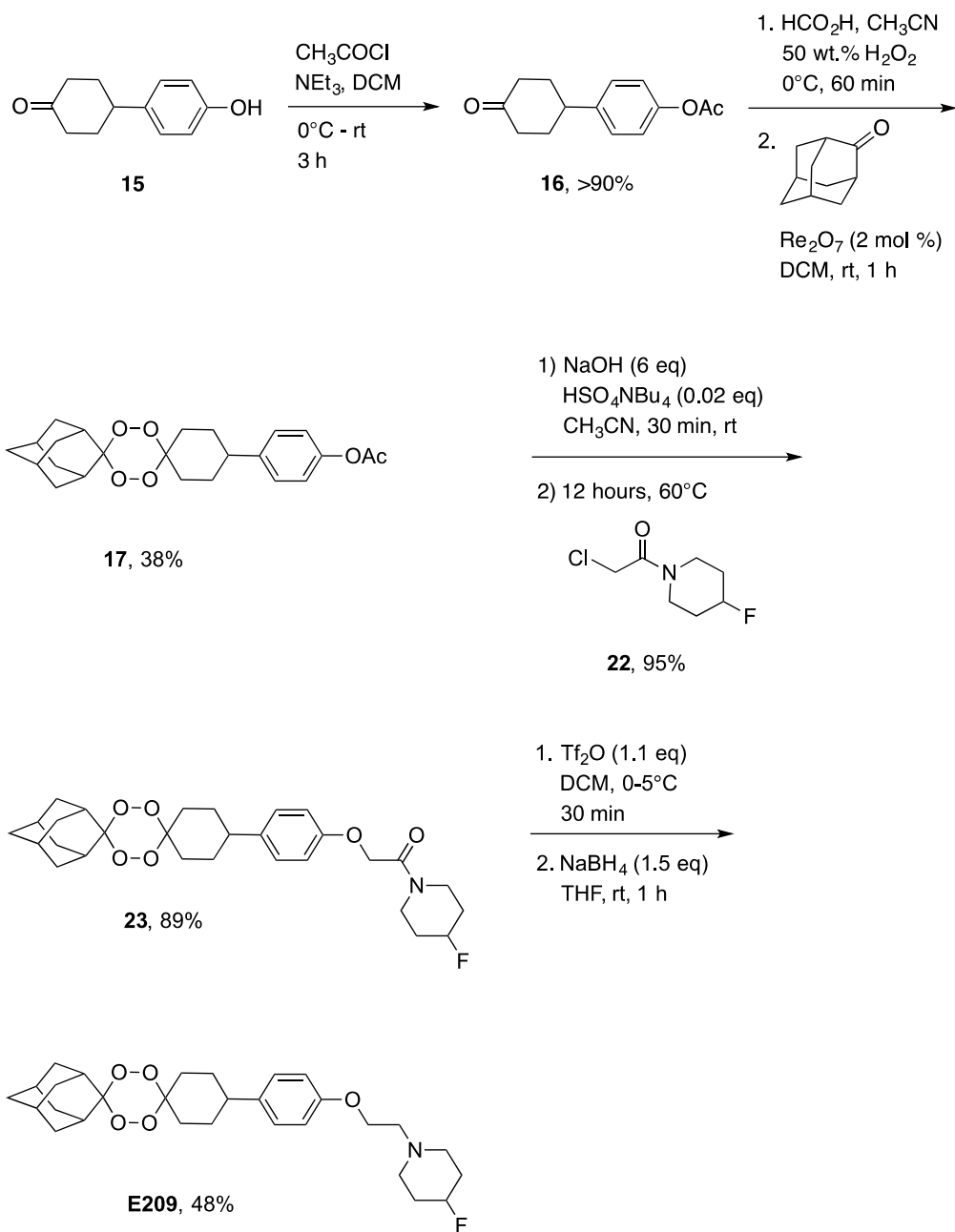
The highest yield of the desired amine product (E209) was observed when 1.1 equivalents of triflic anhydride were combined with 1.5 equivalents of sodium borohydride (Scheme 5.24). The original paper quotes the use of 1.3 equivalents of sodium borohydride; however, the reaction proved to be incomplete in this case. Increasing this further to 2.0 equivalents resulted in a reduced yield, potentially due to the formation of borane complexes with the product.



Scheme 5.24. The triflic anhydride activated reduction of amide **23** using sodium borohydride

Reduced yields were seen on scales below 200 mg but this method proved successful when trialled on scales up to 1 g. The overall successful synthetic route for Alternative Strategy 2 is shown in Scheme 5.25.

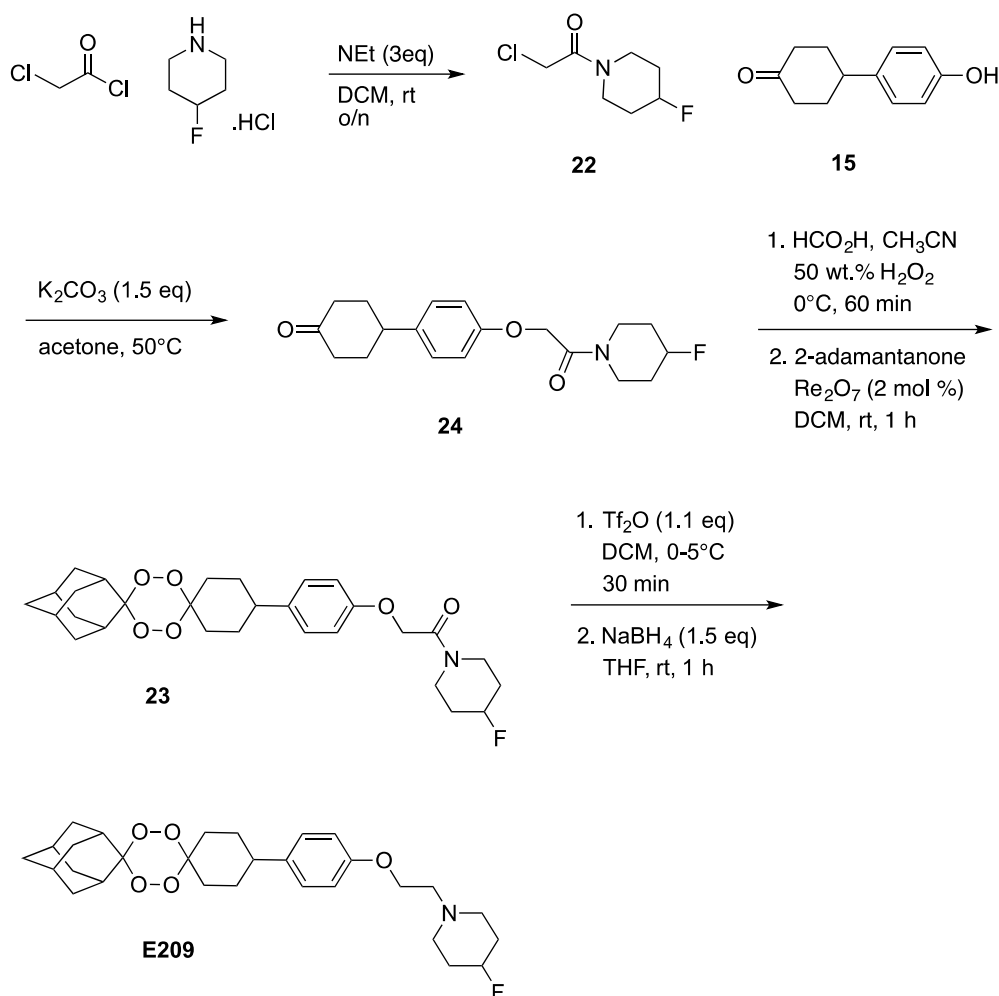
This method reduced the number of steps required to generate E209 to five and avoided the use of an ozonolysis reaction. Therefore the original aims of this project have been achieved. The main drawback of this pathway was the low yield for the tetraoxane forming step; at only 38% it was the lowest yielding step of the whole synthesis. As this step is close to the start of this synthetic pathway, it meant repeat reactions were required in order to obtain enough material to move forward. Another strategy was proposed in which the same steps were used but the order of each step was rearranged in order to move the tetraoxane-forming step towards the end of the synthetic pathway.



Scheme 5.25. Overall synthesis of E209 using Alternative Strategy 2

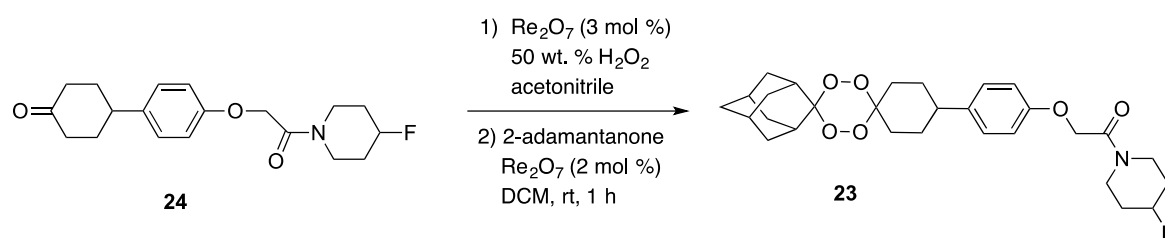
5.2.6 Alternative Strategy 3

The aim of this strategy was to move the tetraoxane-forming step towards the end of the synthetic pathway in order to reduce the number of repeat reactions required for this low-yielding reaction, and to reduce the total number of steps overall. The planned pathway is shown below in Scheme 5.26.



Scheme 5.26. The original pathway planned for the synthesis of E209

The first step in the pathway involved the synthesis of 2-chloro-1-(4-fluoropiperidin-1-yl)ethan-1-one (**22**) using methods described in Section 5.2.5. Amide **22** was then coupled to 4-(4-hydroxyphenyl)cyclohexan-1-one (**15**) using potassium carbonate in acetone. Initially, 1.5 equivalents of potassium carbonate were used, and the resulting reaction mixture was warmed to 50°C for 48 hours.

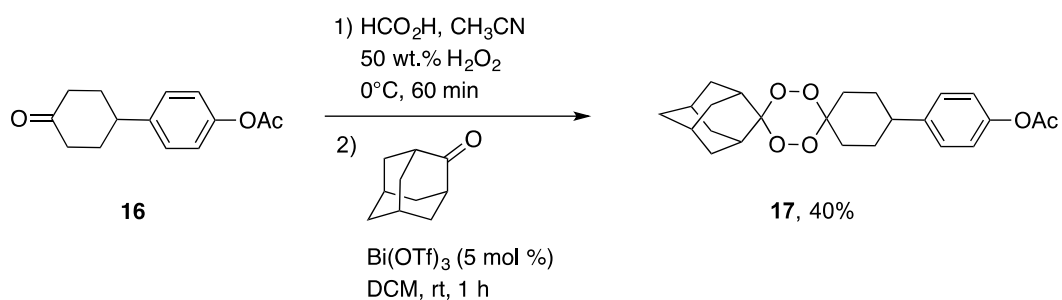


Scheme 5.28. The second method applied for the synthesis of compound **23**

Unfortunately the same result was observed using this method, even after repeating with fresh catalyst and hydrogen peroxide solution. The main issue with this transformation was likely linked to the ability of compound **24** to form a bis-hydroperoxide intermediate. The bis-hydroperoxide could have been so unstable that it immediately decomposed back to the starting ketone, or the starting ketone might have been so stable that the formation of the bis-hydroperoxide intermediate was highly unfavoured. Therefore this strategy was sidelined and alternative methods for improving the yield of the tetraoxane-forming step were investigated instead.

5.2.7 Improving the yield of the tetraoxane-forming step

Not only is rhenium(VII) oxide an expensive catalyst, the yields observed when using this reagent to carry out tetraoxane-forming steps were low and inconsistent; varying from 35-45%. Therefore WuXi AppTec carried out a catalyst screen in order to find a cheaper and more efficient catalyst for this transformation. They identified bismuth(III) triflate as a potential cheaper alternative to rhenium(VII) oxide (bismuth(III) triflate 5 g = £52.50 vs. rhenium(VII) oxide 5 g = £138.50, Sigma Aldrich 7/8/2016).^{67,68} The synthesis of **17** was repeated using this catalyst as a replacement (Scheme 5.29).



Scheme 5.29. Tetraoxane formation using a bismuth catalyst

The yield for this transformation was similar and the cost of the bismuth catalyst was significantly lower, therefore making this a more favourable choice.

As the proposed mechanism for the second stage of this reaction involved a cyclocondensation reaction between the bis-hydroperoxide intermediate and adamantanone, it was suggested that the water molecules released could hydrolyse the bis-hydroperoxide back to the starting ketone.⁶⁹ This could potentially explain the large amounts of starting ketone (**16**) that were recovered at the end of the reaction, despite all of the ketone (**16**) being consumed to form the bis-hydroperoxide in the first step.

It was suggested that the use of 4\AA molecular sieves could help to improve the yield for this step by absorbing the water released and preventing it from hydrolysing the intermediate bis-hydroperoxide.⁷⁰ Therefore the bismuth(III) triflate catalysed step was repeated using molecular sieves in order to investigate this hypothesis. It proved to be correct, and an increased yield of 60% was observed.

The results of this research are summarised in Table 5.7. A cheaper and more efficient route for the important tetraoxane-forming step was developed, which could be applied to future work in this area.

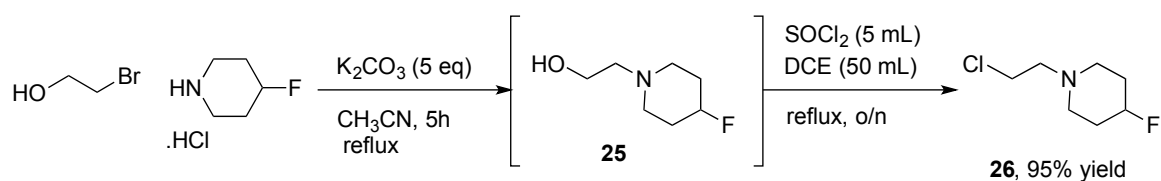
Reagent	Yield
Re ₂ O ₇	35-45%
Bi(OTf) ₃	40%
Bi(OTf) ₃ + 4Å molecular sieves	60%

Table 5.7. A summary of the catalysts used for tetraoxane ring formation

5.2.8 Alternative Strategy 4

With a greatly improved yield for the tetraoxane-forming step, attention turned back to Alternative Strategy 2. This was the best synthesis trialled for the generation of E209; however, the amide reduction step was relatively low yielding, despite optimisation of conditions (see Scheme 5.25). Therefore a literature search was conducted for conditions that could generate the amine side chain directly and eliminating the requirement for a reduction step.

A method was found within the original OZ439 patent for the generation of 1-(2-chloroethyl)-4-fluoropiperidine (**26**).⁷¹ This route generates a hydroxyl intermediate (**25**) *in situ* before forming the corresponding chloro analogue (Scheme 5.30).

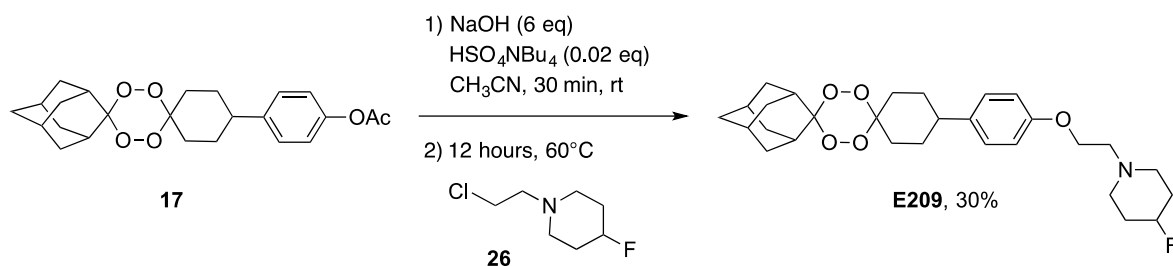


Scheme 5.30. The synthesis of 1-(2-chloroethyl)-4-fluoropiperidine (**26**) from 2-bromoethanol and 4-fluoropiperidine hydrochloride

This method proved highly successful, with the desired product obtained in a 95% yield from 2-bromoethanol and 4-fluoropiperidine. The intermediate hydroxyl (**25**) was not analysed; the reaction mixture was simply filtered and concentrated before setting up the second step. TLC was used to monitor these

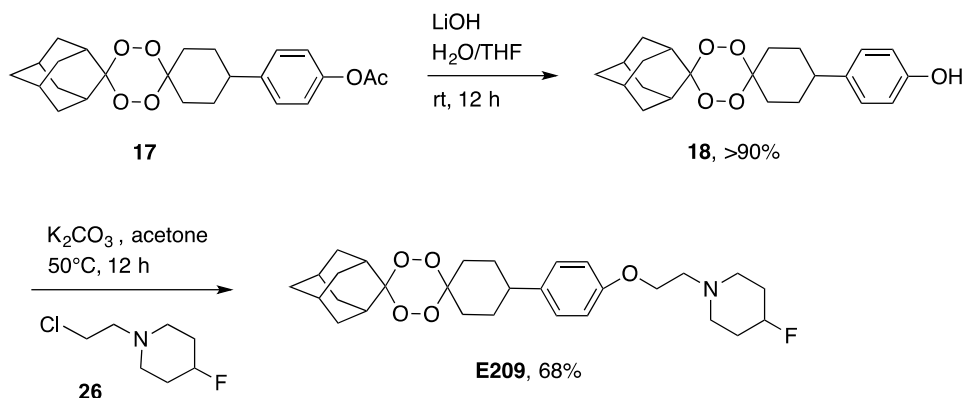
reactions in order to observe consumption of the starting materials and intermediates.

1-(2-Chloroethyl)-4-fluoropiperidine (**26**) was then coupled to the acetate (**17**) using the one-pot hydrolysis and alkylation method described previously (Section 6.2.5). Despite observing high yields with the amide side chain, only a 30% yield was obtained with this amine (Scheme 5.31).



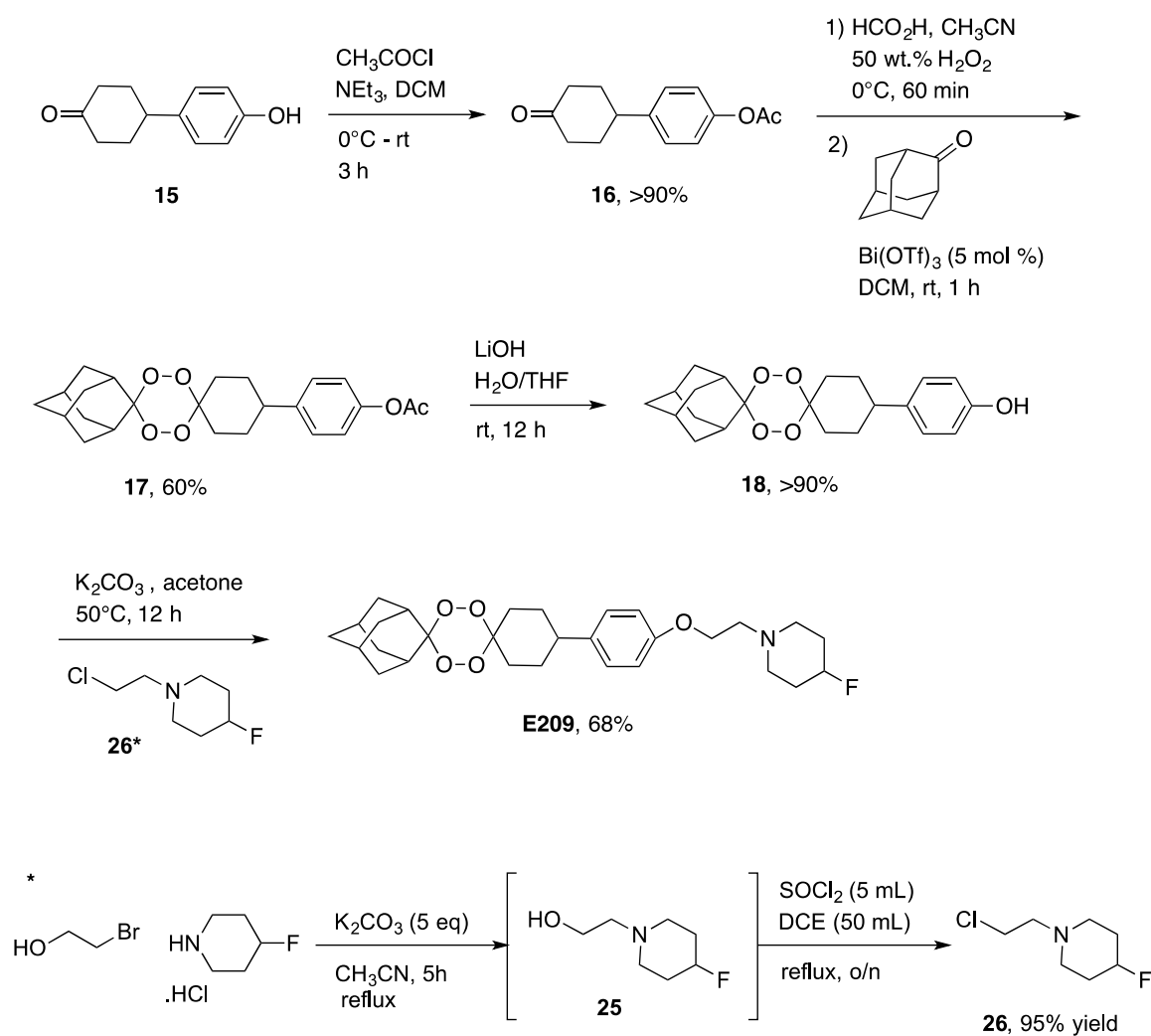
Scheme 5.31. One-pot synthesis of E209 from tetraoxane acetate (**17**) and 1-(2-chloroethyl)-4-fluoropiperidine (**26**)

This transformation was instead carried out in two steps. The first step involved the removal of the acetate using lithium hydroxide and the second was a straightforward nucleophilic substitution reaction between the phenol (**18**) and 1-(2-chloroethyl)-4-fluoropiperidine (**26**) (Scheme 5.32).



Scheme 5.32. Acetate removal and subsequent nucleophilic substitution to generate E209

Despite requiring an extra step, a much-improved yield of 68% was obtained when coupling using the phenol (**18**) rather than the acetate (**17**). The overall synthetic pathway comprised of five simple high-yielding steps, avoiding the use of an ozonolysis reaction and expensive reagents (Scheme 5.33).



Scheme 5.33. Synthesis of E209 using Strategy 4

5.2.9 Conclusion

A number of different routes for the synthesis of E209 were explored, with a reduced number of steps and avoiding the use of an ozonolysis reaction. Initial methods exploring the introduction of an acetal were unsuccessful; therefore a

variety of amide reductions were investigated. A number of these reduction methods proved unsuccessful; however, a triflic anhydride/sodium borohydride method gave the desired product in a 48% yield. A drawback of this route was the low yield for the tetraoxane-forming step. Strategy 3 looked at rearranging the order of each step in order to place this reaction towards the end of the synthetic pathway; however, this proved unsuccessful. Alternative conditions were then trialled in order to improve the yield of this tetraoxane-forming step, and the replacement of rhenium(VII) oxide with bismuth(III) triflate, along with the use of molecular sieves gave a significantly improved yield of 60%.

The final strategy looked at forming the amine side chain first, before coupling with the tetraoxane acetate (**17**). Although a few modifications were required, this strategy proved the most successful, producing E209 in a series of five high-yielding steps.

The aims of this project have not only been met but also surpassed:

- The synthetic pathway to E209 has been successfully optimised for scale up
- E209 is the first tetraoxane to be synthesised with a pharmacokinetic profile comparable to the lead trioxolane OZ439
- E209 is compatible with a single dose cure and suitable for deployment as part of a drug combination

Every aspect of the desired product profile for a novel tetraoxane antimalarial has been achieved and the profile for E209 is comparable to OZ439 in (Figure 5.9). E209 is now in candidate selection for clinical trials.

	E209	OZ439
Simple synthesis	yes	yes
Short number of steps	5	4
Aqueous solubility	>8 mg/mL	6.8 mg/mL
Activity IC ₅₀ <10 nM	5.1 nM	8 nM
Single dose mouse survival	26 days	30 days
Rat blood stability/T _{1/2}	13 hours	>15 hours

Figure 5.9. A comparison of E209 and OZ439

5.3 Back-up Compound

The small intestine is around 7 m long and is the main organ responsible for digestion and absorption of nutrients, vitamins and orally administered drug compounds. When empty (fasted) the pH is around 6.5; however, after a meal (fed state) the pH lowers to around 5. This change in pH can have a significant affect on the solubility of a drug and ultimately result in very different pharmacokinetic profiles for the same compound.^{72,73}

Both E209 and OZ439 were tested for solubility in both Fasted State Stimulated Intestinal Fluid (FaSSIF, pH = 6.5) and Fed State Stimulated Intestinal Fluid (FeSSIF, pH of 5.0) media (Table 5.8). These fluids simulate the juices of the small intestine in both a fasted state and after a meal.

Compound	Media	Solubility ($\mu\text{g/mL}$)	
		1h	4h
OZ439	FeSSIF (pH 5.0)	>1500	>1500
	FaSSIF (pH 6.5)	120	122
E209 mesylate	FeSSIF (pH 5.0)	3355	4495
	FaSSIF (pH 6.5)	117	132

Table 5.8: Solubility data measured at 37°C over a 4-hour incubation period. All solubility values refer to the free base equivalent

E209 showed the best overall solubility, displaying moderate solubility under fasted-state (FaSSIF) conditions and a significant enhancement under fed-state (FeSSIF) conditions. However, this large difference in solubility can lead to a pronounced food effect, where changes in pH in the gastrointestinal tract result in a variable PK profile.⁷⁴

E209 has a higher pKa than OZ439 (12.91 vs. 8 respectively (values calculated using Pipeline Pilot 2017)); therefore the change in pH from 6.5 to 5.0 could have a greater effect on the degree of ionisation for E209. A greater degree of ionisation, could be responsible for the significant increase in solubility observed at pH 6.5, resulting in a food-effect. Therefore another tetraoxane compound was designed and synthesised that was structurally similar to E209, but with a lower pKa, with the aim of preventing the significant change in solubility between fasted and fed states. The structure of this compound is shown below (Figure 5.10). The only difference between E209 and the back-up compound (N327) is the replacement of 4-fluoropiperidine with piperidine in the side-chain.

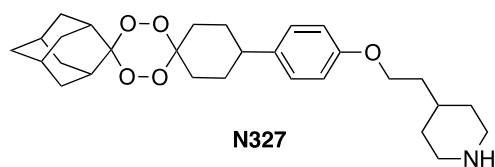
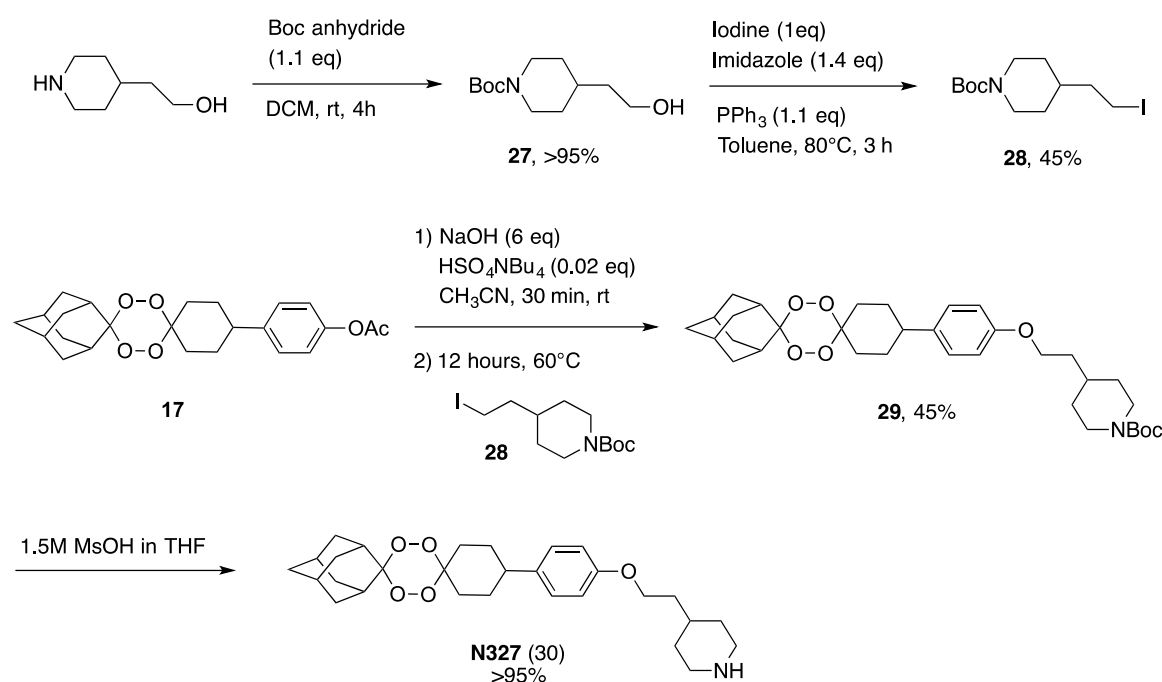


Figure 5.10. The structure of N327 – a back-up compound for E209

5.3.1 Synthesis

The synthesis of N327 is shown in Scheme 5.34.

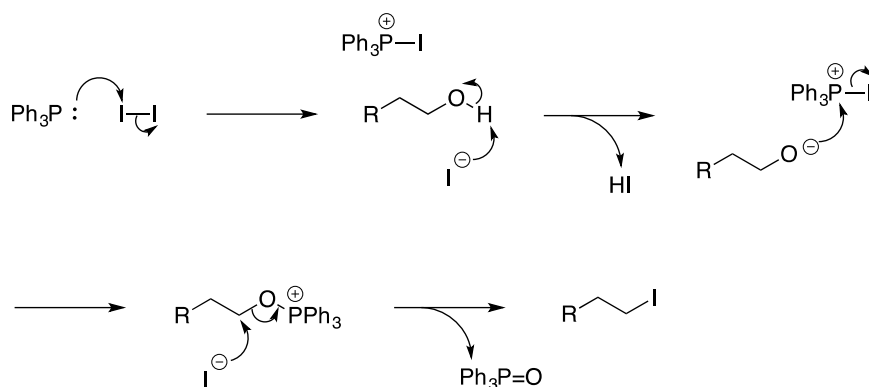


Scheme 5.34. Synthesis of N327 (30) - a back-up compound for E209

The first step involved the boc-protection of 4-piperidine ethanol in order to prevent the amine from interfering with subsequent steps.⁷⁵ Initial attempts to build the side chain in a different order were unsuccessful for this reason. Di-*tert*-butyl dicarbonate is a useful protecting group as it not only allows for transformations to be carried out that would be incompatible with free amines

but is also easily removed under acidic condition.⁷⁶

The next step was to convert the alcohol (**27**) to an alkyl iodide (**28**). This reaction, named after Rolf Appel, is driven by the formation of a strong phosphorous-oxygen bond.⁷⁷ The mechanism can be seen below (Scheme 5.35) and it shows the liberation of both hydrogen iodide and triphenylphosphine oxide. Imidazole was used to capture the hydrogen iodide produced; however, triphenylphosphine oxide was difficult to remove from the product.⁷⁸ The yield of pure product for this step was only 45% as some product was still contaminated with triphenylphosphine oxide, even after purification.



Scheme 5.35. Mechanism of the Appel reaction

Once the alkyl iodide (**28**) was formed, it was coupled to tetraoxane acetate **17**, using the one-pot method described previously. The yield for this step was only 45%. If this synthesis were to be repeated, it might be advantageous to remove the acetate first, before carrying out the nucleophilic substitution; thus forming **29** in two steps rather than one.

The final step in this synthesis involved the removal of the boc-protecting group to reveal the free amine. Common reagents for this transformation include trifluoroacetic acid (TFA) or hydrochloric acid in methanol.^{79,80} The use of TFA successfully removed the boc-group; however, it also led to degradation of the tetraoxane ring. The use of hydrochloric acid in a variety of solvents, including THF, dioxane and methanol was also unsuccessful; whilst the tetraoxane scaffold

remained intact, the boc-group was not removed.

It was therefore decided to use methanesulfonic acid, as this was employed in the synthesis of Vennerstrom's trioxolane compounds.⁷¹ This successfully removed the boc-protecting group whilst leaving the tetraoxane moiety intact, producing the mesylate salt of N327 (**30**) in a quantitative yield. Some of this mesylate salt was also treated with sodium hydroxide to produce the free base of N327 as well.

5.3.2 Conclusion

The back-up compound, designed to reduce the apparent food effect observed with E209, was successfully synthesised in a series of six high-yielding steps. Both the free base of N327 and the mesylate salt were sent for biological testing and testing data is eagerly awaited.

5.4 Experimental

5.4.1 General Background

5.4.1.1 Handling peroxides

Whilst no incidents were encountered in the course of this work, any preparative work with peroxides, particularly those with high active oxygen content, should be conducted with an awareness of the potential for spontaneous and exothermic decomposition reactions. A strict set of rules should be adhered to when forming tetraoxanes in order to avoid the occurrence of such events:

1. These procedures should not be carried out on a larger scale than 10 mmol of starting ketone
2. A blast shield should be placed in front of the reaction and the fume cupboard sash should be fully closed
3. The volume of any solution containing hydrogen peroxide should not be reduced– an aqueous work up should be carried out first to remove it
4. Filtration steps should be carried out using fluted filter paper only – no sinter funnels
5. Concentration of the final compound, before purification, should be carried out on a rotary evaporator inside a fume cupboard. A blast shield should be placed in front of the rotary evaporator and the fume cupboard sash should be fully closed
6. When using a rotary evaporator the water bath temperature should not exceed 20°C and the vacuum should be released slowly.

5.4.1.2 Setting up reactions

All reactions and purifications were carried out in a fume cupboard with appropriate PPE in place. Reactions sensitive to air and moisture were carried out in oven-dried glassware sealed with rubber septa. A nitrogen or argon atmosphere was achieved by manifold or balloon. Sensitive liquids and solutions were transferred via single-use syringes, free from latex and silicone oil.

Reactions, which required heating, were heated in an oil bath and fitted with a reflux condenser. All reactions were stirred using a Teflon coated magnetic stirrer bar and organic solutions were concentrated using a Büchi rotary evaporator with a vacuum pump.

5.4.1.3 Purification of reagents and organic solvents

Anhydrous solvents were obtained from Sigma Aldrich.

All reagents were purchased from Sigma Aldrich, Alfa Aesar and Apollo Scientific and were used without further purification.

5.4.1.4 Purification of products

Analytical thin layer chromatography (TLC) was carried out using Merck TLC Silica gel 60 F₂₅₄ aluminium sheets and visualized under UV or by appropriate stain. Iodine, *p*-anisaldehyde and potassium permanganate were most useful for visualizing tetraoxane compounds. Column chromatography was carried out using Sigma Aldrich technical grade silica gel (pore size 60 Å, 230-400 mesh particle size, 40-63 µm particle size).

5.4.1.5 Analysis

¹H NMR Spectra were recorded on a Bruker AMX400 (400 MHz) or Bruker AMX500 (500 MHz). The chemical shifts (δ) are described in parts per million (ppm) downfield from an internal standard of tetramethylsilane. Multiplicities are singlet (s), doublet (d), triplet (t), quartet (q), doublet of doublets (dd), doublet of triplets (dt), triplet of doublets (td), doublet of doublet of doublets (ddd) and multiplet (m). Coupling values are measured in Hz. ¹³C NMR spectra were also recorded on a Bruker AMX400 (101 MHz) and chemical shifts are reported relative to a residual solvent peak. Mass Spectra were recorded on a Micromass LCT or an Agilent QTOF 7200 Mass Spectrometer using chemical ionisation (CI) or electron spray (ES). Microanalyses (%C, %H, %N) were carried out in the University of Liverpool Microanalysis laboratory.

5.4.2 General Procedures

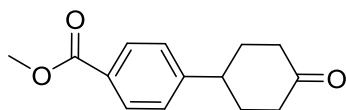
5.4.2.1 General procedure A: Amine formation

To a stirred solution of 4-((1r,3r,5r,7r)-dispiro[adamantane-2,3'-[1,2,4,5]tetraoxane-6',1''-cyclohexan]-4''-yl)benzyl methanesulfonate (1 eq) in anhydrous DCM (40 mL/g) were added triethylamine (2 eq) and the required amine (2 eq) at 0°C. The reaction mixture was stirred at room temperature over a period of 12 hours. The resulting reaction mixture was diluted with DCM (50 mL) and washed with water (3 x 20 mL) and brine (10 mL). The organic phase was dried over Na₂SO₄, filtered and concentrated under reduced pressure. The crude residue was then purified by flash column chromatography to give the desired amine.

5.4.2.2 General Procedure B: A one-pot hydrolysis and alkylation of the tetraoxane acetate unit

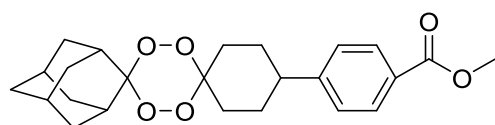
To a stirred solution of 4-(dispiro[cyclohexane-1,3'-[1,2,4,5]tetraoxane-6',2''-tricyclo[3.3.1.1^{3,7}]decan]4-yl)phenyl acetate (1 eq) in acetonitrile (20 mL/g) were added powdered sodium hydroxide (6 eq) and tetrabutylammonium hydrogensulfate (0.2 eq). The resulting turbid solution was warmed to 25°C for one hour. A solution of the required alkyl halide (2 eq) in acetonitrile (20 mL/g) was then added and the resulting reaction mixture was heated to 60°C overnight. The inorganic solid was then filtered off and washed thoroughly with DCM. The filtrate was then washed with water (20 mL) and brine (20 mL), dried over MgSO₄, filtered and concentrated under reduced pressure. The crude products were then purified by flash chromatography.

5.4.3 Experimental



Methyl 4-(4-oxocyclohexyl)benzoate (2).⁹

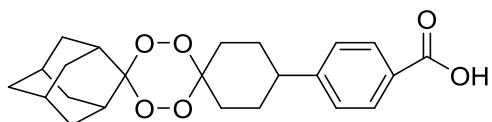
A solution of oxalyl chloride (1.31 mL, 15.3 mmol) in DCM (20 mL) was added to a suspension of 4-phenylcyclohexanone (2 g, 11.5 mmol) and AlCl₃ (4.14 g, 31.1 mmol) in DCM (20 mL) at 0°C. The reaction mixture was stirred at 0°C for 1 hour then at room temperature for 2 hours. A mixture of methanol (10 mL) and pyridine (2.3 mL) was added drop-wise to the reaction mixture, which was left to stand overnight. The reaction mixture was then washed with water (30 mL), 3N HCl (20 mL), NaHCO₃ (30 mL), dried over NaSO₄, filtered and concentrated under reduced pressure. Purification by flash column chromatography gave the title compound as a white solid (1.73 g, 65% yield): ¹H NMR (400 MHz, CDCl₃) δ = 8.00 (d, *J* = 8 Hz, 2H), 7.32 (d, *J* = 8 Hz, 2H), 3.92 (s, 2H), 3.10 (tt, *J* = 11 Hz, 3.0 Hz, 1H), 2.53 (dd, *J* = 10 Hz, 5 Hz, 4H), 2.28-2.20 (m, 2H), 2.03-1.90 (m, 2H) ppm; ¹³C NMR (101 MHz, CDCl₃) δ = 211.0, 167.3, 150.5, 130.4, 129.0, 127.2, 52.5, 43.2, 41.6, 34.2 ppm; HRMS (ES, *m/z*) calcd for [C₁₄H₁₆NaO₃] (M+Na)⁺ 255.0997, found 255.0989.



Methyl 4-(((1r,3r,5r,7r)-dispiro[adamantane-2,3'-[1,2,4,5]tetraoxane-6',1''-cyclohexan]-4''-yl)benzoate (4).¹⁴

To a stirred solution of methyl 4-(4-oxocyclohexyl)benzoate (2g, 8.5 mmol) in acetonitrile (10 mL) were added formic acid (10 mL) and 50% H₂O₂ (8 mL) at 0°C. The resulting reaction mixture was stirred for 30 min at 0°C, warmed to room temperature and diluted with water (30 mL). The resulting mixture was extracted with DCM (3 x 30 mL). The combined organic layers were then washed with water (3 x 30 mL) and brine (30 mL), dried over MgSO₄, filtered and

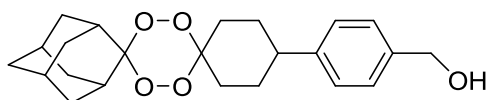
concentrated under reduced pressure. The resulting white solid was then re-dissolved in anhydrous DCM (15 mL) and added to a stirring solution of 2-adamantanone (1.91 g, 12.8 mmol) and rhenium (VII) oxide (82 mg, 0.17 mmol) in DCM (20 mL) at room temperature. The reaction mixture was stirred for 1 hour, filtered through a plug of silica and concentrated. Purification by flash column chromatography gave the title compound as a white powder (1.69 g, 48% yield): ^1H NMR (400 MHz, CDCl_3) δ = 7.89 (d, J = 8 Hz, 2H), 7.22 (d, J = 8 Hz, 2H), 3.83 (s, 3H), 2.60 (tt, J = 12 Hz, 4 Hz, 1H), 2.06-1.44 (m, 23H) ppm; ^{13}C NMR (101 MHz, CDCl_3) δ = 167.4, 151.6, 130.2, 128.7, 127.3, 111.0, 107.7, 52.5, 44.1, 37.4, 34.7, 33.6, 29.9, 27.5 ppm; LRMS (ES, m/z) calcd for $[\text{C}_{24}\text{H}_{30}\text{NaO}_6]$ ($\text{M}+\text{Na}$) $^+$ 437.1940, found 437.2.



4-((1r,3r,5r,7r)-Dispiro[adamantane-2,3'-[1,2,4,5]tetraoxane-6',1''-cyclohexan]-4''-yl)benzoic acid.

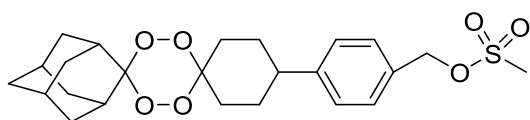
A solution of methyl 4-((1r,3r,5r,7r)-dispiro[adamantane-2,3'-[1,2,4,5]tetraoxane-6',1''-cyclohexan]-4''-yl)benzoate (1.59 g, 3.86 mmol) in 10% w/v potassium hydroxide/methanol (12.6 mL) was stirred at reflux for 90 min. The solution was allowed to cool to room temperature before concentrating under reduced pressure. The resulting residue was taken up in water (15 mL) and washed with diethyl ether (3 x 20 mL). The aqueous layer was acidified with concentrated hydrochloric acid and a white precipitate formed. Diethyl ether (20 mL) was added to dissolve the precipitate and the aqueous phase was extracted with diethyl ether (2 x 20 mL). The combined organic phases were washed with brine (30 mL), dried over Na_2SO_4 , filtered and concentrated under reduced pressure to give a white solid. Recrystallization from ethanol gave the title compound as a white solid (1.54 g, 91% yield): ^1H NMR (400 MHz, CDCl_3) δ = 8.04 (d, J = 8 Hz, 2H), 7.34 (d, J = 8 Hz, 2H), 2.75-2.66 (m, 1H), 2.12-1.45 (m, 22H) ppm; ^{13}C NMR (101 MHz, CDCl_3) δ = 171.3, 155.3, 132.8, 131.0, 129.1, 127.3,

126.8, 114.4, 44.5, 36.7, 33.8, 32.9, 27.9, 25.8 ppm; HRMS (ES, m/z) calcd for $[C_{23}H_{27}O_6]^-$ (M-H) $^-$ 399.1808, found 399.1808.



4-((1r,3r,5r,7r)-Dispiro[adamantane-2,3'-[1,2,4,5]tetraoxane-6',1''-cyclohexan]-4''-yl)phenyl)methanol (5).

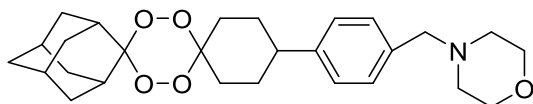
To a stirred solution at 0°C of methyl 4-(4-oxocyclohexyl)benzoate (1.5 g, 3.65 mmol) in THF (50 mL) was added $LiAlH_4$ (0.28 g, 7.29 mmol). The suspension was stirred at 0°C and was monitored by TLC to determine the consumption of the benzoate. The reaction mixture was quenched with 1N HCl and was then extracted with ethyl acetate (3 x 30 mL). The combined organic layers were dried over Na_2SO_4 , filtered and concentrated under reduced pressure. Purification by flash column chromatography gave the title compound as a white solid (1.36 g, >95% yield): 1H NMR (400 MHz, $CDCl_3$) δ = 7.27 (d, J = 8 Hz, 2H), 7.21 (d, J = 8 Hz, 2H), 4.62 (s, 2H), 2.62 (tt, J = 11 Hz, 4 Hz, 1H), 2.08-1.57 (m, 22H) ppm; ^{13}C NMR (101 MHz, $CDCl_3$) δ = 145.9, 139.3, 127.6, 110.9, 107.9, 65.6, 60.8, 43.8, 37.4, 36.2, 34.7, 33.6, 30.1, 27.5 ppm; HRMS (ES, m/z) calcd for $[C_{23}H_{30}NaO_5]^+$ (M+Na) $^+$ 409.1991, found 409.1990.



4-((1r,3r,5r,7r)-Dispiro[adamantane-2,3'-[1,2,4,5]tetraoxane-6',1''-cyclohexan]-4''-yl)benzyl methanesulfonate (6).

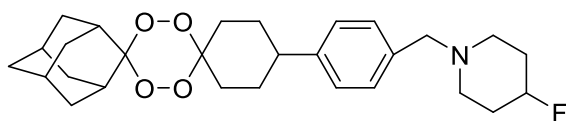
Methanesulfonyl chloride (0.26 mL, 3.36 mmol) and triethylamine (0.50 mL, 3.62 mmol) were added at 0°C under nitrogen atmosphere to a solution of 4-((1r,3r,5r,7r)-dispiro[adamantane-2,3'-[1,2,4,5]tetraoxane-6',1''-cyclohexan]-4''-yl)phenyl)methanol (698 mg, 1.81 mmol) in anhydrous THF (30 mL). The reaction mixture was warmed to room temperature and stirred for 90 minutes. The reaction mixture was then diluted with brine and extracted with ethyl

acetate (3 x 30 mL). The combined organics were then dried over Na₂SO₄, filtered and concentrated under reduced pressure to give the title compound as colourless oil (722 mg, 86% yield): ¹H NMR (400 MHz, CDCl₃) δ = 7.36 (d, *J* = 8 Hz, 2H), 7.27 (d, *J* = 8 Hz, 2H), 5.21 (s, 2H), 2.92 (s, 3H), 2.64 (tt, *J* = 11 Hz, 4 Hz, 1H), 2.09-1.56 (m, 22H) ppm; HRMS (ES, *m/z*) calcd for [C₂₄H₃₂NaO₇] (M+Na)⁺ 487.1766, found 487.176.



4-(4-((1r,3r,5r,7r)-Dispiro[adamantane-2,3'-[1,2,4,5]tetraoxane-6',1''-cyclohexan]-4''-yl)benzyl)morpholine (N205 (7)).

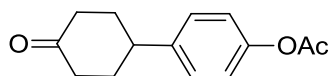
General procedure A was followed using morpholine (0.1 mL, 1.11 mmol) to give the title compound as a white solid (97 mg, 48% yield): Mp 138-140°C; ¹H NMR (400 MHz, CDCl₃) δ = 7.24 (d, *J* = 8 Hz, 2H), 7.17 (d, *J* = 8 Hz, 2H), 3.73-3.68 (m, 4H), 3.46 (s, 2H), 2.67-2.54 (m, 1H), 2.43 (bs, 4H), 2.09-1.58 (m, 22H) ppm; ¹³C NMR (101 MHz, CDCl₃) δ = 145.2, 136.0, 129.7, 127.1, 110.9, 107.9, 67.4, 63.6, 54.0, 43.8, 37.4, 34.8, 33.6, 33.4, 32.3, 30.1, 27.5 ppm; HRMS (CI, *m/z*) calcd for [C₂₇H₃₈NO₅] (M+H)⁺ 456.2750, found 456.2762.



1-(4-((1r,3r,5r,7r)-dispiro[adamantane-2,3'-[1,2,4,5]tetraoxane-6',1''-cyclohexan]-4''-yl)benzyl)-4-fluoropiperidine (N214 (8)).

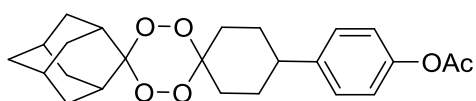
General procedure A was followed using 4-fluoropiperidine hydrochloride (141 mg, 1.6 mmol) to give the title compound as a white solid (159 mg, 52% yield): Mp 122-124°C; ¹H NMR (400 MHz, CDCl₃) δ = 7.23 (d, *J* = 8 Hz, 2H), 7.17 (d, *J* = 8 Hz, 2H), 4.79-4.53 (m, 1H), 3.46 (s, 2H), 2.64-2.53 (m, 5H), 2.40-2.31 (m, 4H), 2.06-1.54 (m, 22H) ppm; ¹³C NMR (101 MHz, CDCl₃) δ = 145.1, 136.6, 129.6, 127.1, 110.9, 107.9, 90.0, 88.3, 63.1, 50.0, 43.8, 37.4, 34.7, 33.6, 32.3, 31.9, 30.6,

27.5 ppm; HRMS (CI, m/z) calcd for $[C_{28}H_{39}NO_4F]$ (M+H)⁺ 472.2863, found 472.2859.



4-(4-Oxocyclohexyl)phenyl acetate (16).

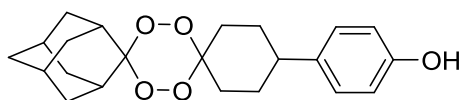
To a stirred solution of 4-(4-hydroxyphenyl)cyclohexanone (4 g, 21.0 mmol) and triethylamine (5.85 mL, 42.0 mmol) in anhydrous dichloromethane was added acetic anhydride (5.96 mL, 63.0 mmol) at 0°C. The reaction mixture was then allowed to warm to room temperature and stirred for 2 hours. The reaction mixture was then washed with water (3 x 30 mL), sodium bicarbonate (2 x 30 mL) and brine (30 mL). The organic layer was dried with MgSO₄, filtered and concentrated under reduced pressure. The resulting residue was triturated using *n*-hexane and diethyl ether to yield 4-(4-oxocyclohexyl)phenyl acetate (4.56 g, 95% yield) as a white solid. ¹H NMR (400 MHz, CDCl₃) δ = 7.25 (d, J = 8 Hz, 2H), 7.04 (d, J = 8 Hz, 2H), 3.03 (t, J = 12 Hz, 1H), 2.51 (dd, J = 11, 4 Hz, 2H), 2.30 (s, 3H), 2.22 (d, J = 14 Hz, 2H), 1.98 – 1.86 (m, 2H) ppm; ¹³C NMR (101 MHz, CDCl₃) δ = 211.06, 169.76, 149.32, 142.42, 127.78, 121.76, 42.35, 41.44, 34.13, 21.26 ppm; HRMS (ES, m/z) calcd for $[C_{14}H_{16}NaO_3]$ (M+Na)⁺ 255.0997, found 255.0995.



4-(Dispiro[cyclohexane-1,3'-[1,2,4,5]tetroxane-6',2''-tricyclo[3.3.1.1.3,7]decan]4-yl)phenyl acetate (17).¹⁴

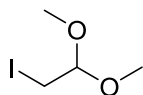
To a stirred solution of 4-(4-oxocyclohexyl)phenyl acetate (2 g, 8.61 mmol) in acetonitrile (10 mL) and formic acid (10 mL) was slowly added hydrogen peroxide solution (9 mL, 50 wt. % in H₂O) at 0°C. The reaction mixture was then stirred at room temperature for 1 hour. The reaction mixture was diluted with water before extracting with DCM (3 x 30 mL). The combined organic layers were then washed with water (3 x 30 mL) and brine (30 mL), dried over MgSO₄,

filtered and concentrated under reduced pressure. The resulting white solid was then re-dissolved in anhydrous DCM (15 mL) before addition of 2-adamantanone (1.68 g, 11.18 mmol) and rhenium(VII) oxide (0.17 mmol, 83 mg). The resulting mixture was stirred under a nitrogen atmosphere at room temperature for 2 hours. The reaction mixture was then filtered through a pad of silica and concentrated. Purification by column chromatography (5% ethyl acetate/*n*-hexane) gave the title compound (1.49 g, 41% yield) as a white solid: ^1H NMR (400 MHz, CDCl_3) δ = 7.22 (d, J = 8 Hz, 2H), 7.00 (d, J = 8 Hz, 2H), 2.61 (t, J = 12 Hz, 1H), 2.29 (s, 3H), 2.13 – 1.55 (m, 22H) ppm; ^{13}C NMR (101 MHz, CDCl_3) δ = 169.84, 149.08, 143.55, 127.93, 121.53, 110.66, 107.58, 47.11, 43.25, 39.39, 37.09, 36.43, 33.30, 27.58, 27.20, 21.28 ppm; HRMS (ES, m/z) calcd for $[\text{C}_{24}\text{H}_{30}\text{NaO}_6]$ ($\text{M}+\text{Na}$) $^+$ 437.1940, found 437.1937.



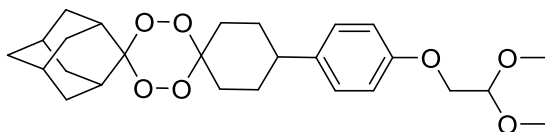
4-(Dispiro[cyclohexane-1,3'-[1,2,4,5]tetroxane-6',2''-tricyclo[3.3.1.1.3,7]decan]4-yl)phenol (18).

To a stirred solution of 4-(dispiro[cyclohexane-1,3'-[1,2,4,5]tetroxane-6',2''-tricyclo[3.3.1.1.3,7]decan]4-yl)phenyl acetate (730 mg, 1.76 mmol) in THF (8 mL) was added lithium hydroxide (126 mg, 5.28 mmol) in water (4 mL). The reaction mixture was then stirred at room temperature for 2 hours. The reaction mixture was neutralised with dilute hydrochloric acid before carefully removing the THF under reduced pressure. The resulting colourless solution was extracted with DCM (3 x 30 mL). The combined organics were washed with brine (30 mL), dried over MgSO_4 , filtered and concentrated under reduced pressure to give the title compound as a white solid (544 mg, 83% yield): ^1H NMR (400 MHz, CDCl_3) δ = 7.09 (d, J = 8 Hz, 2H), 6.76 (d, J = 8 Hz, 2H), 4.63 (s, 1H), 3.26 - 3.20 (m, 2H), 2.55 (t, J = 11 Hz, 1H), 2.12 – 1.60 (m, 20H); ^{13}C NMR (101 MHz, CDCl_3) δ = 153.98, 138.42, 128.06, 115.33, 110.64, 107.70, 42.93, 39.42, 38.64, 37.12, 33.32, 27.22 ppm; LRMS (ES, m/z) calcd for $[\text{C}_{22}\text{H}_{28}\text{NaO}_5]^+$ ($\text{M}+\text{Na}$) $^+$ 395.1834, found 395.2.



2-Iodo-1,1-dimethoxyethane.⁸¹

Sodium iodide (1.06 g, 7.10 mmol) was added to a solution of 2-bromo-1,1-dimethoxyethane (0.7 mL, 5.92 mmol), in acetone (10 mL), in a sealed tube. The resulting solution was heated to 120°C overnight. 1% aqueous sodium sulfite solution (10 mL) was then added to quench the reaction before extraction with ethyl acetate (3 x 20 mL). The combined organics were then washed with water (30 mL) and brine (30 mL), dried over MgSO₄, filtered and concentrated under reduced pressure to give the title compound as a yellow liquid (550 mg, 43% yield): ¹H NMR (400 MHz, CDCl₃) δ = 4.48 (t, *J* = 5 Hz, 1H), 3.38 (s, 6H), 3.21 (d, *J* = 5 Hz, 2H) ppm; ¹³C NMR (101 MHz, CDCl₃) δ = 103.51, 53.87, 4.26 ppm; Sample too volatile for MS.



(1r,3r,5r,7r)-4''-(4-(2,2-Dimethoxyethoxy)phenyl)dispiro[adamantane-2,3'-[1,2,4,5]tetraoxane-6',1''-cyclohexane] (21).

Method 1:

To a stirred solution of 4-(dispiro[cyclohexane-1,3'-[1,2,4,5]tetraoxane-6',2''-tricyclo[3.3.1.1^{3,7}]decan]4-yl)phenol (300 mg, 0.81 mmol) in acetonitrile (30 mL) was added potassium carbonate (668 mg, 4.84 mmol) and 2-bromo-1,1-dimethoxyethane (0.42 mL, 3.54 mmol). The resulting reaction mixture was heated to 80°C for 3 days. The reaction mixture was then diluted with water and extracted with ethyl acetate (3 x 30 mL). The combined organics were washed with brine (30 mL), dried over MgSO₄, filtered and concentrated under reduced pressure to give the title compound as a white solid (50 mg, 13% yield).

Method 2:

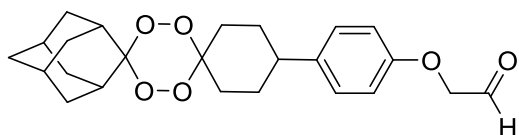
General procedure B was followed using 2-bromo-1,1-dimethoxyethane (0.29 mL, 2.42 mmol). Purification by column chromatography (20:1 *n*-hexane/ethyl acetate) gave the title compound as a white solid (98 mg, 18% yield).

Method 3:

General procedure B was followed using 2-iodo-1,1-dimethoxyethane (536 mg, 2.48 mmol). Purification by column chromatography (20:1 *n*-hexane/ethyl acetate) gave the title compound as a white solid (77 mg, 14% yield).

Analysis:

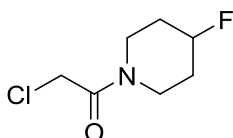
^1H NMR (400 MHz, CDCl_3) δ = 7.13 (d, J = 8 Hz, 2H), 6.86 (d, J = 8 Hz, 2H), 4.71 (t, J = 5 Hz, 1H), 3.98 (d, J = 5 Hz, 2H), 3.45 (s, 6H), 2.56 (t, J = 11 Hz, 1H), 2.09 – 1.61 (m, 22H) ppm; ^{13}C NMR (101 MHz, CDCl_3) δ = 157.08, 138.73, 127.86, 114.71, 110.62, 107.69, 102.30, 67.79, 54.18, 42.93, 37.13, 33.32, 29.87, 27.23 ppm; HRMS (ES, m/z) calcd for $[\text{C}_{26}\text{H}_{36}\text{NaO}_7]^+$ ($\text{M}+\text{Na}$) $^+$ 483.2359, found 483.2354.



2-(4-((1r,3r,5r,7r)-Dispiro[adamantane-2,3'-[1,2,4,5]tetraoxane-6',1''-cyclohexan]-4''-yl)phenoxy)acetaldehyde (20).

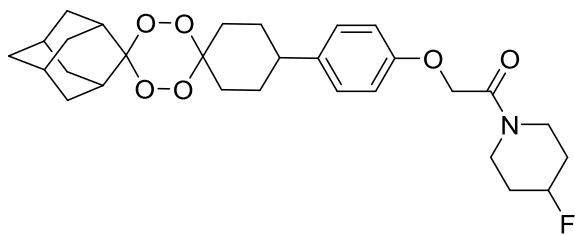
To a stirred solution of (1r,3r,5r,7r)-4''-(4-(2,2-dimethoxyethoxy)phenyl)dispiro[adamantane-2,3'-[1,2,4,5]tetraoxane-6',1''-cyclohexane] (98 mg, 0.21 mmol) in anhydrous THF (10 mL) and acetone (5 mL) was added 4N HCl (10 mL) at 0°C. The reaction mixture was then warmed to room temperature and stirred overnight. The reaction mixture was then neutralised with 2M NaOH and extracted with ethyl acetate (3 x 30mL). The combined organics were then washed with water (30 mL) and brine (30 mL), dried over MgSO_4 , filtered and concentrated under reduced pressure. The resulting colourless oil was taken forward without further purification (88 mg, 90% yield): ^1H NMR (400 MHz, CDCl_3) δ = 9.86 (s, 1H), 7.17 (d, J = 9 Hz, 2H), 6.83

(d, $J = 9$ Hz, 2H), 4.55 (s, 2H), 3.70 (t, $J = 6$ Hz, 1H), 3.59 (t, $J = 6$ Hz, 1H), 3.33 – 3.15 (m, 2H), 2.62 – 2.53 (m, 2H), 2.03 – 1.56 (m, 17H) ppm; ^{13}C NMR (101 MHz, CDCl_3) $\delta = 199.80, 156.23, 139.67, 128.17, 114.67, 110.66, 107.63, 72.95, 45.04, 42.93, 39.41, 37.11, 33.31, 30.47, 30.08, 29.41, 29.18, 27.22$ ppm; HRMS (ES, m/z) calcd for $[\text{C}_{25}\text{H}_{34}\text{NaO}_7]^+$ ($\text{M}+\text{Na}+\text{MeOH}$) $^+$ 469.2202, found 469.2194.



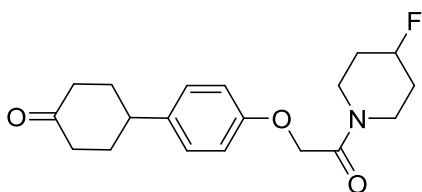
2-Chloro-1-(4-fluoropiperidin-1-yl)ethan-1-one (22).

To a stirred solution of 4-fluoropiperidine hydrochloride (402 mg, 2.88 mmol) in anhydrous DCM (30 mL) was added chloroacetyl chloride (0.17 mL, 2.21 mmol) and triethylamine (0.92 mL, 6.63 mmol). The resulting reaction mixture was stirred overnight under a nitrogen atmosphere. The reaction mixture was then diluted with water (30 mL) and extracted with DCM (3 x 30 mL). The combined organic layers were washed with 2M HCl (20 mL), NaHCO_3 (20 mL) and brine (30 mL). The organic layer was then dried over MgSO_4 , filtered and concentrated under reduced pressure to give the title compound as a yellow oil (385 mg, >95% yield): ^1H NMR (400 MHz, CDCl_3) $\delta = 4.90$ (d, $J = 47$ Hz, 1H), 4.15 – 4.02 (m, 2H), 3.95 (dt, $J = 10, 5$ Hz, 1H), 3.67 – 3.50 (m, 2H), 3.49 – 3.38 (m, 1H), 2.01 – 1.74 (m, 4H) ppm; ^{13}C NMR (101 MHz, CDCl_3) $\delta = 165.19, 88.08, 86.38, 42.38, 42.33, 41.08, 38.22, 38.17, 31.74, 31.54, 30.84, 30.64$ ppm; LRMS (CI, m/z) calcd for $[\text{C}_7\text{H}_{12}\text{ClFNO}]^+$ ($\text{M}+\text{H}$) $^+$ 180.0591, found 180.1.



2-(4-((1r,3r,5r,7r)-Dispiro[adamantane-2,3'-[1,2,4,5]tetraoxane-6',1''-cyclohexan]-4''-yl)phenoxy)-1-(4-fluoropiperidin-1-yl)ethan-1-one (23).⁵³

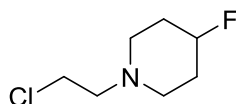
General procedure B was followed using 2-chloro-1-(4-fluoropiperidin-1-yl)ethan-1-one (260 mg, 1.45 mmol). Purification by column chromatography (5:1 *n*-hexane/ethyl acetate) gave the title compound as a white solid (331 mg, 89% yield): ¹H NMR (400 MHz, CDCl₃) δ = 7.14 (d, *J* = 8 Hz, 2H), 6.87 (d, *J* = 8 Hz, 2H), 4.87 (d, *J* = 47 Hz, 1H), 4.72 – 4.60 (m, 2H), 3.91 (dt, *J* = 9, 4 Hz, 1H), 3.62 (t, *J* = 6, 2H), 3.53 – 3.42 (m, 1H), 3.35 – 3.14 (m, 2H), 2.61 – 2.52 (m, 1H), 2.07 – 1.57 (m, 24H) ppm; ¹³C NMR (101 MHz, CDCl₃) δ = 166.67, 156.38, 139.31, 128.05, 114.57, 110.64, 107.65, 88.42, 86.72, 68.08, 42.90, 41.47, 38.20, 37.08, 33.29, 31.95, 31.75, 31.05, 30.85, 27.19 ppm; HRMS (ES, *m/z*) calcd for [C₂₉H₃₈NNaO₆]⁺ (M+Na)⁺ 538.2581, found 538.2577.



4-(4-(2-(4-Fluoropiperidin-1-yl)-2-oxoethoxy)phenyl)cyclohexan-1-one (24).

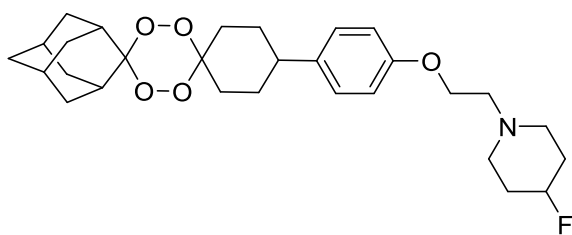
To a stirred solution of 4-(4-hydroxyphenyl)cyclohexanone (191 mg, 1.00 mmol) in acetone (30 mL) was added potassium carbonate (207 mg, 1.10 mmol) and 2-chloro-1-(4-fluoropiperidin-1-yl)ethan-1-one (198 mg, 1.10 mmol). The resulting turbid solution was heated to 50°C overnight. TLC showed the presence of starting materials, therefore anhydrous DMF (10 mL) was added to the reaction mixture to aid solubility. The resulting solution was stirred for a further 18 hours. The reaction mixture was then washed with NaHCO₃ (3 x 30 mL), water (30 mL) and brine (30 mL). The organic phase was then dried over MgSO₄, filtered and concentrated under reduced pressure to give the crude product as a

cream solid. Purification by column chromatography (5:1 (increasing to 5:3) *n*-hexane/ethyl acetate) gave the title compound as a white solid (254 mg, 76% yield): ^1H NMR (400 MHz, CDCl_3) δ = 7.17 (d, J = 9 Hz, 2H), 6.94 – 6.87 (d, J = 9 Hz, 2H), 4.98 – 4.77 (m, 1H), 4.74 – 4.62 (m, 2H), 3.91 (dt, J = 13, 5 Hz, 1H), 3.69 – 3.58 (m, 2H), 3.56 – 3.42 (m, 1H), 2.99 (tt, J = 12, 3 Hz, 1H), 2.60 – 2.42 (m, 4H), 2.25 – 2.16 (m, 2H), 1.99 – 1.71 (m, 6H) ppm; ^{13}C NMR (101 MHz, CDCl_3) δ = 211.32, 166.60, 156.63, 138.15, 127.92, 114.77, 88.38, 86.68, 68.06, 42.05, 41.50, 41.41, 38.27, 38.21, 34.27, 31.97, 31.77, 31.07, 30.86 ppm; HRMS (ES, m/z) calcd for $[\text{C}_{19}\text{H}_{24}\text{FNNaO}_3]^+$ ($\text{M}+\text{Na}$) $^+$ 356.1638, found 353.1634.



1-(2-Chloroethyl)-4-fluoropiperidine (26).¹⁰

To a stirred solution of 4-fluoropiperidine hydrochloride (1 g, 7.16 mmol) and potassium carbonate (4.95 g, 35.8 mmol) in acetonitrile (40 mL) was added 2-bromoethanol (1.01 mL, 14.3 mmol). The resulting solution was refluxed for 5 hours and cooled to room temperature. The reaction mixture was then filtered and the resulting filtrate was concentrated under reduced pressure. The resulting residue was dissolved in 1,2-dichloroethane (40 mL) and thionyl chloride (5 mL) was added at room temperature. The reaction mixture was then refluxed overnight under a nitrogen atmosphere. The reaction mixture was concentrated under reduced pressure and the resulting residue washed thoroughly with diethyl ether. Drying under reduced pressure gave the title compound as a white solid (1.13 g, 95% yield): ^1H NMR (500 MHz, CDCl_3) δ = 5.02 (d, J = 47 Hz, 1H), 4.11 (t, J = 7 Hz, 2H), 3.56 (dd, J = 12, 3 Hz, 2H), 3.39 (dd, J = 11, 6 Hz, 2H), 3.22 – 3.13 (m, 2H), 2.74 – 2.56 (m, 2H), 2.25 – 2.16 (m, 2H) ppm; ^{13}C NMR (101 MHz, CDCl_3) δ = 84.16, 82.45, 58.55, 48.22, 36.52, 27.91, 27.71 ppm; HRMS (CI, m/z) calcd for $[\text{C}_7\text{H}_{14}\text{ClFN}]^+$ ($\text{M}+\text{H}$) $^+$ 166.0799, found 166.0789.



1-(2-(4-((1r,3r,5r,7r)-Dispiro[adamantane-2,3'-[1,2,4,5]tetraoxane-6',1''-cyclohexan]-4''-yl)phenoxy)ethyl)-4-fluoropiperidine (14).

Method 1:

To a stirred solution of 2-(4-((1r,3r,5r,7r)-dispiro[adamantane-2,3'-[1,2,4,5]tetraoxane-6',1''-cyclohexan]-4''-yl)phenoxy)acetaldehyde (77 mg, 0.19 mmol) in anhydrous DCM (10 mL) was added 4-fluoropiperidine hydrochloride (39 mg, 0.28 mmol). The resulting solution was stirred at room temperature for 3 hours. Sodium triacetoxyborohydride (60 mg, 0.28 mmol) was then added and the reaction mixture stirred overnight under a nitrogen atmosphere. The reaction mixture was adjusted to pH 8 using NaHCO₃ before filtering through a pad of celite. The filtrate was extracted with DCM (3 x 20 mL) and the combined organics were washed with brine (30 mL), dried over Na₂SO₄, filtered and concentrated under reduced pressure. Purification by column chromatography (1:1 *n*-hexane/ethyl acetate rising to 100% ethyl acetate) gave the title compound as a pale yellow solid (64 mg, 68% yield).

Method 2:

To a stirred solution of 2-(4-((1r,3r,5r,7r)-dispiro[adamantane-2,3'-[1,2,4,5]tetraoxane-6',1''-cyclohexan]-4''-yl)phenoxy)-1-(4-fluoropiperidin-1-yl)ethan-1-one (133 mg, 0.26 mmol) in anhydrous DCM (10 mL) was added trifluoromethanesulfonic anhydride (0.05 mL, 0.29 mmol) at 0°C. The resulting colourless solution was stirred under a nitrogen atmosphere for 30 minutes. Sodium borohydride (15 mg, 0.39 mmol) and THF (5 mL, dropwise) were then added to the reaction mixture and it was allowed to warm to room temperature before stirring overnight. The pH was adjusted to 11 by addition of saturated aqueous sodium carbonate solution at 0 °C. The cooled aqueous solution was extracted with ethyl acetate (3 x 30 mL). The combined organic layers were washed with brine (30 mL), dried over anhydrous Na₂SO₄, filtered, and

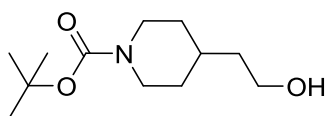
concentrated under reduced pressure. Purification by column chromatography (1:1 *n*-hexane/ethyl acetate rising to 100% ethyl acetate) gave the title compound as a pale yellow solid (62 mg, 48% yield).⁶⁵

Method 3:

General procedure B was followed using 1-(2-chloroethyl)-4-fluoropiperidine (122 mg, 0.74 mmol) to give the title compound as a pale yellow solid (70 mg, 38% yield).

Analysis:

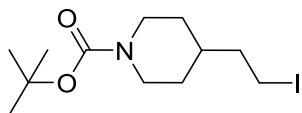
¹H NMR (400 MHz, CDCl₃) δ = 7.13 (d, *J* = 9 Hz, 2H), 6.83 (d, *J* = 9 Hz, 2H), 4.70 (d, *J* = 48 Hz, 1H), 4.09 (t, *J* = 6 Hz, 2H), 3.48 – 3.37 (m, 2H), 3.33 – 3.16 (m, 2H), 2.83 (t, *J* = 6 Hz, 2H), 2.77 – 2.68 (m, 2H), 2.61 – 2.51 (m, 3H), 2.03 – 1.60 (m, 22H) ppm; ¹³C NMR (101 MHz, CDCl₃) δ = 157.2, 139.0, 128.2, 114.9, 110.9, 107.9, 66.3, 65.5, 57.3, 49.7, 43.2, 37.4, 34.8, 33.6, 30.9, 27.5, 22.2 ppm; HRMS (CI, *m/z*) calcd for [C₂₉H₄₁FNO₅]⁺ (M+Na)⁺ 502.2969, found 502.2962; Anal. Calcd for C₂₉H₄₀FNO₅: C, 69.44; H, 8.04; N, 2.79. Found: C, 69.57; H, 8.29; N, 2.41; IR (neat) ν 2929 (m, C-H aromatic), 1510 (m, C-C aromatic), 1234 (m, C-N), 1128 (s, C-O ether) cm⁻¹.



***tert*-Butyl 4-(2-hydroxyethyl)piperidine-1-carboxylate (27).**⁸²

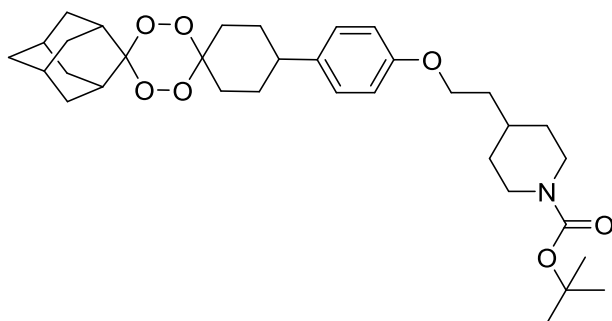
To a stirred solution of 4-piperidineethanol (500 mg, 3.90 mmol) in anhydrous DCM was added di-*tert*-butyl dicarbonate (929 mg, 4.26 mmol) at 0°C. The resulting colourless solution was stirred at room temperature for 4 hours. The solution was then washed with water (30 mL) and brine (30 mL), dried over MgSO₄, filtered and concentrated under reduced pressure to give the title compound as a colourless oil (880 mg, >95% yield): ¹H NMR (400 MHz, CDCl₃) δ = 4.10 (br, 2H), 3.70 (dd, *J* = 12, 6 Hz, 2H), 2.69 (t, *J* = 12 Hz, 2H), 1.71 – 1.47 (m, 5H), 1.45 (s, 9H), 1.29 (dd, *J* = 11, 6 Hz, 1H), 1.12 (dd, *J* = 13, 4 Hz, 2H) ppm; ¹³C

NMR (101 MHz, CDCl₃) δ = 155.04, 79.39, 60.46, 39.45, 32.72, 32.29, 28.62, 27.57 ppm; HRMS (CI, m/z) calcd for [C₁₂H₂₄NO₃]⁺ (M+H)⁺ 230.1756, found 230.1753.



***tert*-Butyl 4-(2-iodoethyl)piperidine-1-carboxylate (28).**⁸²

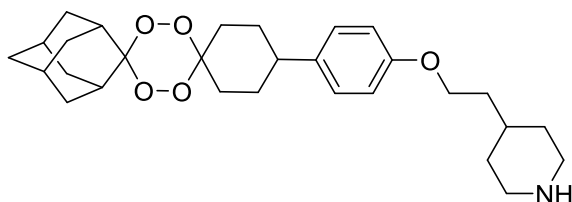
To a stirred solution of *tert*-butyl 4-(2-hydroxyethyl)piperidine-1-carboxylate (400 mg, 1.74 mmol) in anhydrous toluene (30 mL) was added iodine (663 mg, 5.22 mmol), imidazole (166 mg, 2.44 mmol) and triphenylphosphine (503 mg, 1.92 mmol). The resulting orange solution was heated to 80°C for 3 hours. The reaction mixture was then concentrated under reduced pressure and the resulting crude residue purified by column chromatography (10:1 *n*-hexane/ethyl acetate) to give the title compound as a colourless oil (263 mg, 45% yield): ¹H NMR (400 MHz, CDCl₃) δ = 4.18 – 3.97 (m, 2H), 3.21 (t, J = 7 Hz, 2H), 2.70 (t, J = 12 Hz, 2H), 1.77 (q, J = 7 Hz, 2H), 1.65 (d, J = 13 Hz, 2H), 1.61 – 1.58 (m, 1H), 1.45 (s, 9H), 1.10 (dd, J = 12, 4 Hz, 2H) ppm; ¹³C NMR (101 MHz, CDCl₃) δ = 154.96, 79.49, 43.81, 40.07, 36.79, 31.36, 28.61, 4.04 ppm; HRMS (ES, m/z) calcd for [C₁₂H₂₂INNaO₂]⁺ (M+Na)⁺ 362.0593, found 362.0590.



***tert*-Butyl 4-(2-(4-((1r,3r,5r,7r)-dispiro[adamantane-2,3'-[1,2,4,5]tetraoxane-6',1''-cyclohexan]-4''-yl)phenoxy)ethyl)piperidine-1-carboxylate (29).**

General procedure B was followed using *tert*-butyl 4-(2-iodoethyl)piperidine-1-carboxylate (250 mg, 0.74 mmol). Purification by column chromatography (20:1

n-hexane/ethyl acetate) gave the title compound as a white solid (96 mg, 45% yield): ¹H NMR (400 MHz, CDCl₃) δ = 7.13 (d, *J* = 9 Hz, 2H), 6.82 (d, *J* = 9 Hz, 2H), 4.09 (br s, 2H), 3.98 (t, *J* = 6 Hz, 2H), 3.33 – 3.15 (m, 2H), 2.70 (t, *J* = 12 Hz, 2H), 2.56 (t, *J* = 11 Hz, 2H), 2.08 – 1.54 (m, 25H), 1.45 (s, 9H), 1.21 – 1.10 (m, 2H) ppm; ¹³C NMR (101 MHz, CDCl₃) δ = 157.50, 155.03, 138.21, 127.85, 114.44, 110.63, 107.70, 79.41, 65.38, 60.55, 42.93, 37.10, 35.97, 33.30, 33.07, 32.22, 28.61, 27.93, 27.20, 21.21, 14.34 ppm; HRMS (ES, *m/z*) calcd for [C₃₄H₄₉NNaO₇]⁺ (*M*+Na)⁺ 606.3407, found 606.3398.



4-(2-(4-((1r,3r,5r,7r)-Dispiro[adamantane-2,3'-[1,2,4,5]tetraoxane-6',1''-cyclohexan]-4''-yl)phenoxy)ethyl)piperidine (30).

tert-Butyl 4-(2-(4-((1r,3r,5r,7r)-dispiro[adamantane-2,3'-[1,2,4,5]tetraoxane-6',1''-cyclohexan]-4''-yl)phenoxy)ethyl)piperidine-1-carboxylate (174 mg, 0.29 mmol) was dissolved in a 1.5 M solution of methane sulfonic acid (6 mL). The resulting solution was stirred at room temperature for 6 hours. The reaction mixture was then neutralised with 2 M NaOH and extracted with ethyl acetate (3 x 30 mL). The combined organics were washed with brine (30 mL), dried over Na₂SO₄, filtered and concentrated under reduced pressure to give the crude product as a cream solid. Trituration with diethyl ether gave the title compound as a white solid (129 mg, 90% yield): ¹H NMR (400 MHz, CDCl₃) δ = 7.13 (d, *J* = 9 Hz, 2H), 6.82 (d, *J* = 9 Hz, 2H), 3.97 (t, *J* = 6 Hz, 2H), 3.32 – 3.17 (m, 2H), 3.10 (d, *J* = 12 Hz, 2H), 2.62 (t, *J* = 12 Hz, 2H), 2.30 (br s, 1H), 2.07 – 1.58 (m, 25H), 1.24 – 1.17 (m, 2H) ppm; ¹³C NMR (101 MHz, CDCl₃) δ = 157.57, 138.14, 127.83, 114.46, 110.62, 107.71, 65.39, 46.55, 42.93, 37.10, 36.49, 33.30, 27.21 ppm; HRMS (ES, *m/z*) calcd for [C₂₉H₄₁NNaO₅]⁺ (*M*+Na)⁺ 506.2882, found 506. 2873.

5.5 References

- 1 D. T. Manallack, R. J. Prankerd, E. Yuriev, T. I. Oprea and D. K. Chalmers, *Chem. Soc. Rev.*, 2013, **42**, 485–496.
- 2 S. A. Charman, S. Arbe-Barnes, I. C. Bathurst, R. Brun, M. Campbell, W. N. Charman, F. C. K. Chiu, J. Chollet, J. C. Craft, D. J. Creek, Y. Dong, H. Matile, M. Maurer, J. Morizzi, T. Nguyen, P. Papastogiannidis, C. Scheurer, D. M. Shackleford, K. Sriraghavan, L. Stingelin, Y. Tang, H. Urwyler, X. Wang, K. L. White, S. Wittlin, L. Zhou and J. L. Vennerstrom, *Proc. Natl. Acad. Sci. U.S.A.*, 2011, **108**, 4400–4405.
- 3 M. Reichman and H. Gill, in *Drug Metabolism Handbook: Concepts and Applications*, ed. A. F. Nassar, P. F. Hollenberg and J. Scatina, Wiley, Hoboken, 2009, ch. 7, pp. 129–167.
- 4 M. E. Aulton, *Pharmaceutics: The Science of Dosage Form Design*, Churchill Livingstone, London, 2002.
- 5 D. R. Spring, *Org. Biomol. Chem.*, 2003, **1**, 3867–3870.
- 6 C. F. J. Barnard, *Organometallics*, 2008, **27**, 5402–5422.
- 7 J. R. Martinelli, D. A. Watson, D. M. M. Freckmann, T. E. Barder and S. L. Buchwald, *J. Org. Chem.*, 2008, **73**, 7102–7107.
- 8 L. Cotarca and H. Eckert, *Phosgenations: A Handbook*, Wiley, Hoboken, 2006.
- 9 R. Buchecker, M. Schadt and A. Villiger, US Pat., 5 185 098, 1993.
- 10 Y. Dong and J. L. Vennerstrom, *J. Org. Chem.*, 1998, **63**, 8582–8585.
- 11 J. R. Sanderson, A. G. Zeiler and R. J. Wilterdink, *J. Org. Chem.*, 1975, **40**, 2239–2241.
- 12 G. L. Ellis, R. Amewu, S. Sabbani, P. A. Stocks, A. Shone, D. Stanford, P. Gibbons, J. Davies, L. Vivas, S. Charnaud, E. Bongard, C. Hall, K. Rimmer, S. Lozanom, M. Jesús, D. Gargallo, S. A. Ward and P. M. O'Neill, *J. Med. Chem.*, 2008, **51**, 2170–2177.
- 13 D. Farcasiu and D. Hancu, *J. Chem. Soc. Faraday Trans.*, 1997, **93**, 2161–2165.
- 14 P. Ghorai and P. H. Dussault, *Org. Lett.*, 2009, **11**, 213–216.

- 15 P. Ghorai and P. H. Dussault, *Org. Lett.*, 2008, **10**, 4577–4579.
- 16 D. E. Clark, *Peroxides and Peroxide Forming Compounds*, University of Nebraska, 2000.
- 17 C. W. Jones, J. H. Clark and M. J. Braithwaite, *Applications of Hydrogen Peroxide and Derivatives*, The Royal Society of Chemistry, Cambridge, 1999.
- 18 D. E. Clark, *Chem. Health Saf.*, 2000, **8**, 12–22.
- 19 K. Tadpetch and S. D. Rychnovsky, *Org. Lett.*, 2008, **10**, 4839–4842.
- 20 J. Clayden, N. Greeves and S. Warren, *Organic Chemistry*, OUP Oxford, 2012.
- 21 M. S. Singh, *Advanced Organic Chemistry: Reactions And Mechanisms*, Pearson Education, London, 2004.
- 22 M. Kah and C. D. Brown, *Chemosphere*, 2008, **72**, 1401–1408.
- 23 ChemAxon | Calculator Plugins, <https://www.chemaxon.com/marvin-archive/3.4.3/marvin/chemaxon/marvin/help/calculator-plugins.html>, (accessed December 2016) .
- 24 G. Evans, *A Handbook of Bioanalysis and Drug Metabolism*, CRC Press, Boca Raton, 2004.
- 25 G. L. Amidon, H. Lennernäs, V. P. Shah and J. R. Crison, *Pharm. Res.*, 1995, **12**, 413–420.
- 26 S. M. Berge, L. D. Bighley and D. C. Monkhouse, *J. Pharm. Sci.*, 1977, **66**, 1–19.
- 27 P. H. Stahl and C. G. Wermuth, *Handbook of Pharmaceutical Salts Properties, Selection, and Use*, Wiley, Hoboken, 2008.
- 28 D. P. Elder, E. Delaney, A. Teasdale, S. Eyley, V. D. Reif, K. Jacq, K. L. Facchine, R. S. Oestrich, P. Sandra and F. David, *J. Pharm. Sci.*, 2010, **99**, 2948–2961.
- 29 MMV | Developing a single-dose malaria cure, <http://www.mmv.org/newsroom/interviews/developing-single-dose-malaria-cure>, (accessed December 2016).
- 30 Cambridge MedChem | Distribution and Plasma Protein Binding, <http://www.cambridgemedchemconsulting.com/resources/ADME/distribution.html>, (accessed December 2016).
- 31 S. M. Pond and T. N. Tozer, *Clin. Pharmacokinet.*, 1984, **9**, 1–25.

- 32 W. A. Ritschel and G. L. Kearns, *Handbook of Basic Pharmacokinetics ... including Clinical Applications*, American Pharmacists Association, Washington, 2009.
- 33 M. J. Bosma and A. M. Carroll, *Annu. Rev. Immunol.*, 1991, **9**, 323–350.
- 34 R. Ito, T. Takahashi, I. Katano and M. Ito, *Cell. Mol. Immunol.*, 2012, **9**, 208–214.
- 35 T. Pearson, D. L. Greiner and L. D. Shultz, *Curr. Top. Microbiol. Immunol.*, 2008, **324**, 25–51.
- 36 M. A. Brehm, L. D. Shultz and D. L. Greiner, *Curr. Opin. Endocrinol. Diabetes Obes.*, 2010, **17**, 120–125.
- 37 L. Vivas, L. Rattray, L. Stewart, E. Bongard, B. L. Robinson, W. Peters and S. L. Croft, *Acta Trop.*, 2008, **105**, 222–228.
- 38 V. Ravikumar, A. Fin, N. Sakai and S. Matile, *Supramol. Chem.*, 2011, **23**, 69–73.
- 39 B. Dayal, G. Salen, B. Toome, G. S. Tint, S. Shefer and J. Padia, *Steroids*, 1990, **55**, 233–237.
- 40 M. B. Smith, *Organic Chemistry: An Acid-Base Approach, Second Edition*, CRC Press, Boca Raton, 2016.
- 41 J. F. McGarrity and J. Prodoliet, *J. Org. Chem.*, 1984, **49**, 4465–4470.
- 42 M. R. Buchmeiser, *Polymeric Materials in Organic Synthesis and Catalysis*, Wiley, Hoboken, 2006.
- 43 R. Criegee, *Angew. Chemie Int. Ed.*, 1975, **14**, 745–752.
- 44 C. Geletneky and S. Berger, *Eur. J. Org. Chem.*, 1998, **8**, 1625–1627.
- 45 S. Warren and P. Wyatt, *Organic Synthesis: The Disconnection Approach, 2nd Edition*, Wiley, Hoboken, 2008.
- 46 A. F. Abdel-Magid, K. G. Carson, B. D. Harris, C. A. Maryanoff and R. D. Shah, *J. Org. Chem.*, 1996, **61**, 3849–3862.
- 47 A. F. Abdel-Magid and S. J. Mehrman, *Org. Process Res. Dev.*, 2006, **10**, 971–1031.
- 48 P. S. Bailey and R. E. Erikson, *Org. Synth.*, 1961, **41**, 41–45.
- 49 S. A. Epstein and N. M. Donahue, *J. Phys. Chem. A*, 2008, **112**, 13535–13541.
- 50 P. G. M. Wuts, *Greene's Protective Groups in Organic Synthesis*, Wiley, Hoboken, 2014.

- 51 K. D. Deshayes, in *Encyclopedia of Reagents for Organic Synthesis*, John Wiley & Sons, Ltd, Hoboken, 2001.
- 52 V. K. Ahluwalia and R. Aggarwal, *Comprehensive Practical Organic Chemistry: Preparations And Quantitative Analysis*, Universities Press (India) Pvt. Limited, Hyderabad, 2000.
- 53 S.-H. Lau, A. Galván, R. R. Merchant, C. Battilocchio, J. A. Souto, M. B. Berry and S. V. Ley, *Org. Lett.*, 2015, **17**, 3218–3221.
- 54 W. Weber and G. W. Gokel, *Phase Transfer Catalysis in Organic Synthesis*, Springer-Verlag, Berlin, 1977.
- 55 Finkelstein reaction, in *Comprehensive Organic Name Reactions and Reagents*, ed. Z. Wang, John Wiley & Sons, Inc., Hoboken, 2010, pp. 1060–1063.
- 56 Sigma-Aldrich | 4-(chloroacetyl)morpholine,
<http://www.sigmaaldrich.com/catalog/product/aldrich/699357?lang=en®ion=GB>, (accessed December 2016).
- 57 S. Rossi, M. Benaglia, E. Massolo and L. Raimondi, *Cat. Sci. Technol.*, 2014, **4**, 2708–2723.
- 58 A. Volkov, PhD Thesis, Stockholm University, 2016.
- 59 S. Das, D. Addis, S. Zhou, K. Junge and M. Beller, *J. Am. Chem. Soc.*, 2010, **132**, 1770–1771.
- 60 F. Bousejra-El Garah, M. H.-L. Wong, R. K. Amewu, S. Muangnoicharoen, J. L. Maggs, J.-L. Stigliani, B. K. Park, J. Chadwick, S. A. Ward and P. M. O'Neill, *J. Med. Chem.*, 2011, **54**, 6443–6455.
- 61 J. Seyden-Penne, *Reductions by the Alumino- and Borohydrides in Organic Synthesis*, Wiley-VCH, Weinheim, 1997.
- 62 J. Pesti and G. L. Larson, *Org. Process Res. Dev.*, 2016, **20**, 1164–1181.
- 63 H. Akamatsu, S. Kusumoto and K. Fukase, *Tetrahedron Lett.*, 2002, **43**, 8867–8869.
- 64 G. Barbe and A. B. Charette, *J. Am. Chem. Soc.*, 2008, **130**, 18–19.
- 65 S.-H. Xiang, J. Xu, H.-Q. Yuan and P.-Q. Huang, *Synlett*, 2010, **16**, 1829–1832.
- 66 ChemGuide - The Effect of Temperature on Reaction Rates,
<http://www.chemguide.co.uk/physical/basicrates/temperature.html>,
(accessed August 2016).

- 67 Sigma-Aldrich - Bismuth (III) trifluoromethanesulfonate,
<http://www.sigmaaldrich.com/catalog/product/aldrich/633305?lang=en®ion=GB>, (accessed August 2016).
- 68 Sigma-Aldrich - Rhenium (VII) oxide,
<http://www.sigmaaldrich.com/catalog/substance/rheniumviiioxide48441131468711?lang=en®ion=GB>, (accessed August 2016).
- 69 A. B. Rode, K. Chung, Y.-W. Kim and I. S. Hong, *Energy & Fuels*, 2010, **24**, 1636–1639.
- 70 T. Matsuura, J. W. Bode, Y. Hachisu and K. Suzuki, *Synlett*, 2003, **11**, 1746–1748.
- 71 J. L. Vennerstrom, Y. Dong, S. A. Charman, S. Wittlin, J. Chollet, X. Wang, K. Sriraghavan, L. Zhou, H. Matile and W. N. Charman, US Pat., 2008/0125441 A1, 2008.
- 72 R. Khadka, J. Ro, H. Kim, I. Kim, J. T. Kim, H. Kim, J. M. Cho, G. Yun and J. Lee, *Asian J. Pharmacol.*, 2014, **9**, 304–316.
- 73 R. V. Mantri, R. Sanghvi and H. J. Zhu, in *Developing Solid Oral Dosage Forms: Pharmaceutical Theory and Practice*, ed. Y. Qiu, Y. Chen, G. G. Z. Zhang, L. Liu and W. Porter, Elsevier Science, Amsterdam, 2nd edn, 2016, ch. 1, pp. 3–22.
- 74 B. N. Singh, *Clin. Pharmacokinet.*, 1999, **37**, 213–255.
- 75 P. G. M. Wuts and T. W. Greene, *Greene's Protective Groups in Organic Synthesis*, John Wiley & Sons, Inc., Hoboken, 2007.
- 76 Y. Basel and A. Hassner, *J. Org. Chem.*, 2000, **65**, 6368–6380.
- 77 R. Appel, *Angew. Chemie Int. Ed.*, 1975, **14**, 801–811.
- 78 D. W. Allen, in *Organophosphorus Chemistry*, ed. D. W. Allen, D. Loakes and J. C. Tebby, Royal Society of Chemistry, Cambridge, 2015, vol. 44, ch. 1, pp. 1–55.
- 79 S. E. Blondelle and R. A. Houghten, *Int. J. Pept. Protein Res.*, 2009, **41**, 522–527.
- 80 G. Han, M. Tamaki and V. J. Hruby, *J. Pept. Res.*, 2001, **58**, 338–341.
- 81 S. A. Snyder, A. P. Brucks, D. S. Treitler and I. Moga, *J. Am. Chem. Soc.*, 2012, **134**, 17714–17721.
- 82 B. C. Askew, R. A. Bednar, B. Bednar, D. A. Claremon, J. J. Cook, C. J.

McIntyre, C. A. Hunt, R. J. Gould, R. J. Lynch, J. J. Lynch, S. L. Gaul, M. T.
Stranieri, G. R. Sitko, M. A. Holahan, J. D. Glass, T. Hamill, L. M. Gorham, T.
Prueksaritanont, J. J. Baldwin and G. D. Hartman, *J. Med. Chem.*, 1997, **40**,
1779–1788.

Chapter VI

Conclusions

Table of Contents

6.1 General Summary	321
6.2 IspD	322
6.2.1 Conclusions	322
6.2.2 Future work	326
6.3 1,2,4,5-Tetraoxanes	328
6.3.1 Conclusions	328
6.3.2 Future Work	332
6.4 References	332

6.1 General Summary

Due to the increasing emergence of resistance towards commonly used therapies, there is an ever-urgent need for novel antimalarial drug compounds.¹ This research led to the development of two chemically distinct groups of molecules that were designed to inhibit very different *Plasmodium falciparum* targets.

A library of benzisothiazolinone compounds was generated to target the IspD enzyme, a novel target in antimalarial drug discovery.² Many of these compounds displayed low micromolar inhibitory activity against both enzymatic and phenotypic assays *in vitro* and an investigation into structure-activity relationships around the core of these benzisothiazolinones was also conducted. The most potent compound to emerge, a CH₂ linked benzisoselenazolone (Chapter 3 Section 3.7), had an IC₅₀ of 0.17 μM against *PfIspD* and 5.54 μM against *Pf3D7*. These compounds represent a novel class of IspD inhibitor, which have the potential for further development as antimalarial agents.

A number of novel 1,2,4,5-tetraoxane compounds were also designed, which have the potential to target a number of important parasite proteins upon activation (see Chapter 4 Section 4.1.2).³ The most potent analogue, N205, had an IC₅₀ of 1.3 nM and an average mouse survival of 26.3 days (66% cure rate) following a single dose. Furthermore, the synthetic pathways used to generate these 1,2,4,5-tetraoxanes were optimised, and a lead compound emerged. E209 is comparable, in terms of both efficacy and PK/PD profiles, to OZ439, and is a candidate for pre-clinical development.

The results of both projects are summarised herein, along with potential areas for further research.

6.2 IspD

6.2.1 Conclusions

The aims of this particular project were to generate a library of compounds designed to target the IspD enzyme and to explore structure-activity relationships around the hit template that was identified from an initial high throughput screen. A library of over 30 compounds was therefore synthesised, and the inhibitory activity of these compounds was tested against both enzymatic (*PfIspD*) and phenotypic (3D7 whole cell) *in vitro* assays. Furthermore, a variety of modifications and substitutions were introduced in order to explore structure-activity relationships around the benzisothiazolinone core. The most active compounds to emerge from each drug class are summarised below in Figure 6.1.

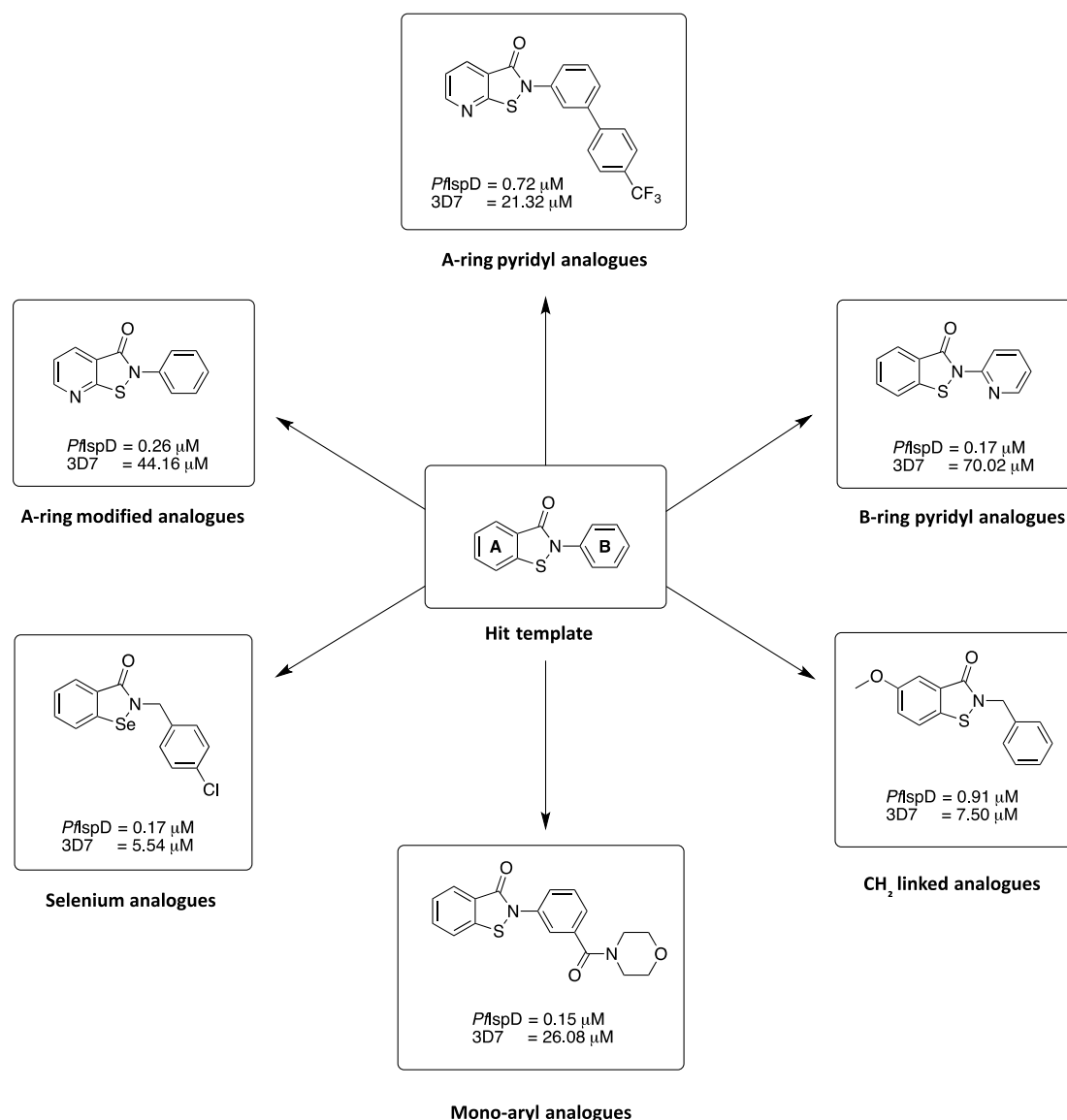


Figure 6.1. A summary of the most potent compounds developed as part of this structure-activity relationship

A number of compounds displayed low micromolar activity against *PflspD* but whole cell 3D7 activity was not comparable. The lipophilicity of a number of compounds was increased in order to help improve whole cell potency, and this was achieved; however, a drop in inhibitory activity against the enzyme was also observed.⁴ This effect is clearly seen between B-ring pyridyl compounds **47** and **48** (Figure 6.2). Compound **47** had an IC_{50} of 0.17 μM vs. *PflspD* but a disappointing activity of 70.02 μM against the whole cell assay. Introduction of an additional benzene ring into the side chain led to compound **48**, which is

more lipophilic (3.95 vs. 1.86 for compound **47**) and has more potent activity against the whole cell assay, IC₅₀ = 0.90 μM. However, potency against *Pf*lspD dropped by an order of magnitude.

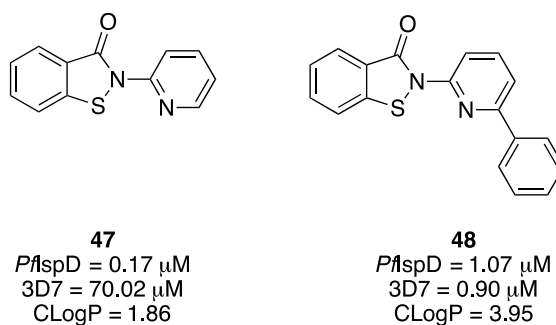


Figure 6.2. A comparison of B-ring pyridyl analogues

A number of compounds also appeared to display off-target effects. Compounds **29** and **35** (Figure 6.3) lacked antimalarial activity against *Pf*lspD, yet exhibited micromolar inhibition of the phenotypic assay. These compounds could be selectively targeting a different enzyme in the MEP pathway, as a number of these enzymes are closely linked, or they could be targeting somewhere different altogether.⁵ Off-target activity of this nature is undesirable in drug compounds.⁶

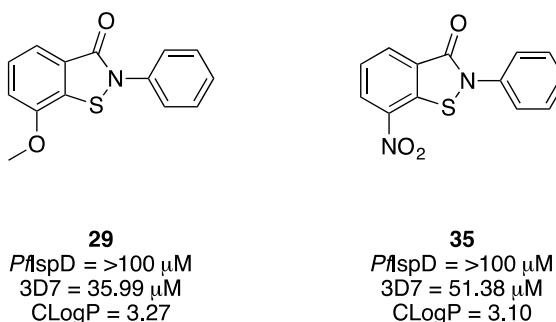


Figure 6.3. Off-target effects observed in A-ring modified analogues

The most potent inhibitor of IspD was compound **1**, a mono-aryl analogue with a morpholine solubilising group (Figure 6.4), which had an IC₅₀ of 0.15 μM against *PflspD*; however, its whole cell inhibitory activity was not comparable. The most promising compound to emerge from this research was the CH₂ linked benzoselenazolone **75** (Figure 6.4), which exhibited potent activity against both *PflspD* and phenotypic 3D7 assays. In fact, all of the CH₂ linked benzoselenazolones displayed more potent activities than the analogous benzisothiazolinones. Compound **75** has the greatest potential for further development as a novel drug candidate and the next steps would be to investigate the inhibitory activity of this compound and determine its pharmacokinetic profile in an *in vivo* model.

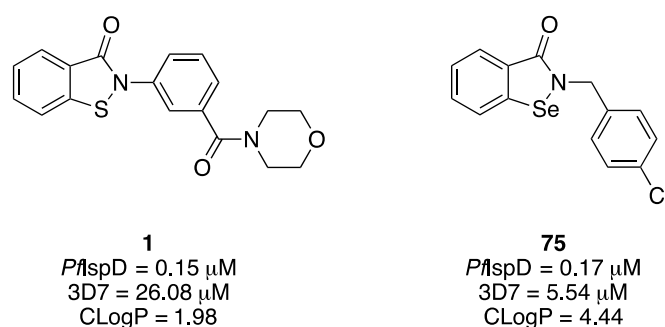
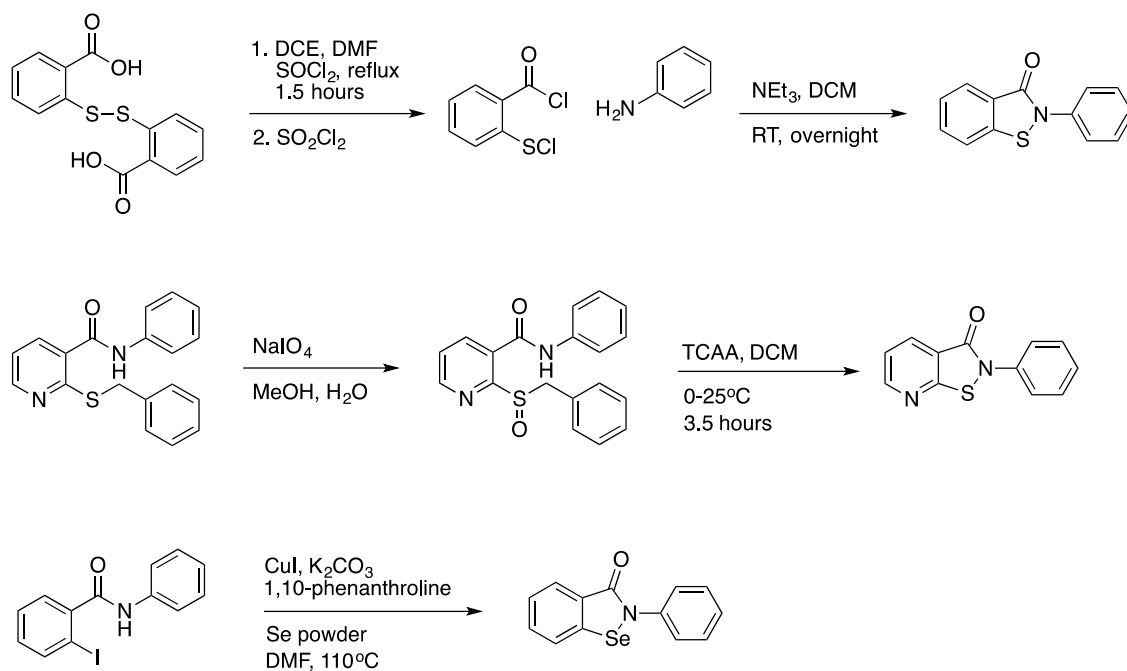


Figure 6.4. The most potent compounds to emerge from this structure-activity relationship exploration

Finally, a number of different methods to synthesise the isothiazolinone core were investigated and the most effective routes for the synthesis of benzisothiazolinones, pyridoisothiazolinones and benzoselenazolones are summarised in Scheme 6.1.^{7,8,9}



Scheme 6.1. A number of successful routes employed to generate an isothiazolinone core

6.2.2 Future work

Compound **75** has the potential for further development as a novel drug candidate and the next stage would be to investigate its inhibitory activity and pharmacokinetic profile *in vivo*.¹⁰ There is also further scope for expansion of this structure-activity relationship study, especially around the mono-aryl and CH₂ linked benzisosenazolone series. These were the most potent groups to be developed in this research; however, only 3 compounds were synthesised in each. Ideally, a novel antimalarial compound would exhibit nanomolar activity against the target rather than micromolar; therefore, further work could be done to develop these compounds, including the incorporation of different substituents/solubilising groups and changing their positions on the ring (Figure 6.5).¹¹ Further modifications could also be made to the A-ring, including the incorporation of a pyridyl group or substitution with fluorine, which can have a dramatic effect on biological activity.^{12,13}

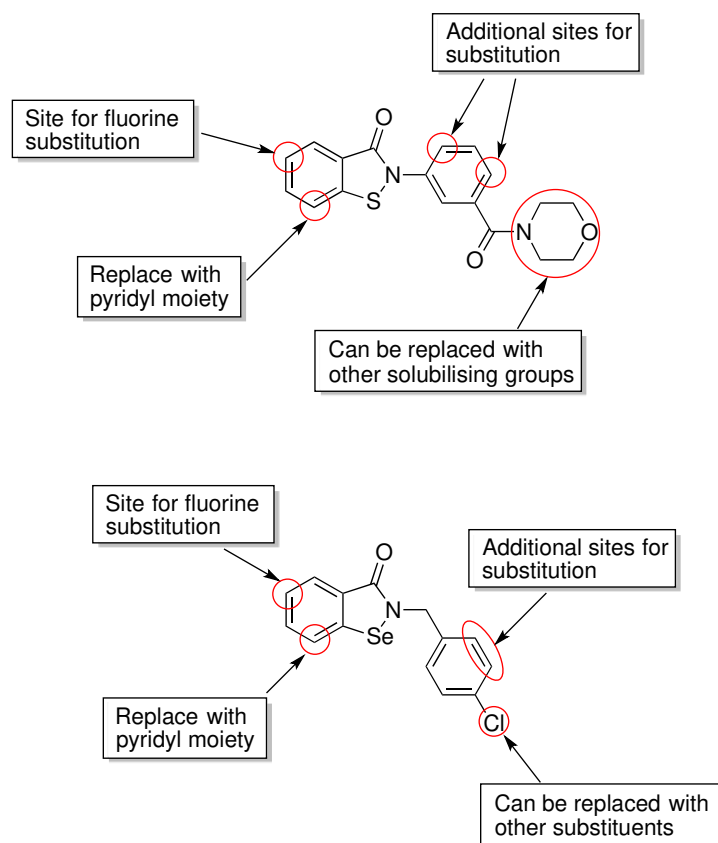


Figure 6.5. Potential for further expansion of this structure-activity relationship

Finally, a fluorescent labelling study could be used in order to identify the molecular targets of the compounds that exhibited off-target activity (e.g. compounds **29** and **35**).¹⁴

6.3 1,2,4,5-Tetraoxanes

6.3.1 Conclusions

The first aim of this project was to synthesise a 1,2,4,5-tetraoxane with the optimal, metabolically stable side chain that would maintain the potency and solubility of RKA182 whilst increasing stability, in order to move towards a single dose cure.¹⁵ A number of parameters were established for the desired target product profile:

- Simple, achiral synthesis
- Short number of steps in the synthetic pathway (≤ 5)
- Aqueous solubility >5 mg/mL
- $IC_{50} < 10$ nM
- Long single dose mouse survival i.e. >20 days survival of an infected mouse following a single 30 mg/kg dose

A benzylamino series was therefore developed. The benzyl moiety was incorporated to help lipophilicity and solubilising amine side chains were included to help maintain a good level of aqueous solubility, which would allow for ease of formulation and administration.^{11,16} The most active compound to emerge from this series was N205 (Figure 6.6).

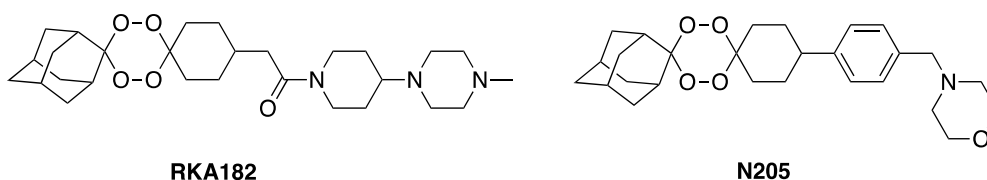


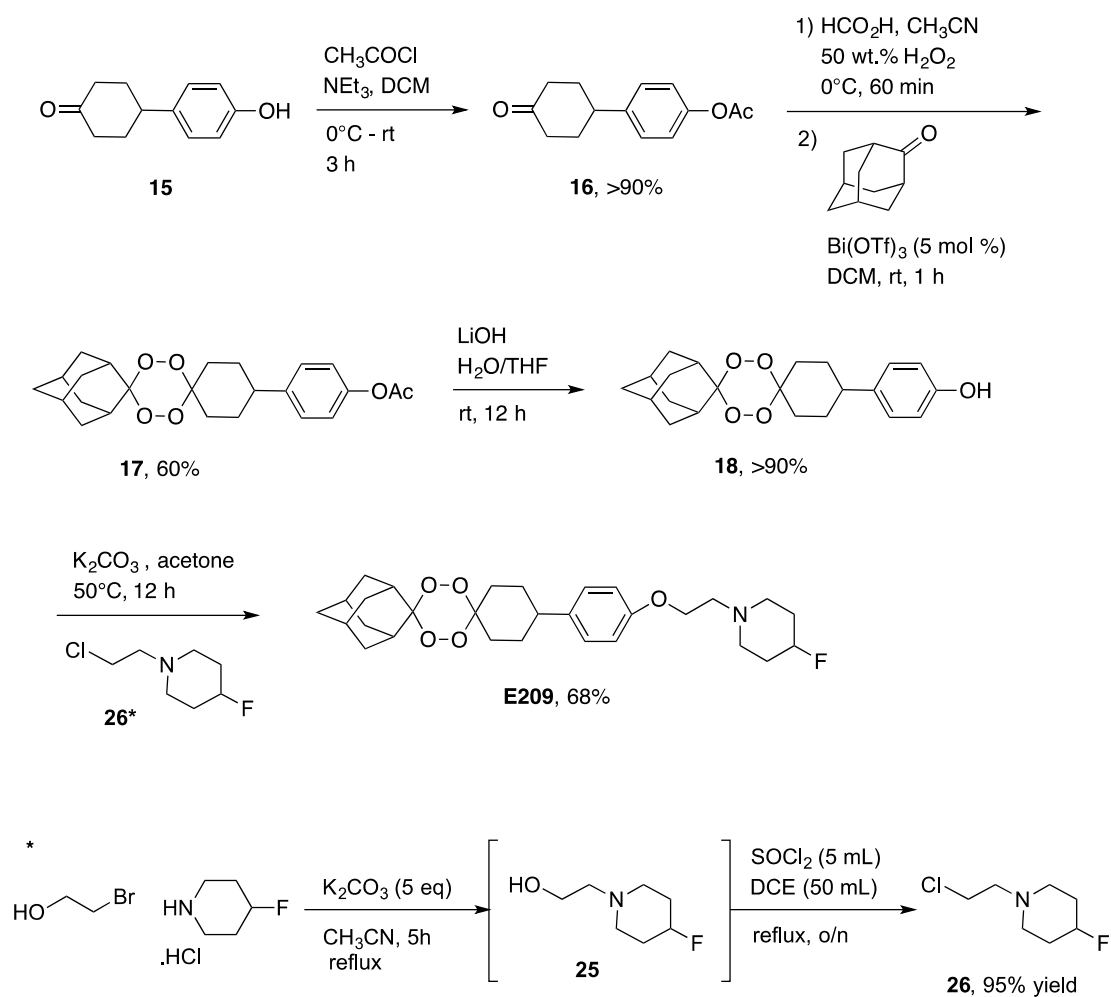
Figure 6.6. The structures of RKA182 and N205 – novel 1,2,4,5-tetraoxane antimalarials

N205 met a number of the criteria set out for the target product (Figure 6.7). IC_{50} data shows that N205 is not only a more potent antimalarial than RKA182 but also better suited for a single-dose cure, which is a current priority for MMV.¹⁷

	RKA182	N205
Simple synthesis	yes	yes
Short number of steps	4	5
Aqueous solubility	>40 mg/mL	>9 mg/mL
Activity IC ₅₀ <10 nM	4.9 nM	1.3 nM
Single dose mouse survival	11.4 days	26.3 days

Figure 6.7. A comparison between the product profile of RKA182 and N205

The second aim of this project was to simplify the synthetic pathway used to generate E209; a potent 1,2,4,5-tetraoxane, with excellent activity and stability profiles. The original synthesis of E209 involved a large number of steps and a potentially hazardous ozonolysis reaction, making this route unsuitable for scale-up.¹⁸ A number of alternative routes were investigated and the final successful pathway is outlined in Scheme 6.2.



Scheme 6.2. A simplified pathway developed for the synthesis of E209

This modified pathway provides an alternative route that is much more suitable for scale-up and allows E209 to be produced in a series of five simple, high-yielding steps that eliminate the requirement for an ozonolysis reaction. The product profile of E209 is now comparable to that of the lead trioxolane compound in development, OZ439 (Figure 6.8). As a result, E209 is now in candidate selection for clinical trials.¹⁹

	E209	OZ439
Simple synthesis	yes	yes
Short number of steps	5	4
Aqueous solubility	>8 mg/mL	6.8 mg/mL
Activity IC ₅₀ <10 nM	5.1 nM	8 nM
Single dose mouse survival	26 days	30 days
Rat blood stability/T _{1/2}	13 hours	>15 hours

Figure 6.8. A comparison between the product profile of E209 and OZ439

The final task was to produce a compound that was structurally similar to E209 but with a lower pka, with the aim of preventing the significant change in solubility observed for E209 between fasted and fed states.²⁰ The structure of this back-up compound (N327) is shown below (Figure 6.9) and the only structural difference between this analogue and E209 is the replacement of 4-fluoropiperidine with piperidine in the side-chain.

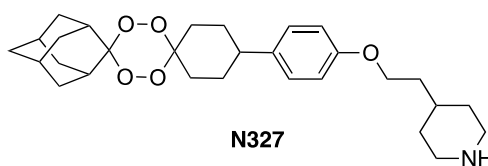


Figure 6.9. The chemical structure of N327, a potential back-up compound for E209

6.3.2 Future Work

Biological data on the back-up compound for E209, N327, is eagerly awaited; however, further research may be necessary in order to identify a compound that is structurally similar to E209 yet does not exhibit such a pronounced food effect (as a result of changes in solubility between fasted and fed states).

6.4 References

- 1 A. Alam, M. Goyal, M. S. Iqbal, C. Pal, S. Dey, S. Bindu, P. Maity and U. Bandyopadhyay, *Expert Rev. Clin. Pharmacol.*, 2009, **2**, 469–489.
- 2 L. S. Imlay, C. M. Armstrong, M. C. Masters, T. Li, K. E. Price, R. L. Edwards, K. M. Mann, L. X. Li, C. L. Stallings, N. G. Berry, P. M. O'Neill and A. R. Odom, *ACS Infect. Dis.*, 2015, **1**, 157–167.
- 3 H. M. Ismail, V. Barton, M. Phanchana, S. Charoensutthivarakul, M. H. L. Wong, J. Hemingway, G. A. Biagini, P. M. O'Neill and S. A. Ward, *Proc. Natl. Acad. Sci. U. S. A.*, 2016, **113**, 2080–2085.
- 4 P. D. Leeson and B. Springthorpe, *Nat. Rev. Drug Discov.*, 2007, **6**, 881–890.
- 5 M. V. Sponsel, *J. Plant Growth Regul.*, 2001, **20**, 332–345.
- 6 A. L. Hopkins, in *The Practice of Medicinal Chemistry*, ed. C. G. Wermuth, D. Aldous, P. Raboisson and D. Rognan, Elsevier Science, Amsterdam, 4th edn, 2015, ch. 16, pp. 395–407
- 7 B. S. Bhakuni, S. J. Balkrishna, A. Kumar and S. Kumar, *Tetrahedron Lett.*, 2012, **53**, 1354–1357.
- 8 S. W. Wright, J. J. Petraitis, M. M. Abelman, D. G. Batt, L. L. Bostrom, R. L. Corbett, C. P. Decicco, S. V. Di Meo and B. Freimark, *J. Med. Chem.*, 1994, **37**, 3071–3078.
- 9 Y. Uchida and S. Kozuka, *J. Chem. Soc. Chem. Commun.*, 1981, 510–511.
- 10 T. Tuntland, B. Ethell, T. Kosaka, F. Blasco, R. X. Zang, M. Jain, T. Gould and K. Hoffmaster, *Front. Pharmacol.*, 2014, **5**, 174.
- 11 C. Bissantz, B. Kuhn and M. Stahl, *J. Med. Chem.*, 2010, **53**, 5061–5084.
- 12 S. Purser, P. R. Moore, S. Swallow and V. Gouverneur, *Chem. Soc. Rev.*, 2008, **37**, 320–330.

- 13 B. K. Park and N. R. Kitteringham, *Drug Metab. Rev.*, 1994, **26**, 605–643.
- 14 U. Eckstein-Ludwig, R. J. Webb, I. D. A. van Goethem, J. M. East, A. G. Lee, M. Kimura, P. M. O'Neill, P. G. Bray, S. A. Ward and S. Krishna, *Nature*, 2003, **424**, 957–961.
- 15 P. M. O'Neill, R. K. Amewu, G. L. Nixon, F. Bousejra ElGarah, M. Mungthin, J. Chadwick, A. E. Shone, L. Vivas, H. Lander, V. Barton, S. Muangnoicharoen, P. G. Bray, J. Davies, B. K. Park, S. Wittlin, R. Brun, M. Preschel, K. Zhang and S. A. Ward, *Angew. Chemie Int. Ed.*, 2010, **49**, 5693–5697.
- 16 C. W. Pouton, *Eur. J. Pharm. Sci.*, 2006, **29**, 278–287.
- 17 MMV | Developing a single-dose malaria cure,
<http://www.mmv.org/newsroom/interviews/developing-single-dose-malaria-cure>, (accessed December 2016).
- 18 P. S. Bailey and R. E. Erikson, *Org. Synth.*, 1961, **41**, 41-45.
- 19 S. A. Charman, S. Arbe-Barnes, I. C. Bathurst, R. Brun, M. Campbell, W. N. Charman, F. C. K. Chiu, J. Chollet, J. C. Craft, D. J. Creek, Y. Dong, H. Matile, M. Maurer, J. Morizzi, T. Nguyen, P. Papastogiannidis, C. Scheurer, D. M. Shackleford, K. Sriraghavan, L. Stingelin, Y. Tang, H. Urwyler, X. Wang, K. L. White, S. Wittlin, L. Zhou and J. L. Vennerstrom, *Proc. Natl. Acad. Sci. U.S.A.*, 2011, **108**, 4400–4405.
- 20 B. N. Singh, *Clin. Pharmacokinet.*, 1999, **37**, 213–255.